University of Southampton

Active control of sound transmission

By Martin Eric Johnson

A thesis submitted for the degree of
Doctor of Philosophy.

Signal Processing and Control Group
Institute of Sound and Vibration Research
Faculty of Engineering and Applied Science

May 1996

UNIVERSITY OF SOUTHAMPTON
ABSTRACT
Faculty of Engineering and Applied Science
Institute of Sound and Vibration Research
Doctor of Philosophy

Active control of sound transmission

By Martin Eric Johnson

This thesis is concerned with the active control of sound transmission through structures. A particular emphasis of the work is the reduction of the complexity of the controller required to achieve good attenuations by the use of distributed sensors and actuators.

The theory of radiation modes, which is a technique for decomposing the velocity profile of a radiator into a set of independently radiating velocity distributions, is presented first. The first radiation mode of a structure is shown to be the dominant radiator of sound at low frequencies and to have an amplitude which is well approximated by the volume velocity of the structure. The cancellation of volume velocity is suggested as a good strategy for reducing the sound power radiation at low frequencies. Radiation mode theory is more generally shown to be a convenient method for determining the complexity of the control system required to reduce the sound radiation from a structure.

The design of a volume velocity sensor for beams and rectangular plates with fixed boundary conditions is suggested. This design uses a pattern of quadratically shaped strips etched into the electrode of a sheet of PVDF (piezoelectric) film.

The strategy of volume velocity cancellation is initially investigated using a computer simulation and is shown to perform well at low frequencies, when compared with the optimal strategy of sound power minimization. In controlling sound radiation a compact secondary actuator can increase the average velocity of the panel and thus increases the pressure generated close to the panel. The use of a matched actuator/sensor pair, consisting of a volume velocity sensor and a uniform-force actuator, is shown to reduce control spillover and thus avoid increasing the plate velocity when controlling sound radiation. The transfer response between such a matched actuator and sensor is also shown to be minimum phase, which has important implications for the performance of the control system. A distributed sensor and actuator would also be beneficial in the active control of sound transmission into a cylinder, which is also briefly examined.

The manufacture and testing of a volume velocity sensor is described and the output of the sensor is shown to compare well with the volume velocity measured using the average of 49 point measurements on a clamped plate excited by a primary source. An experiment is presented in which a piezoelectric ceramic actuator, attached to the plate, is driven to cancel the output of the volume velocity sensor while the plate is excited at a single frequency by a primary acoustic source. Large reductions in the radiated sound power can then be achieved.

An experiment is also described in which the volume velocity sensor is used with a feedback system to cancel broadband noise. Good reductions are achieved in the average output of the sensor, resulting in substantial reductions in the radiated sound.

Contents

Acknowledgements

I would like to acknowledge the support given to this work by the Department of Trade and Industry and by the European Space Agency.

I have been fortunate to have found a superb supervisor in Professor Elliott who has been more amenable to the 'randomly knock on someone's door and ask a silly question' approach to learning than could be reasonably expected from a man in his position. I also extend my appreciation to all of the other members of the SPCG who have been subjected to this technique over the past three years. I would like to give special thanks to Boaz Rafaely for helping me with the feedback control experiments and being a general egg-head on IMC.

I would like to thank (as has become customary) the 'Arlott room inhabitants' for their contribution. While adding greatly to the author's appreciation of political issues and philosophy in general they have also succeeded in delaying the completion of this thesis by a number of months.

The contribution from my parents goes far beyond the obvious one made some twenty six years ago. Their ceaseless and unconditional support has given me a foundation on which it has been very easy to build and I thank them for the abundance of love which they have given me over the years. Finally, I would like to thank my fiancée Debs without whom everything would seem somewhat pointless.

Chapter 1

Introduction

1.1 A definition of active control

Active control can be defined as a method of altering the behaviour of a system by the introduction into the system of an energy source whose output is dependent on the response of the system. Methods of altering the behaviour of a system without the introduction of an energy source are termed *passive control methods.*

As a scientific or engineering term "active control systems" is most often used to describe the set of active control systems operating on electrical or mechanical machines to achieve some electrical or mechanical effect. There are of course a large number of examples of biological active control systems such as salinity control in cells [61] or the steering of a motor vehicle by a human being. In the context of the active control of sound, active control systems are comprised of both electrical and mechanical components.

A review of the entire field of active control of sound will not be given here as there are a number of published reviews and books on the subject [31, 40, 71]. However, the main elements of an active control system will be described so that the contribution of this thesis can be put into context.

1.2 The components of an active control system

Active control systems are used to alter the response of a system in an attempt to produce a more desirable outcome. In the application of active control systems for the control of sound, the desirable response is generally defined to be no sound at all. This is not always the case, as active control systems can be used for the equalization of acoustic enclosures [59] or to modify the characteristics of noise or error signals [19, 20]. For the purposes of this thesis, however, the objective will always be to reduce the acoustic levels as far as possible.

In nearly all applications of active sound control the desired state is zero sound pressure *in a region* of the total system. The physical size of this region is usually determined by the type of disturbance and the frequency range of interest. The low frequency tonal noise produced by propeller driven aircraft can be controlled using an active control system to achieve reductions throughout the entire aircraft cabin [71] although the external sound field (which is part of the total system) is virtually unaffected by the control system. For higher frequency tonal noise, active control systems have been used to produce "zones of quiet" in an enclosure to achieve reduced noise levels close to the head of an observer [71]. With active headsets [71], which are able to reduce the levels of low to medium frequency random or transient noise, the region under control is a very small volume inside the headset cavity.

Most active control systems and all of those considered in the work presented in this thesis, are based on the principle of linear superposition, that is, the altered or final response of the system is due to a *linear* combination of the original response and the response produced by the control system. The acoustic levels in a system will be reduced if the control system creates an acoustic field that is similar to the original field but out of phase with it, such that the two fields interfere destructively.

It is possible in principle to achieve any desired response (i.e. perfect control) if the response of a system can be measured exactly and the control system has the ability to affect the system in any arbitrary manner. In any real system the response of the system will not be determined with complete accuracy and the control system will not be able to influence the system in any arbitrary manner. The engineering task is to design an active control system which is simple/cheap/light enough to be practical

and still achieve good performance i.e. produce a good approximation of the desired response.

The three main components of an active control system are shown in figure 1.1 and will be briefly described in the following sections.

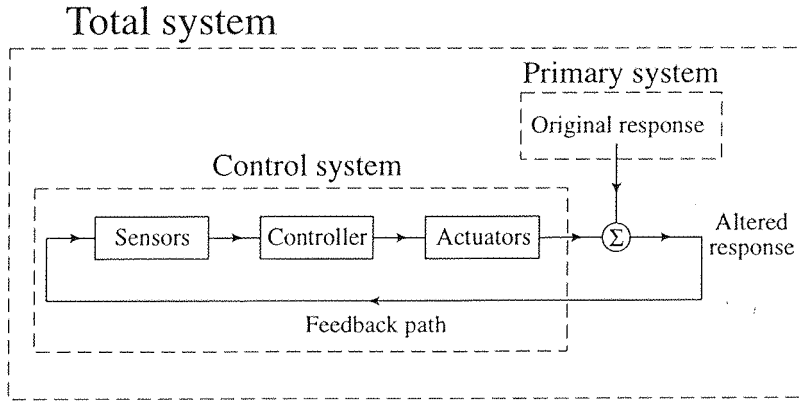

Figure 1.1: The basic components of an active control system.

Sensors

For any control system to operate it must be able to measure the response of the system. If it did not it would lack any criteria on which to operate. The response of a system is determined via *sensors* which collect information about the system and feed this information back to the controller. As will be discussed later in this chapter, the control systems used in the active control of sound are generally termed "feedforward" or "feedback" although in practice both of these control systems use information about the response of the total system.

In the interest of simplifying the control system, it is important to extract, via the sensors, information about the system which is important for the purposes of attaining the desired response. By using a large number of sensors the controller is required to sort out or filter large amounts of information. However, if the sensors are carefully designed some of the "sorting out" or filtering can be done in the physical domain and the computational pressure on the controller can be reduced. Chapters 2, 3 and 4 of this thesis discuss methods of characterizing and measuring parameters which are important for the reduction of radiated sound levels. This facilitates a reduction

in the number of sensors required to achieve good control and hence reduces the need for a complex (and often expensive) controller.

The controller

The controller is the part of the active control system which manipulates information. It receives information from the sensors, processes the information and passes the altered information on to the actuators. The creation of practical active control systems for controlling sound has been made possible primarily by the development of fast digital signal processors. The increases in performance of these D.S.P components are continually allowing more active control applications to become practical.

In feedforward control systems the inputs to the controller are split into two types. Inputs that are used to drive the actuators (reference signals) and inputs that are designed to monitor the performance of the system and alter the response of the controller (error signals). Reference signals are usually taken close to the source of the primary disturbance (for example an engine) and are often largely unaffected by the outputs of the actuators (although this is not always the case [71]). The reference signals are taken "upstream" (with regards to time) of the region of the total system under control and are "feed forward", through the controller, to the actuators which predominantly affect the control region of the total system (figure 1.2a). The error signals, which monitor the response of the region of the system under control, are then used to adapt the way in which the controller manipulates the reference signals such that the error signals are reduced.

Feedback control (figure 1.2b) is used in situations where it is difficult to obtain a good reference signal, for example where the sources of the sound are spatially distributed or the source is not sufficiently "upstream". Feedback controllers use error signals to directly drive the actuators and by doing this run the risk of becoming unstable. Feedback controllers will be discussed in more detail in chapter 8 of this thesis.

Actuators

Actuators are the means by which the control system affects the response of the total system. By having a limited set of actuators the control system can only influence a

(a) Feedforward control system

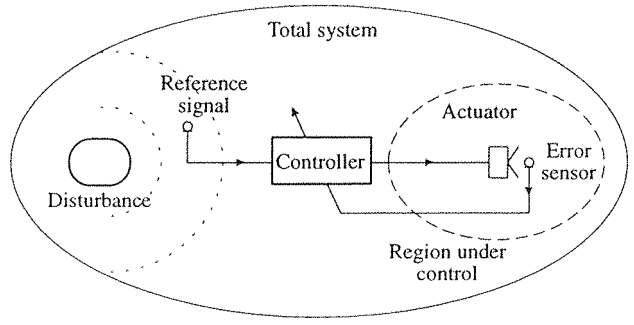

(b) Feedback control system

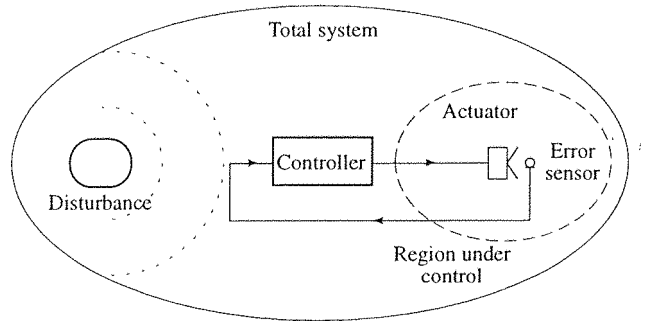

Figure 1.2: Feedforward and feedback control systems. An acoustic analogy is used here but any arbitrary set of actuators and sensors could be used.

subset of the total set of possible responses of the system. It is therefore important that the actuators are able to produce a response that is closely related to the original response of the system. As with the design of the sensing system, large numbers of actuators could potentially be used to achieve this response, thus placing a large computational pressure on the controller. Alternatively, a few carefully designed actuators could be used to reduce the need for a large processing ability. The design of the actuators cannot be viewed separately from the design of the sensing system and careful design of a sensor/actuator pair can significantly increase performance as will be described in chapter 5.

1.3 Structural acoustic control

In general the region under control is spatially separated from the source of the disturbance as illustrated in figure 1.2a. The acoustic disturbance inside an aircraft cabin due to propeller engines is an example of such a case. There is therefore some

path through which the disturbance propagates from the noise source to the region of the system under control. In an attempt to reduce the power transmitted from the source to the region under control, a control system can be placed at some point along the path. In general this path involves a structural component which radiates sound into the region under control. Control of the sound using a control system placed on the structure, that is having structural sensors and actuators, is termed *active structural acoustic control* [18]. This thesis is principally concerned with the active structural acoustic control of sound radiation from panels.

1.4 The structure and contribution of this thesis

The main objective of the work presented in this thesis is the investigation of active control systems which reduce the sound transmission through a panel using distributed structural sensors and actuators. The distributed sensors and actuators are designed to make the electrical control requirements as simple as possible.

Chapter two of this thesis is concerned with the radiation of sound from vibrating surfaces. First, the standard methods of calculating the sound field radiated by a vibrating surface are presented. It is then shown that the radiation from a surface can be decomposed into a set of independently radiating velocity distributions or "radiation modes". A method of calculating the radiation mode shapes and efficiencies using near-field parameters (an elemental radiator approach) is introduced [33]. The resultant radiation mode shapes for a beam are calculated and compared with the radiation mode shapes calculated using a formulation in terms of structural modes. The elemental radiator approach is shown to be an unbiased method of calculating the radiation mode shapes. The independence of the acoustic radiation by individual radiation modes is given a physical interpretation in terms of velocity and pressure distributions. To demonstrate the advantages of the radiation mode approach, the efficiencies of the radiation modes as a function of frequency are presented and compared with the radiation efficiencies of structural modes. The number of parameters required to produce a good estimate of the total sound power radiation are show to be greatly reduced by using the radiation mode approach. For completeness the radiation modes are viewed in terms of multipole expansions and wavenumber expansions.

Chapter three of this thesis investigates the properties of radiation modes [55] in more depth. The radiation modes for various sources radiating into one, two and three dimensional acoustic fields are investigated and the shapes of the radiation modes in these environments are calculated. In all cases the amplitude of the lowest order radiation mode at low frequencies is well approximated by the volume velocity of the surface and it is also shown that the first radiation mode is the dominant radiator of sound in this frequency region. Radiation modes are shown to group into sets of the same order with each mode order having a similar variation in radiation efficiency with frequency (at low frequencies). The number of radiation modes in these sets is shown to be a function of the dimensionality of the acoustic field and the dimensionality of the acoustic source. The radiation modes are linked to *spherical harmonics* which correspond to the radiation modes for a vibrating sphere [67]. Radiation modes appear to produce no circulation in the intensity field and therefore have the property of producing far-field directivity patterns that correspond directly to their surface velocities. A general theory for radiation modes into enclosures is presented and the shapes and efficiencies of these modes are calculated for some specific examples.

Chapter four is concerned with distributed piezoelectric transducers and the design of volume velocity sensors. The piezoelectric theory necessary for the design of distributed transducers for plates and beams is presented. The spatial sensitivity necessary to create volume velocity sensors for beams with fixed ends, simply supported plates and clamped plates are derived and a method of creating a uni-directional sensor is suggested [49, 50]. Designs for a two-dimensional volume velocity sensor are subjected to error analysis and the "quadratic strip" design is selected as the most suitable. The number of point sensors required to create an equivalent volume velocity sensor is calculated and is shown to be prohibitively large.

The theoretical performance of various active control strategies, including the cancellation of volume velocity, are investigated using computer simulations in chapter five of this thesis. The transmission of sound power though a rectangular flexible panel mounted on a baffle is used as an example. The cancellation of volume velocity is shown to give results which compare well with the optimal strategy of sound power minimization [52, 53] although cancellation of volume velocity is potentially far easier to implement practically. Active structural acoustic control is often explained in

terms of a change in the amplitudes of the structural modes in a process which has been termed *modal restructuring.* It is shown that the mechanisms of control can be understood more easily by considering the changes in the amplitudes of the radiation modes. A consequence of controlling the sound power radiation using conventional actuators and sensors is that the vibration levels on the panel and the sound pressure levels near the panel can be greatly increased. A practical method of overcoming this problem, by using a matched distributed sensor/actuator pair, is suggested. It is also shown that a matched sensor/actuator pair will have a minimum phase relationship which suggests the possibility of using feedback efficient controllers for the control of broadband acoustic disturbances [53].

Chapter six of this thesis presents the active control of sound transmission into a cylinder. The investigation has three stages: (i) theoretical investigation, (ii) predicted control using data measured from a real system and (iii) feedforward active control of a real system. This progressive method of investigation is shown to be a very useful approach to the investigation of active structural acoustic control. Although there are potentially large numbers of structural and acoustic modes with natural frequencies in the frequency range of interest, the interaction between these sets of modes can be dominated by only a few or even a single structural mode. A reduction in the amplitudes of these structural modes can therefore achieve significant reductions in the sound transmission into the cylinder. An active control system with only a few actuators can thus produce significant attenuations. It is shown experimentally that by using a single channel feedforward active control system, the sound transmission of single frequency sound into the cylinder can be reduced over a broad range of excitation frequencies [51].

Chapter seven describes the construction and testing of a volume velocity sensor developed using PVDF film. The two-dimensional distributed sensor is tested on a thin aluminium plate with clamped boundary conditions. The sensor output is found to compare favorably with the volume velocity measured using a seven by seven grid of point measurements when the plate is excited using an acoustic source or a structural actuator. With the plate excited using a primary acoustic source, a small piezoelectric ceramic actuator is then used as a secondary source to cancel the output of the volume velocity sensor on the plate at a single frequency. Large attenuations in

the radiated sound power from the plate are then achieved over most of the frequency range of interest. This process is repeated using an inertial actuator as a secondary source, again with good results. The addition of the inertial actuator to the structure alters the structural response on the plate and demonstrates that the sensor is robust to changes in the behaviour of the plate.

Chapter eight describes theoretical and experimental work on the control of sound radiation due to a broadband disturbance on a plate, using a volume velocity sensor in a feedback control system. An internal model control approach to feedback control is used. Significant reductions in the output of the volume velocity sensor are achieved in both computer simulations and in an experiment. The reductions in the output of the volume velocity sensor also produced attenuations in the sound pressure level at a microphone close to the radiating panel.

Finally chapter nine of this thesis presents the conclusions of this thesis and discusses some ideas for future development.

Chapter 2

Acoustic Radiation

2.1 Introduction

Sound radiation from vibrating surfaces is responsible for many of the problems encountered by acoustical engineers. To formulate effective methods of reducing acoustic radiation, using either active or passive methods, it is necessary to gain an appreciation for the mechanisms which cause acoustic radiation. This chapter will outline some of the important techniques for calculating and analysing the acoustic radiation from vibrating surfaces and will introduce the theory of *radiation modes* which is central to the work presented in this thesis.

2.2 Radiation from vibrating surfaces

2.2.1 Radiation from a monopole source

Consider a very small sphere placed in an infinite, homogeneous and isotropic fluid where the radius of the sphere is varying harmonically with time (figure 2.1) [58]. To maintain linearity it is assumed that the change in radius of the sphere is small compared to the average radius of the sphere. The oscillating surface will produce an outgoing harmonic spherical acoustic wave which can be written in complex form as,

$$p(r,t) = \frac{A}{r} e^{j(\omega t - kr)} \tag{2.1}$$

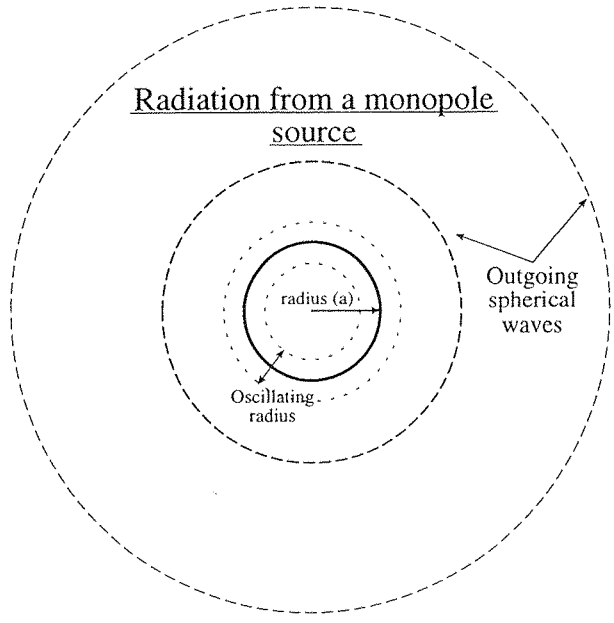

Figure 2.1: A monopole source radiating sound into free space.

where ω is the frequency of oscillation in radians per second, k is the wavenumber which equals ω/c where c is the speed of sound in the fluid and the pressure $p(r,t)$ is a function of time t and radial distance r. The pressure decreases as a function of distance $1/r$ as the wave spreads spherically outwards. The variable A is a function of the complex surface velocity of the sphere v, and is given by [71],

$$A = \frac{j\omega\rho_0 S_s}{4\pi} v \tag{2.2}$$

where S_s is the mean surface area of the sphere, ρ_0 is the mean density of the fluid and it is assumed that the radius of the sphere is much smaller than the acoustic wavelength.

The radiation from a pulsating sphere with uniform radial velocity is totally symmetric and an infinite planar baffle can be placed through the centre of the sphere without affecting the pressure field created. The radiation from a pulsating half sphere, which is baffled, will therefore radiate sound into a hemisphere such that,

$$p(r,t) = \frac{j\omega\rho_0}{2\pi r} e^{j(\omega t - kr)} q \tag{2.3}$$

where q is the source strength which is given by $q = S_h v$ and S_h is the surface of a

hemisphere. If a source is much smaller than an acoustic wavelength then the shape of the source becomes unimportant and it is only necessary to consider the source strength (i.e. rate of change of volume). For example, equation 2.3 can be used to calculate the radiation from a small baffled rectangular element where the source strength is given by $q = S_{rect}v$ where S_{rect} is the surface area of the element and v is the uniform surface velocity [67].

2.2.2 Rayleigh's integral: a far-field approach

The radiation from a planar baffled surface with an arbitrary velocity distribution $v(x, y)$ can be calculated using the Rayleigh integral [8, 38, 86]. This is achieved by considering a vibrating surface to be composed of an infinite number of infinitesimal elemental sources on a rigid baffle (equation 2.3). By integrating over the surface, with the source strength being proportional to the vibration amplitude at each point, the pressure in the far-field can be calculated. Much of the work presented in this thesis concerns the radiation of sound from rectangular panels and in this section a rectangular baffled surface will be used as an example.

For simplicity the time dependence $e^{j\omega t}$ will be suppressed in the following equations. The complex far-field pressure $p(r, \theta, \varphi)$ due to a velocity distribution $v(x, y)$ is given by,

$$p(r, \theta, \varphi) = \frac{j\omega\rho_0}{2\pi r} \int_0^{l_y} \int_0^{l_x} v(x, y) e^{j((\alpha x/l_x)+(\beta y/l_y))} \mathrm{d}x\mathrm{d}y \tag{2.4}$$

where θ and φ are spherical coordinates, l_x is the length of the rectangular vibrating surface and l_y is the width of the rectangular vibrating surface. Figure 2.2 shows the coordinate system used for this calculation. The coefficients α and β are given by,

$$\begin{aligned} \alpha &= kl_x \sin\theta \cos\varphi \\ \beta &= kl_y \sin\theta \sin\varphi \end{aligned} \tag{2.5}$$

To calculate the acoustic power W radiated by the velocity distribution $v(x, y)$ the mean square far-field pressure is integrated over the hemisphere with radius r such that $r \gg \lambda$ where λ is the acoustic wavelength.

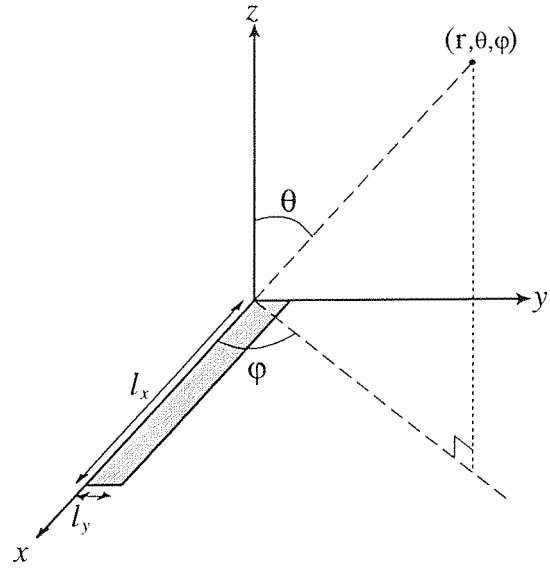

Figure 2.2: Coordinate system used for the calculation of the far-field pressure created by a vibrating rectangular surface.

$$W = \int_0^{2\pi} \int_0^{\frac{\pi}{2}} \frac{|p(r,\theta,\varphi)|^2 r^2 \sin\theta}{2\rho_0 c} \mathrm{d}\theta \mathrm{d}\varphi \tag{2.6}$$

Wallace [86, 87] derived analytical solutions to this equation for some specific cases where the acoustic wavelength is large in comparison to the size of the surface and the velocity distribution $v(x,y)$ is given by the structural mode shapes for a simply supported beam or plate.

2.2.3 Radiation in terms of elemental radiators: a near-field approach

The sound power radiation can also be calculated by considering the vibrating surface to be made up of a *finite* number I of elemental radiators each of which act as monopole sources. If the i^{th} element has a velocity amplitude v_i which is proportional to the true velocity at that point i.e.

$$v_i = v(x_i, y_i) \tag{2.7}$$

where x_i and y_i describe the spatial position of the centre of the i^{th} element, and suf-

ficiently large numbers of equally sized sources are used, then a good approximation to the acoustic radiation can be achieved. The size of the elemental sources must be considerably smaller than both the acoustic and structural wavelengths if spatial aliasing effects are to be avoided. This "finite element approach" allows the calculation of both the near-field and far-field pressures and the power radiated by each of the elemental sources, when operating together, can be calculated and summed to give an estimate of the total radiated power. At a single frequency the acoustic power radiated by the i^{th} element (W_i), will be due to the complex velocity of the i^{th} element (v_i) and the complex pressure (p_i) at the i^{th} element [38],

$$W_i = \frac{S}{2}\mathcal{R}(v_i^* p_i) \tag{2.8}$$

where S is the elemental area, $\mathcal{R}$ denotes the real part of the bracketed quantity and $*$ denotes conjugation. It should be noted that the pressure at the i^{th} element p_i is due to the action of all of the sources present. Since the dimensions of the element are much smaller than an acoustic wavelength, it is assumed that the pressure over the surface of the element remains constant i.e. $p_i = p(x_i, y_i)$. The power radiated by the I elemental sources can be written as the sum of all the components W_i for $i = 1$ to I and can be conveniently written in vector form such that $\boldsymbol{v}$ is an I-length complex vector of elemental velocities and $\boldsymbol{p}$ is an I-length complex vector of pressures at the elemental positions and so,

$$W = \frac{S}{2}\sum_{i=1}^{I}\mathcal{R}(v_i^* p_i) = \frac{S}{2}\mathcal{R}(\boldsymbol{v}^H \boldsymbol{p}) \tag{2.9}$$

where the superscript H denotes a Hermitian transpose (conjugate transpose). If it is assumed that the surface considered encompasses all of the vibrating surfaces present (i.e. this surface could be made up of a number of smaller spatially separated surfaces) the pressure at each of the elementary positions can be expressed as a function of the vibration of all the elemental sources,

$$\boldsymbol{p} = \boldsymbol{Z}\boldsymbol{v} \tag{2.10}$$

where $\boldsymbol{Z}$ is a $I \times I$ matrix of specific acoustic transfer impedances relating the complex

pressure at every element to the complex velocity of every element. Substituting equation 2.10 into equation 2.9 then gives an expression for the total acoustic power radiation purely as a function of the velocity of the elements,

$$W = \frac{S}{2}\mathcal{R}(\boldsymbol{v}^H \boldsymbol{Z}\boldsymbol{v}) = \boldsymbol{v}^H \boldsymbol{R}\boldsymbol{v} \tag{2.11}$$

where $\boldsymbol{R} = \frac{S}{2}\mathcal{R}(\boldsymbol{Z})$ and therefore the matrix $\boldsymbol{R}$ is purely real. $\boldsymbol{R}$ is also symmetric due to reciprocity and must be positive definite on physical grounds since the power output must be greater than zero unless the velocity is zero ($W > 0 \ \forall \ \boldsymbol{v} \neq 0$). The diagonal coefficients of the matrix $\boldsymbol{R}_{ii}$ describes the self-radiation resistances for each element and the non-diagonal terms $\boldsymbol{R}_{ij}$ describe the mutual-radiation resistance terms due to the interaction of two elements. The radiation of sound power from different structures placed in different environments can be expressed by equation 2.11 with different forms of the matrix $\boldsymbol{R}$.

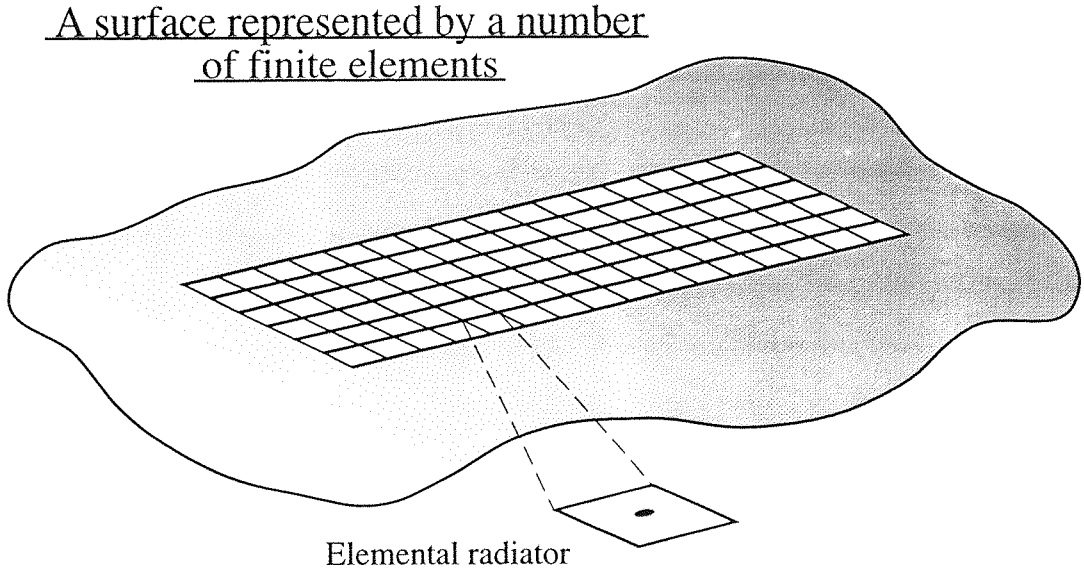

Figure 2.3: A baffled surface represented by a number of elements.

For the case of the acoustic radiation by a vibrating planar surface placed on an infinite baffle (figure 2.3) the coefficients of the matrix $\boldsymbol{Z}$ can be calculated analytically. If the vibration of the surface is approximated by a number of elemental sources, the specific acoustic transfer impedance between the i^{th} and j^{th} elements is given by (from equation 2.3),

$$Z_{ij} = \frac{j\omega\rho_0 S}{2\pi r_{ij}} e^{-jkr_{ij}} \tag{2.12}$$

where r_{ij} is the distance between the i^{th} and j^{th} elements. The ij^{th} element of the matrix $\boldsymbol{R}$ (equation 2.11) can now be calculated as [85],

$$R_{ij} = \frac{\omega^2\rho_0 S^2}{4\pi c}\left[\frac{\sin(kr_{ij})}{kr_{ij}}\right] \tag{2.13}$$

The coefficients in the matrix $\boldsymbol{R}$ are therefore proportional to a *sinc* function of the distance between elements and the wavenumber (kr_{ij}).

2.2.4 Radiation from structural modes

It is often convenient to describe the vibration of a structure in terms of a set of structural modes each with a resonant frequency and a specified mode shape. Any structural mode which has an out-of-plane vibration component will radiate sound. However, in low viscosity fluids modes which describe the in-plane vibration of the structure will not radiate a significant amount of sound power [38].

To completely describe the vibrational behaviour of the structure, an infinite number of structural modes would be required. However, good approximations to the structure's behaviour, over a limited frequency range, can be obtained using only a finite number N of structural modes. The amplitude of the n^{th} structural mode at a given frequency can be represented by a complex variable a_n. The velocity of the surface can therefore be approximated as,

$$v(x,y) \approx \sum_{n=1}^{N} a_n \phi_n(x,y) \tag{2.14}$$

where the velocity in the radial direction $v(x,y)$ is dependent on its spatial coordinates (x,y) and is approximated by a summation of structural mode shapes (or eigenfunctions) $\phi_n(x,y)$. An $N-$length complex vector $\boldsymbol{a}$ can be used to represent a finite set of complex mode amplitudes. The sound power W radiated by the structure can then be calculated by multiplying the vector of mode amplitudes ($\boldsymbol{a}$) by a finite $N \times N$ matrix $\boldsymbol{M}$ of *self-* and *mutual*-radiation resistances [7, 23].

$$W = \boldsymbol{a}^H \boldsymbol{M} \boldsymbol{a} \tag{2.15}$$

The diagonal coefficients of $\boldsymbol{M}$ represent the self-radiation resistances of the structural modes and the radiation from a single mode is equal to the modulus of its amplitude squared times its self-radiation resistance. The off-diagonal terms in $\boldsymbol{M}$ represent the mutual-radiation resistances which determine the sound power radiation due to the cross coupling of two modes. This component of the radiated power will be equal to the conjugate product of the two mode amplitudes times the corresponding mutual-radiation resistance term. If reciprocity is assumed then the matrix $\boldsymbol{M}$ must be symmetric. It is also positive definite on physical grounds since the power radiated must be greater than zero unless all of the mode amplitudes are zero ($W > 0 \ \forall \ \boldsymbol{a} \neq 0$). The radiation of sound power from different structures placed in different environments can be expressed by equation 2.15 with different forms of the matrix $\boldsymbol{M}$.

The values of the matrix coefficients M_{nm} can be calculated using either the far-field or near-field approaches described in the two preceding sections. The diagonal terms in the matrix $\boldsymbol{M}$ describe the power radiation due to a single mode and can be calculated from the far-field method (equation 2.6) as [7, 86, 87, 88],

$$M_{nn} = \int_0^{2\pi} \int_0^{\frac{\pi}{2}} \frac{|p_n|^2 r^2 \sin\theta}{2\rho_0 c} \mathrm{d}\theta \mathrm{d}\varphi \tag{2.16}$$

where p_n is the far-field pressure due to the n^{th} structural mode (excited with unit amplitude) and can be calculated by setting $v(x,y) = \phi_n(x,y)$ in equation 2.4. The diagonal terms can also be calculated using the near-field method by calculating the velocity at every elemental position due to the n^{th} structural mode to create a vector of velocities $\boldsymbol{v}_n$. The velocity of the i^{th} element due to the n^{th} mode is given as,

$$(v_n)_i = \phi_n(x_i, y_i) \tag{2.17}$$

where x_i and y_i are the spatial coordinates of the i^{th} element. The diagonal matrix coefficients M_{nn} can then be calculated as,

$$M_{nn} = \boldsymbol{v}_n^H \boldsymbol{R} \boldsymbol{v}_n \tag{2.18}$$

where $\boldsymbol{v}_n$ is a I-length vector of elemental velocities which approximate the continuous velocity distribution due to the n^{th} structural mode $\phi_n(x, y)$ and where $\boldsymbol{R}$ can, for the infinite baffle case, be calculated analytically from equation 2.13. The off-diagonal terms in M describe the radiation due to the interaction of two structural modes and can be calculated using the far-field approach as,

$$M_{nm} = \int_0^{2\pi} \int_0^{\frac{\pi}{2}} \frac{p_n^* p_m r^2 \sin\theta}{2\rho_0 c} \mathrm{d}\theta \mathrm{d}\varphi \tag{2.19}$$

where p_n and p_m are the far-field pressures due to the n^{th} and m^{th} modes respectively (equation 2.4). Using the near-field approach M_{nm} can be calculated as,

$$M_{nm} = \boldsymbol{v}_n^H \boldsymbol{R} \boldsymbol{v}_m \tag{2.20}$$

If all of the elements of the matrix $\boldsymbol{M}$ are known then the sound power radiation from any general combination of mode amplitudes $\boldsymbol{a}$ can be calculated (equation 2.15).

All the elements in the matrix $\boldsymbol{M}$ can be calculated in one step by defining a matrix whose rows are equal to the elemental velocities due to each structural mode i.e. $\boldsymbol{\Phi}^T = [\boldsymbol{v}_1^T \boldsymbol{v}_2^T \ldots \boldsymbol{v}_n^T]$. The vector of elemental velocities for any arbitrary set of mode amplitudes can then be calculated as,

$$\boldsymbol{v} = \boldsymbol{\Phi} \boldsymbol{a} \tag{2.21}$$

Using equation 2.11 the total power output can be written as,

$$W = \boldsymbol{v}^H \boldsymbol{R} \boldsymbol{v} = \boldsymbol{a}^H \boldsymbol{\Phi}^H \boldsymbol{R} \boldsymbol{\Phi} \boldsymbol{a} \tag{2.22}$$

The matrix of self and mutual radiation resistances for the structural modes $\boldsymbol{M}$, given in equation 2.15 must therefore be equal to $\boldsymbol{\Phi}^H \boldsymbol{R} \boldsymbol{\Phi}$ (equation 2.22).

$$\boldsymbol{M} = \boldsymbol{\Phi}^H \boldsymbol{R} \boldsymbol{\Phi} \tag{2.23}$$

2.3 Radiation mode theory

2.3.1 Formulation in terms of structural modes

Because the matrix $\boldsymbol{M}$ is normal (i.e. it is real, symmetric and positive definite) it has an eigenvector/eigenvalue decomposition which can be written as [7, 23],

$$\boldsymbol{M} = \boldsymbol{P}^T \boldsymbol{\Omega} \boldsymbol{P} \tag{2.24}$$

$\boldsymbol{P}$ is an $N \times N$ unitary matrix of orthogonal real eigenvectors and $\boldsymbol{\Omega}$ is an $N \times N$ diagonal matrix of positive real eigenvalues. Equation 2.24 can be substituted into equation 2.15 to produce an alternative expression for the sound power radiation,

$$W = \boldsymbol{a}^H \boldsymbol{M} \boldsymbol{a} = \boldsymbol{a}^H \boldsymbol{P}^T \boldsymbol{\Omega} \boldsymbol{P} \boldsymbol{a} \tag{2.25}$$

By defining a set of transformed modes such that the mode amplitudes $\boldsymbol{b} = \boldsymbol{P}\boldsymbol{a}$, the expression for the radiated power can be rewritten as,

$$W = \boldsymbol{b}^H \boldsymbol{\Omega} \boldsymbol{b} = \sum_{n=1}^{N} \Omega_n |b_n|^2 \tag{2.26}$$

Because the matrix $\boldsymbol{\Omega}$ is diagonal the radiation can be expressed as a sum of the modulus squared amplitudes of the elements of the vector $\boldsymbol{b}$ times their corresponding eigenvalues. By combining a set of structural modes, whose amplitudes are defined by the rows in the matrix $\boldsymbol{P}$, velocity distributions are thus created that radiate sound *independently.* These independently radiating velocity distributions are termed *radiation modes* and their mode amplitudes are given by the coefficients in the vector $\boldsymbol{b}$. The mutual-radiation resistance terms, unlike those in matrix $\boldsymbol{M}$, are all zero. Each radiation mode corresponds to a velocity distribution over the surface which is orthogonal to all of the other radiation modes and whose radiation is unaffected by the amplitudes of other radiation modes.

This formulation for sound radiation was used by Baumann *et al.* [7] who were concerned with the use of structural actuators to actively control the acoustic radiation from impulsively excited structures using a feedback control strategy. The nature of

the disturbance prohibited the use of far-field microphones as sensors since the pressure signal would arrive at the feedback controller, and therefore the actuators, *after* the disturbance had passed. Unless the disturbance is periodic, then time delays in a feedback control system cause large reductions in performance [36]. Cunefare [23] also calculated the radiation modes using an eigenvector/eigenvalue decomposition of a finite matrix of self and mutual radiation efficiencies for the structural modes.

The shapes of the first four radiation modes for a simply supported beam of vanishingly small width are shown in figure 2.4 and were calculated using the first ten structural modes [33, 80]. These mode shapes were calculated for an excitation frequency which corresponds to a non-dimensional frequency kl of 0.1, where l is the length of the beam and k is the wavenumber.

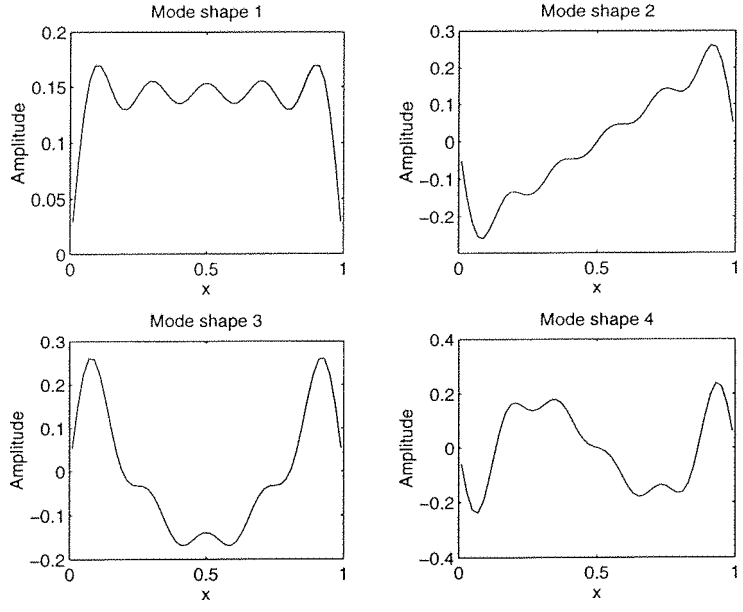

Figure 2.4: The first four radiation mode shapes calculated from the first ten structural modes of a simply supported beam ($kl = 0.1$).

2.3.2 Formulation in terms of elemental radiators

A very similar line of reasoning can be followed to derive the radiation modes from a set of elemental radiators. Since the matrix $\boldsymbol{R}$ is also real, symmetric and positive definite it also has an eigenvector/eigenvalue decomposition which produces orthogonal real eigenvectors with positive real eigenvalues. Therefore $\boldsymbol{R} = \boldsymbol{Q}^T \boldsymbol{\Lambda} \boldsymbol{Q}$ where $\boldsymbol{Q}$

is a real and unitary matrix of orthonormal eigenvectors and $\boldsymbol{\Lambda}$ is a diagonal matrix of eigenvalues λ_i which are all positive real numbers. Equation 2.11, which describes the radiated power in terms of I elemental velocities, can now be written as,

$$W = \boldsymbol{v}^H \boldsymbol{Q}^T \boldsymbol{\Lambda} \boldsymbol{Q} \boldsymbol{v} \tag{2.27}$$

By defining the amplitudes of a set of velocity distributions as $\boldsymbol{y} = \boldsymbol{Q}\boldsymbol{v}$, where $\boldsymbol{y}$ is an I-length vector, equation 2.27 can be rewritten as [33],

$$W = \boldsymbol{y}^H \boldsymbol{\Lambda} \boldsymbol{y} = \sum_{i=1}^{I} \lambda_i |y_i|^2 \tag{2.28}$$

The velocity distributions defined by the eigenvectors in the columns of the $\boldsymbol{Q}$ matrix radiate sound independently and are the same *radiation modes* as defined in the previous section (equation 2.24). It is again possible to calculate the total radiated power as a sum of individual mode amplitudes squared times a corresponding eigenvalue.

The shapes of the first four radiation modes for a baffled beam, which is of vanishingly small width, have been calculated using the elemental radiator approach and are shown in figure 2.5 [33]. For this example fifty elements were used to model the behaviour of the beam. The non-dimensional frequency kl again equals 0.1 for comparison with the radiation modes calculated using the structural mode approach. The shape of the first radiation mode at low frequencies is almost uniform across the radiator and hence the amplitude of the first radiation mode is very nearly proportional to the net volume velocity of the beam. The second mode is a rocking mode (dipole type) followed by higher order modes.

The shapes of the radiation modes calculated using the elemental radiator approach (figure 2.5) differ slightly from those calculated using the structural mode approach (figure 2.4). The shapes of the radiation modes calculated using structural modes are biased because in the example chosen all of the structural modes have zero displacement at the ends of the beam (simply supported). To construct the first radiation mode shape a number of sine waves (structural modes) are added together in an attempt to produce a uniform displacement across the beam. This is impossible using a finite number of sine waves and produces an effect due to the Gibbs phenomena at the ends.

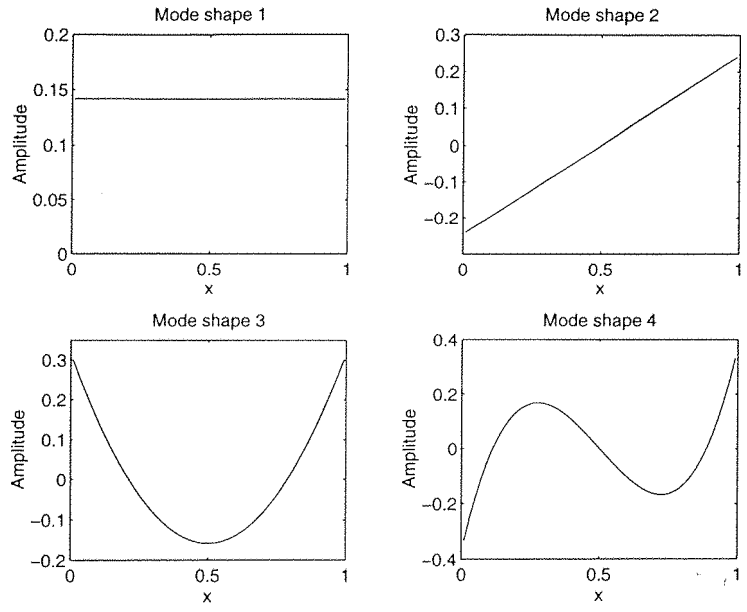

Figure 2.5: The first four radiation mode shapes calculated from the elemental radiator approach ($kl = 0.1$).

The shapes of the radiation modes calculated using the elemental radiator approach are determined by the eigenvectors of $\boldsymbol{R}$ and although this is a function of the geometry of the surface, it is independent of the dynamic properties of the surface. Therefore, the structural mode content of a vibrating structure will affect the amplitudes of the radiation modes but will not affect their shapes or radiation efficiencies. The radiation mode shapes derived using the elemental radiation approach are unbiased and independent of any structural dynamics.

A similar formulation to the one carried out above was presented by Photiadis [74] and Borgiotti [9, 10] who described a region S in an acoustic field where the acoustic pressure could be completely described by the velocity of a surface D which contained all of the acoustic sources. They were concerned with the radiation into some specific far-field region whereas the above formulation is concerned with global radiation. The behaviour of the source D and the region S were approximated by a discrete number of points and a matrix $\boldsymbol{G}$ was derived which described the pressures at m discrete points in the region S due to the n discrete surface velocities on the radiating surface D (figure 2.6). A singular value decomposition (instead of an eigenvector decomposition) was performed on the matrix $\boldsymbol{G}$ to produce a set of orthogonal velocity distributions on D that would radiate sound *independently* into the region S. Borgiotti [9] also

noted that these radiation modes and their radiation efficiencies were only dependent on the geometry of the source and the region S and were independent of the structural characteristics of the radiating surface.

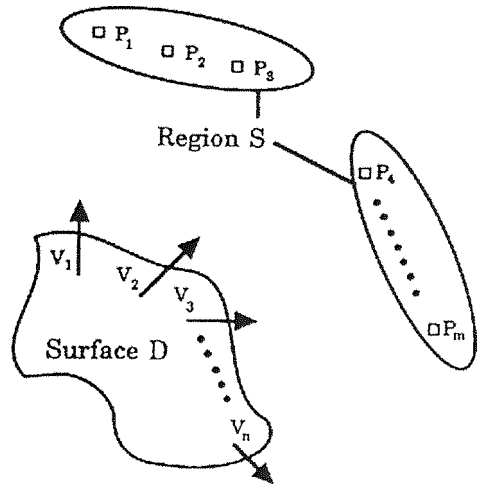

Figure 2.6: Diagram from paper by Photiadis showing the radiation from a surface D into a region S.

Snyder and Tanaka [80] also showed that the power radiated by a surface could be described by the velocity of the surface and the acoustic pressure at the surface (i.e. near-field parameters only). They presented the radiation mode shapes for a baffled beam which were calculated using the summation of rather a small number of structural modes and compared closely to those presented in figure 2.4.

2.3.3 Independence of radiation modes

The sound power radiation from a vibrating surface is a summation of the real part of the conjugate product of the velocity and the pressure at every point on the surface (equation 2.9). To investigate the interaction of the sound radiated from structural modes, the pressure and velocity distributions for three structural modes have been investigated. Only the pressure which is in-phase with the velocity will produce any power output and therefore the amplitude of the velocity and the in-phase part of the pressure are plotted for comparison in figure 2.7 for an excitation frequency corresponding to $kl = 1$. The first, third and fifth structural modes for a simply supported

baffled beam all produce pressure distributions whose real parts are nearly constant along the length of the beam since the source is small compared to a wavelength at this excitation frequency. The vibration of any odd structural mode will therefore interact with the pressure distributions created by any other odd structural modes so that

$$\int_0^{l_x} v^*_{odd}(x) p_{odd}(x) \mathrm{d}x \neq 0 \tag{2.29}$$

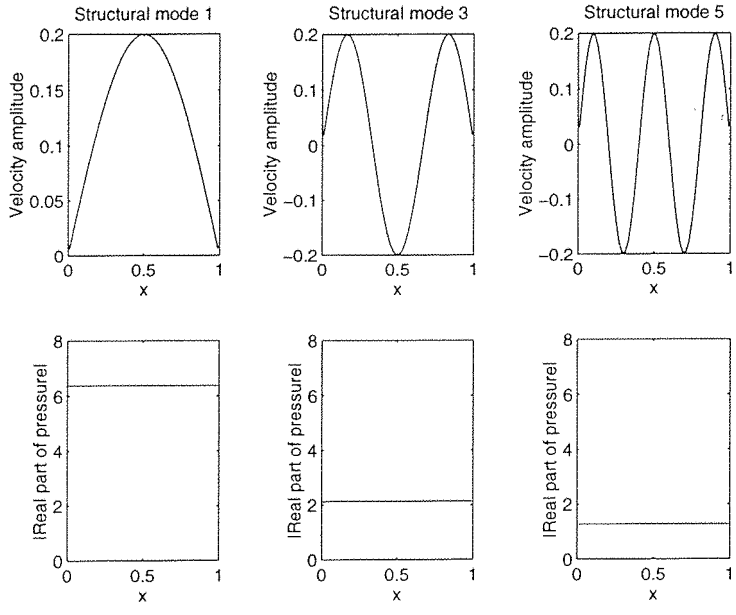

Figure 2.7: Velocity distributions and in-phase pressure distributions (real part) due to the first, third and fifth structural modes of a simply supported beam.

where $p_{odd}(x)$ is the in-phase pressure distribution due to any odd structural mode and $v_{odd}(x)$ is the velocity distribution of any odd structural mode. There is also similar interaction between all of the even structural modes. It is this interaction that causes many of the off-diagonal terms in $\boldsymbol{M}$ to be non-zero. Although the velocity distributions of the structural modes in this case are orthogonal to one another their in-phase pressure distributions are not.

Figure 2.8 plots the velocity and the in-phase pressure distributions for the first three radiation modes. In this case the in-phase part of the pressure distribution is spatially similar to the velocity distribution. The velocity distributions are orthogonal to all of the other vibration *and* pressure distributions. There is therefore no inter-

action between the velocity distribution due to one radiation mode and the pressure distribution due to another radiation mode and therefore,

$$\int_0^{l_x} (v_i^{rad}(x))^* p_j^{rad}(x) \mathrm{d}x = 0 \quad \text{if } i \neq j \tag{2.30}$$

where $p_i^{rad}(x)$ is the in-phase pressure distribution due to the i^{th} radiation mode and $v_j^{rad}(x)$ is the velocity distribution of the j^{th} radiation mode.

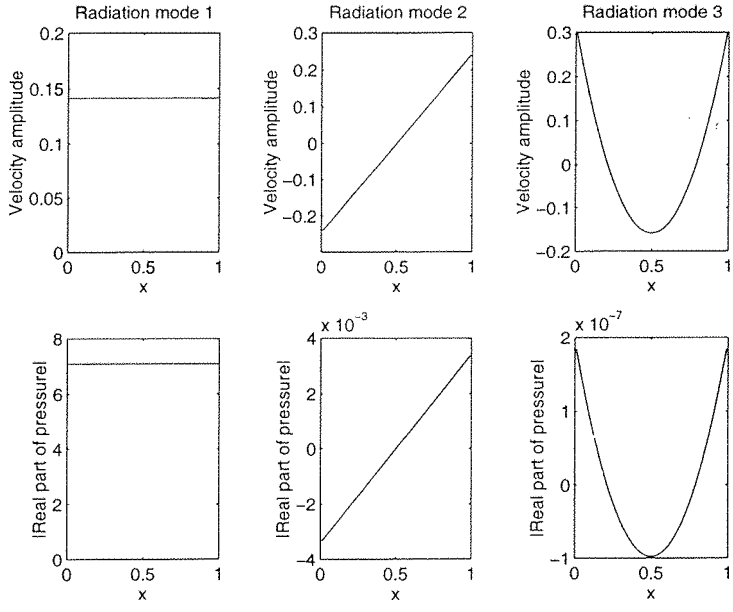

Figure 2.8: Velocity distributions and in-phase pressure distributions (real part) due to the first, second and third radiation modes of a beam.

The inter-dependence of the radiation from structural modes implies that a reduction in amplitude of one structural mode could cause an *increase* in the total sound power radiation [43]. The reduction of individual structural mode amplitudes as a strategy for controlling the total radiated sound power may therefore be unsuccessful. A reduction in the amplitude of a radiation mode, however, *guarantees* a reduction in the total sound power output. A more detailed comparison of active control strategies will be presented in chapter 5.

2.3.4 Radiation efficiencies as a function of frequency

In section 2.2.4 it was demonstrated that the self- and mutual-radiation resistances (the matrix $\boldsymbol{M}$) of the structural modes could be calculated from the matrix $\boldsymbol{R}$ of specific acoustic transfer impedances and the matrix of structural mode shapes $\boldsymbol{\Phi}$. The coefficients in the matrix $\boldsymbol{R}$ (and hence those in the matrix $\boldsymbol{M}$) are a function of frequency and therefore the efficiencies with which structural modes and radiation modes radiate sound can be plotted as a function of non-dimensional frequency. The efficiency is defined to be the ratio of the acoustic power output to the mean squared surface velocity. For a velocity distribution $v(x,y)$ the radiation efficiency σ will therefore be given by,

$$\sigma = \frac{W_v}{\int\int v^2(x,y)\mathrm{d}x\mathrm{d}y} \tag{2.31}$$

where W_v is the sound power due to the velocity $v(x,y)$. If the radiator is approximated using a number of finite elements the radiation efficiency can be conveniently calculated from the vectors $\boldsymbol{v}$ and $\boldsymbol{R}$ by,

$$\sigma = \frac{\boldsymbol{v}^H \boldsymbol{R} \boldsymbol{v}}{S_e \boldsymbol{v}^H \boldsymbol{v}} \tag{2.32}$$

where S_e is the surface area of an element. Some of the examples used in this chapter and chapter 3 describe the radiation of sound from one-dimensional structures. For such cases it is not possible to calculate an absolute value of efficiency without assuming a finite source width (i.e. S_e is difficult to define). In these cases the efficiency plots will be in arbitrary units.

The self- and mutual-radiation resistances M_{11}, M_{22}, M_{33}, M_{13}, M_{15} and M_{24} for a simply supported baffled beam are plotted in figure 2.9. The radiation resistances are proportional to the efficiencies with which the structural modes radiate sound although the mutual radiation resistance terms relate the efficiency with which *two* structural modes radiate or absorb sound power when operating together. The odd-odd coefficients are the most efficient radiators of sound at low frequencies and have a $6dB$ per octave rise in efficiency with frequency which is similar to the efficiency of a monopole source. The even-even coefficients have a $12dB$ per octave rise in

efficiency with frequency at low frequencies which is the same as a dipole source [67]. To estimate the sound power radiated from a baffled beam at low frequencies the amplitudes of all of the significantly excited odd structural modes would have to be known. At higher frequencies it is only the self-radiation resistances that are important since in this frequency range the structural modes begin to radiate sound independently.

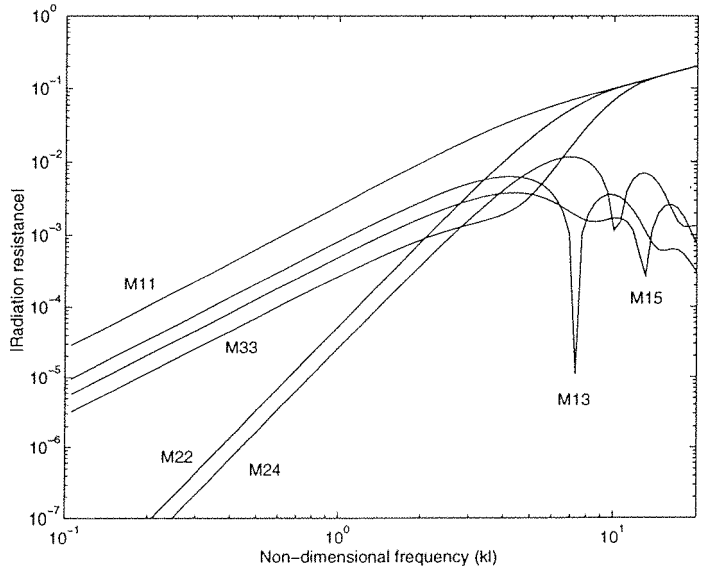

Figure 2.9: Radiation resistances of the structural modes of a baffled beam as a function of frequency.

The radiation efficiencies of the radiation modes as a function of frequency are plotted in figure 2.10 and show that only the first radiation mode is dominant in the radiation of sound at low frequencies. Higher order radiation modes become progressively poorer at radiating sound at lower frequencies. This implies that at low frequencies the amplitude of the first radiation mode will act as a good estimate of the total radiated sound power in most cases. The amplitude of the first radiation mode (figure 2.8) is almost proportional to the volume velocity of the beam. Therefore at low frequencies a reduction in the volume velocity of a structure, which may be achieved using an active control system, will in most cases lead to a reduction in sound power radiation [52, 53, 54]. Cunefare [24] and Burdisso and Fuller [11] have suggested using an active control system to drive the vibration of a structure such that it matches the shape of a higher order (poorly efficient) radiation mode. This

would have a similar effect to using an active control system to cancel the amplitude of the lower order (efficiently radiating) radiation modes.

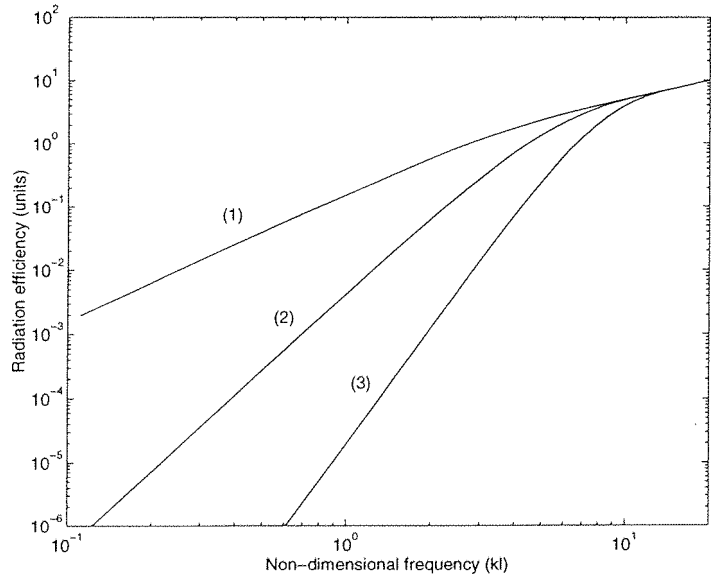

Figure 2.10: Radiation efficiencies of the first three radiation modes as a function of frequency.

2.3.5 Radiation mode shapes as a function of frequency

Unlike structural modes the shapes of the radiation modes are a function of frequency. Figure 2.11 shows the shapes of the first three radiation modes for a baffled beam where the non-dimensional frequency (kl) is varied from 1 to 10.

The shapes of the lower order radiation modes are the first to alter as the frequency is increased. However, in the low frequency region where the radiation from the first radiation mode is dominant (i.e. $15dB$ greater than the radiation efficiency of the second radiation mode for $kl \leq 1$), the lower order radiation mode shapes remain reasonably constant. The shape of the first radiation mode at $kl = 1$ varies by 0.015% from the shape of the first radiation mode as $kl \Rightarrow 0$.

The shapes and efficiencies of the radiation modes of a finite beam as a function of frequency have also been presented by Naghshineh and Koopman [70].

The shapes of the radiation modes are a function of frequency and therefore any active control system which cancels the volume velocity of a panel, for example, will

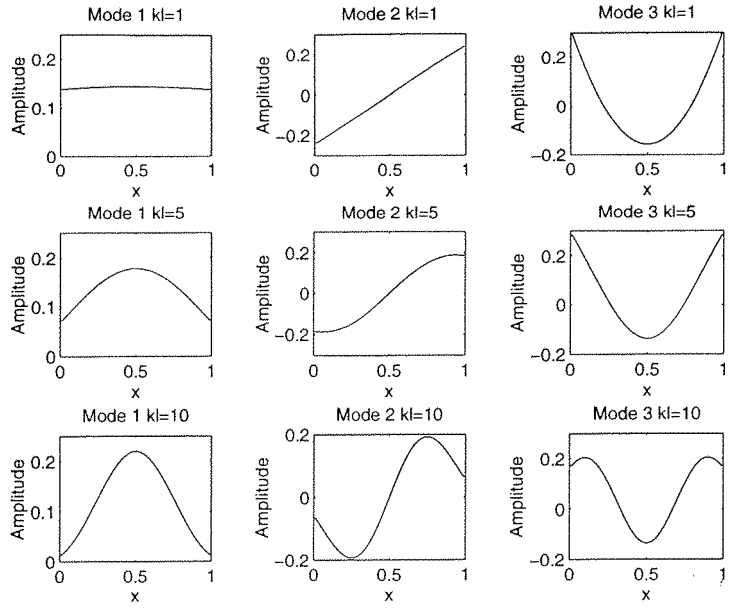

Figure 2.11: The first three radiation mode shapes for a baffled beam calculated from the elemental radiator approach ($kl = 1, 5, 10$).

be cancelling an *approximation* to the first radiation mode. Figure 2.12 shows the radiation efficiencies of three fixed velocity distributions which are equal to the first three radiation mode shapes at very low frequency ($kl \Rightarrow 0$). The interaction between the first and third modes, resulting in the term M_{13}, produces a radiation efficiency comparable with the efficiency of the second mode. It would, in principle, be possible to create an active control system which cancelled the outputs of a number of sensors which measured the true amplitudes of a number of radiation modes. The spatial sensitivity of these sensors would then have to be a function of frequency.

Using fixed shaped sensors the outputs would only be exactly equal to the radiation mode amplitudes at a single frequency. After cancelling the volume velocity, for example (the approximation to the first radiation mode), there would remain a residual first radiation mode component which would radiate a similar amount of sound power to that from the higher order radiation modes. This implies that cancelling the output of many fixed shaped sensors may not achieve significant increases in attenuation over cancelling a single sensor output for frequencies where kl is close to unity. For frequencies where kl is much smaller than unity it is only necessary to cancel the amplitude of the first radiation mode to achieve large reductions in the sound power radiation and hence higher order radiation mode sensors are not required.

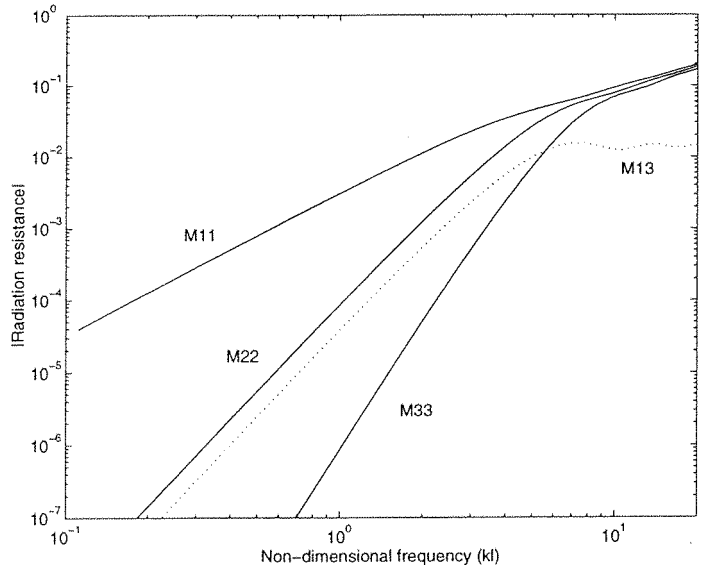

Figure 2.12: Radiation efficiencies of three modes whose shapes correspond to the first three radiation modes at very low frequency. The dotted line represents the efficiency due to the interaction of the first and third modes.

2.3.6 Multipoles

The radiation of sound from a number of spatially separated sources or by a vibrating surface can be represented by an equivalent set of multipoles (monopoles, dipoles, quadrupoles etc.) acting at a single point [57, 71]. This technique should not be confused with the decomposition of the vibration of a surface into radiation modes. Multipoles do *not* radiate sound power independently. For example, the radiation of sound power from a monopole and a quadrupole is coupled which can be very easily demonstrated by considering at the real part of the pressure field created by a quadrupole source which is placed close to a monopole source (figure 2.13). If the real part of the pressure created by the quadrupole source is non-zero at the position of the monopole then the radiation of sound power from the monopole must be due in part to the amplitude of the quadrupole source. If the quadrupole and monopole sources are placed coincidentally (on top of one another) then the real part of the pressure at the position of the monopole due to the quadrupole is given in the free field by,

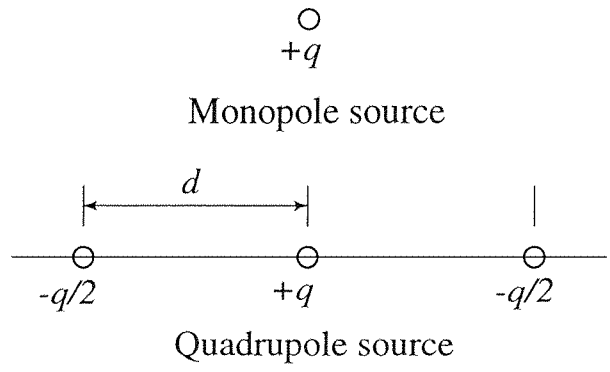

Figure 2.13: A monopole and a longitudinal quadrupole source.

$$\mathcal{R}\{p\} = \left(1 - \frac{\sin(kd)}{kd}\right) Z_0 q \tag{2.33}$$

where d is distance between the sources of the quadrupole and $Z_0 = \omega^2 \rho S^2 / 2\pi c$. Unless $kd = n\pi$, where n is an integer, then the real part of the pressure is non zero and the radiation is coupled.

The equivalent multipole strengths which represent the radiation from a vanishingly thin beam can be calculated using the equation [57, 71],

$$Q_n = \frac{l_y}{n!} \int_{-\frac{l_x}{2}}^{\frac{l_x}{2}} v(x)(x - x_0)^{n-1} \mathrm{d}x \tag{2.34}$$

where Q_n is the n^{th} multipole's source strength, x_0 is the position of the multipole, l_x is the length of the beam which is positioned between $l_x/2$ and $-l_x/2$, l_y is the width of the beam and $v(x)$ describes the velocity along the length of the beam. It should be noted that there is only a single n^{th} order multipole for this one dimensional source distribution. To calculate the multipole strengths the velocity distribution $v(x)$ multiplied by the relevant term $(x - x_0)^{n-1}$ is integrated over the length of the beam. If for instance $x_0 = 0$ then these terms form a set of functions $(1, x, x^2, x^3, ...)$.

The equivalent multipole expansions which represents the radiation from the radiation mode shapes of a baffled vanishingly thin beam, where the multipole expansion is taken at the centre of the beam, are shown in figure 2.14. The multipole source which is equivalent to the first radiation mode (volumetric mode) has even-pole strengths (i.e. monopole, quadrupole etc.) which are constant with frequency but decreasing

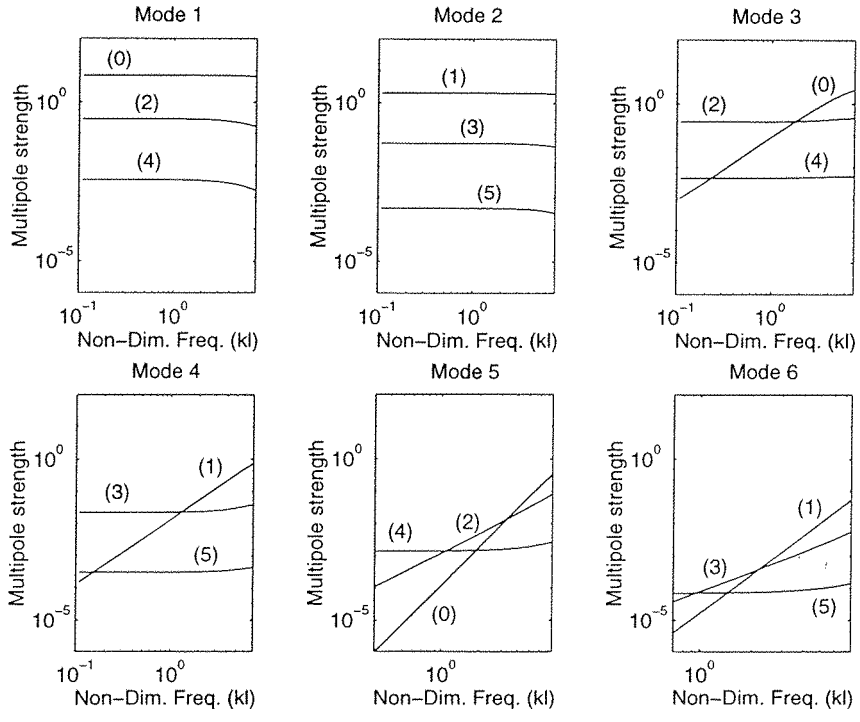

Figure 2.14: The first six equivalent multipole source strengths which represent the radiation from the first six radiation modes for a vanishingly thin beam.

with multipole order. Similarly the second radiation mode will have equivalent odd-pole source strengths which are constant with frequency but decreasing with multipole order. The equivalent multipole to the third radiation mode has a monopole strength which increases with frequency and the amplitude of the other even-poles remain relatively constant. Higher order radiation modes, for example the fifth radiation mode, have equivalent lower order multipole source strengths that roll off at different rates with the lowest order multipole source strength rolling off at the fastest rate.

The first radiation mode contributes to all of the even multipole source strengths but is the only significant contributor to the monopole source strength at low frequencies. The second radiation mode will contribute significantly to all of the odd multipole strengths but is the only significant contributor to the dipole source strength at low frequencies. To accurately calculate the source strengths of the first n multipoles at low frequencies it would thus only be necessary to consider the first n radiation modes.

Nelson *et al.* calculated the minimum power output for a single monopole source radi-

ating into free space which was actively controlled by a number of secondary sources [72]. One of the examples taken was a configuration very similar to a longitudinal quadrupole source, where the source in the centre acted as a primary source and the two outer sources acted as secondary sources. The minimum power output of this configuration, W_{min}, was found to be substantially less than the power output of a longitudinal quadrupole source, W_{quad}. At low frequencies the ratio of minimum power output of the array to the power radiated by the monopole source alone, W_{mono}, was calculated as $W_{min}/W_{mono} = (kd)^4/45$. The ratio of the power radiated by the quadrupole source to the power radiated by the monopole source however was calculated as $W_{quad}/W_{mono} = (kd)^4/20$ where d is defined in figure 2.13 and it is assumed that d is very small compared to a wavelength.

The radiation mode shapes and efficiencies for this three-source configuration can be calculated by performing an eigenvector/eigenvalue decomposition on the three by three matrix of transfer impedances $\boldsymbol{R}$, which is calculated using equation 2.13. The amplitudes of the radiation modes and the sound power radiation from each mode can then be calculated for a given source strength distribution. There are only three radiation modes and if the amplitudes of these modes are denoted y_1, y_2 and y_3 then the total radiated power can be written as (equation 2.28),

$$W = \lambda_1 |y|_1^2 + \lambda_2 |y|_2^2 + \lambda_3 |y|_3^2 \tag{2.35}$$

where λ_1, λ_2 and λ_3 are the radiation efficiencies of the radiation modes, which are plotted in figure 2.15 as a function of kd. At low values of kd the radiation efficiencies vary as $(kd)^{2n}$ where n is the mode order. From figure 2.15 it is observed that at low frequencies the radiation efficiency of the third radiation mode is related to the radiation efficiency of the first radiation mode by the expression,

$$\lambda_3 = \frac{2}{405}(kd)^4 \lambda_1 \tag{2.36}$$

From the shapes of the radiation modes it is possible to calculate the contribution of a given source strength distribution to the three radiation mode components. If the source in the centre has a source strength denoted q_p and the two outer sources have identical source strengths given by $q_{s1} = q_{s2} = q_s$ then it is found that the amplitude

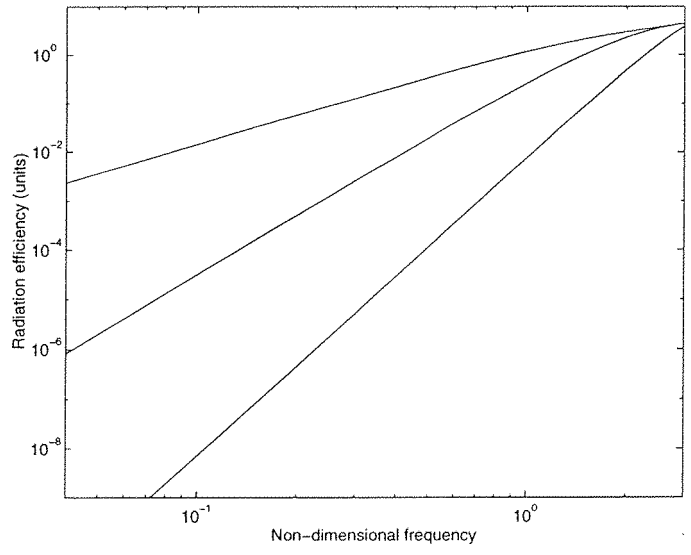

Figure 2.15: Radiation efficiencies of the three radiation modes of a three source configuration as a function of non-dimensional frequency.

of the first radiation mode can be approximated, for small values of kd, by,

$$y_1 = \frac{q_p}{\sqrt{3}}\left[1 + \frac{(kd)^2}{9}\ldots\right] + \frac{2q_s}{\sqrt{3}}\left[1 - \frac{(kd)^2}{18}\ldots\right] \tag{2.37}$$

For a source strength distribution which corresponds to a monopole source, i.e. $q_s = 0$, the power radiated is dominated by the first radiation mode component. At low values of kd the amplitude of the first radiation mode component can be approximated by $y_{1_{mono}} = \frac{q_p}{\sqrt{3}}$ since higher order terms in kd can be ignored (equation 2.37). From equation 2.35 the power output can then be calculated as $W_{mono} = \frac{\lambda_1 |q_p|^2}{3}$.

For a source strength distribution which corresponds to a quadrupole source, i.e. $q_s = -q_p/2$, the second radiation mode component has an amplitude of zero since the source distribution is symmetric. The amplitude of the third radiation mode component is a constant for low values of kd and is given by $y_3 = \sqrt{\frac{3}{2}}q_p$. Using equation 2.37 the amplitude of the first radiation mode component for the quadrupole source can be calculated as $y_1 = \frac{(kd)^2}{\sqrt{108}}q_p$. The power output of the quadrupole source can therefore be written in terms of the power radiated by its first radiation mode component (W_1) plus the power radiated by its third radiation mode component (W_3) and these are given by,

$$W_1 = \lambda_1 y_1^2 = \frac{(kd)^4}{108}\lambda_1 |q_p|^2 = \frac{(kd)^4}{36} W_{mono} \tag{2.38}$$

and using equation 2.36,

$$W_3 = \lambda_3 y_3^2 = \frac{(kd)^4}{135}\lambda_1 |q_p|^2 = \frac{(kd)^4}{45} W_{mono} \tag{2.39}$$

such that,

$$W_{quad} = W_1 + W_3 = \frac{(kd)^4}{20} W_{mono} \tag{2.40}$$

It should be noted that the numbers quoted in the equations above are all limiting values for $kd \Rightarrow 0$.

In the limit of $kd \Rightarrow 0$ the power radiated by the third radiation mode component of the quadrupole source (equation 2.39) is the same as the power radiated by the source distribution for which the power output is minimized. The fact that $W_{min} = W_3$ implies that the action of the secondary sources is to cancel the amplitude of the first radiation mode component. Nelson *et al.* calculated the optimal secondary source strengths q_{so} which minimize the sound power output due to the primary source strength q_p in the limit of $kd \Rightarrow 0$, as,

$$q_{so} = -q_p \left[\frac{1}{2} + \frac{(kd)^2}{12} \cdots \right] \tag{2.41}$$

By setting q_s equal to q_{so} and substituting into equation 2.37 it can be shown that the amplitude of the first radiation mode is zero to order $(kd)^2$ and therefore it is only the third radiation mode component that radiates sound for this source distribution as $kd \Rightarrow 0$. In the limit of $kd \Rightarrow 0$ the distribution of source strengths which minimizes the total radiated sound power is thus equivalent to the third radiation mode for this source configuration.

2.3.7 Wavenumber expansions

The radiation of sound from a vibrating surface into an adjacent fluid can also be considered in terms of wave propagation. A structural wave travelling along the

surface of the structure will create a velocity distribution in the fluid which travels parallel to the surface at the same speed as the structural wave (figure 2.16). The acoustic and the structural wave are therefore matched at the surface of the structure and the angle at which the acoustic wave propagates is dependent upon the speed of sound in air and the speed of the structural wave. If the structural wave on an infinite structure travels slower than the speed of sound in the fluid then there will be no sound radiated into the far-field because there is no angle at which the acoustic wave and the structural wave are matched and only a near-field disturbance will be created. Structural waves which travel faster than the speed of sound in the fluid are said to be supersonic and those which travel slower than the speed of sound in the fluid are said to be subsonic.

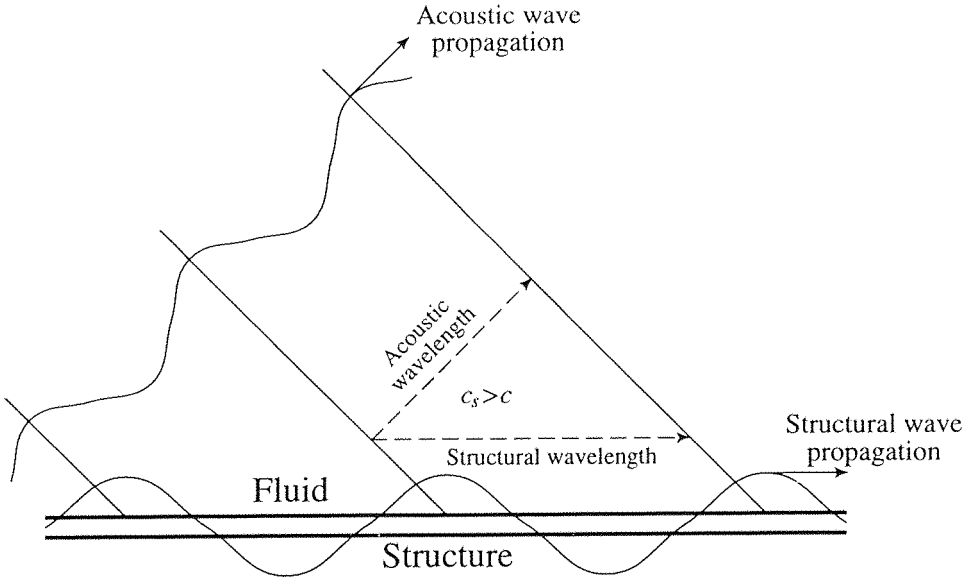

Figure 2.16: A structural wave radiating into a fluid where the structural wavespeed c_s is faster than the speed of sound in the fluid c.

For a given surface velocity distribution $v(x)$ the wavenumber components $F(k)$ can be calculated by using a Fourier integral [38].

$$F(k) = \int_{-\infty}^{\infty} v(x) e^{-jkx} \mathrm{d}x \tag{2.42}$$

The Fourier integral of a harmonic structural wave travelling on an infinite surface will produce a single delta function in the wavenumber domain. If the surface is

finite then, in effect, a rectangular *window* is placed over the function and this has the effect of spreading the spectrum of the signal in the wavenumber domain. This causes waves which travel subsonically on an infinite surface and therefore radiate no sound, to produce supersonic components when the surface is finite i.e. the signal is windowed.

Figure 2.17 shows the wavenumber transform for the first six structural modes of a simply supported beam of length l and having vanishingly small width. For a given frequency of vibration ω there will be a cut-on wavenumber $k_0 = \frac{\omega}{c}$ below which all of the wavenumber components are supersonic and will radiate sound. In the low wavenumber region, $kl \ll 1$ for example, the odd ordered structural modes have a significant wavenumber content and therefore all radiate sound to a similar degree. The wavenumber content of the even modes falls off at low values of k and therefore become increasingly inefficient at radiating sound at low frequencies. Figure 2.18 shows the wavenumber content of the first five radiation modes for $k_0 l = 0.3$ and as shown the wavenumber amplitudes become increasingly lower as the radiation mode order increases.

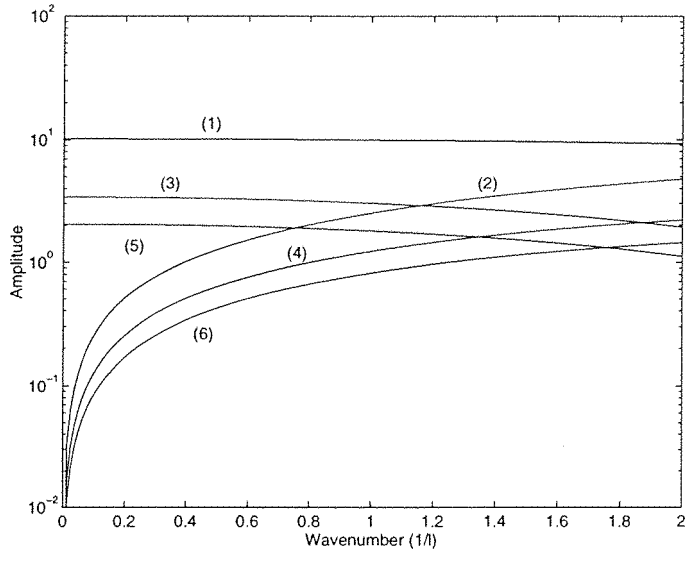

Figure 2.17: The wavenumber transform for the first six structural modes of a simply supported beam.

The shapes of the radiation modes remain reasonably constant for all $k_0 l < 1$, as described in section 2.3.5, and therefore their wavenumber spectra will also be sim-

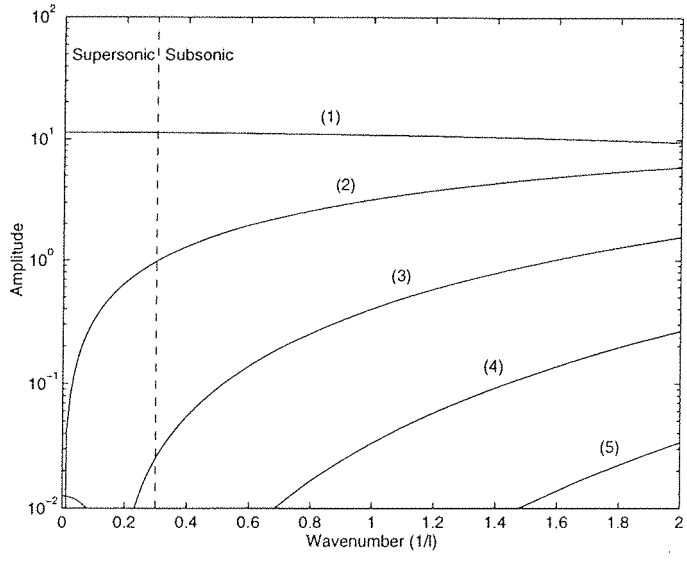

Figure 2.18: The wavenumber transform for the first five radiation modes of a baffled beam where $k_0 l = 0.3$.

ilar. As $k_0 l$ becomes very small and so $k_0 \ll 1/l$ the only radiation mode with a significant supersonic component will be the first. The wavenumber spectrum of the first radiation mode is a *sinc* function if $k_0 l \ll 1$ but the first zero of this function is beyond the range of k plotted in figure 2.18.

2.4 Conclusions

In this chapter an analysis of the radiation of sound from vibrating surfaces has been presented. Both near-field and far-field method for calculating the sound power radiation have been described. The near-field method for calculating the sound power radiation provides a straight forward way of numerically calculating radiated power. The integration of the pressure squared levels in the far-field does not often yield an analytical solution and it is generally necessary to employ numerical methods which can be more complicated than those using the near-field method.

It is convenient to describe the vibration of structures as a combination of a set of structural modes. In terms of the vibration, each structural mode responds almost *independently* and the vibrational energy in each mode in separated. The convenience

of viewing the vibration of a structure in terms of structural modes does *not* carry over to the radiation of sound. The acoustic radiation from each structural mode is coupled to the radiation of other structural modes. To interpret the radiation of sound, the engineer must not only consider the amplitudes of all of the structural modes but must also consider their inter-relationships. Alternatively, the vibration of a structure can be viewed in terms of a set of *radiation modes* which radiate sound independently. The shapes of the radiation modes can be derived from the structural mode shapes or more fundamentally from an elemental radiator approach. The properties of the radiation modes are unaffected by the structural properties of the system and are only dependent upon the geometry of the surface and the acoustic environment into which they radiate.

Radiation modes can also be viewed in terms of their multipole expansions. At low frequencies, the first radiation mode has the only significant monopole strength, the first and third radiation modes have the only significant quadrupole strengths etc. This is also true for the even modes where the second radiation mode is the dominant contributor to the dipole moment. Therefore, the amplitudes of the first n multipoles will be accurately described by the first n radiation modes at low frequencies.

At low frequencies where the source is considerably smaller than an acoustic wavelength the first radiation mode is much more efficient at radiating sound than the higher order radiation modes. Many structural modes however, will radiate sound with similar efficiencies and with large inter-modal coupling. For example, all of the odd modes of a simply supported beam have significant wavenumber amplitudes at low values of k. However the radiation modes exhibit progressively smaller wavenumber amplitudes at low values of k as the radiation mode order increases. In the low frequency region the amplitude of the first radiation mode is well approximated by the volume velocity of the structure and by reducing the level of the volume velocity and hence the first radiation mode, large reductions in the sound power radiation could be achieved. Volume velocity cancellation as a technique for controlling sound power radiation will be developed more fully in chapter 5 of this thesis. Attempting to reduce the sound power radiation by measuring and altering the amplitudes of the structural modes is a far more complex undertaking.

Radiation modes can be useful in designing both active and passive methods for

reducing the sound radiation from vibrating structures. Naghshineh showed that secondary actuators could be used to control the efficiently radiating radiation modes and therefore reduce the sound radiated from a beam [69, 70]. Snyder and Tanaka [80] suggested creating radiation mode sensors which would directly measure the amplitude of a radiation mode and could be used as error sensors in an active control system. Active control of the output of a distributed volume velocity sensor can thus be considered as the limiting case of Snyder and Tanaka's strategy. In terms of passive control, Naghshineh *et al.* [68] showed that a beam could be tailored to have a structural mode shape that corresponded to the shape of a poorly efficient radiation mode. This was achieved by changing the cross-sectional area of the beam as a function of distance along the beam. Therefore, a beam could be designed such that the structural modes of the beam would correspond to poorly radiating radiation modes and hence be inherently "weak radiators" of sound.

Chapter 3

Properties of radiation modes

3.1 Introduction

In this chapter the properties of radiation modes are investigated, for radiation from various types of sources into various types of acoustic field. The complexity of an active control system which achieves good attenuation in sound power radiation from a source, is dependent upon the number of significantly radiating radiation modes. It is therefore important to examine various radiation conditions to determine the number of efficiently radiating radiation modes and to calculate their dependence on frequency.

3.2 Radiation modes and radiation into infinite spaces

3.2.1 Radiation into one-dimensional fields

Consider the radiation of sound into an infinite duct which is assumed to have a vanishingly small cross-sectional area such that the acoustic field acts one-dimensionally (figure 3.1). The excitation is assumed to be harmonic and the time dependence term $e^{j\omega t}$ will be suppressed in the following equations. The complex pressure field created by the radiation from a compact vibrating element placed in a duct is given by [71],

$$p(x) = \frac{\rho_0 c v S_e}{2S_d} e^{-jkr} \tag{3.1}$$

ρ_0 is the density of the acoustic fluid, c is the speed of sound, v is the complex velocity of the source, S_e is the surface area of the elemental source, S_d is the cross-sectional area of the duct, k is the wavenumber and the pressure in the duct $p(x)$ is a function of r which is the distance between the source and the observer at x. The pressure does not reduce with distance as it does in the free-field case because the field is contained and there is no spherical or circular spreading.

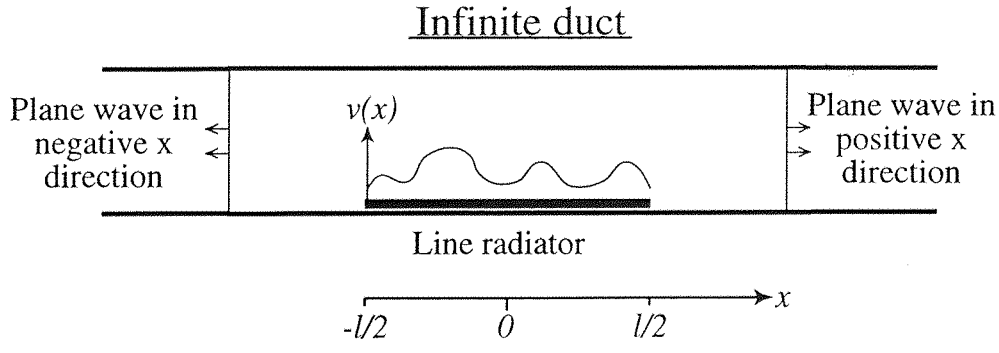

Figure 3.1: A line source radiating into a one-dimensional duct.

Consider a line source of length l radiating into the duct at a single frequency. If this source is approximated using a finite number I of equally sized and spaced elements then the coefficients of the impedance matrix $\boldsymbol{Z}$ (equation 2.10) can be calculated as,

$$Z_{ij} = \frac{\rho_0 c S_e}{2S_d} e^{-jkr_{ij}} \tag{3.2}$$

where r_{ij} is the distance between the i^{th} and j^{th} elements. The coefficients of the radiation resistance matrix $\boldsymbol{R}$, which is the real part of the impedance matrix $\boldsymbol{Z}$ (equation 2.11), can then be written as,

$$R_{ij} = \left(\frac{\rho_0 c S_e}{2S_d}\right) cos(kr_{ij}) \tag{3.3}$$

The radiation mode shapes and efficiencies can then be calculated from the eigenvalue/eigenvector decomposition of $\boldsymbol{R}$. The radiation of sound into an infinite one-dimensional duct at a single frequency is a unique case because the pressure in the

far-field (i.e. at the ends of the duct) can be completely described using only two wave amplitudes. Therefore only two independent sources are necessary to create any desired far-field condition. The matrix $\boldsymbol{R}$ has rank 2 in this case and therefore only two radiation modes exist. The efficiencies of these two modes, as a function of frequency, are shown in figure 3.2. The efficiency of the radiator is dependent on the cross-sectional area of the duct and for convenience the area is adjusted such that the efficiencies of the radiation modes tends to unity at high frequencies.

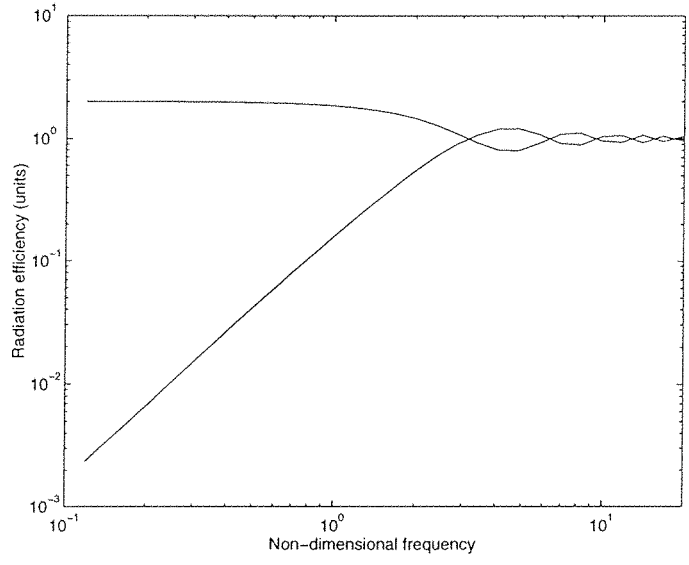

Figure 3.2: Radiation efficiencies of the two radiation modes for a line source (one dimensional beam) radiating into a duct as a function of non-dimensional frequency.

The shapes of the two radiation modes, when kl is equal to 0.1, are shown in figure 3.3 and correspond to a piston source, which generates two in-phase pressure waves in both directions along the infinite duct, and a "dipole" type source which generates two out of phase plane waves but much less efficiently. The radiation mode shapes for the high frequency case where $kl = 7$ are shown in figure 3.4 The shapes of the two radiation modes are found to have the form $\cos(kx)$ and $\sin(kx)$ and this can be shown analytically. The real part of the pressure $\mathcal{R}(p(x))$ for a line source ($\mathcal{R}$ denotes the real part of) is given by,

$$\mathcal{R}(p(x)) = C \int_{\frac{-l}{2}}^{\frac{l}{2}} v(x') \cos(k(x - x'))\mathrm{d}x' \tag{3.4}$$

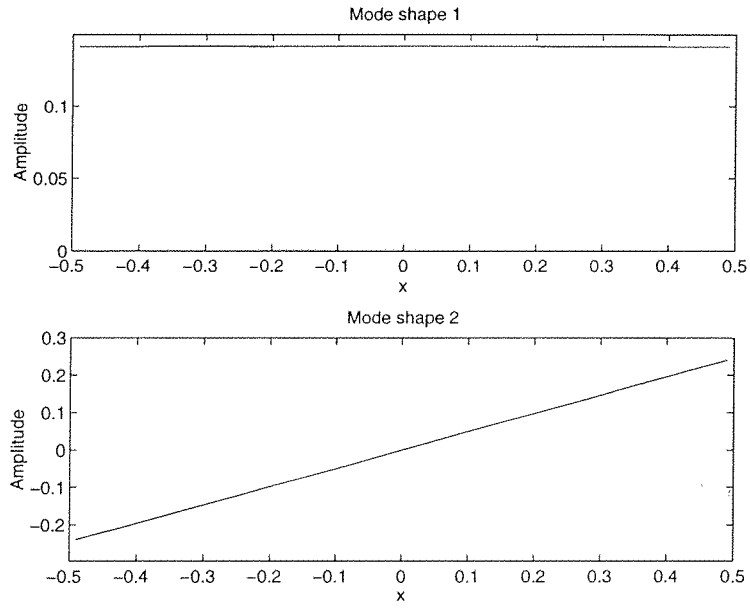

Figure 3.3: The shapes of the two radiation modes where $kl = 0.1$.

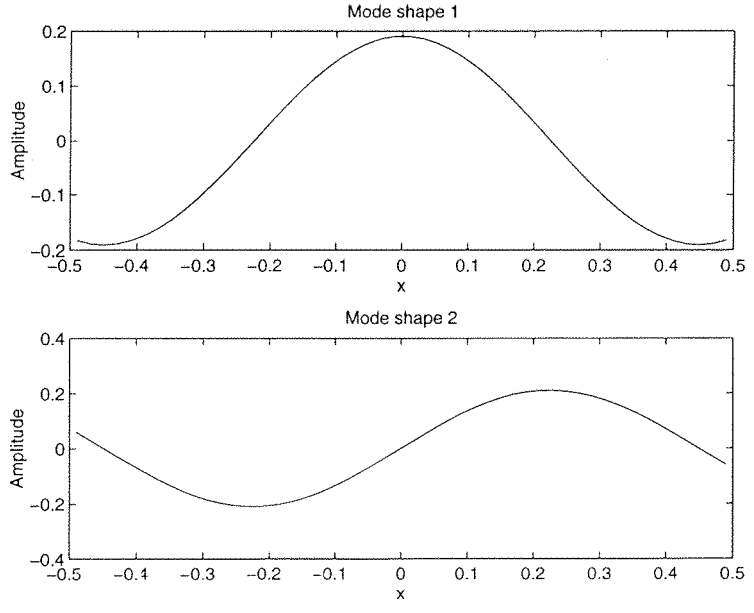

Figure 3.4: The shapes of the two radiation modes where $kl = 7$.

where $v(x')$ is a general velocity distribution and $C = \rho_0 c l_w / 2S_d$ where l_w is the width of the source. Two solutions are assumed for the radiation mode shapes such that $v_1(x') = \alpha cos(kx')$ and $v_2(x') = \beta sin(kx')$. The mode shape v_1 is substituted into equation 3.4 to obtain the in-phase pressure distribution due to the first radiation mode.

$$\mathcal{R}(p_1(x)) = \alpha C \int_{\frac{-l}{2}}^{\frac{l}{2}} \cos(kx') \cos(k(x - x'))\mathrm{d}x' \tag{3.5}$$

This integral can be divided into two separate parts by using the trigonometric relationship $2\cos(A)\cos(B) = \cos(A + B) + \cos(A - B)$. The resulting integral then becomes,

$$\mathcal{R}(p_1(x)) = \left[\frac{kl + \sin(kl)}{2k}\right] \alpha C \cos(kx) \tag{3.6}$$

As has been shown in section 2.3.3, the real part of the pressure distribution due to a radiation mode must have the same spatial dependency as the velocity distribution. Equation 3.6 shows that the real part of the pressure varies spatially with a $\cos(kx)$ dependence. It is therefore spatially similar to the velocity distribution $v_1(x)$ and must be an eigenfunction (or radiation mode) of equation 3.4. The ratio of the real part of the pressure to the velocity is a constant for a given frequency (eigenvalue) and is proportional to the radiation efficiency. This ratio is given by,

$$\frac{\mathcal{R}(p_1(x))}{v_1(x)} = C\left[\frac{kl + \sin(kl)}{2k}\right] \tag{3.7}$$

This ratio tends to Cl at low values of k and to $Cl/2$ at high values of k.

The above calculation can be undertaken for the second velocity distribution $v_2(x')$ and the resulting ratio (eigenvalue) is given by,

$$\frac{\mathcal{R}(p_2(x))}{v_2(x)} = C\left[\frac{kl - \sin(kl)}{2k}\right] \tag{3.8}$$

As k tends to zero the pressure/velocity ratio for the second radiation mode becomes,

$$\frac{\mathcal{R}(p_2(x))}{v_2(x)} \approx Cl\left[\frac{(kl)^2}{12}\right] \tag{3.9}$$

This ratio accounts for the poor radiation efficiency of the second radiation mode where kl is small, as seen in figure 4. At high values of k this pressure/velocity ratio also tends to $Cl/2$.

In principle, the total sound power output of any source radiating into an infinite duct can be reduced to zero using a two channel active control system. If the primary source is small compared to an acoustic wavelength and has a significant monopole component then a single secondary monopole source placed very close to the primary will be able to achieve large attenuations in the sound power radiation.

3.2.2 Radiation into two-dimensional fields

Consider the radiation from a source into an infinite two-dimensional field so that the acoustic wave created by a point source spreads outwards as a circle of increasing radius (figure 3.5). Such a point source will create a harmonic pressure field which has an in-phase component of the form [84],

$$\mathcal{R}\{p(r)\} = A\,[J_0(kr)]\,v \tag{3.10}$$

where the time dependence $e^{j\omega t}$ has again been suppressed, J_0 is a zeroth order bessel function of the first kind, r is the distance between the observer and the source, v is the velocity at the source's surface and A is a constant that is dependent on the particular physical example. Examples of such two-dimensional acoustic fields are the radiation from a source in very shallow water of constant depth [84], the radiation from a source in a plane parallel waveguide [84] and the radiation from an infinitely long pulsating cylinder [67].

Similarly, an infinite plate which has a surface velocity due to bending waves travelling in two-dimensions has an in-phase component of the surface velocity due to a point force of the form [47],

$$\mathcal{R}\{v(r)\} = B\,[J_0(kr)]\,f \tag{3.11}$$

where B is a constant and v is the velocity of the surface due to the force f. The radiation modes for this example have been investigated by Bardou *et al.* [5, 6] and

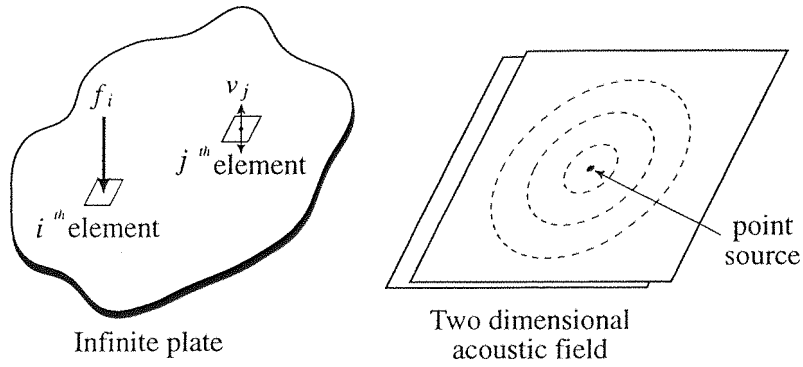

Figure 3.5: Radiation into a two dimensional field.

are similar to those for the acoustic case.

The radiation of sound/vibration into a two-dimensional field due to a distributed source can be approximated by a number of point sources. A matrix $\boldsymbol{R}$ which represents the real part of the transfer impedances between these point sources will be given by,

$$R_{ij} = A\left[J_0(kr_{ij})\right] \tag{3.12}$$

where r_{ij} is the distance between the i^{th} and j^{th} elements and A is a constant. The radiation mode shapes and efficiencies can then be calculated from the eigenvalue/eigenvector decomposition of the matrix $\boldsymbol{R}$.

A line radiator

In this section the radiation from a number of elemental sources which are arranged in a line on the two dimensional plane shown in figure 3.5 are investigated. The matrix $\boldsymbol{R}$ can be calculated for a number of frequencies and the radiation efficiencies of the radiation modes can be derived.

The radiation efficiencies of the first four radiation modes as a function of frequency are shown in figure 3.6. Fifty equaliy sized and equally spaced elements were used to approximate the radiation from the line radiator. For this configuration there are fifty radiation modes which at low frequencies become increasingly less efficient at radiating sound as the mode order increases. The first radiation mode has a

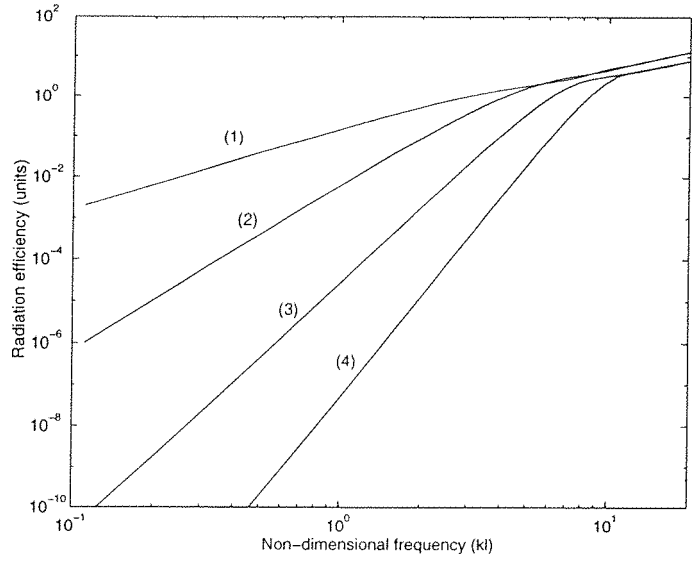

Figure 3.6: The radiation efficiencies of the first four radiation modes for a line source radiating into a two-dimensional field.

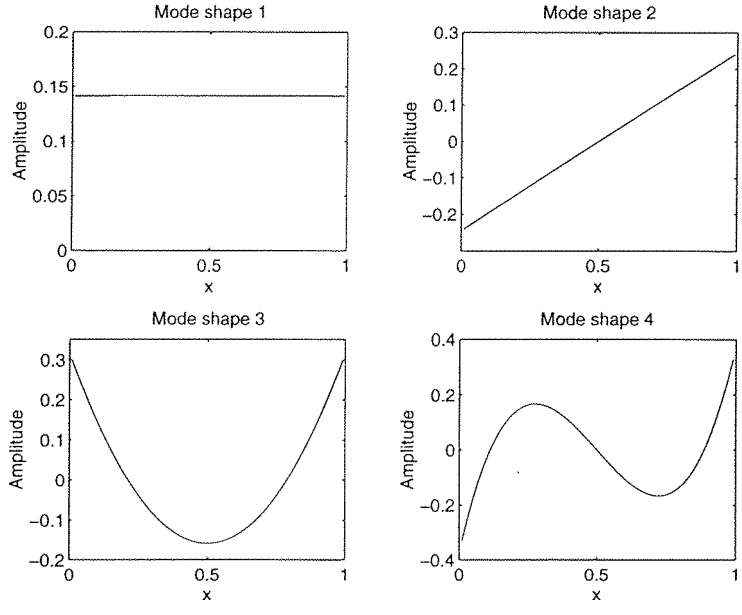

Figure 3.7: The radiation mode shapes of the first four radiation modes for a line source radiating into a two-dimensional field.

radiation efficiency which is proportional to $(kl)^2$ at low frequencies and higher order radiation modes have an efficiency which is proportional to higher order terms i.e. $(kl)^4, (kl)^6 \ldots (kl)^{2n}$ where n is the mode order. There are in principle an infinite number of radiation modes for a continuous source but only the first fifty can be calculated by modelling the radiation using fifty elements. The shapes of the first four radiation modes for $kl = 0.1$ are shown in figure 3.7. At low frequencies the first radiation mode is by far the most significant radiator of sound and its amplitude is well approximated by the volume velocity of the structure. In most cases, a reduction in the volume velocity of the structure will, in the low frequency region, cause a large reduction in the sound power radiation. A multichannel control system could in principle use additional secondary sources to control additional radiation modes. For this example where each higher order radiation mode is significantly less efficient than the lower order radiation modes (figure 3.6) each additional secondary source should achieve significant additional attenuation.

A rectangular radiator

All real sources have a finite width and the radiation from a one-dimensional line source defines the limiting case for a very long thin radiator. A more realistic source is a rectangular radiator, which can be approximated using a number of elements and for the results presented here a 12×12 grid of elements was used. The rectangle had a width to length ratio of 0.89. The radiation efficiencies of the first seven radiation modes as a function of non-dimensional frequency are shown in figure 3.8.

With the exception of the first mode, the radiation modes are grouped into sets of two. These sets of modes become increasingly inefficient at radiating sound as the frequency decreases. At low frequencies the first radiation mode is again by far the most efficient radiator of sound. The first radiation mode has a radiation efficiency which is proportional to $(kl)^2$ at low frequencies and higher order radiation modes have an efficiency which is proportional to higher order terms i.e. $(kl)^4, (kl)^6 \ldots (kl)^{2n}$ where n is the mode order. The shapes of the first four radiation modes are shown in figure 3.9 where the first radiation mode is a piston type mode at low frequencies and therefore its amplitude is well approximated by the volume velocity of the source. The next two modes, which are of the same order, are rocking modes (dipole type)

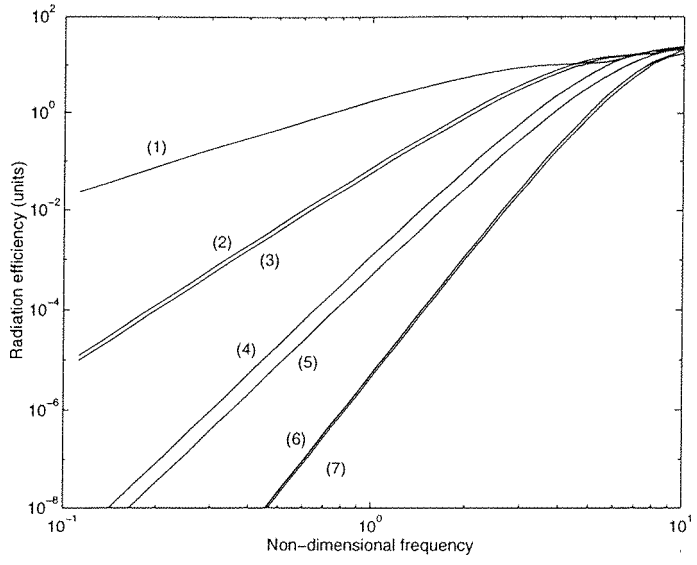

Figure 3.8: The radiation efficiencies of the first seven radiation modes for a rectangular source radiating into a two-dimensional field.

followed by a quadrupole type mode. At high frequencies, where the source becomes large compared to a wavelength, many of the radiation modes begin to radiate sound efficiently.

The efficiencies of the radiation from two radiation modes of the same order are slightly different due to the radiator being non-square. As the length to width ratio becomes larger the separation between the efficiencies of two modes of the same order increases. In the limit of the ratio tending to infinity the efficiencies become those of a line radiator.

For this example an additional control channel in a multichannel control system will not necessarily lead to a significant increase in attenuation. If a two channel control system were used to cancel the first two radiation modes then the third radiation mode, which has a similar efficiency to the second radiation mode, would dominate the sound power radiation from the structure. It would require a three channel control system to cancel both of the second order radiation modes and lead to a significant increase in attenuation. Additional increases in attenuation would require two additional channels in the control system.

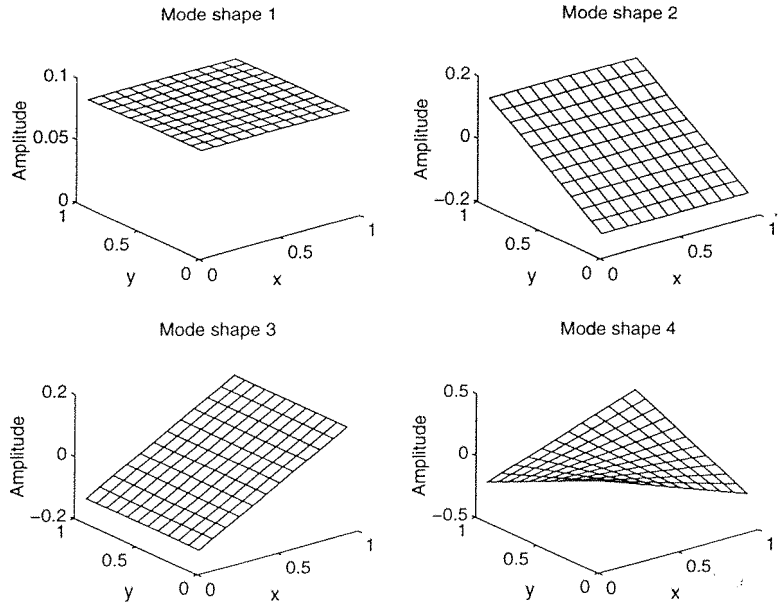

Figure 3.9: The radiation mode shapes of the first four radiation modes for a rectangular source radiating into a two-dimensional field.

3.2.3 Radiation into three-dimensional fields

This section will look at the radiation of sound into an infinite three-dimensional field. The theory used to calculate the radiation modes for sources radiating into three-dimensional space is given in section 2.2.3 of this thesis.

A line radiator

The radiation from a line source into a three-dimensional field has been covered briefly in chapter 2 but will be repeated here. The shapes of the first four radiation modes for a line source (e.g. a baffled beam, which is of vanishingly small width) are calculated by modelling the source using fifty elements. The resulting shapes, where the non-dimensional frequency kl equals 0.1, and are shown in figure 3.10 [25, 33]. The shape of the first radiation mode at low frequencies is almost uniform across the radiator and hence the amplitude of the first radiation mode is very nearly proportional to the net volume velocity of the beam. The second mode is a rocking mode (dipole type) followed by higher order modes. These are very similar to the radiation mode shapes for a line radiator radiating into a two-dimensional field (figure 3.6).

The radiation efficiencies of the first 4 radiation modes as a function of frequency

are shown in figure 3.11 with each higher order mode have a larger rate of change of efficiency with frequency i.e. $(kl)^{2n}$ where n is the mode order.

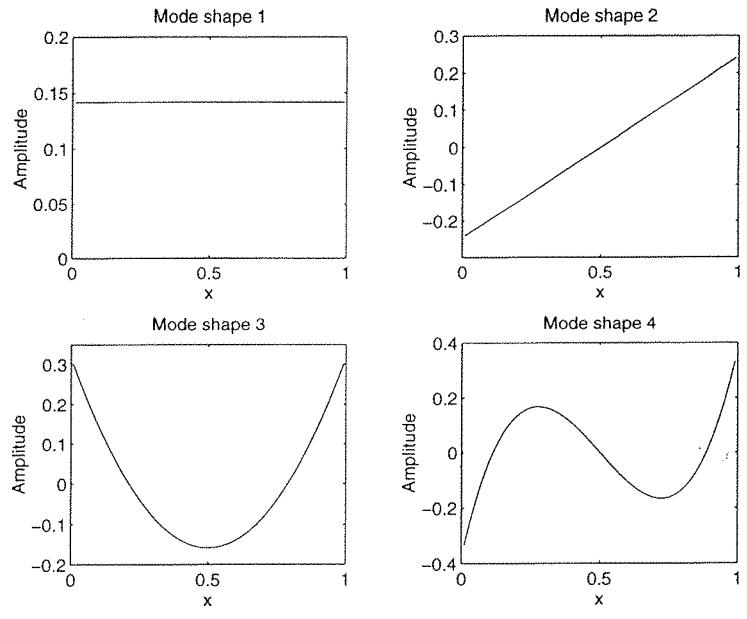

Figure 3.10: The first four radiation mode shapes for a line radiator radiating into a three-dimensional free-field($kl = 0.1$).

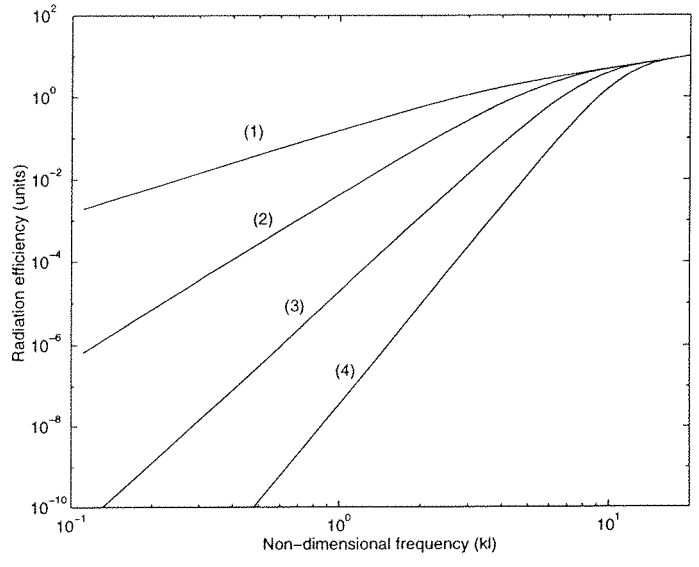

Figure 3.11: The radiation efficiencies for the first four radiation modes for a line source radiating into a three-dimensional field.

A rectangular radiator

In this section the radiation from a baffled rectangular radiator into a three-dimensional hemisphere is considered. The radiator is approximated by a 12×12 grid of elemental radiators whose width to length ratio is 0.89. Figure 3.12 shown the radiation efficiencies of the first ten radiation modes for a rectangular surface radiating into free space. The radiation modes are grouped into sets with the same rate of change of efficiency with respect to frequency when $kl < 1$ i.e. are of the same order. These groups are of increasing size $1, 2, 3, 4, ...$ with each larger set becoming increasingly inefficient at radiating sound at low frequencies i.e. $(kl)^{2n}$ where n is the mode order. A multichannel control system will in this example require progressively larger additional numbers of secondary sources to achieve each additional increase in attenuation.

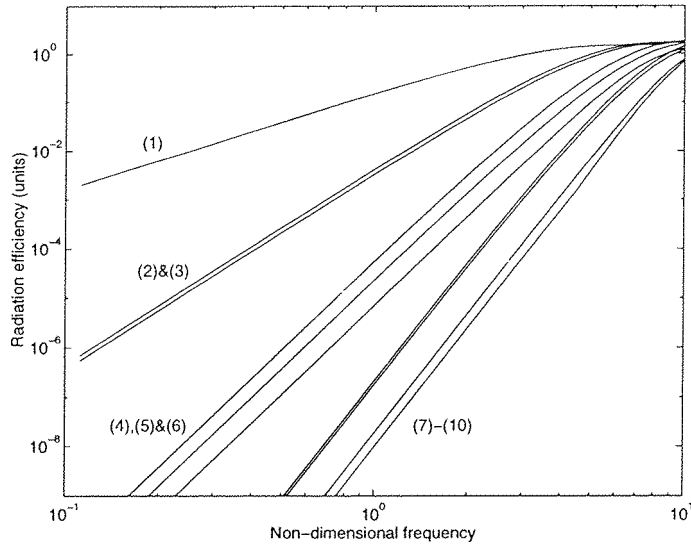

Figure 3.12: The radiation efficiencies of the first ten radiation modes for a rectangular source radiating into a three-dimensional free-field.

The shapes of the first six radiation modes are shown in figure 3.13. Most of these mode shapes look similar to the radiation mode shapes for a rectangular radiator radiating into a two-dimensional field (figure 3.9) with the exception of mode shape 6 which does not exist for the case of the two-dimensional field. The existence of this and other additional modes for the three dimensional case will be considered in section 3.3.

Currey and Cunefare [27] have calculated radiation mode shapes for baffled rectangular panels using boundary element techniques and their work closely supports the results presented here.

It should be noted that the radiation from a baffled source on a plane into a hemispherical space is of exactly the same form as that of an unbaffled source into a full three-dimensional spherical space if the velocity on either side of the source is identical and opposite.

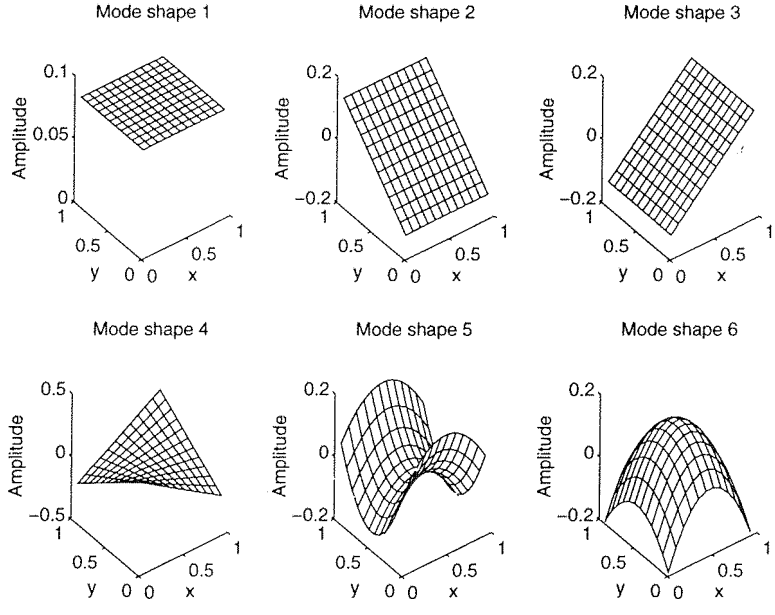

Figure 3.13: The radiation mode shapes of the first six radiation modes for a rectangular source radiating into a three-dimensional free-field.

A transparent cuboid radiator

A transparent cuboid radiator is used as an example of a three-dimensional radiator and is approximated by using a $6 \times 6 \times 6$ grid of elemental radiators. The length:width:height ratio is 1:0.89:0.82. For simplicity the radiator is assumed to be transparent and therefore the pressure at one element due to the radiation from another element is considered to be the same as if the two elements were in a free field. This allows easy calculation of the impedance matrix $\boldsymbol{Z}$. The radiation efficiencies of the first nine radiation modes for this three-dimensional radiator radiating into free space is shown in figure 3.14. The radiation modes are arranged in to sets

of increasing size such that each higher order set contains two additional modes (i.e. $1, 3, 5, 7, ...$). A simple graphical representation of the first four radiation mode shapes at low frequency is given in figure 3.15. The first mode is a monopole type source with the next three modes being dipole type sources.

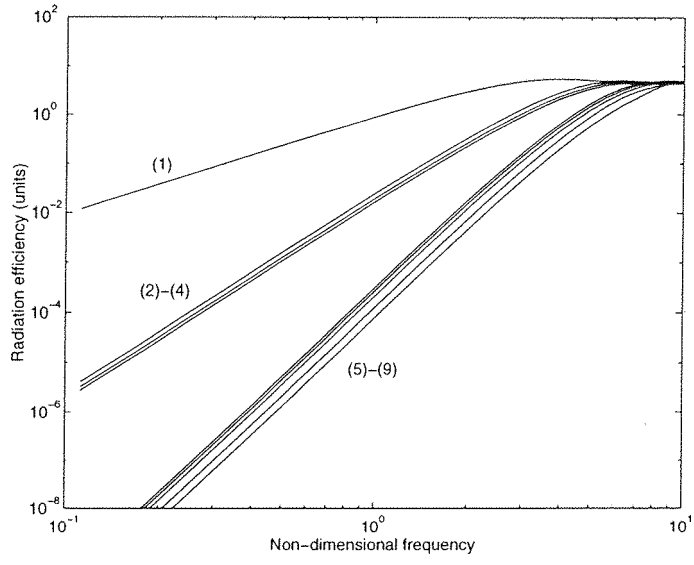

Figure 3.14: The radiation efficiencies of the first nine radiation modes for a transparent cuboid source radiating into a three-dimensional free-field.

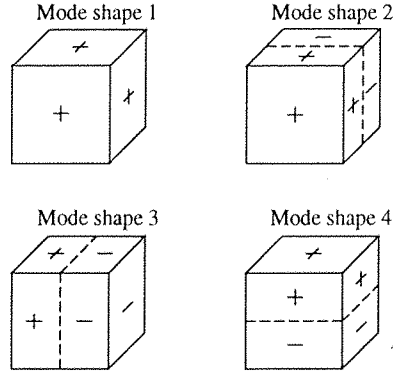

Figure 3.15: The first four radiation mode shapes for a transparent cuboid radiator radiating into free space at low frequency.

For this example it would require three additional secondary sources to gain a significant increase in attenuation over a single channel control system. An additional increase in attenuation would then require five more secondary sources to cancel all of the five third order radiation modes.

3.3 Directivity properties and intensity fields

The number of radiation modes with the same order is dependent on both the dimension of the radiator and the dimension of the acoustic (or vibration) field. In an attempt to understand the reasons for this behaviour some of the properties of radiation modes will be developed in more detail.

The time-average intensity fields created by the radiation of sound from a vibrating beam are shown in figure 3.16 where the non-dimensional frequency (kl) is equal to one [39]. The top lefthand graph shows the intensity field for the radiation from the first structural mode of a simply supported beam. At this frequency the power output at every point on the surface is greater than or equal to zero. However, for the third structural mode (top righthand graph) the centre third of the surface is absorbing energy, even though the output of the two sides is positive, and there is circulation in the intensity field. The sound power which reaches the far field perpendicular to the surface will have been radiated by two spatially separated areas on the surface of the beam. The bottom lefthand and bottom righthand graphs in figure 3.16 shown the radiation from the first and third radiation modes where the sound power radiated by every part of the surface is greater than or equal to zero for both modes and there is no circulation in the intensity field. This property appears to be true for all radiation modes. In section 2.3.3 it was shown that the in-phase part of the acoustic pressure due to a radiation mode had the same spatial variation as the velocity of the surface due to that radiation mode. This implies that the acoustic power radiated by every part of the surface must be greater than or equal to zero. Therefore there is no absorption of acoustic energy by any part of the surface for a radiation mode. The acoustic energy thus appears to flow directly outwards from the surface into the far-field without any circulation in the intensity field. Since there is no circulation in the intensity field the number of lobes in the far-field directivity pattern for a radiation mode must be the same as the number of sections in the radiation mode shape which are divided by points of zero velocity (stationary points). This is clearly not the case for structural modes since, as shown in the top righthand graph of figure 3.16, there are two stationary points on the surface but there is only a single lobe in the far-field directivity pattern.

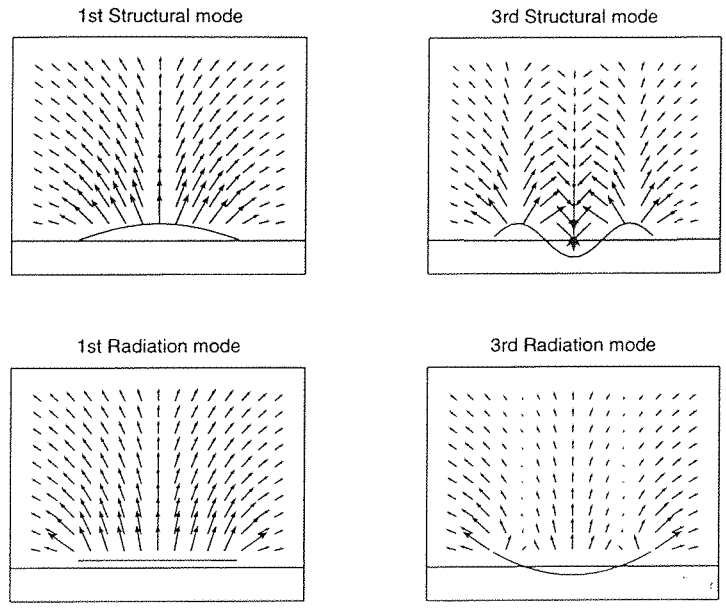

Figure 3.16: The intensity fields produced by the radiation from the first and third structural modes of a simply supported beam and the first and third radiation modes for a beam.

The radiation mode order for a two-dimensional radiator is defined by the number of stationary lines in the radiation mode shape where the stationary lines are lines of zero velocity on the radiator surface. Figure 3.17 shows the stationary lines for the sixth radiation mode of a rectangular radiator, radiating into an infinite three-dimensional space and also the far field directivity pattern for this mode. There are only two stationary lines for this mode, one on the top face and one on the bottom face and hence there are only three lobes. This radiation mode does not exist for the radiation of a rectangular radiator into a two-dimensional field because the third dimension is necessary to allow energy to flow from the top and bottom of the baffled surface.

For the radiation modes of a three-dimensional source stationary planes have to be considered instead of stationary lines. The radiation modes for a three-dimensional source are grouped into larger sets because we can include stationary planes along the $x-y$ axes. Figure 3.18 shows the far-field radiation directivity from the fourth radiation mode for a transparent cuboid radiator which is of order 2 and shown in figure 3.15. This mode cannot exist for a two-dimensional baffled radiator placed in the $x-y$ plane because the generation of this mode requires that elements on the top

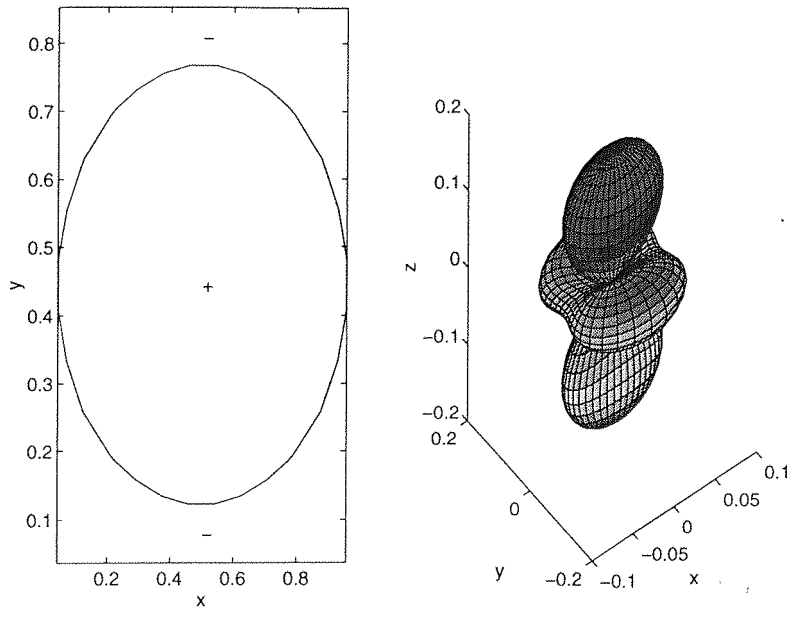

Figure 3.17: The stationary lines and the far-field directivity of the sixth radiation mode of a rectangular radiator radiating into free-space.

and bottom of the plane act out of phase with each other to generate a dipole type source in the z direction.

3.4 Radiation modes and radiation into enclosures

All of the earlier sections in this chapter have dealt with the radiation of sound into infinite spaces. However, many noise problems occur in enclosed spaces and this section will deal with the radiation of sound into enclosures.

3.4.1 General theory

The pressure field in an enclosure at low frequencies can be approximated by the summation of a finite number N of acoustic modes. These modes have defined spatial variations that are fixed and are not a function of frequency for a locally reacting boundary whose properties do not change with frequency. It is assumed that the radiation of sound from a source at the enclosure boundary can be approximated, as in the free-field case, by a number of elemental radiators. The pressure at the i^{th} elemental position will be defined as,

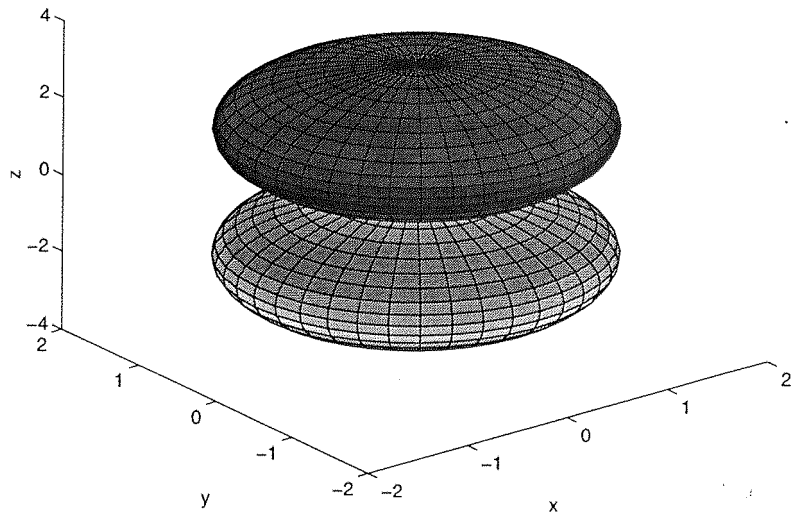

Figure 3.18: The far-field directivity pattern of the fourth radiation mode for a transparent cuboid radiator radiating into free space.

$$p_i = \sum_{n=0}^{N-1} b_n \psi_n(x_i, y_i, z_i) \tag{3.13}$$

where x_i, y_i, z_i define the spatial position of the i^{th} element, b_n is the complex amplitude of the n^{th} mode and ψ_n is the n^{th} acoustic mode shape of the enclosure.

If the sound in the enclosure is due purely to the I elemental sources which are assumed small compared to a wavelength, then the amplitude of the n^{th} acoustic mode can be approximated as,

$$b_n = A_n^a \sum_{i=1}^{I} \psi_n(x_i, y_i, z_i) v_i = A_n^a \boldsymbol{\psi}_n^T \boldsymbol{v} \tag{3.14}$$

where $\boldsymbol{\psi}_n$ is an I-length vector of the pressures due to the n^{th} mode at the I elemental positions, v_i is the velocity of the i^{th} element, $\boldsymbol{v}$ is an I length vector of elemental velocities and A_n^a is the complex resonance term for the n^{th} acoustic mode and is a function of frequency. The complex resonance term is given by [71],

$$A_n^a = \frac{\omega S_e \rho_0 c^2}{V\left[2\zeta_n \omega_n \omega - j(\omega^2 - \omega_n^2)\right]} \tag{3.15}$$

where ω is the frequency of excitation, ω_n is the resonant frequency of the n^{th} mode,

S_e is the elemental area and ζ_n is the damping ratio for the n^{th} mode. If the excitation frequency is close to the resonant frequency of the mode, then the complex resonance term will be large and real.

The complex resonance term quoted above is not used to model the zeroth order acoustic mode because the natural frequency of the zeroth order mode is zero ($\omega_0 = 0$) and hence the damping would also be zero. To make the response at low frequencies more realistic this mode is given a damping equal to half the damping of the first resonant mode i.e.

$$A_0^a = \frac{\omega S_e \rho_0 c^2}{V\left[\zeta_1 \omega_1 \omega - j\omega^2\right]} \tag{3.16}$$

where ζ_1 is the damping ratio for the first resonant mode and ω_1 is the natural frequency of the first resonant mode.

Equation 3.13 and equation 3.14 can be combined in matrix form to calculate the vector of pressures $\boldsymbol{p}$ at the I elemental positions due to the velocity of the elements.

$$\boldsymbol{p} = \boldsymbol{\Psi b} = \boldsymbol{\Psi A^a \Psi^T v} \tag{3.17}$$

The vector $\boldsymbol{b}$ defines the amplitudes of the N modes, the I by N real matrix $\boldsymbol{\Psi}$ defines the pressures due to the N modes at the I elemental positions and $\boldsymbol{A}^a$ is an N by N diagonal matrix of complex resonance terms.

The total power output is given by equation 2.9 and can be rewritten as,

$$W = \frac{S}{2}\mathcal{R}(\boldsymbol{v}^H \boldsymbol{p}) = \frac{S}{2}\boldsymbol{v}^H \boldsymbol{\Psi}\mathcal{R}(\boldsymbol{A}^a)\boldsymbol{\Psi}^T \boldsymbol{v} \tag{3.18}$$

The radiation mode shapes can be calculated by the eigenvector/eigenvalue decomposition of $\boldsymbol{\Psi}\mathcal{R}(\boldsymbol{A}^a)\boldsymbol{\Psi}^T$. The coefficients in $\boldsymbol{A}^a$ will determine how the shapes of the radiation modes will vary with frequency. If a single mode dominates at a single frequency then the radiation mode shapes will be largely determined by the shape of that acoustic mode at the surface of the source.

3.4.2 Finite ducts

Consider the radiation of sound into a finite duct by a line source which is placed along a section of a duct (figure 3.19). For this example the ratio of the source length to duct length is chosen to be 0.2 where the total length of the duct is L and the source is placed between $x = 0.3/L$ and $x = 0.5/L$.

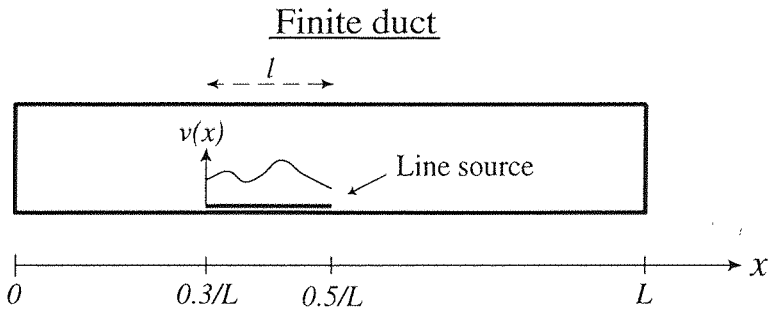

Figure 3.19: A line source of length $l = 0.2L$ radiating into a finite duct.

As was show in section 3.1 an infinite duct has only two radiation modes and the far field pressures can be totally described using only two source strengths. By making the duct finite, the enclosure becomes an infinite degree of freedom system and an infinite number of acoustic modes are required to perfectly describe the internal sound field. An infinite number of radiation modes would also be required to perfectly describe the radiation from a distributed source placed in the finite duct.

Figure 3.20 shows the radiation efficiencies of the first five radiation modes for the line source placed in the duct as a function of non-dimensional frequency kl. The radiation efficiencies of the radiation modes in this case, unlike all of the free-field cases, vary at the same rate (with respect to frequency) at low frequencies except for the first radiation mode. This is due to the dominance of the zeroth order acoustic mode, which is a special case since it is the compliant mode whose amplitude is entirely due to the change in the volume of the enclosure. At low frequencies the higher order radiation modes do not have any volumetric component and therefore cannot couple into the zeroth order acoustic mode.

For an enclosure, the variation of pressure with distance is specified by the shapes of the acoustic modes which are independent of frequency. Any velocity distribution will

couple into the acoustic mode shapes to the same extent regardless of the frequency i.e. $\boldsymbol{\Psi}^T\boldsymbol{v}$ = constant. The only variable factor is due to the complex resonance terms $\boldsymbol{A}^a$. If the shapes of two higher order radiation modes remain reasonably constant at low frequencies then their coupling with the acoustic modes will also remain reasonably constant and their radiation efficiencies will both fall off at the same rate as the complex resonance terms i.e. proportional to $(kl)^2$.

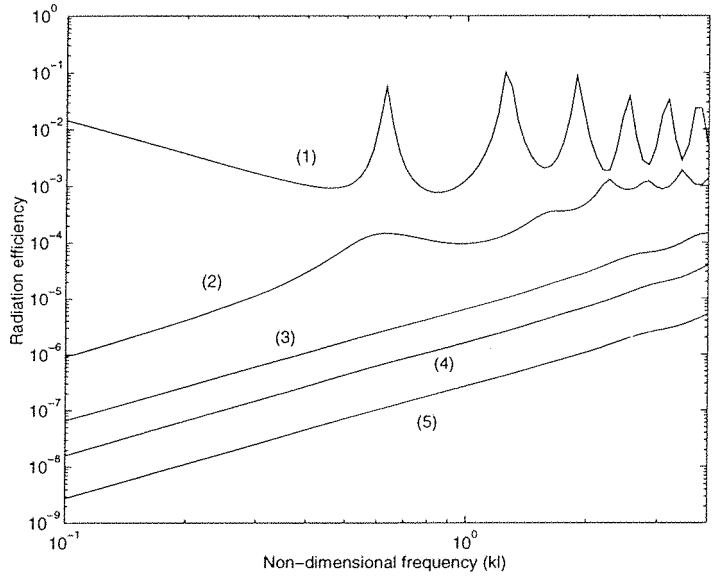

Figure 3.20: The radiation efficiency of the first five radiation modes as a function of frequency for a line source of length $l = 0.2L$ in a finite duct of length L.

The efficiency of the first radiation mode at higher frequency is highly dependent on the resonances in the duct. Equation 3.18 and equation 3.15 show that close to a resonant frequency the matrix $\boldsymbol{A}^a$ will be dominated by a single large coefficient. The shape of the first radiation mode when the excitation frequency is close to a resonant frequency of the mode in the duct is therefore dependent upon the shape of this dominant mode. This is demonstrated by comparing the shape of the first radiation mode at a resonant frequency with the pressure distribution over the surface of the source due to that resonant mode. The shape of the first radiation mode at the first three resonances is shown in figure 3.21 (top graphs) and closely match the pressure distributions (bottom graphs) due to the first, second and third acoustic modes respectively.

The shapes of the first four radiation modes are shown in figure 3.22 where $kl = 1$

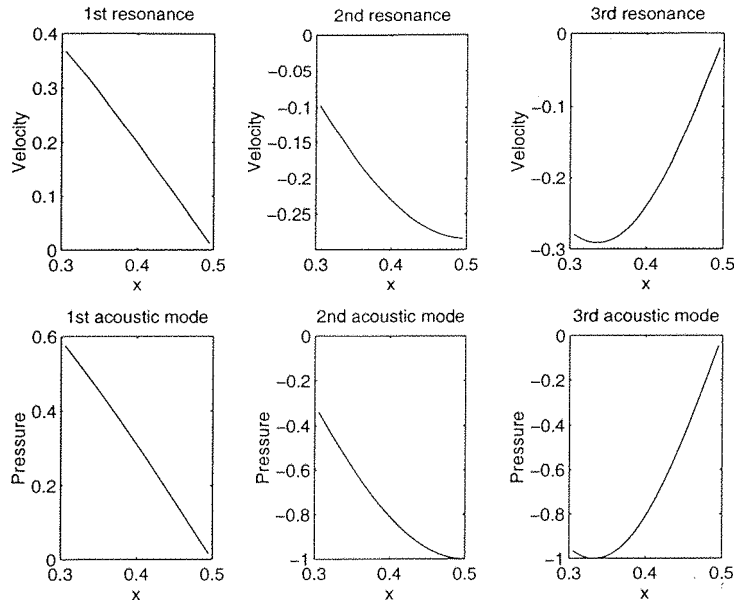

Figure 3.21: The shape of the first radiation mode for a source radiating into a duct at excitation frequencies corresponding to the first three resonances of the duct, compared with the pressure in the first three acoustic mode shapes of the enclosure over the source.

which corresponds to a non-resonant frequency. The radiation mode shapes are not dissimilar to those for the radiation by a line source radiating into an infinite two or three-dimensional field.

The difference in the radiation efficiencies of the radiation modes at a single frequency is dependent upon the size of the source. To investigate the efficiency of the radiation modes as a function of source size, sources of varying size, whose centres are placed at $x = 0.4L$, are examined. Figure 3.23 shows the efficiencies of the first five radiation modes where $kL = 5$ (L being the length of the duct) and the length of the source, l, is varied from $0.005L$ to $0.5L$. The radiation efficiency of the first radiation mode becomes more dominant when the source size is small. If the size of the source is halved then the relative efficiency of the second radiation mode falls by $6dB$. This implies that the cancellation of the first radiation mode of a source will be more effective if the source size is small compared to the size of the duct.

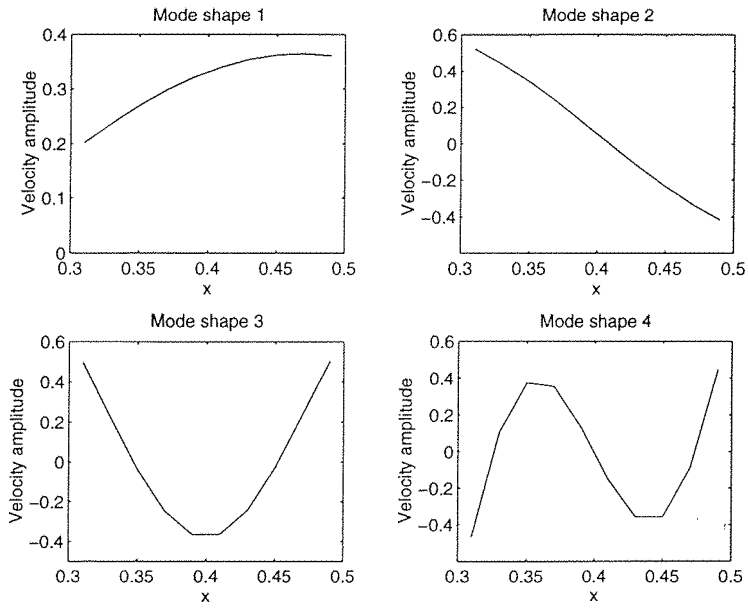

Figure 3.22: The radiation mode shapes of the first four radiation modes for a $0.2m$ source in a finite duct of $1m$ length ($kl = 1$).

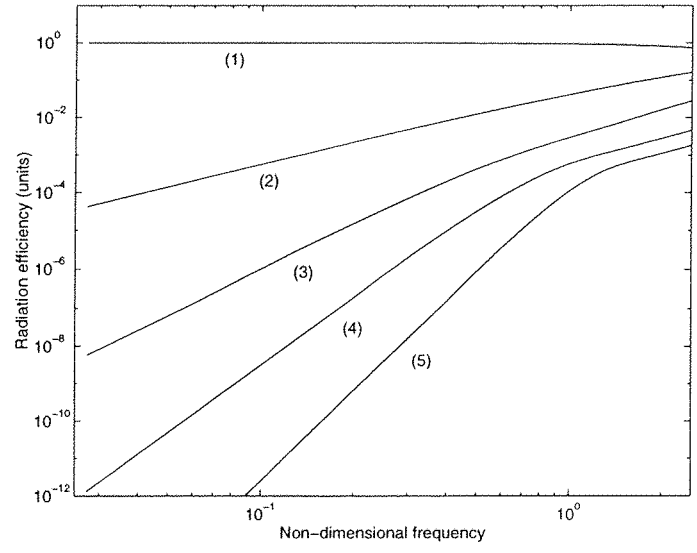

Figure 3.23: The radiation efficiencies of the first five radiation modes for a source whose center is placed at $x = 0.4L$ and whose length, l, varies from $0.005L$ to $0.5L$ (i.e. kl varies from 0.025 to 2.5) where $kL = 5$.

3.4.3 Three-dimensional enclosures

The radiation modes for a rectangular panel radiating into a three-dimensional cuboid (box) enclosure are calculated in this section. The enclosure is of dimensions $6m \times 2.2m \times 2m$ and the source has dimensions $0.2m \times 0.2m$ (figure 3.24). The radiation efficiencies of the first six radiation modes for this source are plotted against frequency in figure 3.25. The radiation efficiencies of the radiation modes are affected by the acoustic resonances of the enclosure such that certain radiation modes may have increased efficiency close to an acoustic resonance. The overall trend is similar to the finite duct case at low frequencies with the radiation efficiencies of the radiation modes all falling off at the same rate with the exception of the first order mode. At higher frequencies, however, the enclosure becomes diffuse and the response at any one frequency is due to the action of a large number of acoustic modes. In this region the radiation modes group into sets whose efficiencies exhibit a frequency dependency of the form $(kl)^2$, $(kl)^4$.... This behaviour is very similar to the radiation modes for a baffled panel radiating into free space (section 3.2.3). Figure 3.26 shows the radiation mode shapes for an excitation frequency corresponding to $kl = 0.6$ where l is the dimension of the source.

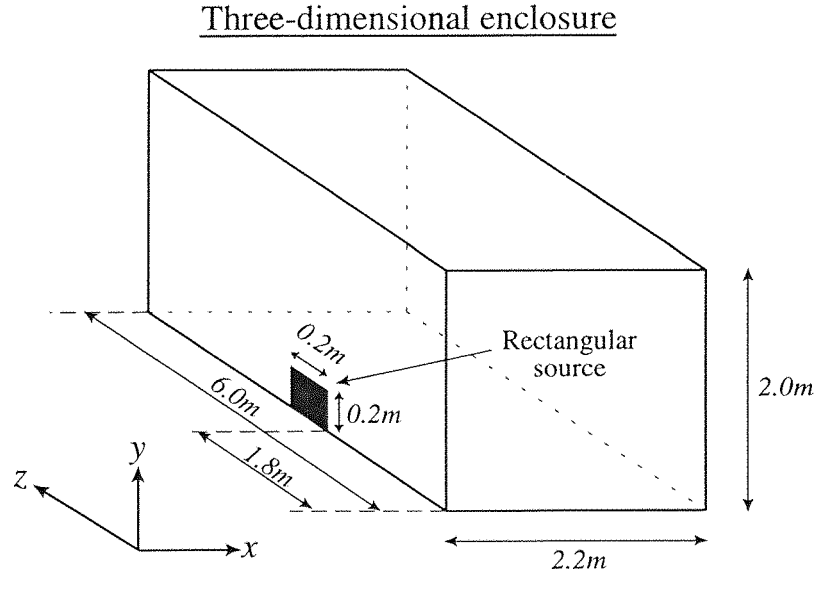

Figure 3.24: A rectangular source radiating into a three dimensional enclosure.

The ratios between the efficiencies of the higher order radiation modes and the effi-

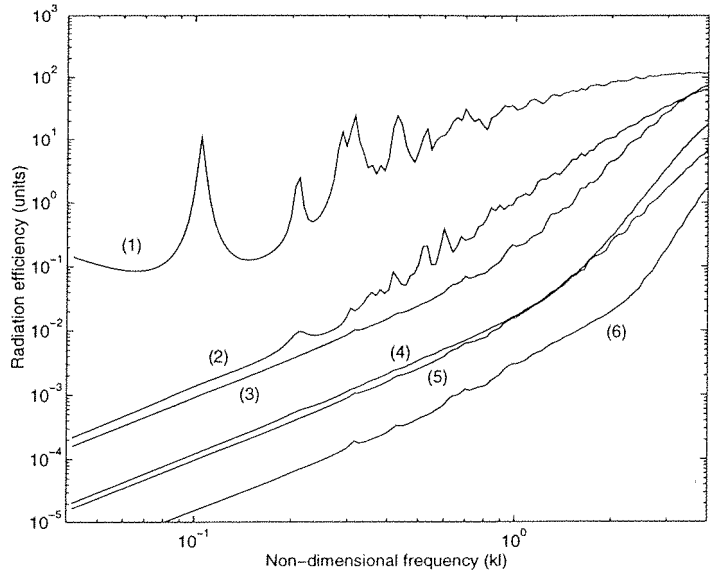

Figure 3.25: The variation of the radiation efficiencies of the first six radiation modes with excitation frequency for a $0.2m$ by $0.2m$ source in a rectangular enclosure of dimension $2m$ by $2.2m$ by $6m$ ($l = 0.2m$).

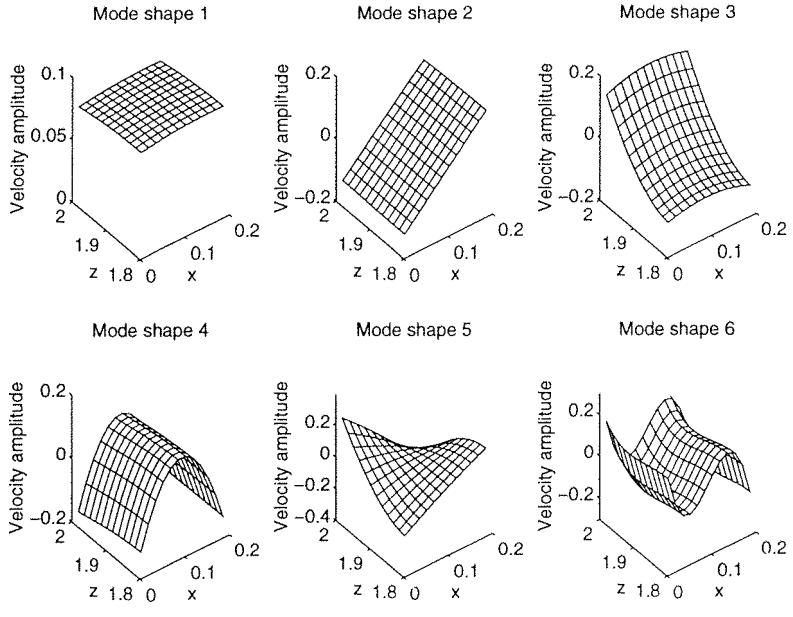

Figure 3.26: The radiation mode shapes of the first six radiation modes for a $0.2m$ by $0.2m$ source in a rectangular enclosure of dimension $2m$ by $2.2m$ by $6m$ ($kl = 0.6$).

ciency of the first radiation mode are a function of the size of the source (Figure 3.27). The radiation modes are grouped into sets of increasing size (1,2,3,...) with each higher order set of radiation modes having an efficiency which is proportional to a higher order term i.e. $(kl)^{2n}$ where n is the mode order. This is very similar to the radiation modes produced by a rectangular baffled source radiating into a three-dimensional infinite field. If the excitation frequency is low then the enclosure can begin to lose its three-dimensional characteristics and the radiation modes will no longer group into the same sets. This is particularly true for enclosures with one dimension significantly smaller than the other two dimensions such that there is a frequency range in which the enclosure acts two-dimensionally.

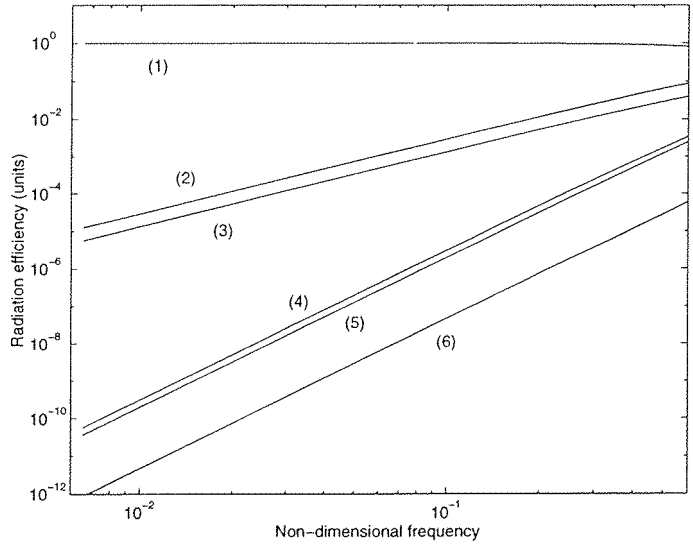

Figure 3.27: The radiation efficiencies of the first six radiation modes for a source whose center is placed at ($x = 0.3$, $y = 0$, $z = 1.9$) and whose size varies from $0.006m$ to $0.6m$ and where the frequency equals $200Hz$.

3.5 Conclusions

To actively control the sound radiation from a vibrating surface it is necessary to have a number of sensors which can accurately measure the sound power radiation. Secondary actuators can then be driven to minimize the measured sound power radiation. There are two mechanisms by which the sound power radiation from structures

may be reduced: (i) the vibration levels are reduced or (ii) the vibrational behaviour is altered such that the radiation efficiency is reduced. It is often difficult in practice to measure the sound power radiation from a structure directly using microphones and as an alternative, structural mode sensors may be used in an attempt to reduce the vibration levels on the structure (strategy (i)). Alternatively, the amplitudes of the radiation modes could be measured using radiation mode sensors and the levels of these could be reduced using secondary actuators (strategy (ii)). The number of significantly excited *structural* modes, at a given frequency, will determine the number of independent secondary sources required to ensure a significant reduction in the *vibration* levels on the structure. The number of significantly radiating *radiation* modes, at a single frequency, will determine the number of independent secondary sources required to ensure that the *radiation* efficiency is significantly reduced. The mechanisms of active control have been discussed more thoroughly by Johnson and Elliott [53] and will be covered in more detail in chapter 5. By determining at a particular frequency the number of efficiently radiating radiation modes and the number of significantly excited structural modes, the engineer can determine the likely success of using either structural mode reduction or radiation mode reduction strategies for controlling the radiated sound power from a vibrating structure.

It has been demonstrated that at low frequencies the radiation modes are grouped into sets with a similar rate of change of radiation efficiency with frequency. The size of these sets is determined by both the dimension of the radiator and the dimension of the field into which the radiator is radiating. The sizes of these sets for the cases of radiation into infinite spaces, considered in section 3.2, are shown in table 3.1. It should be noted that the grouping behaviour of radiation modes is due to the *dimensionality* of the source and the acoustic field but not their shapes. For instance, the radiation modes for a randomly shaped two-dimensional source will exhibit the same grouping behaviour as a rectangular source.

By using a single secondary source to cancel the amplitude of the first radiation mode at low frequency, good attenuations will be achieved in nearly all circumstances. To achieve further reductions the outputs of a number of higher order radiation modes will also have to be cancelled and this implies that for the more complex case of a three-dimensional radiator radiating into a three-dimensional field, three additional

		Dimension of radiator		
		1	2	3
Dimension of field	1	1,1	-	-
	2	1,1,1...	1,2,2,2...	-
	3	1,1,1...	1,2,3,4...	1,3,5,7...

Table 3.1: The number of radiation modes in groups with similar rates of change of radiation efficiency with frequency at low frequencies (same mode order) as a function of source and field dimension.

secondary sources will be required to achieve a significant increase in the attenuation. For the simpler case of a line source radiating into a two or three-dimensional field only a single additional secondary source is required to achieve a significant increase in the attenuation.

The radiation of sound into enclosures has also been investigated. For a fixed source and enclosure geometry the rate of change of the radiation efficiencies of the radiation modes with frequency is the same (approximately) for all of the radiation modes except the first. The relative efficiencies of the radiation modes is dependent on the size of the source in relation to the size of the enclosure. Small source sizes produce large differences in the efficiency of the radiation modes with respect to one another. The rate of change of efficiency of the radiation modes with source size shows a similarity to the behaviour of the radiation modes in a free-field. At high frequencies, when the number of acoustic modes becomes very large, the enclosure becomes "diffuse" and the radiation modes appear to act similarly to the free-field case. The main conclusion is that the active control of the amplitude of the first radiation mode of a panel radiating into an enclosure will achieve better performance for panels that are small compared to the enclosure.

Chapter 4

Distributed piezoelectric transducers

4.1 Introduction to piezoelectric transducers

Piezoelectric materials produce an electric polarization when mechanically stressed (piezoelectric effect) and, reciprocally, produce a mechanical strain when an electrical field is applied (inverse piezoelectric effect) [92]. The piezoelectric effect was first noted in natural crystals by Pierre and Jacques Curie over a century ago [26], and modern piezoelectric materials are widely used as transducers in active control systems.

The work presented in this chapter will concentrate on the use of piezoelectric materials as distributed sensors, but many of the ideas presented in this chapter can be applied to other types of strain sensors.

Most of the strongly piezoelectric materials have crystalline structures and so are brittle and difficult to manufacture into arbitrary shapes. Piezoelectric ceramics are a set of piezoelectric materials that are more versatile than natural crystals as they can be manufactured into a variety of shapes and sizes. They are however brittle, heavy and difficult to manipulate after manufacture. Piezoelectric ceramics are often used as structural actuators because of their high stiffness. They are particularly effective in high frequency applications (acoustic or structural) where only small displacements are necessary. Polyvinylidene fluoride (PVDF), which is a polymer, was found to

have strong piezoelectric properties [56] and also had other useful physical properties. PVDF is lightweight, flexible, can be manufactured into very thin sheets (or films) and can be easily cut into different shapes. Because of these properties, a PVDF sheet can easily be applied to a structure as a surface mounted sensor which measures some distributed function of the surface strain.

Electrical strain gauges, piezoelectric materials and fibre optic refraction gratings [28] can all be used as strain sensors because their physical properties change when a strain is induced in them. Piezoelectric transducers produce a charge, electrical strain gauges change their electrical resistance and fibre optic gauges reflect light of varying frequencies (glass fibres can also be used as strain gauges by measuring the time taken for a beam of light to travel the length of the fibre). All of these effects occur over some finite spatial distance or area. It is often desired that the strain be known at a point on a structure and therefore many of these sensors are designed to be as small as possible. In some applications the desired measurement is of a distributed quantity, for example the amplitude of a structural mode. The amplitude of a structural mode can be approximately measured by processing the outputs of a number of point sensors, but for some applications the number of measurements required becomes prohibitively large. If a system uses a large number of point sensors to measure a distributed quantity all of the sensors must be *matched* and this adds further complexity and cost. It is in these applications that distributed sensors, which measure the integral of the strain over a large area of the structure, may become useful.

Polyvinylidene Fluoride (PVDF) has been widely used to create distributed sensors and actuators for vibration control and structural acoustic control [3, 15, 16, 18, 21, 44, 45, 81]. Many of the earliest applications of PVDF as distributed transducers were for the control of structural vibration. Bailey and Hubbard [3] used a rectangular strip of PVDF as a distributed actuator for the vibration control of a cantilevered beam. The integrated output of an accelerometer positioned at the tip of the beam was used to drive the PVDF actuator in a feedback control system. Using this control system an increase in the damping of the beam was achieved.

Lee [62] developed a "theory of laminated piezoelectric plates for the design of distributed sensors and actuators". This paper is probably the single most important piece of work on distributed piezoelectric transducers. Lee considered most of the

physical possibilities, "bending, torsion, shearing, shrinking and stretching," for a flexible plate and developed the electromechanical relationships for distributed piezoelectric materials under these conditions. Lee also showed that there is a reciprocal relationship for a piezoelectric transducer used as a sensor or an actuator and that this property is "a generic feature of all piezoelectric laminates." Lee and Moon [63] used this theory to design modal sensors/actuators for a cantilevered beam using PVDF film. However, the sensor designed to measure the first structural mode was found in practice to also have a significant sensitivity to the second structural mode of the beam.

Clark and Fuller [18] used two rectangular strips of PVDF in an attempt to sense the odd-odd modes of a plate which are the most efficient radiators of sound. The PVDF sensors were used as error signals in a single frequency feedforward active control system. In the cases presented by these authors, the control system using PVDF sensors produced considerable attenuation on and off resonance.

Gu *et al.* [44] designed PVDF structural modal sensors to measure "a family" of structural modes, for example the amplitudes of the (3,$*$) structural modes where $*$ is an integer. By using a pair of these modal family sensors, one oriented in each direction, a single mode, for example the (3,1) mode, could be measured. The sensor was, however, shown also to be sensitive to other structural modes.

Guigou, Berry and Charette [45, 16] also suggested a method for designing volume velocity sensors for beams and plates using PVDF. The structural modes of the plate are measured experimentally and the sensor is designed to measure the modes of the plate in proportion to their individual contribution to the volume velocity. The sensor was constructed using two shaped strips of PVDF tape, one along each axis. The necessity of experimental modal identification makes this design very "application specific" and sensitive to changes in the plate's behaviour. Snyder *et al.* [81] also created sensors using two strips of PVDF film to measure "transformed modes" or radiation modes. These sensors were also based on a knowledge of the structural mode shapes, although these were calculated analytically.

Distributed piezoelectric transducers can be used both as sensors or actuators and the spatial sensitivity of the transducer remains the same regardless of whether it is

being used to sense or actuate [62, 63]. Most of this chapter will be discussing the production of a volume displacement sensor but in principle such a transducer could also be used as an actuator in which case it would generate a constant force across the surface to which it was attached [53].

4.2 General theory of piezoelectric transducers

For the purposes of this thesis the discussion will be restricted to the use of distributed sensors on thin plates and beams. The relationship between the electrical output of a piezoelectric material and the mechanical strain it undergoes has been thoroughly developed by Lee [62] with a view to the design of distributed sensors and actuators.

All piezoelectric materials have a number of piezoelectric constants which define the relationships between the compressional or shearing strains of the piezoelectric material and an electric field placed (or induced) across any of the three axes. Standard notation uses axes numbered $1, 2$ and 3 and the 3 axis is taken as the axis across which the piezoelectric material is poled. For this work the 3 axis of the piezoelectric will always be taken to be the same as the z axis for the plate or beam (figure 4.1).

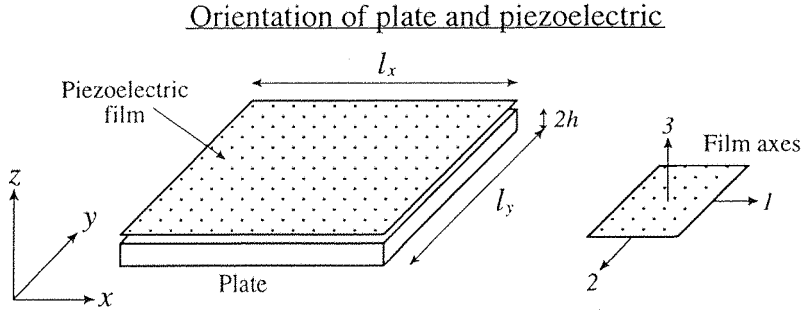

Figure 4.1: The orientation and axes for the plate and the piezoelectric film.

The piezoelectric effect implies that the piezoelectric material can be used to measure strain or, when driven by an electrical voltage, create stresses. The relationship between the electric field and the strain in the material is dependent upon the physical and electrical constraints of the material and therefore the stress levels in the material must also be considered. One form of the constitutive equations is given by [62],

$$\boldsymbol{T} = \boldsymbol{c}^E \boldsymbol{S} - \boldsymbol{e}\boldsymbol{E} \tag{4.1}$$

$$\boldsymbol{D} = \boldsymbol{e}\boldsymbol{S} + \boldsymbol{\epsilon}\boldsymbol{E} \tag{4.2}$$

The stresses along the three axes and the three shear stresses are represented by the vector $\boldsymbol{T}$ which is equal to the 6 by 6 matrix of elastic stiffnesses $\boldsymbol{c}^E$ times the six strains in $\boldsymbol{S}$ minus the 3 by 6 matrix of piezoelectric stress/charge constants $\boldsymbol{e}$ times the electric field intensities across the threes axes $\boldsymbol{E}$. The 3 electric displacements $\boldsymbol{D}$ (charges per unit area) are a function of the vector of strains, the piezoelectric stress/charge constants, the electric field intensities and the 3 by 3 permitivity matrix $\boldsymbol{\epsilon}$.

If a strip of piezoelectric material is attached to the surface of a structure the induced strain in the piezoelectric material can be deduced by measuring the electric displacement across the surface electrodes. In general the electric displacement across the 3-axis of the piezoelectric material is measured to deduce the strain induced along the 1 and 2 axes. The electric field intensities in the 1 and 2 directions will be assumed to be zero. Also due to the geometry of the beam or plate (figure 4.1) the stress/strain in the 3-direction is assumed to be negligible and hence equation 4.2 can be simplified to,

$$D_3 = \epsilon_{33} E_3 + e_{31} S_1 + e_{32} S_2 + e_{36} S_6 \tag{4.3}$$

where e_{31}, e_{32} and e_{36} are piezoelectric constants (coefficients in the matrix $\boldsymbol{e}$), ϵ_{33} is the permitivity and E_3 is the electric field intensity across the z-axis of the film. The subscript 6 on the strain component S_6 refers to shear in the $1-2$ plane. Typical values of the piezoelectric constants for PVDF film are given in table 4.1 [2].

By relating the displacement of the surface of the plate/beam to the strain on the surface the electric displacement due to a given surface displacement can be calculated. Consider a thin rectangular isotropic piate (or beam) having dimensions l_x and l_y, oriented in the x-y plane which has an out of plane displacement w (in the z direction) and inplane displacements u and v in the x and y directions respectively. Consider a piece of piezofilm which is attached to the surface of the plate and covers

the entire surface. The piezofilm is oriented such that the 1 axis of the film is the same as the x axis of the plate. If the film is attached to a charge amplifier, which measures the charge flow while effectively short circuiting the film's electrodes, the contribution due to the E_3 component will be removed. The total charge output (q) of the film, which is the integral over the surface of the electric displacement, can now be written as, [62]

$$q = \int_0^{l_y} \int_0^{l_x} S(x,y) \left[e_{31} \frac{\partial u}{\partial x} + e_{32} \frac{\partial v}{\partial y} + e_{36} \left(\frac{\partial u}{\partial y} + \frac{\partial v}{\partial x} \right) - h e_{31} \frac{\partial^2 w}{\partial x^2} - h e_{32} \frac{\partial^2 w}{\partial y^2} - 2 h e_{36} \frac{\partial^2 w}{\partial x \partial y} \right] \mathrm{d}x\mathrm{d}y \tag{4.4}$$

where h is the film-neutral axis separation and $S(x,y)$ is the spatial sensitivity of the film. The variables u, v and w are all functions of x and y but for simplicity these will not be explicitly expressed in all of the equations. The above equation can be split into two components.

The first component of the charge output is due to the strain caused by the stretching of the midplane of the plate ($\frac{\partial u}{\partial x}$, $\frac{\partial v}{\partial y}$, $\frac{\partial u}{\partial y}$ and $\frac{\partial v}{\partial x}$). If the plate is fixed, then there may be a contribution due to the elongation of the plate when some modes are excited, but this is very small in comparison to the other terms and is generally ignored [63].

The second component is due to the strain caused by the bending of the plate (i.e. $\partial^2 w/\partial x^2$ and $\partial^2 w/\partial y^2$) and is dependent on the distance h between the film and the neutral axis of the plate. Given these conditions and the fact that the value of e_{36} quoted by the manufactures is zero [2] (table 4.1), the equation for the closed circuit charge output q can be simplified to,

$$q = \int_0^{l_y} \int_0^{l_x} -h S(x,y) \left[e_{31} \frac{\partial^2 w}{\partial x^2} + e_{32} \frac{\partial^2 w}{\partial y^2} \right] \mathrm{d}x\mathrm{d}y \tag{4.5}$$

The spatial sensitivity of the film $S(x,y)$ has previously been designed to measure some distributed quantity such as one of the plate's structural modes. The following section will describe the spatial sensitivities required to measure the volume velocity of a plate or beam with fixed boundary conditions.

$e_{31}(N/Vm)$	5.2×10^{-2}
$e_{32}(N/Vm)$	2.1×10^{-2}
$e_{36}(N/Vm)$	0
Young's modulus $Y(Nm^{-2})$	2×10^{9}
Poisson's ratio ν	0.29
Relative permitivity ϵ_{33}/ϵ_0	12
Max. operating field (@ a.c.) $(V/\mu m)$	30

Table 4.1: Constants for PVDF film.

4.3 Volume velocity sensors

It was concluded from the work presented in chapters 2 and 3 that the first radiation mode of a vibrating structure will be the dominant radiator of sound at low frequencies, where the size of the structure is small compared with the acoustic wavelength. It was also shown that the amplitude of the first radiation mode is well approximated by the volume velocity of the source under these conditions. By actively controlling the net volume velocity of a structure it is possible to reduce the level of the the first radiation mode and hence reduce the total sound radiation from the structure at low frequencies.

The sensors described in this section are designed to measure the net volume *displacement* of a structure, but the volume velocity can be easily inferred by differentiating the output of the volume displacement sensor.

The net volume displacement can be defined as,

$$U = \int_0^{l_y} \int_0^{l_x} w(x,y) \mathrm{d}x \mathrm{d}y \tag{4.6}$$

4.3.1 A volume velocity sensor for a beam with fixed ends

To begin, the measurement of the volume velocity of a beam which has fixed ends will be considered. If the beam does not have fixed ends then whole body displacements can occur and these do not cause any surface strain. Therefore, whole body displacements cannot be measured using a strain sensor and hence additional sensors will be required if the ends are not fixed.

For a beam with fixed edges (i.e. pinned or clamped) the displacement w is purely a function of x as there is no bending along the y axis of the beam ($l_x \gg l_y$). By making this assumption equation 4.5 can be further simplified to,

$$q = -hl_y e_{31} \int_0^{l_x} S(x) \frac{\partial^2 w}{\partial x^2} \mathrm{d}x \tag{4.7}$$

It is unnecessary for the sensitivity function $S(x)$ to vary with y since the displacement w is independent of y. By integrating by parts equation 4.7 can be re-expressed as,

$$q = hl_y e_{31} \left[- \left[S(x) \frac{\partial w}{\partial x} \right]_0^{l_x} + \left[\frac{\partial S(x)}{\partial x} w \right]_0^{l_x} - \int_0^{l_x} \frac{\partial^2 S(x)}{\partial x^2} w \mathrm{d}x \right] \tag{4.8}$$

The sensitivity $S(x)$ is defined to be quadratic in the x-direction such that $S(x)$ equals zero when x=0 and x=l_x. This sensitivity was first suggested by Rex [78, 79] and is given by,

$$S(x) = \alpha(l_x x - x^2) \tag{4.9}$$

where α is a constant. Since $S(x)$ has been defined to be zero at x=0 and x=l_x then the first term in equation 4.8 must be zero. Secondly, if the ends of the beam are fixed then the displacement $w(x)$ is zero when x=0 and x=l_x and therefore the second term in equation 4.8 must also be zero. By substituting equation 4.9 into equation 4.8 the charge output can be written as,

$$q = -hl_y e_{31} \int_0^{l_x} \frac{\partial^2 S(x)}{\partial x^2} w(x) \mathrm{d}x = 2hl_y e_{31} \alpha \int_0^{l_x} w(x) \mathrm{d}x = 2he_{31} \alpha U \tag{4.10}$$

By choosing a sensitivity that varies quadratically along the beam the sensor output q is thus directly proportional to the net volume displacement of the beam. If the ends of the beam were not fixed then two additional sensors would be required to measure the whole body displacements at the ends of the beam. This would then allow the calculation of the total volume displacement with arbitrary boundary conditions.

4.3.2 A volume velocity sensor for a clamped plate

Consider a rectangular plate with clamped edges. The plate has variations in its out of plane displacement in the x and y directions and both bending terms in equation 4.5 must be considered.

Equation 4.5 can be separated into two components one describing the charge output due to bending in the x-direction q_x and one describing the output due to bending in the y-direction q_y such that the total charge output q is equal to $q_x + q_y$ [49, 50] where,

$$q_x = \int_0^{l_y} \int_0^{l_x} -hS(x,y)e_{31}\frac{\partial^2 w}{\partial x^2}\mathrm{d}x\mathrm{d}y \tag{4.11}$$

$$q_y = \int_0^{l_y} \int_0^{l_x} -hS(x,y)e_{32}\frac{\partial^2 w}{\partial y^2}\mathrm{d}x\mathrm{d}y \tag{4.12}$$

The inner integral of equation 4.11 can be integrated by parts to arrive at,

$$q_x = he_{31}\int_0^{l_y}\left[-\left[S(x,y)\frac{\partial w}{\partial x}\right]_0^{l_x} + \left[\frac{\partial S(x,y)}{\partial x}w\right]_0^{l_x} - \int_0^{l_x}\frac{\partial^2 S(x,y)}{\partial x^2}w\mathrm{d}x\right]\mathrm{d}y \tag{4.13}$$

$S(x,y)$ is defined to be quadratic in the x-direction such that $S(x,y)$ equals zero when x=0 and x=l_x and that $S(x,y)$ is independent of y.

$$S(x,y) = \alpha(l_x x - x^2) \tag{4.14}$$

where α is a constant. Since $S(x,y) = 0$ at the edges of the plate where $x = 0$ and $x = l_x$ the first component of equation 4.13 is eliminated. If the plate is fixed at the edges (clamped or pinned), $w(l_x, y)$ and $w(0, y)$ will equal zero and therefore the second term in equation 4.13 will also equal zero. The spatial sensitivity given in equation 4.14 can be substituted into equation 4.13 to arrive at an expression for the closed circuit charge output due to bending in the x-direction.

$$q_x = 2he_{31}\alpha\int_0^{l_y}\int_0^{l_x} w(x,y)\mathrm{d}x\mathrm{d}y = 2he_{31}\alpha U \tag{4.15}$$

The output due to bending in the x-direction is therefore proportional to the integrated displacement of the whole surface. It is clear that it is necessary for the output

due to bending in the y-direction (q_y in equation 4.12) to be zero in order for the sensor to measure the integrated displacement of the surface. After some manipulation equation 4.12 can be written, with $S(x,y)$ given by equation 4.14, as [54],

$$q_y = -he_{32}\alpha \int_0^{l_x} S(x,y) \left[\frac{\partial w(x,l_y)}{\partial y} - \frac{\partial w(x,0)}{\partial y} \right] \mathrm{d}x \qquad (4.16)$$

The charge output due to bending in the y direction is therefore dependent on the gradients at the edges of the plate where $y = 0$ and $y = l_y$. For a clamped plate the gradients at these edges (i.e. $\partial w(x,l_y)/\partial y$ and $\partial w(x,0)/\partial y$) are equal to zero and therefore q_y is also zero. The total charge output from the distributed sensor, equation 4.4, will thus be equal to q_x and hence proportional to the integrated displacement of the plate.

4.3.3 A volume velocity sensor for a simply supported plate

For the case of a simply supported plate the gradients at the edges of the plate (i.e. $\partial w(x,l_y)/\partial y$ and $\partial w(x,0)/\partial y$) are non-zero and the q_y component of the charge output must be taken into account. The q_y component can be eliminated by using a matched pair of distributed sensors, the second of which is identical to the first with the exception that the piezoelectric axes are swapped such that the 1 axis of the piezoelectric corresponds to the y axis of the plate (figure 4.2) [49, 50]. The sensitivity functions are the same on both sensors with the same orientation with respect to the x and y axes. Carey and Stulen [15] have also suggested using two PVDF sensors to create a single isotropic sensor. They essentially use the same technique as is being suggested in this section but their objective was to make the sensor equally sensitive to bending in the x and y directions. Our objective is to remove the sensitivity of the sensors to bending in the y direction.

The output of the first sensor q_1, has a component q_x which is proportional to the integrated volume displacement (equation 4.15) and a second component q_y (equation 4.16) which it is necessary to eliminate. The output of the second sensor q_2 will be given by,

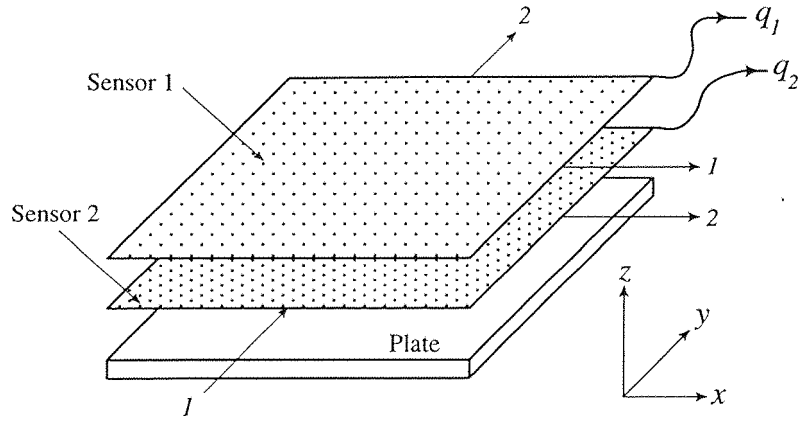

Figure 4.2: The orientation and axes for the sensor configuration required to eliminate the q_y component and hence measure the volume velocity of a simply supported plate.

$$q_2 = \int_0^{l_y} \int_0^{l_x} -hS(x,y) \left[e_{32} \frac{\partial^2 w}{\partial x^2} + e_{31} \frac{\partial^2 w}{\partial y^2} \right] \mathrm{d}x\mathrm{d}y \tag{4.17}$$

This equation is the same as equation 4.5 but with the piezoelectric constants changed around. Using the definitions of q_x and q_y in equations 4.15 and 4.16 the charge output of the second sensor can be written as,

$$q_2 = \frac{e_{32}}{e_{31}} q_x + \frac{e_{31}}{e_{32}} q_y \tag{4.18}$$

If the ratio of the two piezoelectric constants e_{32} and e_{31} are known then the outputs of the two sensors can be combined to eliminate the sensitivity to bending in the y direction.

$$q_0 = q_1 - \frac{e_{32}}{e_{31}} q_2 = q_x \left(1 - \left(\frac{e_{32}}{e_{31}} \right)^2 \right) \tag{4.19}$$

where q_0 is the total output of the two sensors and e_{32}/e_{31} is typically 0.4 [2, 50, 62] so that $q_0 \approx 0.84 q_x$. For this method to be successful the ratio of piezoelectric constants must be accurately known and the two sensors must be fixed to the plate such that they are equally sensitive to any strain on the surface of the plate.

4.3.4 A volume velocity sensor for a plate with arbitrary boundary conditions

The sensors described in the proceeding three sections are designed to measure the volume displacement due to *bending*. If the boundaries of the plate are not fixed then additional sensors will be required to measure the movement of the boundaries. The second term in equation 4.13 will be non-zero if the edges of the plate at $x = 0$ and $x = l_y$ have displacements that are non-zero. The volume displacement sensor described in section 4.3.3 measures the volume displacement relative to these two boundaries. Two one-dimensional volume velocity sensors (section 4.3.1) could be used to measure the volume displacement along these boundaries relative to the corners of the plate. Four accelerometers would then also be required to measure the displacement at the corners of the plate as required to compensate for the second term in equation 4.8. To measure the net volume displacement of a panel with arbitrary boundary conditions using this technique would therefore require seven sensors which would have to be calibrated relative to each other.

The accelerometers could, however, be made from a patch of the same piezoelectric material as the distributed sensor but with a proof mass integrated onto the side not bonded to the plate. Strain effects could be compensated for by using a dummy patch very close to the accelerometer patch. It may also be possible to build distributed accelerometers which measure the average acceleration along an edge of the plate. Using such techniques, would reduce the total number of sensors required to three. Unfortunately the outputs from these accelerometers must still be integrated twice before they can be added to the output of the strain sensor. Even if all transducers could be based on the same piece of piezoelectric film some additional electronics would thus still be required to produce a signal proportional to the volume velocity due to both bending and whole body motion.

4.4 Matched actuators and sensors

In this section some important properties of the transfer response between a distributed actuator and a *matched* distributed sensor will be derived. Matched sensor-

actuator pairs are those in which the spatial distribution of the force input to the structure due to the actuator is the same as that of the spatial sensitivity of the response from the structure at the sensor. Lee [62] showed that there is a reciprocal relationship for any piezoelectric transducer used as a sensor or an actuator. If the closed circuit charge output of a tranducer q is given by,

$$q = \int\int \eta(x,y)w(x,y)\mathrm{d}x\mathrm{d}y \tag{4.20}$$

where $\eta(x,y)$ is the spatial sensitivity to displacement, then the tranducer, when driven by an input voltage u, will excite the structure (which is assumed to have clamped boundary conditions) with a force distribution which is equivalent to,

$$f(x,y) \propto \eta(x,y)u \tag{4.21}$$

where $f(x,y)$ is the equivalent force distribution. Since a single distributed piezoelectric transducer can be operated as either an actuator or a sensor, an identical pair of piezoelectric transducers mounted on either side of the structure would be a good approximation to a matched pair. Alternatively a single piezoelectric actuator can, in principle, be arranged to act simultaneously as both an actuator and a sensor as discussed by Anderson *et al.* [1], Dosch *et al.* [29] and Clark [22], and if such a device could be made to work reliably over a wide range of frequencies it would form an ideal matched actuator-sensor pair.

The complex transverse displacement of a two dimensional structure, $w(x,y,\omega)$, subject to a harmonic excitation at frequency ω, can be represented as a summation of the responses of the structural modes,

$$w(x,y,\omega) = \sum_{i=1}^{\infty} a_i(\omega)\phi_i(x,y) \tag{4.22}$$

where $\phi_i(x,y)$ is the i^{th} mode shape and $a_i(\omega)$ is the amplitude of the i^{th} mode. If the structure is driven by a distributed actuator producing a force distribution on the structure proportional to $\eta(x,y)$, and having an input voltage $u(\omega)$, the resulting amplitude of the i^{th} mode can be written as,

$$a_i(\omega) = u(\omega)A_i^s(\omega)\int\int \phi_i(x,y)\eta(x,y)\mathrm{d}x\mathrm{d}y \tag{4.23}$$

where $A_i^s(\omega)$ is a second order resonance term, which has a maximum response at the natural frequency of the i^{th} mode and is given by,

$$A_{mn}^s = \frac{1}{2\rho_p h[(\omega_{mn}^2 - \omega^2) - j\omega D_{mn}]} \tag{4.24}$$

where ρ_p is the density of the plate, h is half the thickness of the plate, ω_{mn} is the natural frequency of the mn^{th} structural mode and D_{mn} is the damping of the mn^{th} mode and is given by $D = 2\xi\omega_{mn}$. It is assumed that a distributed sensor is implemented whose sensitivity to transverse displacement is identical to that of the distributed actuator. The complex output of this sensor, $q(\omega)$, will then be,

$$q(\omega) = \int\int w(x,y,\omega)\eta(x,y)\mathrm{d}x\mathrm{d}y \tag{4.25}$$

and using equations 4.22 and equation 4.23 this output can be written as [34, 33],

$$q(\omega) = u(\omega)\sum_{i=1}^{\infty} A_i^s(\omega)\left[\int\int \phi_i(x,y)\eta(x,y)\mathrm{d}x\mathrm{d}y\right]^2 \tag{4.26}$$

The term in squared brackets must be real and positive for all of the structural modes and can be written as C_i. The transfer response between the actuator and the matched sensor can thus be written,

$$G(\omega) = \frac{q(\omega)}{u(\omega)} = \sum_{i=1}^{\infty} A_i^s(\omega)C_i \tag{4.27}$$

The phase of each of the modal contributions to the transfer response will thus be equal at their respective natural frequencies. Another way of expressing this property, in the Laplace domain, is that between each of the poles of the transfer response due to the structural modes, there must be zeros [83]. The consequence of this pole-zero structure in the transfer response is that there is no accumulation of phase with increasing frequency. Because all of the zeros of the transfer response are also on the left hand half of the s-plane [83] the response is *minimum phase* [12]. If the output of the transducer is differentiated to give a velocity response, the phase of the

transfer response between the matched transducers will lie between $+90^{o}$ and -90^{o}, and thus the real part of the response will be entirely positive. The implications of this minimum phase property in the design of active control systems will be discussed in section 5.4.5.

The fact that the transfer response of a pair of matched distributed transducers can be made to have an entirely real response is a generalization of the properties of co-located point transducers described by Balas [4], and shares the property of unconditional stability when implemented in a feedback loop. In practice the performance is always limited by the presence of some additional transducer dynamics. It should be finally noted that a whole family of such transducer pairs could be implemented, for example, to measure structural modes. In this case the shaping function of the i^{th} mode shape would be $\eta_i(x,y) = \phi_i(x,y)$, the transfer response would be proportional to $A_i^s(\omega)$ and only the i^{th} sensor would, in principle, would respond to the i^{th} actuator, if the modes were orthogonal. Alternatively a set of matched transducer pairs could be implemented to measure the radiation modes of a structure [33]. In this case however, each sensor would not only respond to its corresponding matched actuator, but in general, would also respond to other actuators. This interaction is not expected to be large however, and it may still be possible to implement stable independent feedback control loops around each actuator/sensor pair.

4.5 Creating an etched piezoelectric film sensor

The design of a two dimensional volume velocity sensor requires a quadratically weighted piezoelectric film. This section is concerned with exploring the practical methods of achieving a quadratically weighted sensitivity. Potentially, spatial weighting could be achieved by varying the distance between the film and the neutral axis of the beam or plate during manufacture. Varying the sensitivity can also be achieved by *doping* or mixing PZT powder with the PVDF matrix [63] or by varying the poling voltage during manufacture. To accomplish these tasks after manufacture, however, is much more difficult but was required here since only commercial uniform sensitivity film was available.

The easiest method for creating a spatial weighting is to cut or etch shapes or strips

into the piezoelectric film. Piezoelectric film is covered with a thin layer of metal which acts as an electrode. The piezoelectric material by its nature has a very high impedance and hence the electrical output will be due purely to areas that are covered by the metal electrode. The electrode can be etched away to produce shaped strips which change the area over which the film is sensitive. To approximate a continuous spatial weighting some of the electrode can be removed where low sensitivity is required and left intact where high sensitivity is required. This in effect keeps $S(x, y)$ constant and instead varies the area over which the integral operates (equation 4.5).

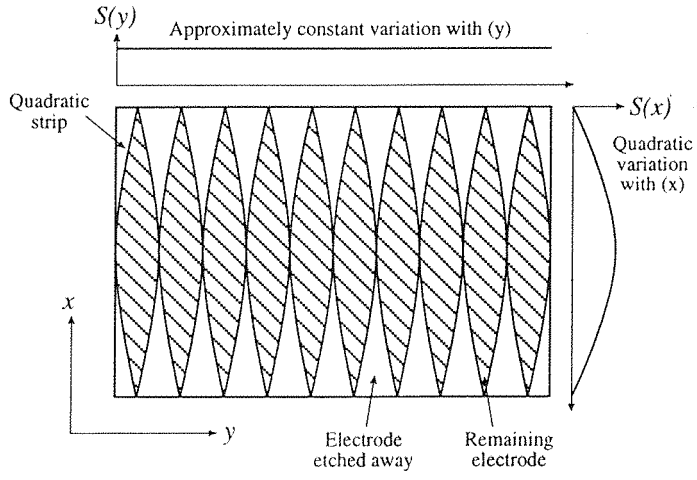

Figure 4.3: A number of quadratically shaped strips etched into the electrode of a piece of piezoelectric film.

To approximate a quadratic sensitivity in the x direction a number of strips whose width varies quadratically with x can be etched into the surface electrode of the film (figure 4.3). If the strips have a sufficiently small width then they will not experience a large change in displacement from one side of the strip to the other. If the wavelength of a structural mode is large compared to the width of the strip this assertion will hold. It is therefore necessary to produce thinner strips to accurately measure higher order modes. This configuration will approximate a quadratically weighted sensitivity in the x-direction while maintaining a constant sensitivity in the y-direction. A quadratic function in the x direction can also be approximated by dividing the surface into a large number of small rectangular strips which could be etched away such that the density of these strips in the x direction varies quadratically (figure 4.4).

To create a reasonably accurate template with which to etch the piezofilm a laser

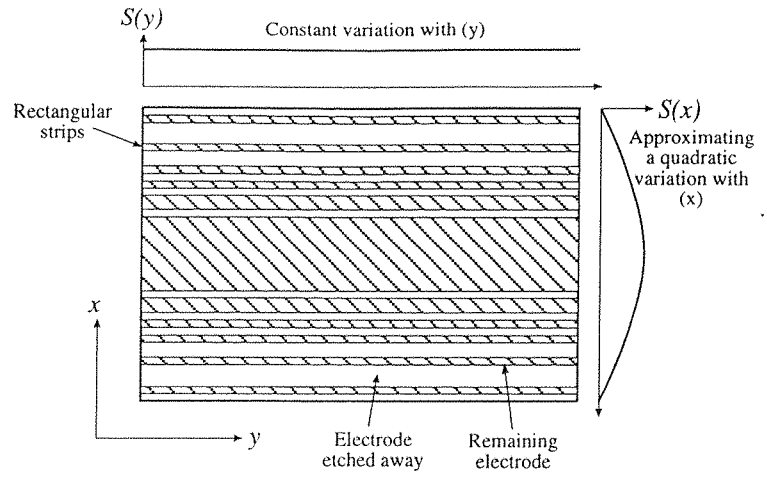

Figure 4.4: A number of rectangular strips etched into the electrode of a piece of piezoelectric film.

printer can be used to print the required image. This image can then be enlarged or reduced, to the required dimensions, onto a transparency. This transparency can then be used as a positive template with which to etch the film using standard circuit board etching techniques. Usually film with copper/nickel metallization is used for etching. It should be noted that the layer of metallization on the film is very much thinner than that covering a circuit board and hence diluted etching solutions should be used.

4.6 Error analysis

The shaping of the electrode surface to create a piezofilm sensor will inevitably produce errors which will affect the performance of the sensor. It is important before manufacture to investigate the sensitivity of the sensor's performance to certain types of error in the manufacture of the sensor. This will allow performance targets to be set for the accuracy of etching required to produce a suitable sensor. It may also be possible to formulate a design which is robust to errors in manufacture and to avoid highly sensitive designs. It is interesting to compare the likely performance errors of a shaped PVDF sensor with the errors to be produced by using an array of point sensors [49, 50]. Some work has been done very recently by Burke *et al.* on transducer tolerance which supports much of the work presented here [13, 14].

The sensitivity of a distributed sensor to errors in design, manufacture, etc. is very case-specific as it depends heavily on the type of structure, the required sensitivity and the definition of "error" that is used. In this section errors in the sensitivity of a volume velocity sensor will be examined but a general theory of transducer sensitivity will not be attempted.

The design of a volume velocity sensor is qualitatively different from many of the distributed modal sensors that have been suggested [15, 63] in that it does not make any assumptions about the structural mode shapes or of the structural properties of the plate. This is important, because experimentally many structural mode sensors have been found to be inaccurate [63, 44, 16] and this may be due to the actual mode shape being significantly different than the theoretical mode shape rather than due to design or etching errors. Because the volume velocity sensor does not assume any particular mode shapes then the errors may be less sensitive to altering structural characteristics. This is borne out experimentally as described in chapter 7.

To quantify the sensor "error" due to etching approximations or other implementation errors it is first necessary to define an error criterion. For a distributed sensor there are a number of different valid error criteria and the definition of the sensing error must reflect the conditions under which the sensor is likely to be applied.

It is assumed that the volume velocity sensor is bonded to a simply supported rectangular plate whose surface displacement can be represented by a modal summation given by,

$$w(x,y) = \sum_{n=0}^{\infty} \sum_{m=0}^{\infty} a_{nm} \phi_{nm} \tag{4.28}$$

where a_{nm} is the amplitude of the nm^{th} structural mode whose eigenfunction ϕ_{nm} is given by,

$$\phi_{nm} = \sin\left(\frac{n\pi x}{l_x}\right) \sin\left(\frac{m\pi y}{l_y}\right) \tag{4.29}$$

where the plate has dimensions l_x and l_y. Assuming the frequency of oscillation ω is known, the volume velocity can be calculated from the spatially averaged surface displacement given by,

$$\overline{w}_{nm} = \frac{a_{nm}}{l_x l_y} \int_0^{l_y} \int_0^{l_x} \phi_{nm} \mathrm{d}x\mathrm{d}y \tag{4.30}$$

where $\overline{w}_{nm}$ is the space averaged displacement of the plate due to the nm^{th} structural mode. This is the quantity we would ideally like to measure (volume displacement). The volume displacement of any even mode will be zero since half of their surface areas will be oscillating out of phase with the other half. For odd-odd modes (n and m are both odd), the spaced averaged displacement $\overline{w}$ is the sum of the modal contributions given by,

$$\overline{w} = \sum_{n=0}^{\infty} \sum_{m=0}^{\infty} \frac{4a_{nm}}{\pi^2 nm} \quad n \text{ and } m \text{ are odd} \tag{4.31}$$

since the integral of displacement over an odd-odd mode shape (equation 4.30) is $4/\pi^2 nm$.

The ideal sensor will therefore only measure the odd-odd modes such that the response to each mode is proportional to the mode amplitude divided by nm. The error can be considered as the deviation of a sensor's response from the ideal response. How this deviation is calculated may depend on the particular application considered. Certain modes in a particular application may be unimportant and hence measurement errors of that mode may also be of little significance. The ideal response, equation 4.31, considers the response to an infinite number of structural modes when practically, only a finite number can be considered. For this application the response of a given design will be compared with the ideal response to the structural modes up to and including $n = 7$ and $m = 7$. The sensor responds to a large number of modes and it is possible to have two measurement errors that cancel each other depending on the relative excitation of the structural modes. It is important at this stage not to assume specific structural mode amplitudes and the error will be defined as the standard deviation of the sensor's response from the ideal response. The sensor's response is normalized such that the sensitivity to the first structural mode is the same as the ideal sensor response. What is important in any specific application is to be able to measure the *relative* volume velocity contributions from the contributing modes. If the relative volume velocity contributions from forty nine modes, all excited to the same extent, can be accurately measured then the sensor should be able to

accurately measure the volume velocity due to any combination of modes likely to be encountered in practice, assuming the amplitudes of high order modes are low. Therefore, this method tests the sensor in a worse case scenario. The normalized sensor response is given by q_o and the normalized error E is given as,

$$E = \frac{\left[\frac{1}{NM-1}\sum_{n=1}^{N}\sum_{m=1}^{M}\left(q_{o_{nm}} - \overline{w}_{nm}\right)^2\right]^{1/2}}{\left[\sum_{n=1}^{N}\sum_{m=1}^{M} q_{0_{nm}}\right]^{1/2}} \tag{4.32}$$

where $\overline{w}_{nm}$ is the spaced averaged displacement of the nm^{th} structural mode, $q_{o_{nm}}$ is the normalized sensor response to the nm^{th} mode and $N = M = 7$. When considering specific applications, this error calculation method may or may not be very useful. The intention here is to explore the possibility of accurately sensing the volume velocity of a large number of structural modes and to provide an understanding of design sensitivity to errors.

4.6.1 Errors in the rectangular strip method

The rectangular strip design produces the desired sensitivity in the y-direction and makes all of its approximations in the x-direction. Unlike the quadratic strip method the rectangular strip method does not have a well-defined mathematical shape that is to be approximated. The accuracy of this design is due to the number of rectangular strips that can be used and the designs have to be carefully chosen. It is assumed that there are a fixed number of uniform elemental strips which can each be active or inactive so that broader strips are generated by activating a number of adjacent elements. There can easily be an astronomical number of combinations of activated and deactivated strips (a hundred elements gives the possibility of 2^{100} different designs) and the selection of a suitable design can be difficult. The design is selected to match a suitable error criterion. Figure 4.5 shows the sensitivity of a sensor optimized to accurately measure the volume displacement of the structural modes up to and including those of seventh order. This graph shows the sensor's response to the (n,1) mode where n is varied from one to fifteen. The sensor's sensitivity to modes not included in the optimization process is very large. To solve this problem larger numbers of modes must be included in the optimization process but this will

inevitably effect the accuracy of the sensor [50]. These findings have been supported in a recent paper by Burke and Sullivan [13]. Because of the sensitivity of this method this design was considered unsuitable and further error analysis will concentrate on the quadratic strip design.

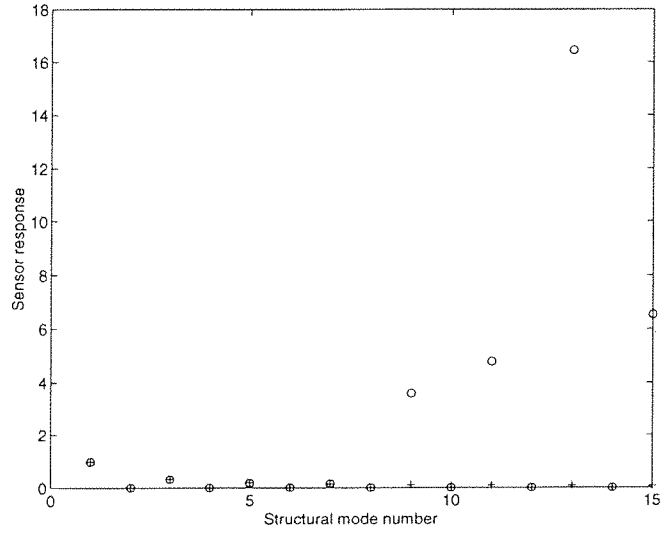

Figure 4.5: The ideal (+) and actual (o) response of a sensor using a rectangular strip design with 240 elements and optimized to measure the volume displacement of the structural modes up to and including those of seventh order.

4.6.2 Errors in the quadratic strip design

The sensitivity of the quadratic strip sensor to four possible sources of error will be considered,

- The error caused by approximating a smooth quadratic curve with a matrix of digitized points.
- Errors due to etching mistakes.
- The error inherent in the design i.e. a finite number of strips.
- Errors due to the ill positioning of the sensor on the plate.

Errors due to digitization

The ideal quadratic strip has a width that varies quadratically with x. To produce a template for etching the piezofilm sensor a laser printed approximation to this ideal shape was used. Initially it is assumed that there are a very large number of strips and that there is perfect positioning and perfect etching. Therefore, any errors in sensing will be due to the digitization of the quadratic shape (figure 4.6). Figure 4.7 shows the sensing error E due to a variation in the number of elements in the y-direction from ten to one thousand. The number of elements in the x-direction will be in practice be much larger than the number of elements in the y-direction and it is therefore the number of elements in the y-direction that will be the significant source of error. Because the error criterion only considers a finite number of modes there is some variability in the error as a function of the number of elements but the overall trend is linear. For a design which uses twenty five strips and covers an A4 piece of paper ($210mm$ by $190mm$ design was used in this work) the number of elements across a single strip using a laser printer is about 200 for a 600dpi printer. This corresponds to a sensing error of the order of 6×10^{-4}.

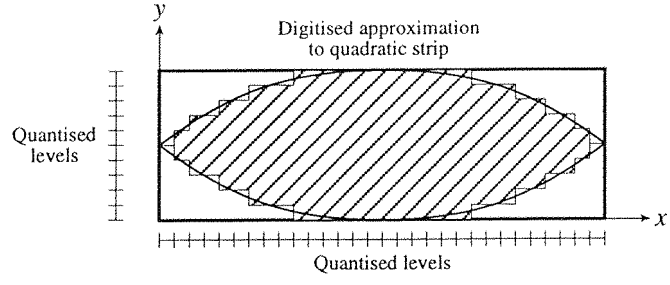

Figure 4.6: The digitized approximation to a continuous quadratic strip.

Errors due to etching mistakes

The errors due to etching mistakes is clearly the most difficult to assess. There is the possibility of the electrode being etched away in positions that it is not supposed to be and the reverse case may also occur. However, if a small area of electrode that is supposed to be etched is not etched, then it will not contribute to the sensor output unless it is electrically connected. Therefore isolated unetched areas of electrode will

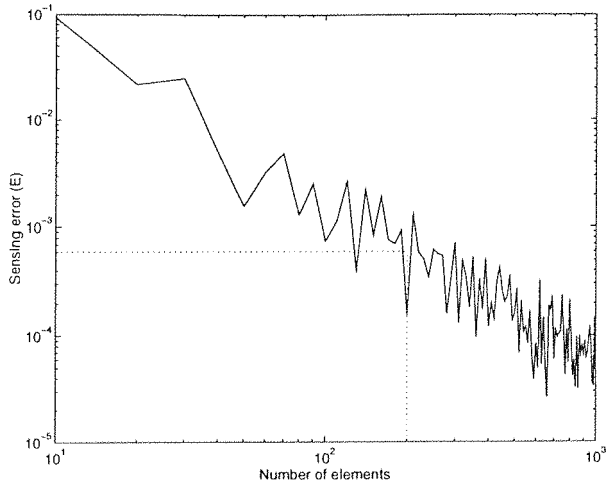

Figure 4.7: The sensing error E due to the digitization of the quadratic strip as a function of the number of elements across each strip. The dotted line shows the error for a design using 200 elements.

not contribute to the sensing error. It is only at the edges of the quadratic strips that remaining electrode areas will be a problem.

The removal of etched areas where they are supposed to remain is a more likely source of sensing error. The erroneous removal of electrode area is most likely to occur at the edges of the quadratic strip. The sensing errors due to this are similar in nature to the errors due to the digitization of the strips. The difference being that the errors occur randomly and are different on every strip. It is difficult to formulate a clear definition of the etching errors for simulation purposes and for this work it is assumed that the etching errors act essentially like digitization errors. For the simple etching technique used for this work an accuracy of up to $0.1mm$ is quoted in the instruction leaflet for RS Positive Photoresist and that is equivalent (for a $250mm$ wide sensor) to an error to length ratio of 4×10^{-4}. This corresponds to the error due to a design using 100 elements per strip as shown in figure 4.7. A 600dpi laser printer has an error to length ratio that is smaller than this (10^{-4}) and therefore it is assumed that the etching errors will be the limiting factor which, from figure 4.7 will produce a worst case sensing error of about 2×10^{-3}.

Errors due to the number of strips used

The error due to the number of strips used is essentially a sampling problem. The structural waves are "sampled" at a number of points and this produces a sensing error. Aliasing should not be a problem as long as the number of strips used is significantly larger than the highest mode order. Because the strips have finite width and do not act as "points" the error calculated by considering them to act as points produces an over-estimate of the error. The results can therefore be considered conservative. Figure 4.8 shows the sensing error E as a function of the number of strips used. By using 25 strips in the design it can be ensured that the sensing error, due to there being a finite number of strips, is smaller ($\approx 2 \times 10^{-4}$) than the other sources of error.

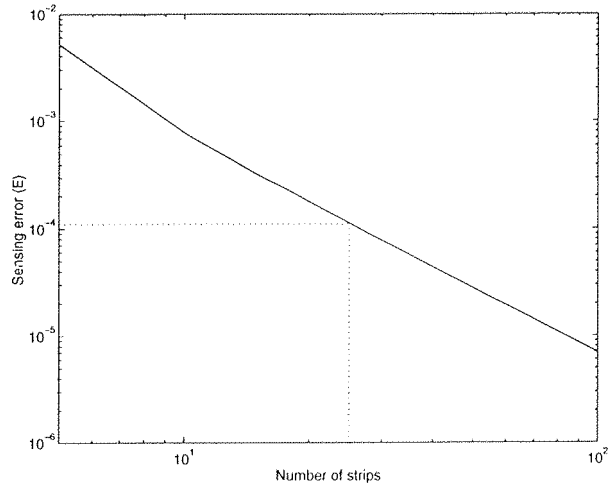

Figure 4.8: The sensing error E as a function of the number of quadratic strips used. The dotted line shows the error for a design using 25 strips.

Errors due to ill-positioning of sensor

The sensing errors due to ill-positioning of the sensor in the x and y directions on to the plate are shown in figure 4.9 and it is assumed that the sensor is the same size as the plate. The sensor seems to be reasonably tolerant to positioning errors with comparatively small sensing errors occurring for positioning errors of up to one hundredth the length of the sensor. If the sensor is position within one percent of the

total length of the sensor (i.e. +/- 2.5mm) then the errors due to positioning should be small in comparison to other sources of error.

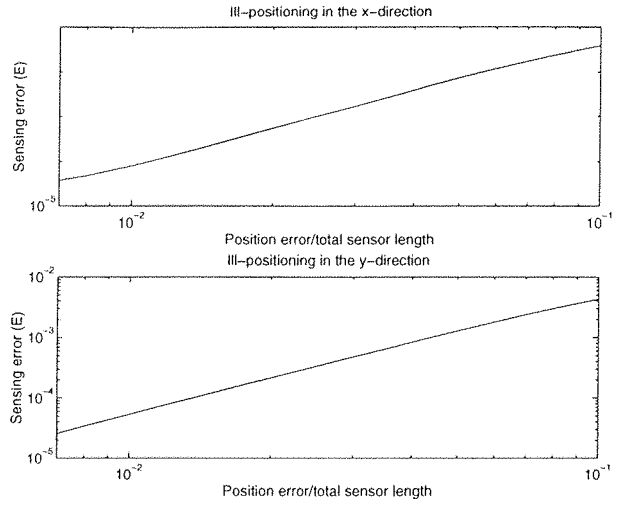

Figure 4.9: The sensing error E as a function of the positioning errors in the x and y-directions. The positioning errors are quoted as a fraction of the total sensor length.

If a sensor was larger than the vibrating surface of a clamped plate, such that the edges of the sensor were positioned under the clamp, then the sensor would not be affected by small changes in position. However, the clamping of piezoelectric film can damage the sensor and for this reason the sensor was designed to be the same size as the exposed vibrating surface of the plate.

4.7 Conclusions

Piezoelectric material and in particular PVDF film can be used as distributed transducers to measure the integral of some distributed quantity (i.e. strain, displacement). By shaping the surface electrode of the film any desired spatial sensitivity can be approximated. A sensor which has a spatial sensitivity that varies quadratically along one of the principle axes will measure the volume displacement of the plate or beam to which it is attached, assuming the plate/beam has fixed edges. For the case of a simply supported plate the design requires two films with different alignments of the piezoelectric axes to produce a true volume displacement sensor. The design of a volume displacement sensor does not make any assumptions about the physical

properties of the plate/beam that is being considered and this property suggests that the sensor will be very robust to changes in the structural properties of the panel. Structural mode sensors are designed to measure some specific mode shape and are therefore very sensitive to any change in the mode shape which may occur due to changes in structure properties or boundary conditions. A volume displacement sensor has the advantage of measuring a quantity that has contributions from many structural modes and is not designed to measure a specific structural mode shape. A change in structural mode shape may change a structural mode's contribution to the volume displacement but does not necessarily alter the accuracy with which the volume displacement is measured.

Two basic designs for shaping the surface electrode have been investigated with the quadratic strip method being chosen over the rectangular strip method on the basis of sensitivity to implementation errors. The errors due to etching mistakes have been shown to be the most likely to effect the overall sensor accuracy. The assessment of the sensing error was intended to give an indication of the sensor's performance over a broad range of applications. The expected accuracy of the sensor (sensing error of 2×10^{-3} as defined by equation 4.32) is equivalent to the accuracy that would be expected using an 8×8 array of matched transducers. If the etching accuracy could be improved such that the limiting error was the digitization of the template then an 11×11 array of matched sensors would be required to produce an equivalent accuracy. Large numbers of matched sensors could be expensive and require a large processing capability.

The volume velocity of a surface, which can be easily inferred from the volume displacement of a surface, is responsible for the majority of the sound power radiation from that surface at low frequencies and therefore by eliminating this quantity the sound power radiation should be reduced. In an active control system a volume velocity sensor could be used as an error sensor for the active reduction of sound power radiation from panels at low frequencies.

The reciprocal nature of the piezoelectric effect allows a transducer designed as a volume velocity sensor to be used as a distributed actuator which will create a uniform force over the surface of the plate. A matched pair of transducers (i.e. a volume velocity sensor and a uniform force actuator) will exhibit minimum phase character-

istics which would, in principle, allow an arbitrarily large feedback gain to be used in a negative gain feedback system without causing instability. The acoustic performance of volume velocity cancellation, with compact and constant force actuators is discussed in chapter 5.

Chapter 5

A theoretical comparison of various active control strategies

5.1 Introduction

The purpose of this chapter is to examine various active control strategies for the reduction of sound transmission through a flexible panel. In particular, the cancellation of volume velocity as an active control strategy for reducing the sound transmission will be investigated. The intention is to actively drive a secondary actuator, which is placed on the structure, to thereby alter the structure's vibrational behaviour such that there is a reduction in the radiated sound power. Cancellation of volume velocity has been suggested as a simple control strategy that would achieve good attenuations in the low frequency region without requiring a complex control system [45, 49].

For the analysis of the control strategies considered here the radiation of sound will be explained in terms of radiation modes [33] (chapter 2). The net volume velocity of a panel is a good estimate of the amplitude of the lowest-order radiation mode which in the low frequency region accounts for the majority of the sound power radiated. Volume velocity can be measured using a single distributed transducer (chapter 4) [45, 49, 54, 80] which can be used as an error sensor in a single channel feedforward active control system for controlling the sound radiation from a vibrating surface. The advantages of this technique are that: (i) only a single surface mounted error sensor is required instead of a number of microphones placed in the acoustic field

[17, 18, 43] and (ii) the control strategy does not need to be tailored specifically for each application.

For the purposes of comparing various control strategies, the radiation from a thin rectangular panel mounted on a baffle and excited by a harmonic plane wave is modelled using computer simulations. Both the sound radiation by the panel into free space and the sound radiation by the panel into enclosures will be considered. A small piezoelectric actuator, placed on the panel, acts as a secondary source which will be adjusted according to four control strategies: (i) to drive the volume velocity of the panel to zero, (ii) to minimize the sound power radiation (optimal strategy), (iii) to minimize the vibration at a point and (iv) to minimize the total kinetic energy of the structure. The second strategy, which is difficult to implement practically, will act as a benchmark against which the performance of the other strategies can be viewed. It is also important to consider the effects of actively controlling the sound transmission through the panel on the sound levels in the near field of the panel and on the structural vibration levels. An increase in the near field sound pressure level could affect an observer positioned near the panel and an increase in the vibration level could increase the fatiguing of the structure and could also cause the structure to exhibit non-linear behaviour.

5.2 Theory

In this section the theory of sound transmission through a thin panel will be developed. The theoretical models of plate excitation by various sources will be described (acoustic and structural sources) as will the model for calculating the sound power radiated by a vibrating plate and the control strategies used to effect control.

5.2.1 Plate excitation due to an incident plane wave

The excitation of a plate due to an incident plane wave can be calculated analytically. The analysis presented here will follow the work of Wang and Fuller [88]. Figure 5.1 shows the co-ordinate system used and the various dimensions and angles used in the analysis. A harmonic plane wave incident on a rigid plate at angles θ and φ will

create a pressure field p_i in the plane of the plate given by,

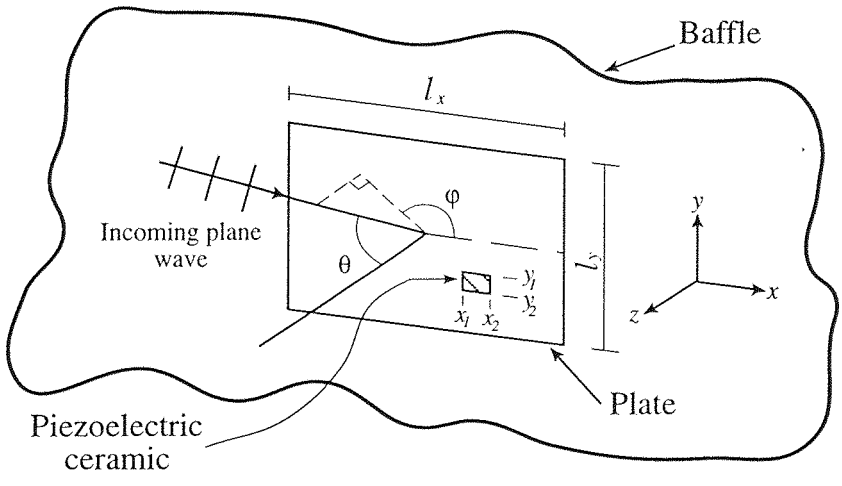

Figure 5.1: The plate configuration used in the numerical experiments

$$p_i(x,y,t) = 2P_i e^{j(\omega t - k_x x - k_y y)} \tag{5.1}$$

where P_i is the amplitude of the incident plane wave which has a wavenumber in the x-direction given by $k_x = -k\sin(\theta)\cos(\varphi)$ and a wavenumber in the y-direction given by $k_y = -k\sin(\theta)\sin(\varphi)$ where k is the wavenumber. For simplicity it will be assumed that the dynamics of the plate do not affect the forcing due to the incident wave and that the pressure on the plate's surface is the same as that for a rigid plate.

For a harmonically excited simply supported panel the displacement of the surface $w(x,y)$ can be described as a sum of modes with sinusoidal mode shapes [89].

$$w(x,y) = \sum_{m=1}^{\infty}\sum_{n=1}^{\infty} a_{mn}\sin(\frac{m\pi x}{l_x})\sin(\frac{n\pi y}{l_y}) \tag{5.2}$$

where the amplitude of the mn^{th} mode is given by a_{mn} and l_x and l_y are the dimensions of the panel in the x and y directions.

The amplitude of a particular mode a_{mn} will be determined by to two main factors: (i) the forcing of the mode F_{mn} due the geometric coupling between the acoustic and structural waves multiplied by the amplitude of the acoustic wave and (ii) the complex resonance term A^s_{mn} which takes into account the frequency of excitation and will be

a maximum where the frequency of excitation matches the natural frequency of the mode. The mode amplitude can therefore be written as

$$a_{mn} = A^s_{mn} F_{mn} \tag{5.3}$$

The complex resonance term is given by,

$$A^s_{mn} = \frac{1}{2\rho_p h \left[(\omega^2_{mn} - \omega^2) - j\omega D_{mn}\right]} \tag{5.4}$$

where ω_{mn} is the natural frequency of the mn^{th} mode, ρ_p is the density of the plate material, h is half the thickness of the plate and D_{mn} is the damping of the mn^{th} mode and is given by $D = 2\xi\omega_{mn}$ (where ξ is the damping ratio). The natural frequencies of the plate, ω_{mn}, can be calculated using standard plate theory [89].

The forcing term for the mn^{th} mode due to an incident wave, F^i_{mn}, is given by,

$$F^i_{mn} = 8 P_i I_m I_n \tag{5.5}$$

where I_m and I_n are due to the geometric coupling between the plane wave and the m and n modes. I_m is given by [88],

$$I_m = \frac{m\pi \left[1 - (-1)^m e^{-j \sin\theta \cos\varphi (\omega l_x / c)}\right]}{[m\pi]^2 - [\sin\theta \cos\varphi (\omega l_x / c)]^2} \tag{5.6}$$

If $m\pi = \pm \sin\theta \cos\varphi (\omega l_x / c)$ the numerator and denominator of the above equation become zero and I_m in this case will be given by,

$$I_m = \frac{j}{2} sgn(\sin\theta \cos\varphi) \tag{5.7}$$

where sgn denotes the sign of the bracketed quantity (i.e. $+1$ or -1). Similarly, I_n is given by,

$$I_n = \frac{n\pi \left[1 - (-1)^n e^{-j \sin\theta \sin\varphi (\omega l_y / c)}\right]}{[n\pi]^2 - [\sin\theta \sin\varphi (\omega l_y / c)]^2} \tag{5.8}$$

and if $n\pi = \pm \sin\theta \sin\varphi (\omega l_y / c)$,

$$I_n = \frac{j}{2} sgn(\sin\theta \sin\varphi) \tag{5.9}$$

These terms can be collected together to determine the mode amplitudes due to the incident wave a^i_{mn},

$$a^i_{mn} = A^s_{mn} F^i_{mn} \tag{5.10}$$

For the simulations carried out in section 5.4 of this chapter eighty one modes ($m =$ 1 to 9, $n = 1$ to 9) were used in the modal summation. This gave a reasonable approximation of the behaviour of the plate over the frequency range of interest.

For the results presented in section 5.4 of this chapter only a single acoustic plane wave was used as a primary excitation. Other more complex acoustic excitations can be created by summing together the contributions from a number of incident plane waves. For example, diffuse acoustic fields comprising a large number of plane waves each with random angles of incidence, amplitudes and phases have been used as primary excitations. The results however are not dissimilar to those where a single incident plane wave has been used.

5.2.2 Plate excitation due to a piezoelectric actuator

A piezoelectric patch placed with edges defined by the lines x_1, x_2, y_1 and y_2 as shown in figure 5.1, was used as a control source. The strain at the surface of a thin, flat, isotropic plate is proportional to the second derivative of displacement (out of plane) with respect to x and y [49]. The forcing of each mode is therefore due to the integral, over the area of the piezoelectric, of the second derivative of the displacement due to that mode (chapter 4).

The resulting modal forcing co-efficients F^c_{mn} are given by [88],

$$F^c_{mn} = Cu \left[\frac{(m/l_x)^2 + (n/l_y)^2)}{mn} \right]$$

$$\left[\cos(\frac{m\pi x_1}{l_x}) - \cos(\frac{m\pi x_2}{l_x}) \right] \left[\cos(\frac{n\pi y_1}{l_y}) - \cos(\frac{n\pi y_2}{l_y}) \right] \tag{5.11}$$

where u is the complex input signal to the piezoelectric and C is a constant which is a function of the material properties of the plate and the piezoelectric, the thickness of the plate and the piezoelectric and the piezoelectric constant of the piezoelectric material. A more complete analysis of the behavior of piezoelectric transducers is given in chapter 4 and by Lee [62].

The total forcing of the structure and hence the structural vibration, will be a superposition of the forcing due to the incoming plane wave (equation 5.5) and the forcing due to the secondary actuator (equation 5.11) i.e. $F_{mn} = F^i_{mn} + F^c_{mn}$. In an attempt to achieve some desired response the control system varies the input voltage to the secondary actuator such that some cost function is minimized.

5.2.3 Radiation of sound from a vibrating plate using a near field approach

The radiation of sound from a vibrating plate mounted on an infinite rigid baffle can be calculated by integrating over the far field the superposition of the acoustic fields radiated by each of the structural modes [88]. This process is mathematically tedious and a near field approach was adopted for this work. The vibration of the surface was approximated by a finite number of elements whose sound power radiation can be calculated using a matrix of acoustic transfer impedances (equation 2.11). The far field method is also an approximation since it requires the summation of a finite number of structural modes. If a sufficiently large number of elements are taken in the near field model then the accuracy will be comparable to that of the far field approach (section 5.4.1). The near field elemental model is also easier to interpret and allows simple calculation of near field pressure levels and optimal control values (section 5.3).

The power radiated by a vibrating panel can be expressed in terms of the velocities of a number of elemental radiators as outlined in chapter 2. In particular equation 2.11 provides a convenient way of calculating radiated power if the acoustic transfer impedances between elements are known. For sources mounted on an infinite baffle in free space the transfer impedance between two elements Z_{ij} is given in equation 2.12. For a specific planar source geometry all of the inter-elemental distances r_{ij}

can be calculated and the acoustic resistance matrix $\boldsymbol{R}$ can thus be calculated using equation 2.13.

The elemental velocities $\boldsymbol{v}$ can be calculated using a summation of a finite number of structural modes whose amplitudes are determined by the contributions from both the primary and secondary sources. The mode amplitude of the mn^{th} mode due to both primary and secondary sources will be given by,

$$a_{mn} = A^s_{mn}[F^i_{mn} + F^c_{mn}] \tag{5.12}$$

If the velocity of an elemental source is taken to be the plate velocity at the centre of the corresponding element then the elemental velocity can be derived by substituting the co-ordinates of the elemental position into the equation for displacement (equation 5.2) and multiplying by $j\omega$ to convert displacement to velocity,

$$v_i = j\omega \sum_{m=1}^{M} \sum_{n=1}^{N} a_{mn} \sin(\frac{m\pi x_i}{l_x}) \sin(\frac{n\pi y_i}{l_y}) \tag{5.13}$$

where x_i and y_i are the co-ordinates of the i^{th} element and M and N are the number of modes used in the modal summation ($M = N = 9$ in the simulations carried out in this chapter). It is also possible to define a set of elemental velocities due only to the incident plane wave $\boldsymbol{v}^i$ and due to the secondary control force $\boldsymbol{v}^c$ by using the individual mode amplitudes a^i_{mn} and a^c_{mn} instead of a_{mn} in the above equation. These velocity vectors can then be used to calculate the power radiation due to any source acting on its own.

5.2.4 Radiation into enclosures

The radiation of sound power into an enclosure due to a vibrating surface is dependent on the mode shapes and the natural frequencies of the acoustic modes of the enclosure (section 3.4.1). The amplitudes of the acoustic modes $\boldsymbol{b}$ is given by,

$$\boldsymbol{b} = \boldsymbol{A}^a \boldsymbol{\Psi}^T \boldsymbol{v} \tag{5.14}$$

where the elemental velocities are given by the vector $\boldsymbol{v}$, the mode shapes over the

radiating surface are represented by the matrix $\boldsymbol{\Psi}$ and $\boldsymbol{A}^a$ is a diagonal matrix of complex resonance terms (equation 3.14 and equation 3.15). If the natural frequencies and the acoustic mode shapes are known then the excitation of the acoustic modes due to any surface velocity vector $\boldsymbol{v}$ can be calculated. From the acoustic mode amplitudes the total acoustic potential energy in the enclosure can be determined.

The acoustic potential energy in the enclosure E_p is the integral of the pressure squared levels throughout the entire enclosure and is given as,

$$E_p = \frac{1}{4\rho_0 c^2} \int_V |p(x)|^2 \mathrm{d}V \tag{5.15}$$

If the acoustic mode shapes are orthogonal and have been normalized such that for the n^{th} mode,

$$\int_V \psi_n^2 \mathrm{d}V = V \tag{5.16}$$

then the total acoustic potential energy can be expressed as,

$$E_p = \frac{1}{4\rho_0 c^2} \boldsymbol{b}^T \boldsymbol{b} \tag{5.17}$$

The total acoustic potential energy is is thus proportional to the sum of the squared acoustic mode amplitudes [71].

5.2.5 Vibration and near field pressure levels

In attempting to control the sound power radiated by a vibrating panel the vibration levels and near field pressure levels on the panel can be increased. In this section a measure of the total kinetic energy in the structure and a measure of the near field pressure levels will be defined.

The sum of the squared velocities of the elemental radiators can be written as,

$$V = \boldsymbol{v}^H \boldsymbol{v} \tag{5.18}$$

this is approximately proportional to the total kinetic energy of the structure and will

be used as a relative measure of the space averaged surface velocity. This parameter can then be calculated before and after control to determine the effects of control on vibration (section 5.4).

A measure of the space averaged mean square acoustic pressure in the near field of the panel can be defined by summing the modulus squared pressure at each of the elemental positions. Since $\boldsymbol{p} = \boldsymbol{Z}\boldsymbol{v}$ is the vector of pressures at the elemental positions, the sum of the squared near field pressures which is written as $\boldsymbol{p}^H\boldsymbol{p}$, is given by,

$$N = \boldsymbol{v}^H \boldsymbol{Z}^H \boldsymbol{Z}\boldsymbol{v} \tag{5.19}$$

N is a measure of the acoustic potential energy present in the near field of the panel and the effects of active control on N are considered in section 5.4. It should be noted that the imaginary part of the elemental self-impedance Z_{ii}, given by equation 2.12, goes to infinity since $r_{ii} = 0$. This is because the elements are modelled as point sources. To deal with this problem in equation 5.19 the self-impedance of any element is taken to be the self-impedance of a baffled pulsating hemisphere of similar surface area where the element is small compared to a wavelength.

5.2.6 Power transmission

Many of the results quoted in the following sections will be expressed in terms of a power transmission ratio. This is defined as the sound power radiated by the panel divided by the sound power incident on the plate if the plate were rigid. The power incident on the plate area if it were rigid (W^i) can be written as [88],

$$W^i = |P_i^2| l_x l_y \cos(\theta)/2\rho_0 c \tag{5.20}$$

Where P_i is the incident pressure in equation 5.1. If the sound power radiated by the other side of the plate is W^r, then the sound transmission ratio (T) can then be written as,

$$T = W^r/W^i \tag{5.21}$$

T is the inverse of the transmission loss which is the form in which results in other publications have often been expressed [88], but the results presented here are presented in terms of T since this is a convenient normalized form of the radiated power.

5.3 Cost functions

In this section four control strategies are presented. The control strategies are: (i) the minimization of total radiated sound power, which is the optimal control strategy for radiation into a free field, (ii) cancellation of volume velocity, (iii) minimization of the sum of the squared velocities and (iv) cancellation of the velocity at a point.

5.3.1 Minimization of total radiated power

As discussed in section 5.2.3, the velocity distribution due to an incident plane wave can be calculated and is represented by the vector $\boldsymbol{v}^i$. Similarly, the velocity distribution due to the secondary control input can be defined as $\boldsymbol{v}^c$. The forcing of the structure by the control force is linearly dependent on the input signal to the source and the velocity distribution $\boldsymbol{v}^c$ is considered to be a combination of the velocity due to a unit input voltage $\boldsymbol{g}$ times some complex control signal u.

$$\boldsymbol{v}^c = \boldsymbol{g}u \tag{5.22}$$

The total velocity of the structure $\boldsymbol{v}$ can now be written as,

$$\boldsymbol{v} = \boldsymbol{v}^i + \boldsymbol{g}u \tag{5.23}$$

and by substituting equation 5.23 into equation 2.11 the sound power radiation can be written as,

$$\begin{aligned} W &= (\boldsymbol{v}^i + \boldsymbol{g}u)^H \boldsymbol{R}(\boldsymbol{v}^i + \boldsymbol{g}u) \\ &= (\boldsymbol{v}^i)^H \boldsymbol{R}\boldsymbol{v}^i + (\boldsymbol{v}^i)^H \boldsymbol{R}\boldsymbol{g}u + u^* \boldsymbol{g}^H \boldsymbol{R}\boldsymbol{v}^i + u^* \boldsymbol{g}^H \boldsymbol{R}\boldsymbol{g}u \end{aligned} \tag{5.24}$$

This equation has a Hermitian quadratic form and can be rewritten in terms of u, the control signal, as,

$$W = u^* A u + u^* b + b^* u + c \tag{5.25}$$

where $A = \boldsymbol{g}^H \boldsymbol{R} \boldsymbol{g}$, $b = \boldsymbol{g}^H \boldsymbol{R} \boldsymbol{v}^i$ and $c = (\boldsymbol{v}^i)^H \boldsymbol{R} \boldsymbol{v}^i$. Given that $\boldsymbol{R}$ is positive definite this function will have a unique minimum value when $u = u_m = -A^{-1}b$ for which the minimum power $W_{min} = c - b^H A^{-1} b$ [71]. This analysis can readily be extended to multichannel systems where there is more than one secondary source present. It should be emphasized that minimization is being performed at a single known excitation frequency and thus represents the best performance that could be obtained using a feedforward control system.

5.3.2 Cancellation of volume velocity

The cancellation of volume velocity will be tested as a strategy for the control of sound power radiation and compared with the results of power minimization. The net complex volume velocity Q of the structure is, within the accuracy of this calculation, given by the sum of the complex velocities at each of the elemental positions and can be written in terms of the velocity vector,

$$Q = \boldsymbol{q}_1^T \boldsymbol{v} \tag{5.26}$$

where $\boldsymbol{q}_1^T$ is a I-length vector (I being the total number of elements) in which every element is unity. If the total velocity of the surface is defined to be a combination of contributions from the primary and secondary sources then the volume velocity can be expressed as,

$$Q = \underbrace{\boldsymbol{q}_1^T \boldsymbol{v}^i}_{primary} + \underbrace{\boldsymbol{q}_1^T \boldsymbol{g} u}_{secondary} \tag{5.27}$$

The optimal secondary source strength u_{vv} which cancels the volume velocity by setting Q to zero [52] can thus be written as,

$$u_{vv} = -\frac{\boldsymbol{q}_1^T \boldsymbol{v}^i}{\boldsymbol{q}_1^T \boldsymbol{g}} \tag{5.28}$$

It should be emphasized that this control strategy does not necessarily drive the velocity of the structure to zero at any point but drives its *average* velocity to zero, so that there is no volumetric contribution from its motion.

If this control strategy were used in a practical control system the optimal secondary source strength u_{vv} could be approached using a steepest decent algorithm to minimize the output of the error sensor squared (i.e. Q^2).

5.3.3 Minimization of the sum of the squared velocities

The minimization of the sum of the squared velocities at the elemental positions is effectively minimizing an estimate of the total kinetic energy of the plate (V). If the vector of velocities at the I elements is given by equation 5.23 the sum of the squared velocities V can be expressed using equation 5.18, as,

$$V = (\boldsymbol{v}^i + \boldsymbol{g}u)^H(\boldsymbol{v}^i + \boldsymbol{g}u) = (\boldsymbol{v}^i)^H\boldsymbol{v}^i + (\boldsymbol{v}^i)^H\boldsymbol{g}u + u^*\boldsymbol{g}^H\boldsymbol{v}^i + u^*\boldsymbol{g}^H\boldsymbol{g}u \tag{5.29}$$

This equation also has a Hermitian quadratic form and can be rewritten in terms of u, the control signal, as,

$$V = u^*Au + u^*b + b^*u + c \tag{5.30}$$

where now $A = \boldsymbol{g}^H\boldsymbol{g}$, $b = \boldsymbol{g}^H\boldsymbol{v}^i$ and $c = (\boldsymbol{v}^i)^H\boldsymbol{v}^i$. This function will have a unique minimum value when $u = u_{kin} = -A^{-1}b$ for which the minimum value of the sum of the squared velocities $V_{min} = c - b^HA^{-1}b$ [71].

5.3.4 Cancellation of the velocity at a point

This is the control strategy which would be implemented by a simple active vibration control system with a single error sensor on the panel. If the velocity at the i^{th} element due to the primary source v_i^i and the velocity at this element due to a unit input voltage to the secondary source g_i are known, then the complex control signal u_{vel} required to cancel the velocity of the i^{th} element is given by,

$$u_{vel} = -\frac{v_i^i}{g_i} \tag{5.31}$$

where g_i is equivalent to the complex transfer impedance between the input to the secondary actuator and the output of a velocity measuring device at the i^{th} position on the plate.

5.4 A comparison of active control strategies

In this section a number of different computer simulations are presented all of which involve the active control of sound radiation from a rectangular panel mounted on an infinite baffle, excited by an incoming harmonic plane wave and radiating into a semi-infinite space. The plate thickness and the secondary actuator are changed to demonstrate various features of the control approaches considered here.

The intention is to compare the effects of the minimization of sound power radiation, the cancellation of volume velocity, the cancellation of the velocity at a point on the panel and the minimization of vibrational energy, on the total acoustic power output of the panel, the vibration levels on the panel and the near field acoustic pressure levels. Acoustic and vibration control will be investigated in terms of radiation modes.

5.4.1 A comparison of results: Near field vs Far field

Wang *et al.* demonstrated [88] that a secondary actuator (or a number of them) could in principle be used to reduce the amount of sound transmitted through a plate mounted on a baffle. They considered the transmission through a $2mm$ thick steel plate, having dimensions $l_x = 380mm$ and $l_y = 300mm$, and used the far field integral approach to calculate the radiated sound power. The physical constants assumed by these authors are given in table 5.1. A similar simulation for a steel plate using the near field approach (section 5.2.3) was carried out and the results compared with those of Wang *et al.* The primary source was assumed to be a plane wave incident on the plate at $\theta = 45^o$ and $\varphi = 0^o$ (figure 5.1) and the secondary input was supplied by a small centrally positioned piezoelectric actuator. In the model used by Wang *et al.* plate damping is not considered, but in the results presented here a small

amount of damping has been added ($\xi = 0.002$) to make the on-resonance response of the system more realistic. The attenuations predicted here achieved using a single centrally located piezoelectric control source adjusted to minimize radiated sound power are within one decibel of the results quoted in the paper by Wang *et al.* [88].

	Density (ρ)	Poisson's ratio (ν)	Young's Modulus (E)
Steel	$7870(kg/m^3)$	0.292	$207 \times 10^9(N/m^2)$
Aluminium	$2720(kg/m^3)$	0.33	$71 \times 10^9(N/m^3)$

Table 5.1: The physical constants for the plate materials used in the simulations.

Figure 5.2 shows the power transmission through the plate before control (solid line), after minimization of the radiated power (dashed line) and after cancelling the volume velocity (dotted line). The strategy of volume velocity cancellation achieves good reductions in sound power transmission especially at low frequencies and these reductions are very similar to those achieved using the optimal control strategy of sound power minimization, except for a frequency region between $400Hz$ and $450Hz$. The reasons for this will be dealt with in the following section.

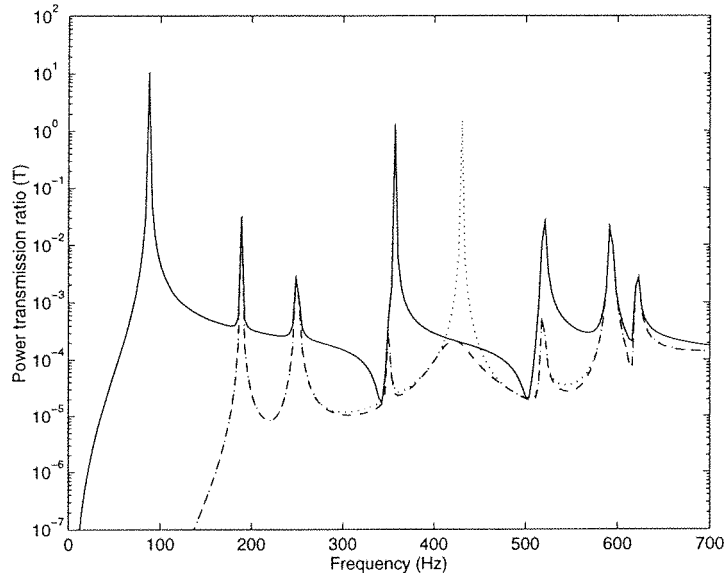

Figure 5.2: The sound power transmission through a $380mm \times 300mm \times 2mm$ steel plate before control (solid), after minimization of radiated sound power (dashed) and after cancellation of volume velocity (dotted) as a function of excitation frequency.

5.4.2 Sound power minimization and volume velocity cancellation

To explore the mechanisms involved in the minimization of sound power radiation, a simulation was carried out in which the modal density was considerably higher than the modal density of the plate considered in the section above. A $1mm$ thick aluminium plate, with dimensions l_x and l_y as above, was assumed. Therefore, at a given frequency this plate has a higher modal density than the $2mm$ steel plate considered in the section above. The plate was then excited by a plane wave incident at $\theta = 45^o$ and $\varphi = 45^o$. Since $\varphi \neq 0$, all of the $n = even$ plate modes were excited (equation 5.8) which further increases the number of modes excited by the primary field in the frequency range considered. A small ($25mm$ by $25mm$) centrally positioned piezoelectric patch was used as a secondary actuator. The resulting sound transmission ratios before and after control when using the strategies of minimization of sound power radiation and cancellation volume velocity are shown in Figure 5.3. It is again clear that significant attenuations in sound power radiation are possible up to about $500Hz$, which corresponds to $kl_x \approx 3.5$, and that up to this frequency there is, in general, little difference between the attenuations achieved using sound power minimization or volume velocity cancellation, apart from very narrow frequency bands at about $220Hz$ and $410Hz$.

To help explain the mechanisms of control the active control of the transmission for a specific excitation frequency of $350Hz$ ($kl = 2.45$, as shown in figure 5.3) will be analysed in more detail. The minimization of the sound power radiation using a single secondary source achieves a $12.5dB$ reduction in the sound transmission ratio at this frequency (figure 5.3). The changes in the structural mode content which cause this large decrease in the sound power radiation will be examined in more detail. Figure 5.4 shows the relative kinetic energies of the first fifty structural modes, before and after the minimization of radiated sound power where $0dB$ represents the *total* kinetic energy of the panel before control. The values of the modal integers m and n corresponding to the ordering used in figure 5.4 are listed in table 5.2. Both before and after control there are a large number of well excited structural modes but there is a significant *increase* in structural vibration *after* control. This data is also displayed

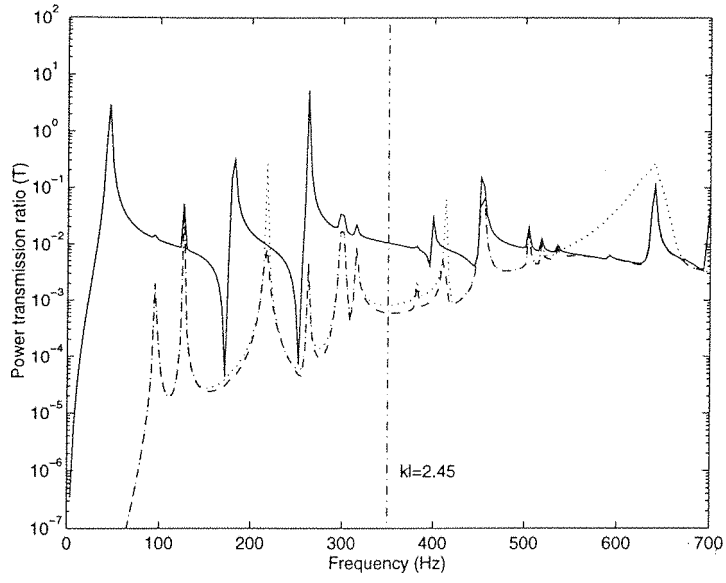

Figure 5.3: The sound power transmission through a $380mm \times 300mm \times 1mm$ aluminium plate before control (solid), after minimization of radiated sound power (dashed) and after cancellation of volume velocity (dotted) as a function of frequency.

in figure 5.5, which illustrates more clearly that paradoxically it is the amplitudes of the efficiently radiating odd-odd structural modes (e.g. the (3,3) mode) which are increased by the action of the secondary source.

		m								
		1	2	3	4	5	6	7	8	9
	1	1	2	5	8	12	18	26	35	43
	2	3	4	6	10	16	22	28	37	46
	3	7	9	11	15	19	25	33	41	-
n	4	13	14	17	21	27	31	39	49	-
	5	20	23	24	29	34	40	48	-	-
	6	30	32	36	38	45	50	-	-	-
	7	42	44	47	-	-	-	-	-	-

Table 5.2: The structural mode numbers as shown in figure 5.4 as a function of their individual modal integers m and n.

When minimizing the total sound power radiation the secondary source alters the amplitudes and phases of the structural modes so that their net radiation efficiency is low. This process is often termed *modal restructuring* [18]. The effect of modal restructuring is to cause the acoustic pressures in the far field due to the individual structural modes to largely cancel each other. In an early paper by Fuller [43] where

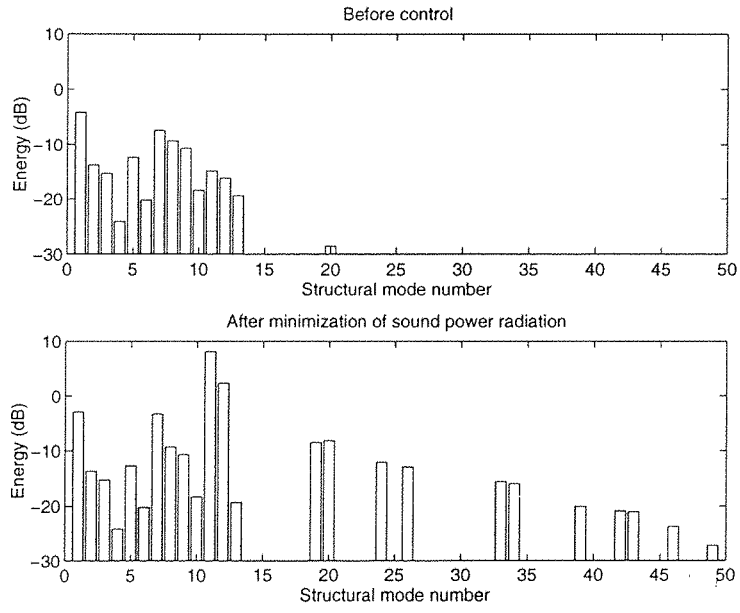

Figure 5.4: The kinetic energy contained in each of the first fifty structural modes of the panel at $350Hz$, before control (top diagram) and after the minimization of sound power radiation (bottom diagram).

he used point forces to control the sound radiation from a circular panel he states that the reductions in acoustic level are due to "the control source modifying the plate source characteristics..." producing a "...lower radiation efficiency." The mechanism by which this is achieved is not immediately obvious. The interaction of not only the amplitudes but also the phases of each of these structural modes must be considered to achieve an understanding of the radiation of the sound. The total power radiated by the structure can be considered as a combination of the power radiated by each of the structural modes. However, the power radiated by any one structural mode is dependent on the amplitudes and phases of all of the other structural modes since their radiation is inter-independent (equation 2.15). It is very difficult to gain a clear understanding of how the structural mode content should be altered to reduce the total sound power radiation. Any attempt to control the sound power radiation by controlling the amplitude of a specific structural mode is only likely to be successful near to the resonant frequency of that mode.

If, however, the vibration of the plate is viewed in terms of a sum of radiation modes, instead of structural modes, the problem is greatly simplified. Figure 5.6 shows the sound power radiated by each of the radiation modes before and after the mini-

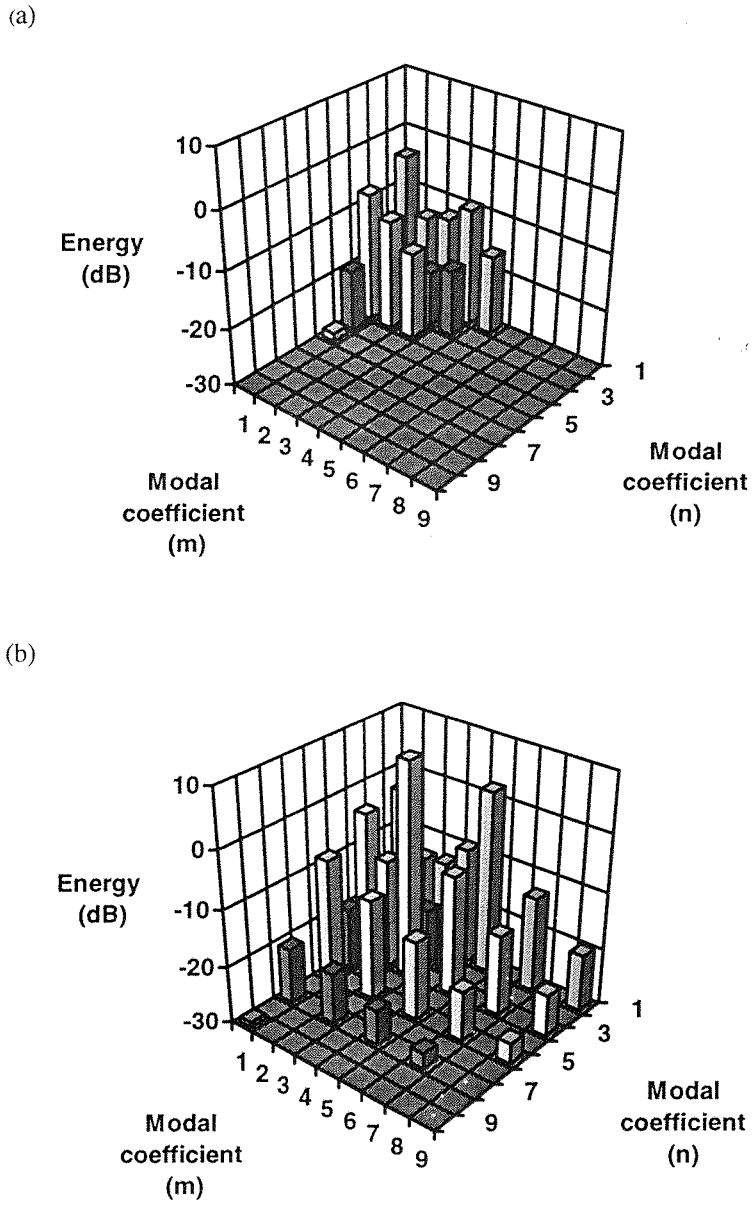

Figure 5.5: The kinetic energy contained in the structural modes of the panel at $350Hz$, (a) before control and (b) after the minimization of sound power radiation.

mization of total radiated sound power, where $0dB$ represents the *total* sound power radiated by the panel before control. Since the radiation from any single radiation mode is independent of the amplitudes of any other radiation mode their individual contribution to the total power radiated can be easily calculated. At $350Hz$ the first radiation mode accounts for 95.6% of the total sound power radiated with no control and the net effect of driving the secondary actuator to minimize the radiated sound power is to substantially reduce the amplitude of the first radiation mode. Although the higher order radiation modes are then also well excited, their radiation efficiencies at $350Hz$ (kl=2.45) (as shown in chapter 2) are very low. The amplitudes of the 5^{th} and 6^{th} radiation modes, in particular, are increased after control but because of their very low radiation efficiencies they do not significantly contribute to the total sound power radiated. The effect of modal restructuring is thus to shift the contribution of the structural modes from well radiating low order radiation modes to higher order poorly radiating radiation modes.

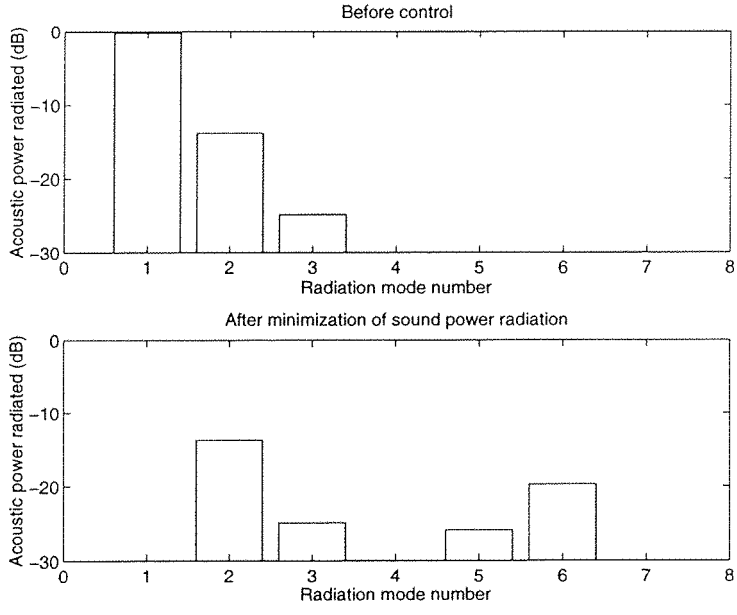

Figure 5.6: The sound power radiated by the first eight radiation modes at $350Hz$, before control (top diagram) and after the minimization of radiated sound power (bottom diagram).

If there are a large number of well excited structural modes present, the ability of the secondary actuator to achieve significant attenuations in sound power radiation can be most readily explained in terms of radiation mode amplitudes. For excitation

frequencies at which the first radiation mode is far more efficiently radiating than the other higher order radiation modes, good control should be possible using a single secondary source. If a number of sensibly placed secondary sources operating at higher excitation frequencies are used, then it is likely that at least that number of radiation modes will be controlled and the ability to achieve good attenuations is dependent on there being an equal or smaller number of well radiating radiation modes than secondary sources. Conversely, for a very stiff plate, where even at high kl values their are relatively few significantly excited structural modes, the ability to achieve significant attenuations is dependent upon the number of significantly excited structural modes compared with the number of control forces. At high frequencies the radiation from structural modes becomes almost independent and it is thus only in the low frequency region that the radiation mode approach is useful, particularly for flexible structures.

As has been shown in chapter 2, the volume velocity of a structure is a good approximation to the amplitude of the first radiation mode at low frequencies. Given also that at low frequencies the first radiation mode is responsible for the majority of the sound power radiation, volume velocity will act as a good measure of sound power radiation from a vibrating surface. For the example quoted above in which the excitation frequency was $350Hz$, the reduction in the sound transmission ratio due to volume velocity cancellation was $11.3dB$ which compares well with the $12.5dB$ of attenuation achieved by using the optimal control strategy of sound power minimization. Although volume velocity cancellation is slightly less effective than the minimization of sound power radiation in attenuating the sound power transmission at low frequencies, the simplifications in the required sensing are enormous. The volume velocity of a plate can be measured using a single distributed sensor whose design is independent of the material properties of the plate and does not have to take into account the exact excitation frequencies or structural mode content of the plate [54] (chapter 4). To measure the sound power radiation from a vibrating panel would potentially require large numbers of matched vibration or acoustic sensors. Volume velocity cancellation is a simple, robust and effective technique for the active control of sound power transmission at low frequencies which only requires a single distributed sensor on the structure.

There are frequencies at which the cancellation of volume velocity can lead to significant increases in the radiated sound power (e.g. $220Hz$ in figure 5.3). This effect is due to the secondary source being unable to efficiently drive the first radiation mode at this frequency. The secondary source excites the structural modes, which in turn contribute to the amplitudes of the radiation modes. Structural modes can be excited by the secondary actuator such that their phases can either lead or lag the phase of the input to the secondary source (equations 5.4 and 5.11). It is possible that a set of structural modes which contribute to the amplitude of the first radiation mode are excited out-of-phase with another set of structural modes which also contribute to the amplitude of the first radiation mode such that their contributions largely cancel each other. Under these circumstances the secondary source will drive extremely hard in an attempt to cancel the amplitude of the first radiation mode and as a result strongly excite higher order radiation modes which will begin to radiate significant amounts of sound power. Using the strategy of volume velocity cancellation the control system has no means of detecting the radiation from higher order radiation modes and hence increases in sound power radiation can occur but only appear to be significant in narrow frequency ranges if kl is small. This can be clearly demonstrated by looking at the frequency response between the input to the secondary source and the output of the volume velocity sensor (figure 5.7). The frequency regions in which the frequency response is very small correspond to the frequency regions in which the secondary source has to drive hard to cancel the volume velocity and so excites the higher order radiation modes and causes an increase in the radiated sound. The increase in radiated power at these frequencies can be controlled by adjusting the secondary source to minimize a cost function which includes both control effort (mean square control signal $|u|^2$) as well as mean square volume velocity such as,

$$J = |Q|^2 + \beta|u|^2 \tag{5.32}$$

Small values of the parameter β give attenuations in the volume velocity and hence radiated sound power which are almost the same as those shown in figure 5.3 but reduce the amplifications around the problem frequencies of $220Hz$ and $410Hz$.

Another way of ensuring that the volume velocity is controllable at every frequency is to use more than one secondary source [32] or a secondary source which couples more

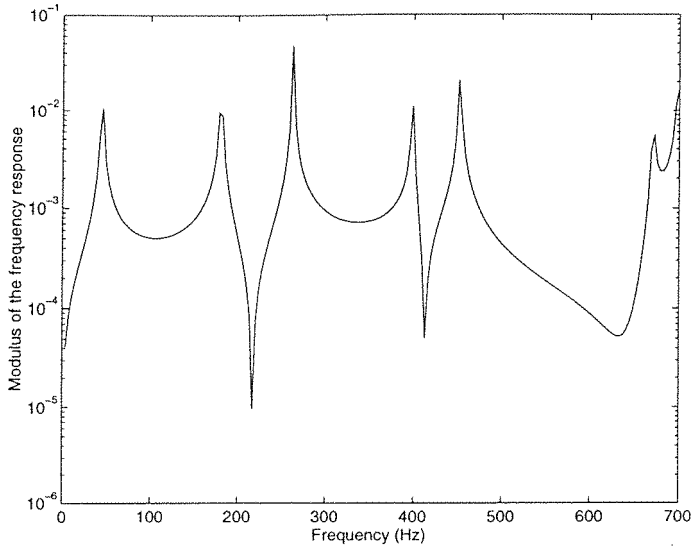

Figure 5.7: The modulus of the frequency response between the input to the piezoelectric actuator and the output of the volume velocity sensor.

effectively to the volume velocity at all frequencies. The design of such a secondary source will be returned to in section 5.4.5.

5.4.3 Other effects: Vibration and near field pressure levels

In attempting to control the sound power transmitted through a panel with the secondary actuator other effects may occur which may not be desirable. For example, significant and often large increases in vibration [60] and near field pressure levels can be generated. Figure 5.8 shows the sum of the squared velocities (V calculated in equation 5.18) for the panel before and after control of both sound power radiation and volume velocity. There can be large increases in the levels of vibration after control, except at very low frequencies where the first structural mode dominates the vibration and the strategies of sound power minimization and minimizing the sum of the squared velocities are equivalent. By minimizing the sound power radiation at $350Hz$ the average level of vibration is increased by $9.9dB$. Although the average level of vibration has increased, the efficiency with which the panel radiates sound power is so significantly decreased that there is still an $12.5dB$ reduction in the sound power radiation. The increase in vibration after control can be thought of as being

due to strong excitation of the higher order radiation modes (as seen in figure 5.6) whose radiation efficiencies at this frequency are still very small in comparison to the radiation efficiency of the first radiation mode.

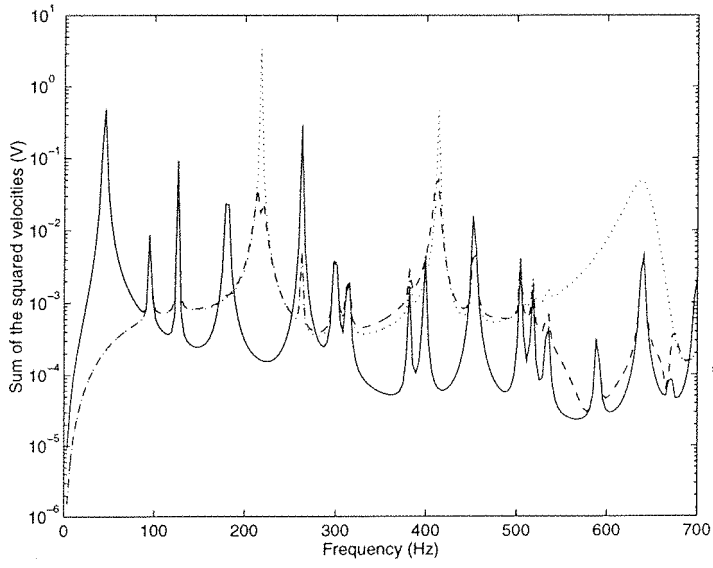

Figure 5.8: The sum of the squared velocities of the elemental radiators before control (solid), after minimization of radiated sound power (dashed) and after cancellation of volume velocity (dotted) as a function of frequency.

As well as the increases in vibration levels there can also be increases in the pressure levels observed near the surface of the panel. This may be undesirable if there is a possibility of an observer close to the surface as well as in the far field. Figure 5.9 shows the mean squared pressure levels at the surface of the panel, calculated using equation 5.19, before and after control using the two control strategies. It is only at low frequencies that the minimization of radiated sound power leads to a large reduction in the sum of the squared pressure (N) and again in some frequency regions large increases can be observed.

The frequency regions where the increases in vibration levels and pressure levels are greatest correspond to frequencies at which the secondary source is incapable of effectively coupling into the first radiation mode. At these frequencies the control system is unable to achieve any significant reductions in sound power radiation using either minimization of sound power radiation or volume velocity cancellation (figure 5.3). It should be noted that there is an increase in the vibration and near-field pressure,

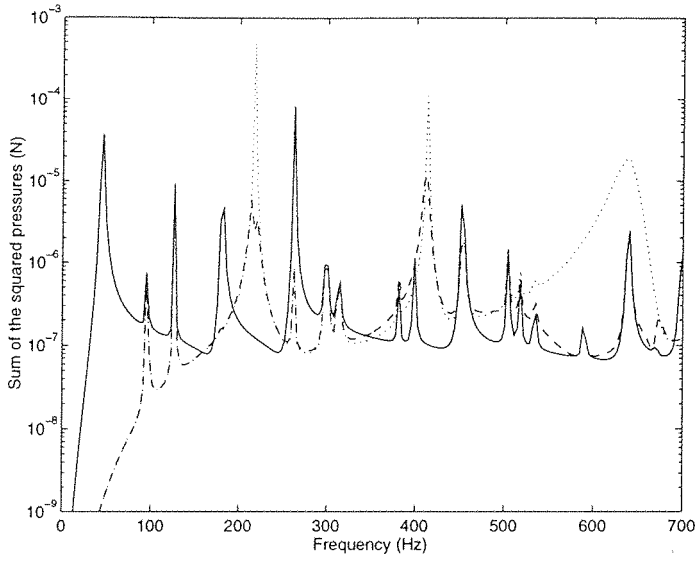

Figure 5.9: The sum of the squared near-field pressures (N) before control (solid), after minimization of radiated sound power (dashed) and after cancellation of volume velocity (dotted) as a function of frequency.

at these frequencies, even when the optimal strategy of sound power minimization is used. This supports the conclusion that it is the secondary actuator which is causing the problem rather than the strategy of volume velocity cancellation.

5.4.4 Vibration control

To further demonstrate that the main mechanism of acoustic control in not always vibration reduction, computer simulations were carried out in which either the vibration at the centre of the plate was cancelled or the kinetic energy of the plate was minimized by the action of the secondary source. The plate configuration used is exactly the same as in the former sections.

Figure 5.10 shows the resulting vibration levels before and after control using these two control strategies. The cancellation of the vibration at the centre of the plate causes increases in the total vibration levels in many frequency regions. The minimization of the sum of the squared velocities of all of the elements results in useful reductions in vibration level up to $300Hz$ but has little or no effect above $400Hz$. For this example, where there is a high structural modal density at low frequencies but

few efficient radiation modes, control of vibration level is significantly more difficult than reductions in the acoustic power output.

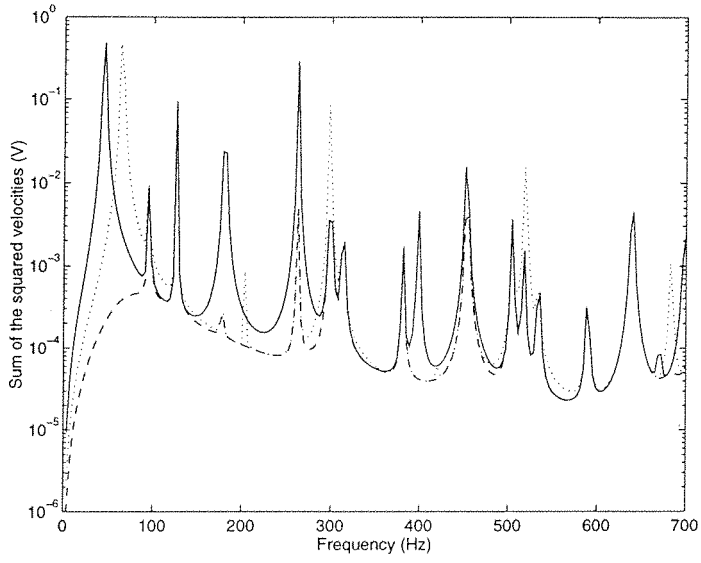

Figure 5.10: The sum of the squared velocities of the elemental radiators before control (solid), after minimization of the sum of the squared velocities (dashed) and after cancellation the vibration in the centre of the plate (dotted) as a function of frequency.

The resulting acoustic power transmission ratios for the two vibration control strategies are shown in figure 5.11 and can be contrasted with the performance of the other control strategies as shown in figure 5.3. The cancellation of the vibration at the centre of the plate is ineffective in controlling the acoustic power transmission through the plate with the exception of a few narrow frequency regions corresponding to the natural frequencies of low order structural modes. Cancellation of the vibration at the centre of the panel pins the centre of the panel and therefore alters the resonant frequencies of the odd-odd structural modes without altering the resonant frequency of any odd-even or even-even structural modes. At very low frequencies, where the plate's response is dominated by the first structural mode, minimization of the sum of the squared velocities produces significant reductions in the acoustic power transmission ratio. Reductions in the transmission ratio are also possible close to a structural mode resonance where the response in dominated by a single structural mode. Over most of the frequency range the minimization of the sum of the squared velocities is ineffective as a technique for controlling the acoustic transmission ratio

for this panel. It does not however produce any significant increases in the acoustic transmission ratio.

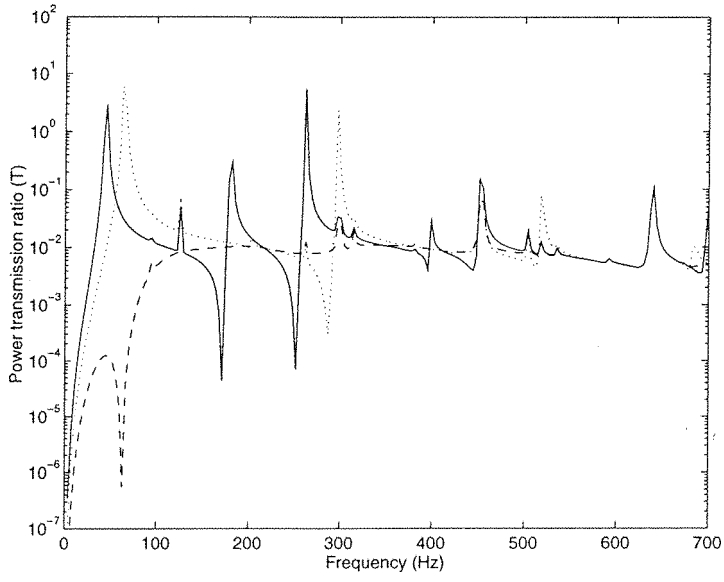

Figure 5.11: The sound power transmission through a $380mm \times 300mm \times 1mm$ aluminium plate before control (solid), after minimization of the sum of the squared velocities (dashed) and after cancellation of the vibration at the centre of the plate (dotted) as a function of frequency.

5.4.5 Reducing control spillover

The increases in vibration and near field pressure levels shown in figures 5.8 and 5.9 are due to the secondary actuator causing *control spillover* [17, 43]. Control spillover is conventionally understood in terms of structural modes, where the secondary actuator excites structural modes that are weakly excited by the primary source in its attempt to control the structural modes which the primary source strongly excites. In the context of sound radiation control, control spillover can be most readily understood in terms of the spillover of radiation modes.

The amount of control spillover is determined by the type and size of the control actuator. If the size of the centrally located piezoelectric actuator used in the simulations is varied, it is found that the amount of control spillover does not vary to a large extent if the size of the actuator is considerably smaller than a structural wavelength. If a point force actuator is used instead of a small piezoelectric actuator (in

the same position) the control spillover is found to occur into lower order structural modes but the extent of the spillover is similar. Piezoelectric actuators are in general more efficient at exciting higher order structural modes (equation 5.11). In general, however, there appears to be no clear preference for either a small piezoelectric or point force actuator and in a given application the relative amounts of spillover from the two types of actuator will be very dependent on the excitation frequency.

If a pair of discrete sensors and actuators are co-located on a structure they will observe and excite the structure in a similar manner [4, 12]. This property also carries over to distributed actuators and sensors (section 4.4). A reciprocal transducer, originally designed as a volume velocity sensor, will generate a uniform force over the surface of the panel when driven by a voltage. If a volume velocity sensor and a uniform-force actuator are used as a sensor/actuator pair to control the sound power radiation, the cancellation of the volume velocity can be achieved without causing increases in the vibration and near field pressure levels. Figure 5.12 shows the sound power transmission before and after control when using a distributed uniform-force actuator. The use of a uniform-force actuator instead of a piezoelectric patch increases the useful frequency range of control to above $600Hz$ and also increases the attenuations possible over the entire frequency range. The control strategies of minimizing sound power and cancelling volume velocity produce extremely similar results in this case. Without any control spillover the vibration (figure 5.13) and the near field pressure (figure 5.14) are not adversely effected by control, and for most of the frequency range significant reductions in these quantities are also observed.

Having matched transducers (for example, a volume velocity sensor and a uniform force actuator) also implies that the transfer function between these transducers is *minimum phase* (section 4.4). The frequency response of a minimum phase system can always, in principle, be exactly compensated for to give an overall response with no delay [71]. In an adaptive feedforward control system the speed of convergence is always limited by the delays in the system under control [71], and so this arrangement of actuator and sensor could result in a very fast acting controller.

The possibility of a feedback controller can also be contemplated in which the output of the volume velocity sensor is fed back to the uniform pressure actuator as shown in figure 5.15a. The equivalent block diagram is shown in figure 5.15b and the overall

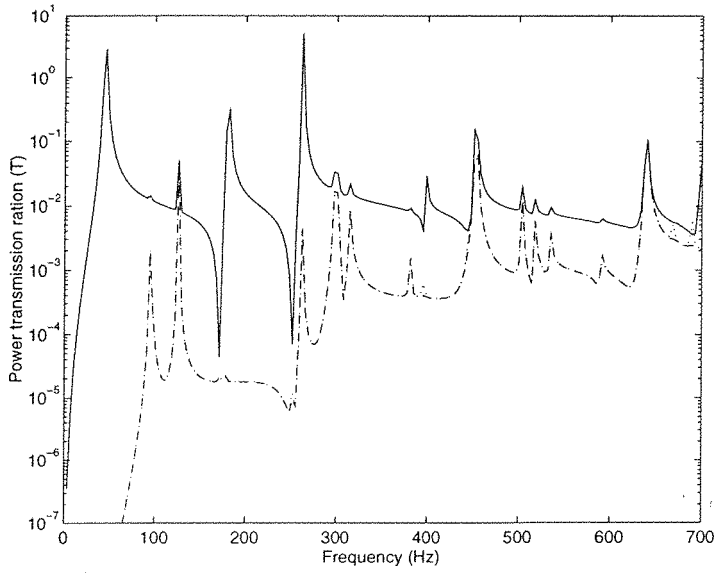

Figure 5.12: The sound power transmission through the panel, using a uniform-force actuator, before control (solid), after minimization of radiated sound power (dashed) and after cancellation of volume velocity (dotted) as a function of frequency.

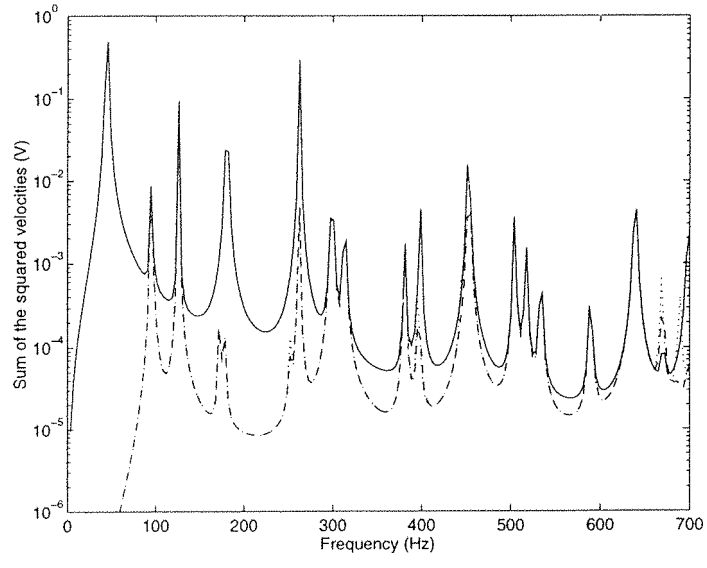

Figure 5.13: The sum of the squared velocities of the elemental radiators before control (solid), after minimization of radiated sound power (dashed) and after cancellation of volume velocity (dotted) when using a uniform-force actuator.

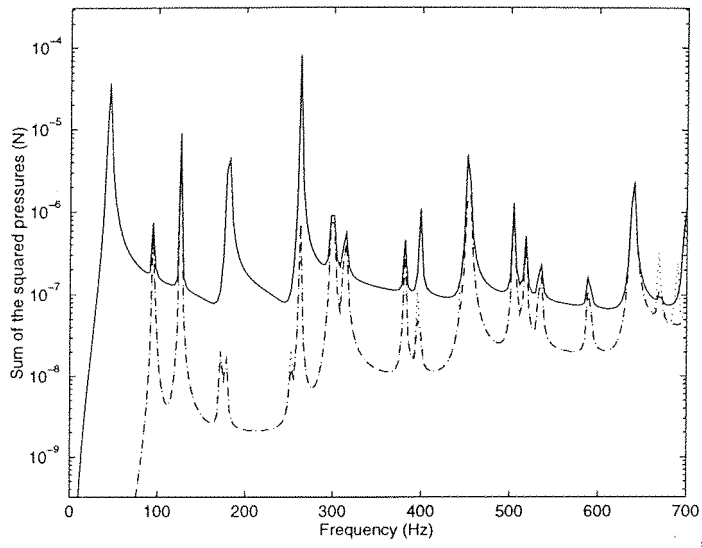

Figure 5.14: The sum of the squared near-field pressures (N) before control (solid), after minimization of radiated sound power (dashed) and after cancellation of volume velocity (dotted) when using a uniform-force actuator.

frequency response from the primary disturbance to the error signal is given by,

$$\frac{e(j\omega)}{d(j\omega)} = \frac{1}{1 + G(j\omega)H(j\omega)} \tag{5.33}$$

If the system under control, $G(j\omega)$, is minimum phase then in principle its response can be perfectly compensated for by the controller $H(j\omega)$, which can also incorporate a large feedback gain such that $1 + G(j\omega)H(j\omega)$ is always entirely real and very large. Under these circumstances $e(j\omega)/d(j\omega)$ is very small and so the performance of the feedback system is the same as the feedforward one. The advantage of a feedback system is that no reference signal is necessary and therefore broadband noise as well as harmonic disturbances can be controlled. Feedback control will be considered in more detail in chapter 8 of this thesis.

5.5 Control of radiation into finite enclosures

The control of sound levels in enclosures is an important application for active control, in particular for cars and aircraft [71]. In this section the effectiveness of cancelling

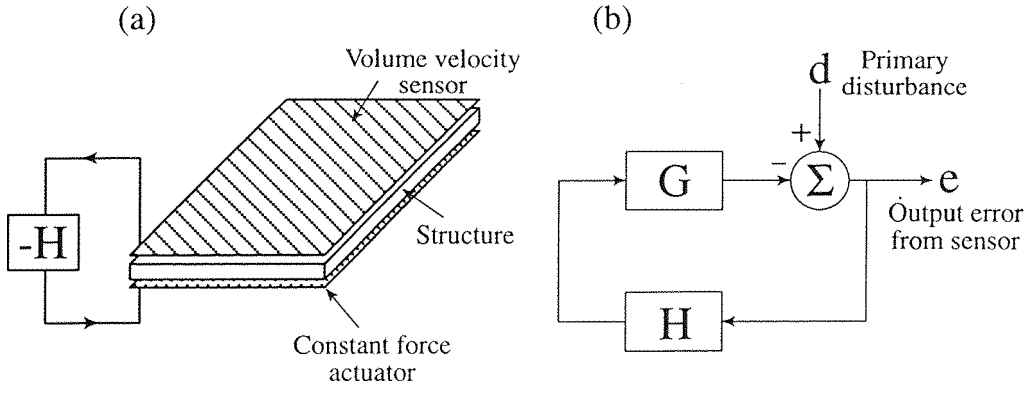

Figure 5.15: A feedback control system using (a) a volume velocity sensor and a uniform-force actuator matched pair and (b) the equivalent block diagram.

the volume velocity of a vibrating panel when it is radiating sound into an enclosed space will be investigated.

The radiation of sound into enclosures differs from the radiation of sound into free space in that the acoustic impedance between two points on a vibrating surface is determined by the acoustic modes in the enclosure and not simply by the distance between the points (equation 3.17).

Power vs Energy

In this thesis the radiation of sound has been dealt with in terms of acoustic *power* output. However, most of the active control systems used to control the sound in enclosures, attempt to minimize the acoustic potential *energy* in the enclosure. The acoustic potential energy in an enclosure will depend upon the acoustic power input to the enclosure and the level of acoustic damping in the enclosure. The minimization of acoustic power output is therefore subtly different from the minimization of the acoustic potential energy in that the minimization of acoustic potential energy places more emphasis on controlling the acoustic modes which have low damping [48]. At a single frequency the acoustic resonances which are well excited will in general have similar natural frequencies and similar acoustic damping. The damping model used in this work, equation 3.15, assumes the damping of a mode to be proportional to its natural frequency (i.e. $2\xi\omega_{mn}$ where ξ is the damping ratio). This implies that the

largest discrepancy between the minimization of sound power and the minimization of acoustic potential energy will occur at low frequencies where there can be a large relative change in the natural frequency of consecutive modes or if the sound absorbing material in the enclosure is distributed such that adjacent modes have a very different damping ratios. The discrepancy between these two methods will also increase with higher levels of damping. In general however, it is found that these two methods produce near identical results and for practical purposes they can in most cases be considered to be the same [48].

To be consistent with earlier work [71], the results given in this section will be presented in terms of the change in the acoustic potential energy in the enclosure .

5.5.1 Control of radiation into a finite duct

The control of a simply supported beam radiating sound into a finite duct is taken as the first and simplest example of the active control of sound transmission into an enclosure (figure 5.16). The internal acoustic response due to an externally incident acoustic plane wave will be affected by the natural resonances of both the beam and the acoustic enclosure.

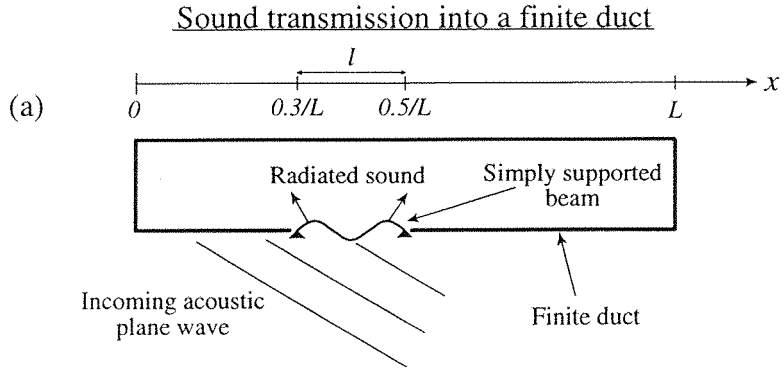

Figure 5.16: The transmission of sound into a finite duct through a single simply supported beam.

Consider a single simply supported $0.5mm$ thick aluminium beam (positioned at $x = 0.3/L$ to $x = 0.5/L$ i.e. $l = 0.2L$) as the only source of sound in a finite duct of length $L = 1m$ (figure 5.16). The damping ratios for the acoustic modes and the beam's structural modes are both taken to be 0.02. The sound in the enclosure is

due to the vibration of the beam which is in turn excited by an incoming plane wave angled at 45° to the duct. The beam is controlled using a single point force actuator located at the centre of the beam. The acoustic potential energy in the duct after the minimization of the sound power radiation of the beam into the duct and after the cancellation of the beam's volume velocity is shown in figure 5.17 in terms of non-dimensional frequency kl. Up to $kl = 1$ the cancellation of volume velocity produces similar reductions in the internal acoustic energy levels as the optimal strategy of minimization of sound power radiation. At higher frequencies the first radiation mode does not dominate the radiation from the beam and little attenuation in the radiated power can be achieved using a single secondary source (section 3.4.2).

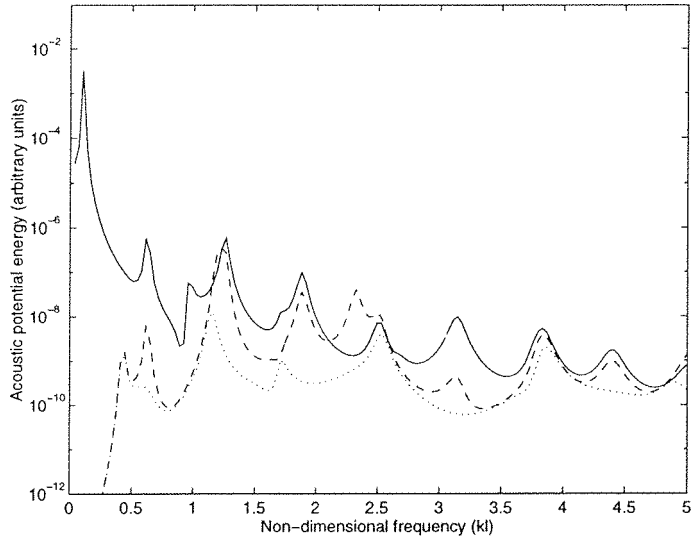

Figure 5.17: The acoustic potential energy in a finite duct due to the primary source (solid), the minimization of the sound power output (dotted) and the cancellation of the volume velocity of the beam (dashed) using a single centrally placed point force actuator as a secondary source.

5.5.2 Control of radiation into a cuboid enclosure

The radiation of sound into a three dimensional cuboid enclosure is a more realistic scenario for the application of an active control system. Figure 5.18 shows the system configuration for the control of sound power into two cuboid enclosures having dimensions $2.2m \times 2.0m \times 6.0m$ and $2.2m \times 1.0m \times 0.8m$. The only acoustic source in

the enclosure is considered to be a rectangular simply supported aluminium plate of $1mm$ thickness whose centre is positioned at $y = 0.19m$, $z = 1.95m$ for enclosure (a) and $y = 0.19m$, $z = 0.55m$ for enclosure (b). The plate has dimensions $l_y = 0.38m$ and $l_z = 0.3m$ with a damping ratio of 0.002 which is the same as for the plate used in the active control simulations described in section 5.4.2. The plate is excited by an incoming plane wave angled at $\theta = 45^o$ and $\varphi = 45^o$ (figure 5.1). The secondary control source is a small piezoelectric actuator positioned at the centre of the plate. The damping ratio for the acoustic modes in the enclosure is taken to be 0.02.

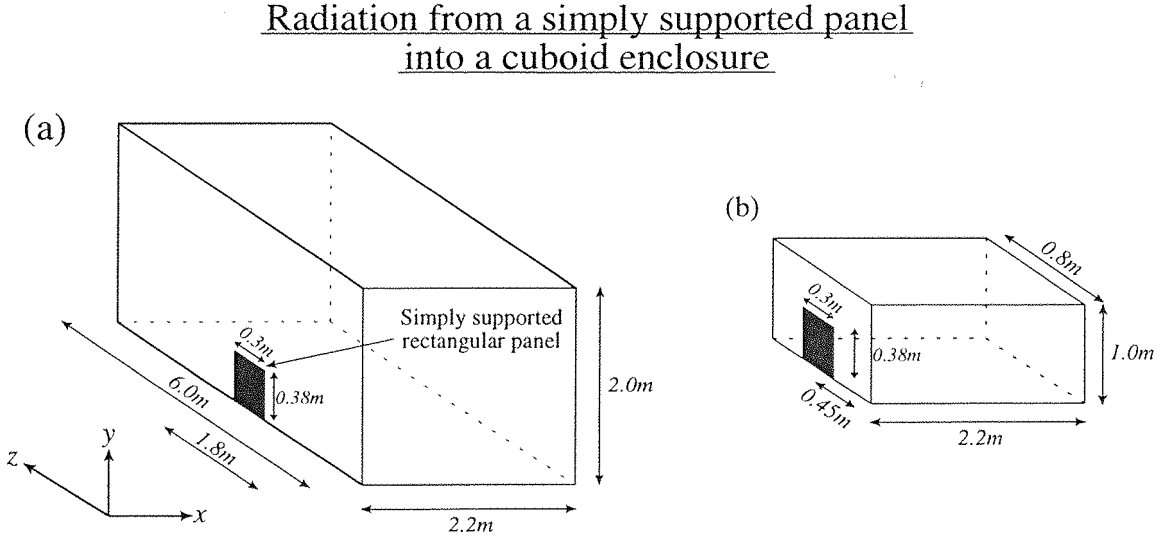

Figure 5.18: A $0.38m \times 0.3m$ rectangular simply supported panel radiating into a three dimensional enclosure of dimensions $2.2m \times 2.0m \times 6.0m$ for enclosure (a) and $2.2m \times 1.0m \times 0.8m$ for enclosure (b).

The reductions in the internal acoustic energy levels are very similar in this case for both the minimization of sound power radiation and for the cancellation of volume velocity (figure 5.19 and figure 5.20). Very good reductions are possible at low frequencies and even at relatively high frequencies significant reductions are still possible for both enclosures (over $12dB$ at $350Hz$ $kl_y \approx 2.45$ in both cases by cancelling volume velocity). The size of the enclosure does not seem to greatly affect the performance of the system. For both enclosures the resonant behaviour of the acoustic potential energy in the enclosure at higher frequencies is principally due to the structural modes of the plate and not the acoustic modes of the enclosure and this can be seen by comparing figures 5.19 and 5.20 with the case where the plate is radiating into free

space shown if figure 5.3. This is because at any one frequency in this region there are a large number of acoustic modes which are significantly excited which tends to flatten the response of the enclosure.

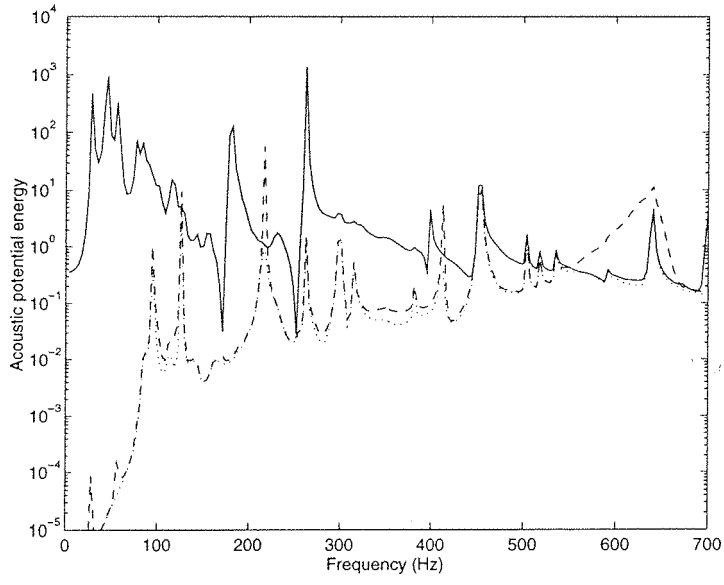

Figure 5.19: The acoustic potential energy in enclosure (a) due to the primary source (solid), the minimization of the sound power output (dotted) and the cancellation of the volume velocity of the plate (dashed) using a single centrally placed piezoelectric actuator as a secondary source.

The acoustic modal overlap factor [71], which is a measure of the number of acoustic resonances which are likely to be present within the $3dB$ bandwidth of a single resonance, increases very rapidly for a three-dimensional enclosure. If the modal overlap factor is large it is unlikely that effects which are due to the dominance of a single mode will be observed and the performance of the system will be due to the combined action of a large number of modes. The modal overlap factor is generally defined to be three at the Schroeder frequency where the enclosure begins to act as a diffuse field [71]. The Schroeder frequency for enclosure (a) is $178Hz$ and for enclosure (b) is $440Hz$. It is known that the average behaviour of an active control system acting in a diffuse field is similar to that in a free field [71]. For the example of a duct, the modal overlap factor does not increase rapidly and therefore the radiation mode shapes are more likely to be dominated by a single acoustic mode.

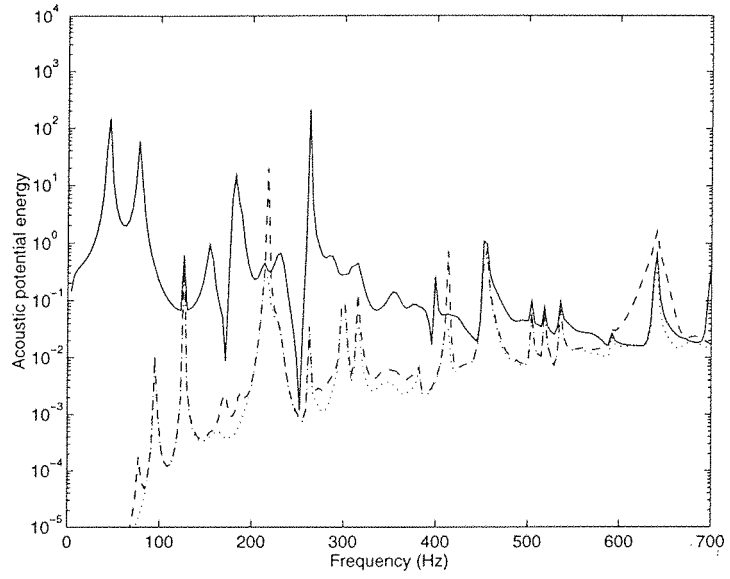

Figure 5.20: The acoustic potential energy in enclosure (b) due to the primary source (solid), the minimization of the sound power output (dotted) and the cancellation of the volume velocity of the plate (dashed) using a single centrally placed piezoelectric actuator as a secondary source.

5.6 Conclusions

The active control of sound power radiation and the active cancellation of volume velocity has been investigated analytically. A series of computer simulations have been carried out in which a panel was excited by a single incident harmonic plane wave and a secondary piezoceramic actuator on the panel is driven to cancel the volume velocity of the panel. For comparison, other control strategies such as minimization of total power output, vibration cancellation at a point and minimization of total kinetic energy, have also been investigated. Both the radiation from a panel mounted on to an infinite baffle radiating into free space and a beam or plate radiating into an enclosure have been investigated to determine the likely performance of these control strategies in various circumstances.

The active control of sound radiation from a panel has previously been formulated in terms of the radiation from a set of structural modes. The radiation of sound from each structural mode, however, is dependent not only on the amplitude of this mode but also on the amplitudes of many of the other structural modes. The interdependence of the acoustic radiation from structural modes makes it difficult to determine

what the basic mechanisms of radiation are, and this in turn makes it difficult to formulate active control strategies. Alternatively, the radiation of sound power can be viewed in terms of a set of orthogonal, independently radiating velocity distributions which are termed *radiation modes*. It has been shown that the first radiation mode is the dominant radiator of sound power at low frequencies and that by reducing the amplitude of the first radiation mode, large reductions in radiated sound power can be achieved. At low frequencies the amplitude of the first radiation mode is well approximated by the net volume velocity of the panel and therefore the cancellation of volume velocity is a very good strategy for the reduction of sound power transmission at low frequencies. This conclusion has been supported by the results of the simulations carried out here, in which the strategies of cancellation of volume velocity and minimization of radiated sound power are compared. The minimization of radiated sound power defines the physical limitations of the control system but is difficult to implement in practice. It has been shown that at low frequencies the cancellation of volume velocity achieves very similar attenuations to that of sound power minimization.

The usefulness of the cancellation of volume velocity as a control strategy carries over to the radiation of sound into finite enclosures which has been investigated for a single panel radiating into different size enclosures. In the one-dimensional duct the modal overlap factor remains low over a large frequency range and hence the response of the system at most frequencies is dominated by a single acoustic mode. This implies that the volume velocity is a poor estimate of the amplitude of the first radiation mode since the shape of the first radiation mode is determined to a large extent by the shape of a single acoustic mode (section 3.4.2). This also implies that there are many frequencies at which the secondary source is poorly coupled to the internal acoustic field and therefore very little control can be achieved regardless of the control strategy used. In three-dimensional enclosures there are a larger number of acoustic modes at high frequencies and on average the control system behaves as if it were in a free field, particularly for the larger enclosure. The radiation mode shapes in this case are similar to those for radiation into a free field (section 3.4.3) and hence the cancellation of volume velocity produces a large reduction in the amplitude of the first radiation mode and therefore a significant reduction in the sound power radiation.

These results suggest that if the panels that form the boundaries of an enclosure (e.g. an aircraft cabin) are controlled locally to cancel the volume velocity, then significant reductions in the overall sound levels can be achieved. If the enclosure has a high acoustic modal density, direct control of the sound field is more difficult and it is more likely that the cancellation of the volume velocity of individual panels will be a more successful strategy for reducing the overall sound pressure levels.

The action of the secondary source in minimizing the sound power radiation from a plate can in many cases cause an increase in the plate's vibration levels and also lead to increases in the plate's near field pressure levels due to control spillover. By using a volume velocity sensor and a uniform-force actuator as a matched actuator/sensor pair, control spillover can be greatly reduced. The control system can then achieve large attenuations in the sound power radiation at low frequencies whilst also reducing the levels of vibration and the near field pressure levels.

The use of a matched pair of transducers can also have additional benefits when used in a feedback control system. The transfer function between a matched actuator/sensor pair will be *minimum phase* and therefore will not accumulate phase with increasing frequency. This suggests that a perfect actuator/sensor matched pair could be used in a feedback system which had an arbitrarily large feedback gain. This feedback system would therefore achieve the same attenuations possible as with a feedforward control system but would require no reference signal and be able to accommodate any type of disturbance, random, transient or harmonic.

Chapter 6

The active control of sound transmission into a cylinder

6.1 Introduction

This chapter is concerned with computer and laboratory experiments on the active control of sound transmission into an enclosed cylinder. The motivation for this work derives from problems experienced in the space industry where payloads may be damaged during launch by the high levels of noise from the engines. Passive noise reduction usually has a large weight penalty associated with it, especially at low frequencies. It is clear that weight is of the utmost importance in the design of launch vehicles and the active reduction of the noise transmission using secondary actuators is potentially a light weight solution. For the purposes of this investigation piezoelectric transducers are used as actuators although it may also be possible to use other types of actuators. Piezoelectric actuators are useful for this application because they produce an excitation without requiring an inertial mass against which to react. In this study a simple single channel feedforward control system is used to reduce the sound transmission into the cylinder from an external harmonic disturbance. Although this disturbance is not a realistic model of the stochastic noise produced by a launcher engine it will serve to demonstrate the potential for controlling the internal noise levels using an active noise control system. The production of a realistic system would require further development and some suggestions will be made regarding the

direction of further work necessary to produce such a system.

The investigation into the feasibility of controlling the sound transmission into a cylinder is undertaken in three progressive steps.

- A simplified mathematical computer model of the real system is constructed to determine the general feasibility for control and to pinpoint the main control issues.
- Frequency response measurements of the real system are taken and used in computer simulation to *predict* the performance of the system.
- A control system is implemented on the structure to measure the system performance and to verify the results of the computer prediction using real data.

This general investigative procedure will also be used in chapters 7 and 8.

6.2 Theory

To access the feasibility of actively controlling sound transmission into an enclosed cylinder, a simple computer model was set up. Rather than providing an exact prediction of the control possible in a practical experiment, the model allowed the general features of the interaction between the structural vibration and the acoustics to be investigated. Circumstances which would facilitate good attenuation using active control methods could then be identified. The natural frequencies of the structural and acoustic modes were taken from the computer model PROXMODE written for an ESA contract undertaken by ISVR Consultancy services in 1987 [75].

The computer model includes the excitation of the structure due to an incoming plane wave and a secondary piezoelectric actuator. By altering the structural vibration, the secondary source can cause a reduction in the noise levels inside the cylinder.

6.2.1 The forcing of the structure due to an incident plane wave

To model the forcing effect of an incoming plane wave on the cylinder, a simple numerical model was constructed. It was assumed that the acoustic field at the surface of the cylinder was unchanged by the presence of the cylinder. Although this assumption may not be realistic in some circumstances (high frequencies for example), it is a useful approximation in the context of this work. The primary concern of this investigation was the active control of acoustic transmission from *any* general external acoustic field into the cylinder. So although this model does not realistically represent the excitation due to an incoming plane wave, it provided a reasonable primary excitation for which possibilities of active control could be explored.

The structural modes (figure 6.1) of a cylinder fitted with two stiff end plates (i.e. acting as simple supports) are given by,

$$\phi_{mn}(x,\theta) = \sin\left(\frac{m\pi x}{l}\right) \begin{matrix}\cos\\ \sin\end{matrix} (n\theta) \tag{6.1}$$

where ϕ_{mn} is the mode shape of the mn^{th} structural mode for a simply supported cylinder with m being the axial mode number and n being circumferential mode number, l is the length of the cylinder and θ describes the angle around the cylinder. The circumferential mode shapes are combinations of sin and cos terms.

In the simulations results presented in this chapter the modes $m = 1$ to 5 and $n = 0$ to 6 were considered. The surface of the cylinder was divided up into 20 elements along its length and 24 elements circumferentially. Therefore, at any one frequency the complex pressures at each elemental position due to an incoming plane wave could be calculated. A generalized forcing function for the mn^{th} structural mode can be calculated by,

$$F^i_{mn} = \boldsymbol{\phi}^T_{mn}\boldsymbol{p}^i \tag{6.2}$$

where the generalized forcing function F^i_{mn} of the mn^{th} mode due to the incident plane wave is approximated by the product of the pressures $\boldsymbol{p}^i$ at the elemental

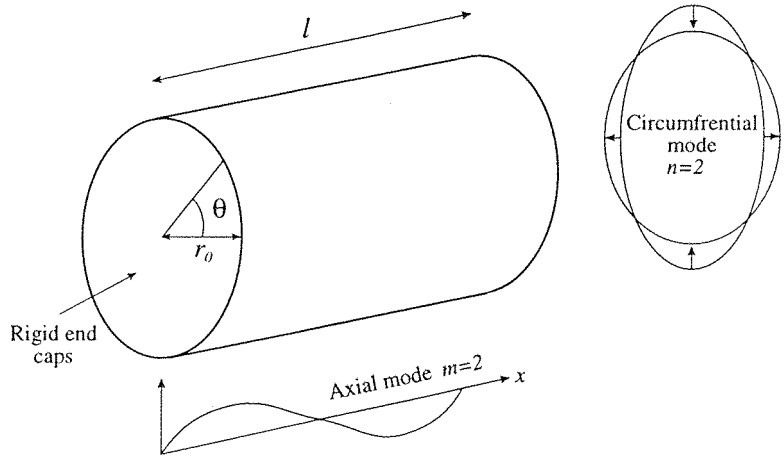

Figure 6.1: The cylinder used for the computer simulations. The $m = 2$, $n = 2$ mode shape is shown as an example.

positions and the value of the mn^{th} mode shape ϕ_{mn} at the elemental positions. The absolute pressures at the elemental positions are dependent upon the amplitude of the incoming plane wave. However, it is the *relative* values of the complex pressure at the surface of the cylinder that is of primary importance and therefore it is assumed that there is some arbitrary amplitude which produces the pressures $\boldsymbol{p}^i$. Throughout this chapter the constants which are necessary for the calculation of the *absolute* levels of excitation will not be explicitly stated as they are unimportant in the context of this preliminary study. The relationship given in equation 6.2 can be extended to include all of the modes considered i.e.

$$\boldsymbol{F}^i = \boldsymbol{\Phi}^T \boldsymbol{p}^i \tag{6.3}$$

where $\boldsymbol{F}^i$ is a complex vector of forcing coefficients and $\boldsymbol{\Phi}$ is a matrix describing all of the mode shape values of the structural modes considered at the elemental positions. To calculate the excitation of each structural mode, the forcing functions need to be multiplied by their respective complex resonance terms. The complex resonance terms are dependent on the natural frequency of the mode considered, the frequency of excitation and the damping of the structure. The complex resonance term for the mn^{th} structural mode is given by,

$$A^s_{mn}(\omega) = \frac{\omega}{D_{mn}\omega - j(\omega^2_{mn} - \omega^2)} \tag{6.4}$$

where D_{mn} is the damping of the mn^{th} mode and is given by $D_{mn} = 2\xi\omega_{mn}$ (where ξ is the damping ratio), A^s_{mn} is the complex resonance term for the mn^{th} structural mode when the forcing frequency is given by ω and ω_{mn} is the natural frequency of the mn^{th} structural mode. The diagonal matrix $\boldsymbol{A}^s$ is a collection of these terms such that the (i,i) term in the matrix represents the complex resonance term for the i^{th} structural mode of the cylinder. The complex resonance term given here is slightly different to the complex resonance term shown in equation 5.4 since it includes a $j\omega$ term to account for the structural modes being expressed in terms of surface velocity instead of surface displacement. The complex resonance term given here also excludes any constants which are not frequency dependent as they are unimportant for this work. The excitation of the structural modes due to the forcing functions and the complex resonance terms is described by,

$$\boldsymbol{a}^i = B^f \boldsymbol{A}^s \boldsymbol{F}^i \tag{6.5}$$

Where $\boldsymbol{a}^i$ is a complex vector of structural mode amplitudes due to the primary incident plane wave and B^f is a constant which relates the forcing of the mode to the excitation. B^f will be a function of the structural properties of the cylinder i.e. stiffness, density etc.

6.2.2 The forcing of the structure due to the secondary piezoelectric

The calculation of the forcing of the structure by the piezoelectric actuator follows the approach of Lester and Lefebvre [64]. This approach models the effect of two piezoelectric ceramic patches placed on opposite sides of the cylinder walls and driven out of phase with one another. This actuator arrangement minimizes the in-plane forces (in-plane forces due to the two actuators tend to cancel) and produces a bending moment. In the experiment presented in section 6.4 only a single piezoelectric patch was used and the in-plane forces produced by the single actuator were not considered.

In a more complete and accurate model these forces would have to be taken into account.

The structural mode shapes given by equation 6.1 can be broken into two parts, one to deal with the sin term and one to deal with the cos term. The centre of the piezoelectric is positioned at (x_c, θ_c) and its dimensions are defined as $(\Delta x, \Delta\theta)$. The equations which define their excitation will also be dependent on the value of n. If $n = 0$ the modal forcing terms are given by,

$$F_{mn}^{c_{\cos}} = \frac{B^{pz} m \Delta\theta}{4} \sin\left(\frac{m\pi\Delta x}{2l}\right) \sin\left(\frac{m\pi x_c}{l}\right)$$
$$F_{mn}^{c_{\sin}} = 0 \tag{6.6}$$

$F_{mn}^{c_{\cos}}$ is the forcing coefficient regarding the cos term and $F_{mn}^{c_{\sin}}$ is related to the sin term. B^{pz} is a constant which relates a unit input to the piezoelectric to the forcing of the modes and is a function of the piezoelectric properties of the ceramic as well as the structural properties of the ceramic, the bonding material and the cylinder. If n is greater than zero then the equations are given by,

$$F_{mn}^{c_{\cos}} = G_{mn} B^{pz} m \Delta\theta \left(\sin\left(\frac{m\pi\Delta x}{2l}\right) \sin\left(\frac{m\pi x_c}{l}\right) \sin\left(\frac{n\Delta\theta}{2}\right) \cos(n\theta_c)\right)$$
$$F_{mn}^{c_{\sin}} = G_{mn} B^{pz} m \Delta\theta \left(\sin\left(\frac{m\pi\Delta x}{2l}\right) \sin\left(\frac{m\pi x_c}{l}\right) \sin\left(\frac{n\Delta\theta}{2}\right) \sin(n\theta_c)\right) \tag{6.7}$$

where G_{mn} is a weighting coefficient given by,

$$G_{mn} = \frac{m}{n} + \frac{nl^2}{m\pi^2 r_0^2} \tag{6.8}$$

and r_0 is the radius of the cylinder. The terms $F_{mn}^{c_{\cos}}$ and $F_{mn}^{c_{\sin}}$ can be combined to produce a vector of forcing terms $\boldsymbol{F}^c$ for all of the structural modes considered. The vector of structural mode amplitudes due to a unit input to the piezoelectric actuator $(\boldsymbol{c}_s)$ will be dependent upon the forcing vector and the vector of complex resonance terms.

$$\boldsymbol{c}_s = B^f \boldsymbol{A}^s \boldsymbol{F}^c \tag{6.9}$$

Because the forcing of the structural modes due to the secondary source is a function of a complex control signal u, which can be altered to affect control (as in section 5.3), the total structural mode amplitudes can be expressed as,

$$\boldsymbol{a} = \boldsymbol{a}^i + \boldsymbol{c}_s u \tag{6.10}$$

6.2.3 Radiation from structural modes into the acoustic cavity

The radiation from the vibrating cylinder into the inner cavity can be described by the coupling between the structural modes and the acoustic modes of the cylindrical cavity. The acoustic mode shapes are given by,

$$\psi_{n'pm'}(x,\theta,r) = J_{n'}(k_r r)\cos\left(\frac{m'\pi x}{L}\right)\begin{matrix}\cos\\ \sin\end{matrix}(n'\theta) \tag{6.11}$$

where $J_{n'}$ is an n'^{th} order Bessel function and k_r is the radial wavenumber determined by the zero normal-particle wall boundary condition as solutions of the equation $J_{n'}(k_r r) = 0$ when $r = r_0$ the cylinder radius [38].

To calculate the coupling between a structural mode and an acoustic mode the product of the two mode shapes is integrated at the cylinder wall (surface area S) and multiplied by the complex resonance term for the acoustic mode i.e.

$$C_{mn,n'pm'} = A^a_{n'pm'}\int_S \psi_{n'pm'}(x,\theta,r)\phi_{mn}(x,\theta)dS \tag{6.12}$$

where $C_{mn,n'pm'}$ is the coupling factor between the mn^{th} structural mode and the $n'pm'^{th}$ acoustic mode and $A^a_{n'pm'}$ is the complex resonance term for the acoustic modes taking the same form as that of equation 3.15. The coupling factors for all of the combinations of structural and acoustic modes can then be represented as a matrix of coupling factors $\boldsymbol{C}$. The coupling matrix $\boldsymbol{C}$ is calculated numerically and can be calculated as,

$$\boldsymbol{C} = \boldsymbol{A}^a\boldsymbol{\Psi}\boldsymbol{\Phi} \tag{6.13}$$

where $\boldsymbol{A}^a$ is a diagonal matrix of complex resonance terms for the acoustic modes and $\boldsymbol{\Psi}$ is a matrix of pressures due to the acoustic mode shapes at the elemental positions on the inner surface of the cylinder.

The acoustic modes considered for these simulations were; $n' = 0$ to 6, $p = 0$ to 2 and $m' = 0$ to 4. The total excitation of each of the acoustic modes is then given by the vector,

$$\boldsymbol{b} = \boldsymbol{b}^i + \boldsymbol{c}_a u \tag{6.14}$$

where,

$$\boldsymbol{b}^i = B^{cup} C \boldsymbol{a}^i \tag{6.15}$$

and

$$\boldsymbol{c}_a = B^{cup} C \boldsymbol{c}_s \tag{6.16}$$

where $\boldsymbol{b}^i$ is a complex vector of acoustic mode amplitudes due to the primary excitation (incident plane wave) and $\boldsymbol{c}_a$ is the complex vector of acoustic mode amplitudes due to the secondary piezoelectric source acting with unit excitation. B^{cup} is a constant which relates the vibration of the structure to the amplitude of the acoustic modes and is a function of the properties of the fluid i.e. density, speed of sound etc.

6.2.4 Minimization of acoustic potential energy

The total acoustic potential energy in the enclosure is proportional to the sum of the squared acoustic mode amplitudes (section 5.2.4).

$$E_p \propto \boldsymbol{b}^H \boldsymbol{b} = (\boldsymbol{b}^i + \boldsymbol{c}_a u)^H (\boldsymbol{b}^i + \boldsymbol{c}_a u) \tag{6.17}$$

which is minimized if the secondary source strength is given by $u = u_{opt}$ where,

$$u_{opt} = -(\boldsymbol{c}_a^H \boldsymbol{c}_a)^{-1} (\boldsymbol{c}_a^H \boldsymbol{a}^i) \tag{6.18}$$

By substituting this optimal secondary source strength into the equation for the total acoustic potential energy (equation 6.17) the attenuation of this parameter can be calculated. For the purposes of calculating the optimal secondary source strength the constants B^f and B^{cup} are unimportant since they affect both the acoustic mode amplitudes $\boldsymbol{b}^i$ and $\boldsymbol{c}_a$ to the same extent and therefore cancel in equation 6.18.

6.3 Results of computer simulations

The computer simulations carried out were intended to give an idea of the effectiveness of an active control system in controlling the acoustic transmission into an enclosed cylinder. The results shown here are examples of the very large number of possible permutations of source position, frequency range, structural characteristics etc. This section will therefore examine configurations similar to those tested experimentally using a composite cylinder previously used for sound transmission experiments [75].

For the results shown here the cylinder length was taken to be $0.94m$, the radius to be $0.45m$, the structural damping factor to be 0.02 and the acoustic damping factor to be 0.005. Thirty five structural modes and one hundred and five acoustic modes are considered in these simulations. The centre of the piezoelectric actuator was placed at $x = 0.3m$ and $\theta = \frac{\pi}{2}$, and was assumed to be $100mm$ long (in x direction) and $45mm$ wide (circumferentially). The mechanical properties of the cylinder are only used in the calculation of the natural frequencies of the structural modes and are not necessary for the calculation of the optimal secondary source strengths (equation 6.18), if the natural frequencies are provided. The properties of the model cylinder and the natural frequencies of the structural and acoustic modes are taken from [75] and tabulated in tables 6.1 to 6.3.

6.3.1 Case 1: Plane wave incident at 45^0

The plane wave primary field in this example was assumed to be incident on the cylinder at an angle of $\varphi = 45^0$ to the x axis and at an angle of $\varphi = 0^0$. The acoustic energy levels before and after control with the optimally adjusted piezoelectric actuator are shown in figure 6.2.

Parameter	Value
Face Plates (CFRP, common)	
Thickness (mm)	1.0
Density $10^3(kg/m^3)$	1.6
Elastic mod. $10^9(N/m^2)$	
Tensile axial	26.2
Tensile circumf.	69.5
Shear in plane	19.3
Core (aluminium honeycomb)	
Thickness (mm)	5
Density (kg/m^3)	48
Shear mod.$10^6(N/m^2)$	
Axial	240
Circumf.	150
Wall	
Length (m)	0.94
Diameter (m)	0.9
Mass/area (kg/m^3)	4.0

Table 6.1: Properties and dimensions of the cylinder used in the active control experiments.

Structural mode (m,n)	Natural frequency (Hz)
(1,4)	268
(1,3)	278
(1,5)	353
(1,2)	467
(1,6)	478
(2,5)	535
(2,4)	586
(2,6)	592

Table 6.2: Predicted natural frequencies of the first few structural modes.

Acoustic mode (n', p, m')	Natural frequency (Hz)
(0,0,0)	0
(0,0,1)	182
(1,0,0)	223
(1,0,1)	288
(0,0,2)	365
(2,0,0)	370
(2,0,1)	413
(1,0,2)	428
(0,1,0)	465
(0,1,1)	499
(3,0,0)	510
(2,0,2)	520

Table 6.3: Predicted natural frequencies of the first few acoustic modes.

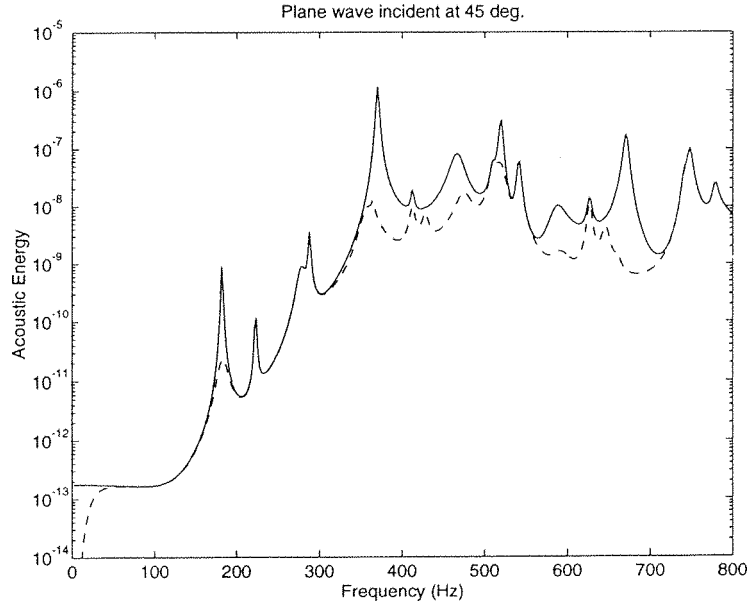

Figure 6.2: The acoustic energy present in the cylindrical cavity before (solid) and after control (dashed) when controlling the transmission due to an incoming plane wave incident at 45^0.

These results show that the control system has the ability in most cases to reduce the acoustic energy due to resonant behaviour. At resonance the response is dominated by a single structural and/or acoustic mode and a single channel system which can couple into this mode will in general be able to achieve good attenuations. What is more interesting is the cases where off-resonant control is achieved. This occurs in two regions in the frequency range considered: (i) $350-500Hz$ and (ii) $550-700Hz$. The off-resonant response of a system inevitably involves more than one mode. Therefore a single channel control system will generally be unable to achieve good attenuations off-resonance. However, the response of the system is determined by the interaction of two sets of modes, and although the off-resonant acoustic behavior may be due to a number of *acoustic* modes they may all be excited to the largest extent by a *single structural mode* even though there are other structural modes excited to a significant extent. The reduction of this structural mode amplitude will therefore produce good off-resonant attenuation. This observation has also been made in connection with sound transmission into a cylinder by Fuller and Jones [42]. The above scenario could equally occur where a single acoustic mode is being excited by a number of structural modes. In this case the actuator could minimize the *net* contribution to that acoustic mode to achieve good off-resonant control.

In the case considered here there are a number of structural *and* acoustic resonances present in the $350-500Hz$ frequency range. The important factor is the *coupling* between the structural and acoustic modes. A single structural mode will not couple into the *majority* of the acoustic modes because they are not matched geometrically. It is therefore possible for numerous structural resonances and acoustic resonances to occur within a frequency range and the coupling to be dominated by the interaction of a single structural mode with a single acoustic mode. In this simulation the $n = 2$, $m = 1$ structural resonance ($467Hz$) has a natural frequency which is fairly close to the $n' = 2$, $p = 0$, $m' = 0$ acoustic mode ($370Hz$). These two modes couple very well geometrically , and most of the other structural and acoustic modes in this frequency range do not couple at all. It is therefore possible amongst a large number of individual resonances to achieve good off-resonant attenuation using a single channel control system. Similarly the control in the $550-700Hz$ range is due to good geometric coupling between the $n = 4$, $m = 2$ structural mode ($586Hz$) and

the $n' = 4$, $p = 0$, $m' = 1$ acoustic mode ($671Hz$).

To demonstrate the importance of the $n = 2$, $m = 1$ structural mode in the transmission of sound in the $350 - 500Hz$ frequency range the simulation was repeated with the amplitude of the $n = 2$, $m = 1$ structural mode set to zero. The resulting sound transmission is greatly reduced over this frequency range as shown in figure 6.3.

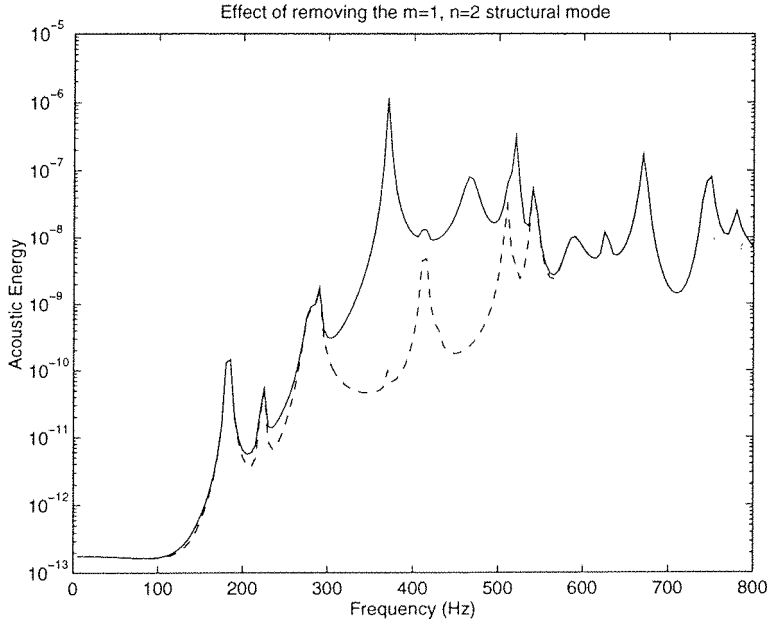

Figure 6.3: The acoustic energy levels due to an incoming plane wave incident at 45^0 (solid) and with the $m = 1$, $n = 2$ structural mode removed.

6.3.2 Case 2: Plane wave incident at 90^0

The second case considered was to some extent simpler than Case 1. The incident plane wave was angled at $\varphi = 90^0$ to the cylinder and therefore the even number longitudinal structural modes were not excited (i.e. $m = 2, 4, 6...$). The attenuations predicted after control with the secondary piezoelectric ceramic optimally adjusted are shown in figure 6.4. In this case there are again significant attenuations possible in the $350 - 450Hz$ frequency range but there is no attenuation in the $550 - 700Hz$ range since the $m = 2$, $n = 4$ mode is not excited by the primary excitation.

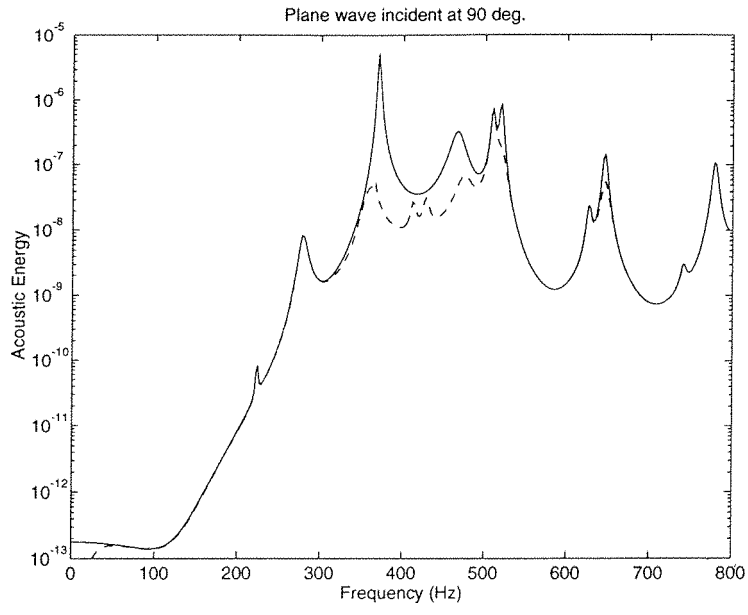

Figure 6.4: The acoustic energy present in the cylindrical cavity before (solid) and after control (dashed) when controlling the transmission due to an incoming plane wave incident at 90^0.

6.4 Experiment

6.4.1 Experimental arrangement

The experimental work was carried out on a model cylinder which was originally constructed as a 1/6 scale model of an Ariane 5 fairing and used in earlier experiments [75]. The cylinder was of dimension $l = 0.94m$ and $r_0 = 0.45m$ (figure 6.5.) and constructed of thin aluminium honeycomb covered by carbon fibre re-enforced plastic. The end caps were made of $8mm$ steel to provide stiff (simply supported) end conditions. The cylinder was suspended from the ceiling of a large anechoic chamber by steel cables connected to the end caps.

The primary sound field for the experiment was generated by an 8 inch loudspeaker. The secondary actuator used was a $100mm \times 45mm \times 2mm$ piezoelectric ceramic plate which was driven via a 1 to 128 step-up transformer to produce high drive voltages from low voltage amplifiers. The actuator can be driven with voltages of over 1000 volts but for the purposes of this experiment it was only necessary to use between 50 and 200 volts. The piezoelectric ceramic was fixed to the cylinder using epoxy

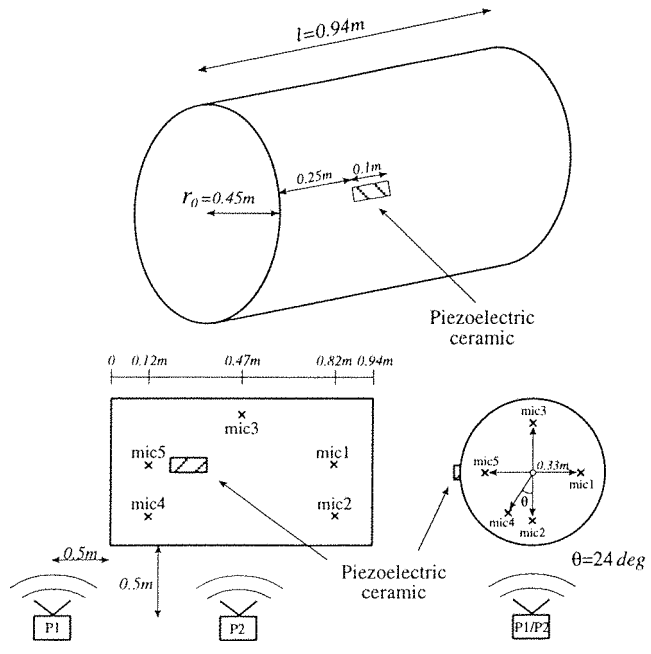

Figure 6.5: The experimental layout of the cylinder showing the microphone locations, the secondary actuator's position and the two primary source positions.

glue and this involved attaching the flat piezoelectric surface to the curved cylinder. Therefore, an epoxy base was cast to produce a flat surface onto which the actuator could be glued. This is probably an undesirable arrangement for high excitation levels and to remedy this problem bases could be made of stiffer material (i.e. metal) or the actuators themselves could be manufactured curved. It may also be possible to integrate the actuators into the face plate construction of the fairing sandwich wall.

To observe the sound pressure inside the cavity, five electret microphones were placed in the positions shown in figure 6.5. A single accelerometer was moved to a number points on the external structure to measure the vibration levels and to detect the structural modes present at various frequencies.

6.4.2 Accelerometer results

The frequency response between the primary or secondary source and an accelerometer placed on the cylinder was measured for various accelerometer locations (figure 6.6).

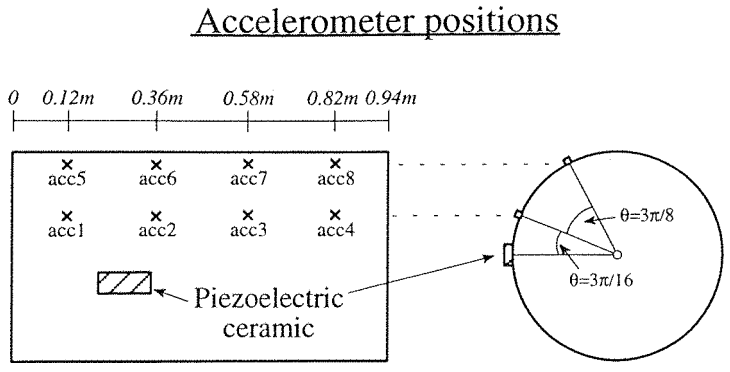

Figure 6.6: The eight accelerometer positions on the cylinder.

These measurements allowed the identification of the structural mode order and a comparison between the measured and predicted natural frequencies. The mode order was deduced from the shape of the measured axial acceleration and the relative phases of the acceleration circumferentially. This was sufficient to identify the first few modes. Figure 6.7, for example, shows the frequency response between the input to the piezoelectric actuator and the accelerometer at position 1.

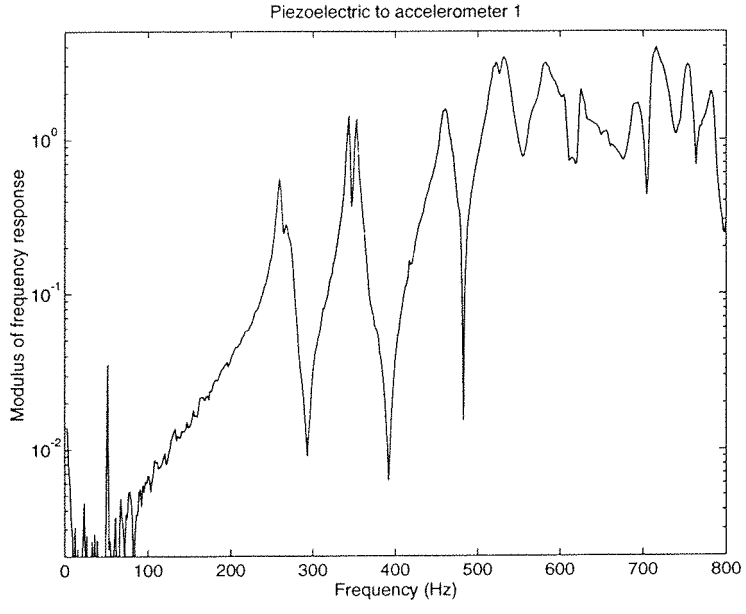

Figure 6.7: The frequency response of accelerometer 1 to the piezoelectric actuator.

The observed natural frequencies of the first few modes fall within 4 percent of the natural frequencies previously predicted (table 6.4). Some of the measured responses

have double peaks (probably due to asymmetries within the cylinder) and therefore both peak frequencies are quoted.

Mode (m,n)	Predicted	Measured
(1,4)	268	259
(1,5)	353	345 or 353
(1,2)	467	461
(2,5)	535	522 or 531

Table 6.4: Predicted and measured natural frequencies of the first few structural modes in Hz.

6.4.3 Broadband frequency response measurements

The frequency responses between the input to the primary source and the five microphones and the frequency responses between the input to the secondary source and the five microphones was measured over the $0 - 800Hz$ frequency range using the apparatus shown in figure 6.8.

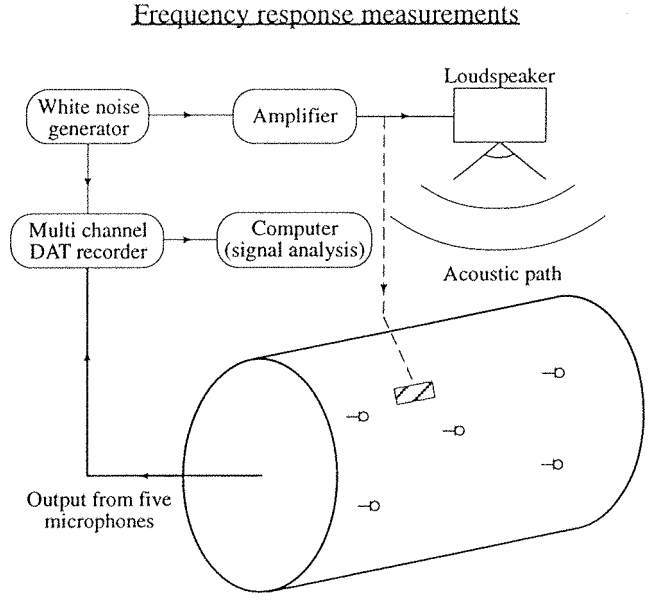

Figure 6.8: The equipment layout used for the frequency response measurements of $\boldsymbol{p}_p$. The measurement of $\boldsymbol{z}$ involves driving the piezoelectric instead of the loudspeaker (dashed line).

This was carried out for the two primary source locations $P1$ and $P2$ which generated primary fields incident on the cylinder at approximately 45^0 and 90^0 for comparison

with the theory in section 6.3. At a single frequency the pressures at the five microphone locations are represented by the five element vector $\boldsymbol{p}_p$. By driving the primary source with white noise the vector $\boldsymbol{p}_p$ could be measured over a range of frequencies and acted as an example of a primary disturbance. The frequency responses between the secondary source and the five microphones was also measured and at a single frequency the pressures due to a unit input to the secondary source are represented by a complex vector $\boldsymbol{z}$. The pressures at the microphones due to the secondary source are therefore given by $\boldsymbol{p}_s = \boldsymbol{z}u$, where u is the complex secondary source strength. The sum of the mean squared pressures at the microphone positions, which is an estimate of the total acoustic potential energy, can then be calculated at a given frequency for any secondary source strength,

$$J = (\boldsymbol{p}_p + \boldsymbol{z}u)^H(\boldsymbol{p}_p + \boldsymbol{z}u) \tag{6.19}$$

where J is the sum of the mean squared pressures at the microphone positions. This equation is very similar to equation 5.29 which describes the kinetic energy in a plate and there is a unique secondary source strength u_{pres} which minimizes this function. This is given by,

$$u_{pres} = -(\boldsymbol{z}^H\boldsymbol{z})^{-1}\boldsymbol{z}^H\boldsymbol{p}_p \tag{6.20}$$

By substituting the optimal secondary source strength calculated from the measured data back into the equation for the sum of the squared pressures (equation 6.19) and dividing by the original pressure (i.e. before control) the ratio of the sum of the squared pressures before and after optimal control can be calculated,

$$\frac{J_{min}}{J_{prim}} = 1 - \frac{\boldsymbol{p}_p^H\boldsymbol{z}\boldsymbol{z}^H\boldsymbol{p}_p}{\boldsymbol{z}^H\boldsymbol{z}\boldsymbol{p}_p^H\boldsymbol{p}_p} \tag{6.21}$$

The sum of the mean squared pressures J_{min} is obtained when the secondary source strength is set to the optimal value u_{pres} and J_{prim} is the sum of the mean squared pressures when $u = 0$ and is given by $J_{prim} = \boldsymbol{p}_p^H\boldsymbol{p}_p$.

The primary disturbance was taken as the sound pressure measured by five microphones when the primary source was driven with white noise. The disturbance there-

fore incorporates the frequency responses of the primary loudspeaker, the microphones and some electronics. These responses will affect the absolute pressure levels before and after control but will not affect the predicted attenuations.

6.4.4 Attenuation prediction

The frequency responses between the primary source $P1$ (at 45°) and the five microphones, is used to produce the solid line graph in figure 6.9, which represents the sum of the squared pressures measured at the microphone positions due to the primary source alone. The dashed line represents the sum of the squared pressures at the microphone positions after optimal control (equation 6.21).

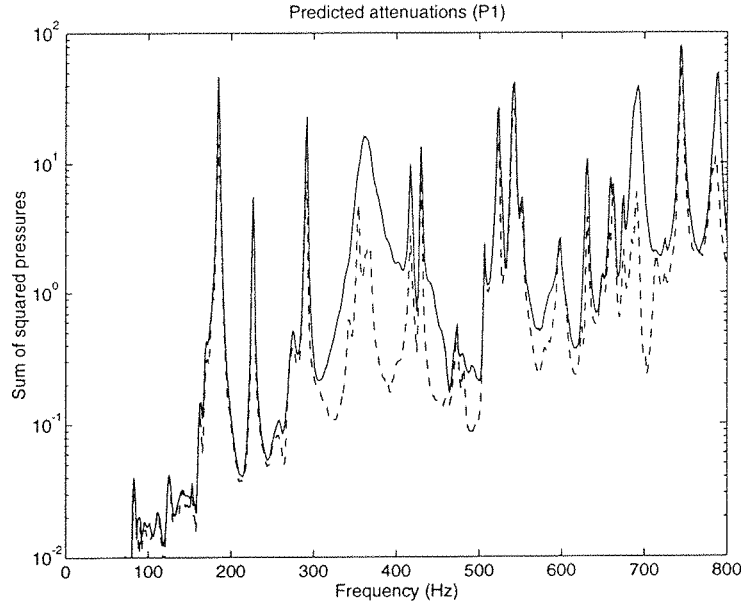

Figure 6.9: The sum of the squared pressures measured at the five microphone positions without control (solid) and the levels predicted after control (dashed) for the primary source P1.

The primary field displays many sharp resonances across the frequency range which all seem to be attenuated to some extent by the control system (between 2 and $5dB$). There are also two regions of significant off resonant control, the first being between $300-450Hz$ and the second between $670-720Hz$. This corresponds very well to the regions of attenuation predicted by the computer model in section 6.3 (figure 6.2).

The predicted attenuations using the frequency response measurements with the primary source $P2$ (90^o) are shown in figure 6.10. It is encouraging to see that the frequency regions of attenuation again corresponded well to those predicted from the computer simulations (figure 6.4). The resonance occurring at $695Hz$ ($n = 4$, $m = 2$) is not nearly as strongly excited as in figure 6.9, and therefore less attenuation is possible. The computer simulation predicted that this mode would not be excited at all if the primary source was in this location but some excitation of every mode can be expected in any practical situation. It this case the attenuations predicted are even larger than with the primary source $P1$ in the $300 - 450Hz$ range with reductions at some frequencies exceeding $20dB$.

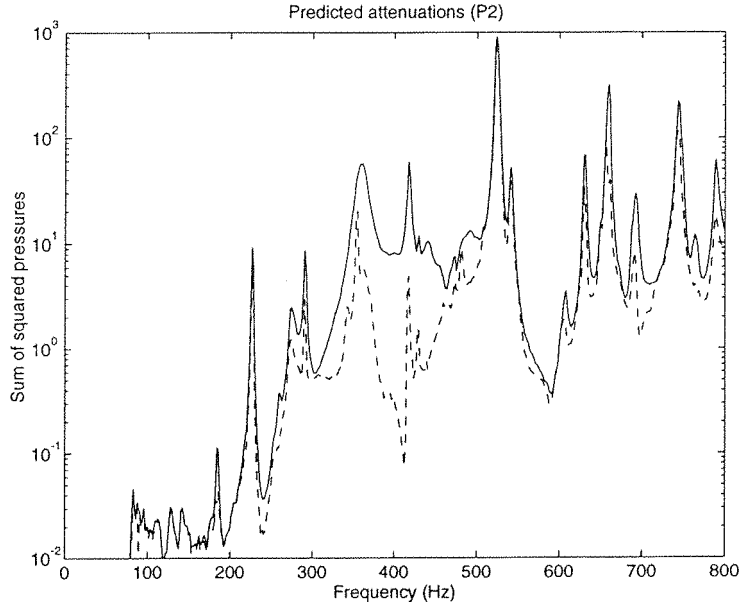

Figure 6.10: The sum of the 5 squared pressures measured at the microphone positions without control (solid) and the levels predicted after control (dashed) for the primary source S2.

6.4.5 Single channel control

By taking frequency response measurements (sections 4.2 and 4.3) the attenuation due to the action of the secondary actuator, over a range of frequencies, can be predicted. To ensure that these predicted attenuations could be achieved in practice, active control experiments were carried out at two frequencies. The control was carried out

manually by altering the phase and amplitude of the input to the secondary source while monitoring the response of the microphones (figure 6.11) when the cylinder was excited by the primary source $P1$ (figure 6.5).

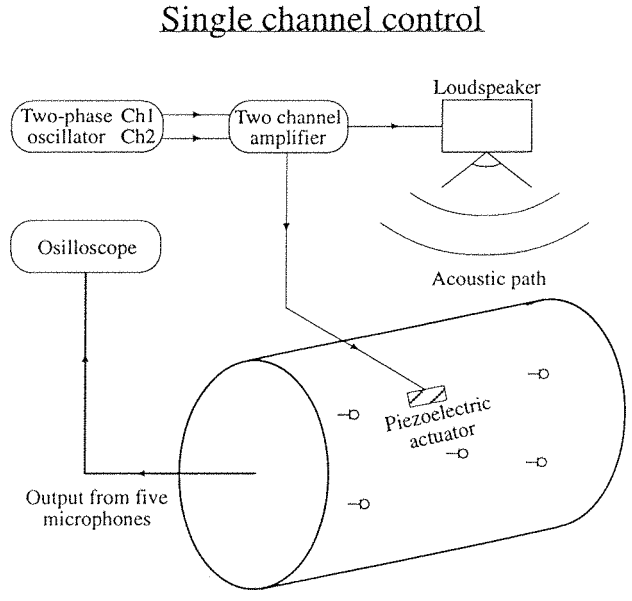

Figure 6.11: The equipment layout used for the active control of sound into the cylinder.

Although this adaption method is crude the results can be directly compared with the predicted attenuations (section 6.4.4) at two frequencies.

6.4.6 Results of single channel control

The control was carried out at two frequencies $359Hz$ and $415Hz$ ($60Hz$ and $69Hz$ full scale). The resulting reductions in mean squared pressure levels measured at the microphone positions after manual control were $10dB$ and $7dB$ respectively. This corresponded very well to the $10.6dB$ and $5.3dB$ in attenuation predicted by the frequency response measurements at these frequencies (figure 6.9).

6.5 Conclusions and discussion

A simple theoretical model has been constructed to determine the acoustic excitation inside a cylinder due to an external plane acoustic wave as a primary source and

a piezoelectric actuator bonded to the cylinder as the secondary source. This has enabled predictions to be made of the attenuations in the total acoustic potential energy inside the cylinder using a single channel feedforward control system operating at a single frequency.

The predicted attenuations are significant $(10 - 20dB)$ in the two frequency regions for which, with the cylinder considered here, the sound transmission into the cylinder is dominated by the interaction between a single structural mode and a single acoustic mode.

Experiments were conducted on a $0.94m$ long by $0.9m$ diameter honeycomb cylinder with rigid end caps which is a 1/6 scale model of an Ariane 5 payload fairing. The pressure was measured with 5 microphones inside the cylinder when excited by an external loudspeaker, representing the primary source, and a $100mm \times 45mm \times 2mm$ piezoceramic patch glued to the cylinder as the secondary source. The potential reductions in the sum of the squared pressures were calculated for pure tone excitation at frequencies up to $800Hz$, and these reductions were similar to those predicted by the theoretical model.

Finally, some single channel active control experiments were conducted at two discrete frequencies in which the internal pressures due to the external loudspeaker were reduced by adjusting the amplitude and phase of the pure tone signal fed to the secondary actuator. Reductions in the sum of the squared internal pressures of $7dB$ and $10dB$ were measured, which compares well with the reductions predicted. These reductions were achieved at $359Hz$ and $415Hz$ corresponding to $60Hz$ and $69Hz$ full scale.

This work demonstrates that although the precise calculation of every feature of sound transmission into a cylinder cannot be represented using a simple theoretical model the important physical aspects which determine the overall performance of an active control system can be easily represented. For the cylinder considered here it was generally the interaction between specific structural and acoustic modes which determined the performance. It has also been demonstrated that these potential reductions can be achieved in practice for a pure tone primary excitation.

This work was carried out on a 1/6 scale model and therefore scaling effects must be

considered. The scaling of the natural frequencies of the acoustic modes is linear but this is not the case for the structural modes and therefore a change in scale will also change the interaction between these two sets of modes. This scale model was designed with this scaling effect in mind and scaling effects would have been partially taken into account. However, given that in this case the attenuations achieved were due to the interaction between the structural and acoustic modes it would be important to repeat the current exercise using data for the full scale model, initially using computer simulations with some experimental verification.

It would also be useful to investigate the additional attenuations achievable by using multiple secondary sources. This would be relatively easy to carry out with a computer simulation. In the experiments presented in this chapter the secondary source was deliberately positioned such that it coupled into the circumferential modes in a similar way to the primary source. This will not be possible in practice and at least two secondary sources will be required to ensure that the control system can couple into a circumferential mode in a similar way to the primary source.

It has been shown that much of the sound transmission over a frequency range can be dominated by a single structural mode. The cancellation of this mode could therefore significantly reduce the sound transmission over that range. A distributed modal sensor has an output which is purely a measure of the amplitude of a specific structural mode and could be used as an error sensor in a feedback control system to reduce that modal amplitude. A modal actuator is the reciprocal of a modal sensor, forcing only a specific mode and not largely affecting the amplitudes of the other structural modes. The problem with the use of modal sensors *without* modal actuators is that the reduction in the amplitude of one mode will in general be accompanied by an increase in the amplitudes of other modes. However, a modal sensor/actuator pair would have the ability to remove the desired structural mode without altering the amplitudes of the other modes. Modal sensors and actuators can be approximated by a number of individual transducers in an array or can be made of distributed material i.e. piezoelectric film. A perfect feedback control system, with a modal actuator and sensor for the $m = 1$, $n = 2$ mode would produce the attenuation shown in figure 6.3. These attenuations would in principle be possible for any primary excitation whether it was random or deterministic.

The largest and most difficult extension of this work will be to control random signals rather than harmonic signals. Potentially there are two approaches which can be taken: (i) a feedforward approach or (ii) a feedback approach.

Feedforward control implies that the primary disturbance can be measured *ahead of time*. This requires that the disturbance is measured before it reaches the fairing. This would be very difficult in practice because the pathways between the engine exhaust and the fairing are very complex. These pathways are also *dynamic* and as conditions change (i.e. speed of launcher, distance from ground, speed of sound etc.) these pathways will vary. It is unlikely that a sufficiently accurate reference signal could be obtained for this application.

Feedback control, however, does not require prior information about the primary signal. A system could be developed that uses feedback control to reduce the sound transmission into the payload bay. The smaller the time delay between the output of the secondary actuator and the control sensor, the better the performance of a feedback system [71]. The time delay due to an acoustic signal travelling from a secondary source to a microphone in the payload bay will generally be larger than that for an actuator/sensor combination placed on the structure. It is therefore likely that a realistic feedback system will involve the use of modal sensors and actuators designed to sense and force specific structural modes or some weighted combination of structural modes.

It has been recently demonstrated that feedback control systems can in principle be used to suppress narrow-band disturbances [37]. Physical performance limitations of such a system can be determined before any experimental work is undertaken. The relatively narrow-band character of the pressure spectrum inside the cylinder (figures 6.9 and 6.10) suggests that a feedback controller could potentially have a high performance. The subject of feedback control and its application to the active control of sound transmission will be dealt with more thoroughly in chapter 8 of this thesis.

Chapter 7

Active control of sound power radiation using a volume velocity sensor

7.1 Introduction

It was shown in chapter 3 that the volume velocity of a surface is responsible for the majority of the sound power radiation at low frequencies i.e. where the dimensions of the surface are not large compared with a wavelength. It has therefore been suggested that at these frequencies the cancellation of volume velocity is an appropriate strategy for reducing the sound power radiation from vibrating surfaces and this is supported by the results of the computer simulations presented in chapter 5. In order to actively cancel the volume velocity of a surface an accurate measure of the volume velocity is required and designs for volume velocity sensors have been suggested in chapter 4 which use piezoelectric material etched or cut into specific shapes. In the experiments described in this chapter such a sensor is tested and used to control the sound power radiation from a rectangular aluminium panel.

A volume velocity sensor was made from PVDF film and the procedure used to manufacture this sensor is briefly described in the following section. This sensor was tested to determine its ability to accurately sense the volume velocity of a thin rectangular plate and was used as an error sensor in an active control system in an

attempt to reduce the acoustic transmission through a plate. The procedure used in the investigation described in this chapter is similar to that used in chapter 6 where predictions are made using measured frequency responses and then real time control is carried out at a number of discrete frequencies.

7.2 Experiments

7.2.1 Apparatus

The piezofilm sensor was tested on a aluminium plate of dimensions ($278mm \times 247mm \times 1mm$). This plate was rigidly clamped to the top of a small rigid box which was placed into a larger box of dry sand (figure 7.1). The clamped boundary conditions removed the sensitivity to bending in the y-direction and allowed the sensor to be manufactured using a single piece of PVDF film (section 4.3.2). A small loudspeaker was placed inside of the box and used to generate a primary disturbance. The rigidity of the inner box and the damping and mass provided by the outer box of sand ensured that the only significant path for the internal sound to travel to the outside was through the clamped aluminium plate. A small piezoceramic actuator ($25mm \times 25mm$) was fixed centrally to the lower side of the plate and used as a secondary actuator. A very small loudspeaker acting as an inertial actuator was used as an alternative secondary source in a separate series of experiments. The piezofilm sensor covered the entire surface of the plate and was fixed to the plate using *3M Spray Mount* adhesive which allowed for some repositioning of the sensor.

7.2.2 Sensor design

The spatial sensitivity required to produce a volume velocity sensor is derived in section 4.3.2. and was achieved in practice using a number of quadratically shaped strips, as shown in figure 4.3. For the frequency range of interest the modal density of the plate was such that 25 quadratic strips were considered to be sufficient to accurately sample the strain on the panel. If the modal density were higher then more strips may have been necessary.

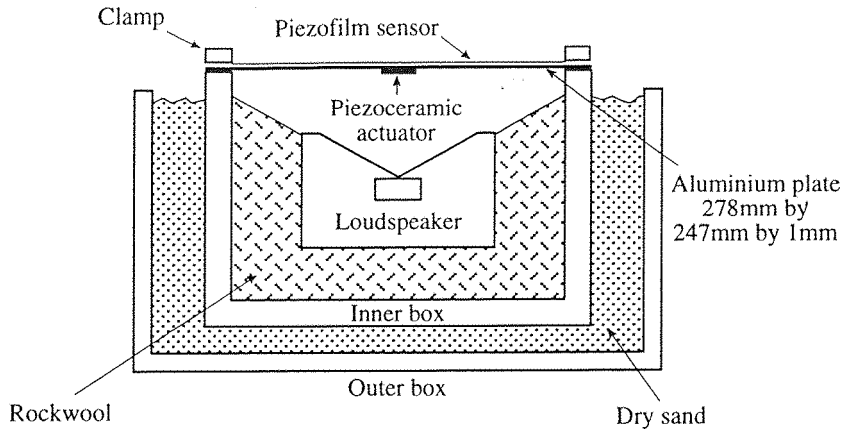

Figure 7.1: The controlled acoustic source used in the experiments.

7.2.3 Sensor construction

To create a reasonably accurate template with which to etch the piezofilm, a $600dpi$ laser printer was used to print the required image. A reduced version of this template is shown in figure 7.2. This image was then enlarged and transferred onto a transparency (final dimensions $278mm \times 247mm$). This transparency could then be used as a positive template with which to etch the film using standard circuit board etching techniques. It should be noted that the layer of metallization on the film is very much thinner than that covering a circuit board and hence diluted etching solutions should be used. The film used was a $52\mu m$ piezofilm with copper/nickel metallization. A digitized photograph of the apparatus is shown in figure 7.3 (without the outer box of sand).

7.2.4 Volume velocity measurements

To verify that the sensor was accurately measuring volume velocity a laser vibrometer was used to measure the velocity at a number of points on the surface of the panel over a seven by seven grid. These measurements were taken when the panel was excited first by the primary source and then by the secondary source. The measured complex velocities at the 49 positions were added together at each frequency to produce an estimate of the total volume velocity of the panel which could then be compared with the output of the piezofilm sensor. If higher order modes of the panel are well

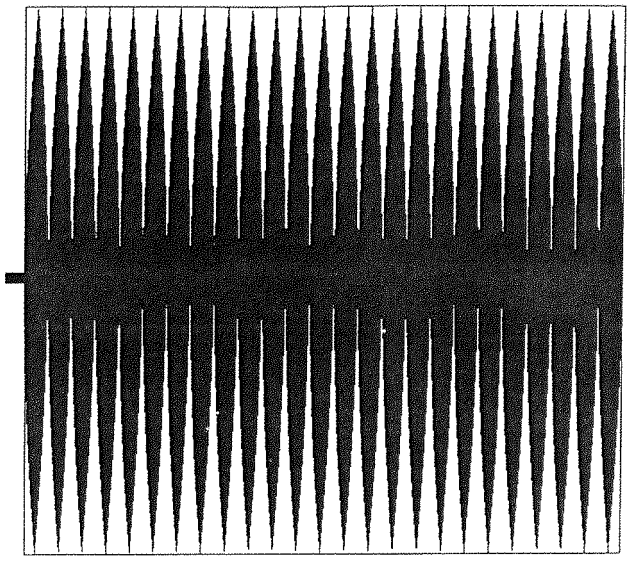

Figure 7.2: Template used to create volume velocity sensor

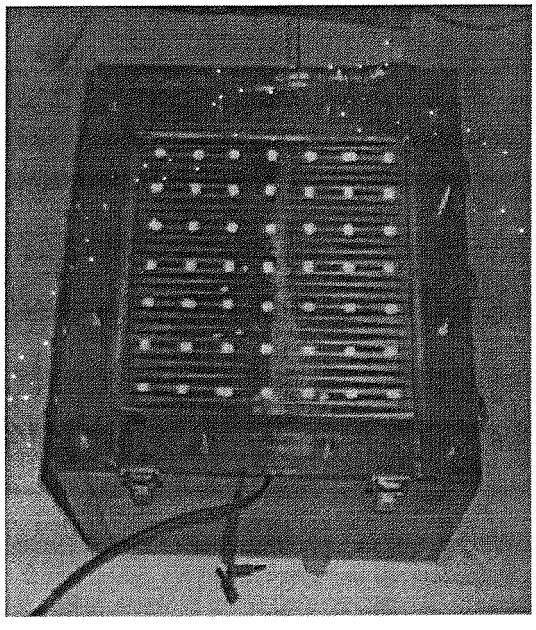

Figure 7.3: A photograph of the piezofilm sensor attached to the clamped plate and attached to a closed box. The reflective tape used for the 49 laser vibrometer measurements can be clearly seen.

excited, the volume velocity estimated by the laser vibrometer measurements will become inaccurate due to spatial aliasing. Above $1000Hz$ the mode order on the plate becomes too high for the laser vibrometer measurements to be useful. For a panel of this size $1000Hz$ corresponds to a kl_x value of 5.1 where k is the wavenumber and l_x is the largest dimension of the plate. Since the cancellation of volume velocity is a more useful strategy at low frequencies it was unlikely that large attenuations would be possible using this technique at frequencies above $1000Hz$.

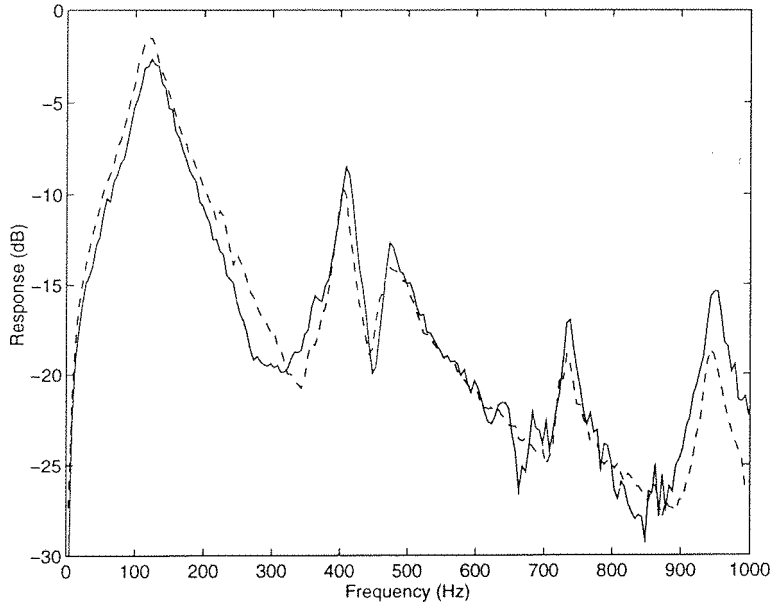

Figure 7.4: The volume velocity estimated using 49 laser vibrometer measurements (dashed) and the output of the piezofilm sensor (solid) when the panel was excited using the primary source.

In figure 7.4 the output of the piezofilm sensor and the volume velocity estimated by the laser vibrometer measurements are compared. The piezofilm sensor was designed to measure volume displacement and therefore the measured output was differentiated to produce the results presented here. Since the piezofilm sensor is uncalibrated the signals are normalized such that they are equal at $550Hz$. It can be seen from figure 7.4 that the output of the distributed sensor closely matches the estimate of the volume velocity, measured by the 49 point sensors, over most of the frequency range.

This procedure was repeated using the secondary actuator to excite the plate. The output of the sensor was again compared with the sum of the velocities at 49 points

on the surface of the panel, as shown in figure 7.5 and was normalized such that the responses were equal at $550Hz$. Again there is good agreement between the volume velocity estimate using the laser vibrometer measurements and the output of the piezoelectric sensor.

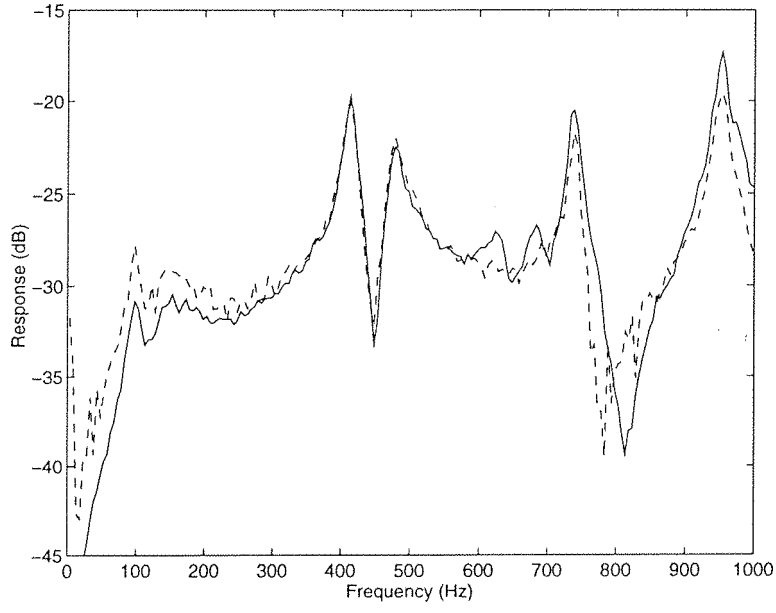

Figure 7.5: The volume velocity estimated using 49 laser vibrometer measurements (dashed) and the output of the piezofilm sensor (solid) when the panel was excited using the secondary source.

It should be noted that the first structural mode is very poorly excited by the secondary source and as this has consequences for control at low frequencies it will be discussed in more detail in section 7.2.5.

7.2.5 Reductions in sound power, predicted using measured frequency responses

If the panel is excited by the primary source, acting at a single frequency, then the amplitude and phase of the secondary source, acting at the same frequency, can be adjusted such that the output of the film sensor is set to zero. This implies that a signal from the primary source (i.e. a reference signal) is fed forward via a controller to the secondary source. In many applications the primary noise source would be an engine (propeller or automobile engine) from which a reference signal could be easily

obtained using a tachometer.

By cancelling the output of the piezofilm sensor it is expected that the sound power radiation would in general be reduced. To measure the potential reductions which could be achieved over a broad frequency range, the frequency responses between the input to the primary source (i.e. the loudspeaker) and ten microphones placed around the panel, and the frequency responses between the secondary source (i.e. the piezoceramic actuator) and the ten microphones, were measured in an anechoic environment. These frequency responses can be manipulated to give predicted reductions in the sum of the squared pressures at the microphone positions, as described in chapter 6. The microphone positions used are illustrated in figure 7.6 and are taken from the ISO 3745 standard for measuring the acoustic power output from a source [46]. Also measured were the frequency responses between the input to the primary source and the output of the piezofilm sensor and the input to the secondary source and the output of the piezofilm sensor. If the secondary source were used to cancel the output of the piezofilm sensor, the effect at the ten microphone positions could be predicted using these measurements. Although the prediction of the performance of the control system using measured frequency responses is an approximate technique, it is an efficient method of calculating the performance at a large number of frequencies without having to actually carry out the control at each frequency. The optimal control possible at the ten microphones using the secondary actuator can also be predicted from the frequency response measurements and can be compared with the cancellation of the output of the piezofilm sensor.

At any one frequency the complex output of the ten microphones due to a unit input to the primary source can be expressed as a ten element complex vector $\boldsymbol{p}_p$. The output of the ten microphones due to the piezoceramic actuator, driven with a complex amplitude u, can be expressed as $\boldsymbol{z}u$ where $\boldsymbol{z}$ is also a ten element complex vector. The vector of total output signals from the ten microphones, when the primary source has a unitary input and the secondary source is driven with a complex amplitude u, is therefore given by $\boldsymbol{p}_p + \boldsymbol{z}u$. The frequency response measurements described above were used to define the elements of the vectors $\boldsymbol{p}_p$ and $\boldsymbol{z}$ for a large number of discrete frequencies across the frequency range considered. The sum of the squared pressures J at a single frequency due to the action of both the primary and the secondary

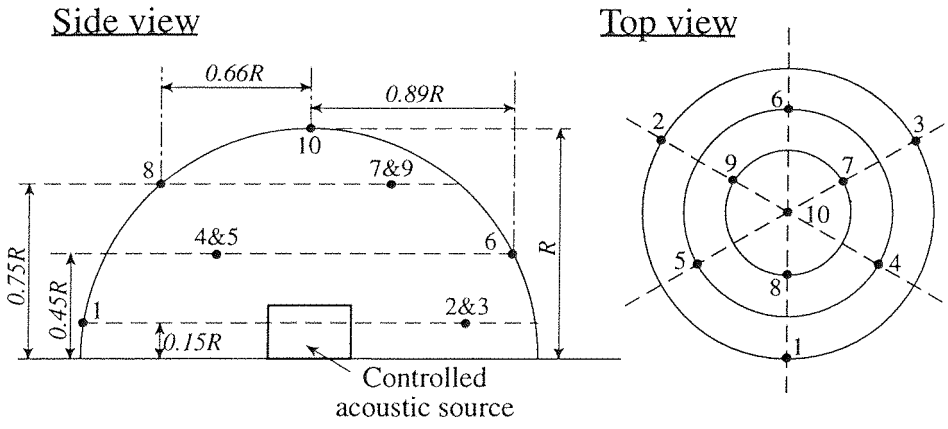

Figure 7.6: Microphone positions used in the active control experiment.

sources is therefore given by,

$$J = (\boldsymbol{p}_p + \boldsymbol{z}u)^H(\boldsymbol{p}_p + \boldsymbol{z}u) \tag{7.1}$$

The sum of the squared pressures at the ten microphone positions due to the primary source alone (i.e. $u = 0$) is given by,

$$J_{prim} = \boldsymbol{p}_p^H \boldsymbol{p}_p \tag{7.2}$$

The output of the the piezofilm sensor due to a unit input to the primary source at a single frequency is given by the complex number d and the output of the piezofilm sensor due to the piezoceramic actuator driven with a complex amplitude u is given by cu where c is a complex scalar. The total piezofilm sensor output is therefore given by $e = d + cu$. The secondary source strength u_{sens} which cancels the output of the piezofilm sensor is thus given by,

$$u_{sens} = -\frac{d}{c} \tag{7.3}$$

If the secondary source is adjusted such that the output of the piezofilm sensor is zero (i.e. amplitude u_{sens}) the sum of the squared pressures at the ten microphone positions J_{sens} can be calculated by substituting the secondary source strength u_{sens} into equation 7.1.

The frequency response measurements ($\boldsymbol{p}_p$ and $\boldsymbol{z}$) can also be used to predict the optimal secondary source strength necessary to minimize the sum of the squared pressures at some or all of the microphones (as in section 6.4.3). The optimal secondary source strength will then be given by,

$$u_{pres} = -(\boldsymbol{z}^H \boldsymbol{z})^{-1} \boldsymbol{z}^H \boldsymbol{p}_p \tag{7.4}$$

By substituting the optimal value for the complex secondary source strength into the equation for the total sum of the squared pressures (equation 7.1) the optimal sum of the squared pressures J_{min} can be calculated.

The values of J_{prim}, J_{sens} and J_{min} can then be compared to determine whether any significant reductions in the sound at the ten microphone positions can be achieved and whether the minimization of the output of the piezofilm sensor gives results which are comparable to the optimal strategy.

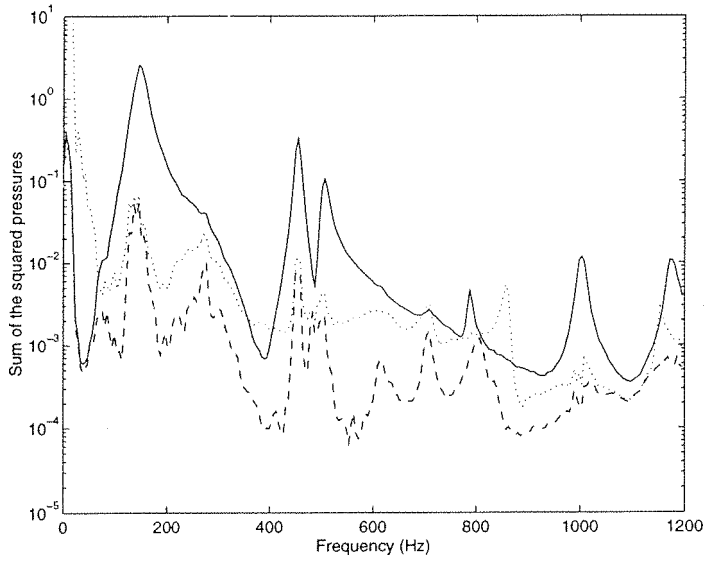

Figure 7.7: The sum of the squared pressures at ten microphone positions before control (solid), the predicted pressure squared levels after minimization of the sum of the squared pressures (dashed) and cancellation of sensor output (dotted) using the piezoelectric actuator as a secondary source.

Figure 7.7 shows the predicted sum of the squared pressures at the ten microphones before and after control using both the optimal strategy, of minimizing the sum of the squared pressures and cancellation of the sensor output. These results were

calculated using measured estimates of $\boldsymbol{p}_p$, $\boldsymbol{z}$, d and c. At very low frequencies (below $70Hz$) the strategy of cancelling the output of the sensor produces increases in the pressure squared levels. This is due to high levels of noise in the frequency response measurements at these frequencies. In this frequency range the vector $\boldsymbol{z}$ is heavily contaminated by noise because the secondary source is very inefficient at exciting the panel, and the radiation efficiency of the panel is very low. This is demonstrated by the fact that the strategy of minimization of the sum of the squared pressures also does not achieve any attenuation in this frequency range. In principle, large attenuations would be possible in this range if a suitable secondary source was used. By cancelling the output of the piezofilm sensor large reductions in the sound power (up to $25dB$ at certain frequencies) are achieved at frequencies between $70Hz$ and $700Hz$ and significant reductions are achieved at some frequencies above this. These experimental results support the conclusions of the computer simulations in chapter 5 by demonstrating that the cancellation of volume velocity is a useful strategy in the control of sound radiation up to excitation frequencies for which $kl \simeq 3.5$ ($700Hz$ in this case). For most of the frequency range the optimal control strategy achieves somewhat higher attenuations than the cancellation of the output of the volume velocity sensor. This is probably due to errors in the estimation of volume velocity by the sensor, since even a small residual level of volume velocity after control would limit the attenuation in the radiated sound. It should be emphasized that the minimization of the sum of the squared pressures requires ten remote error sensors compared with volume velocity cancellation which only requires a single integrated error sensor, and is thus a far more practical control strategy to implement.

At $850Hz$ there is an increase in the sum of the squared pressures at the ten microphones of about $9dB$ after cancellation of the piezofilm sensor output. The secondary source and the piezofilm sensor are very poorly coupled at this frequency (figure 7.5) and this causes the secondary source to drive very hard in an attempt to cancel the output of the sensor and therefore strongly excites higher order radiation modes which at this frequency begin to radiate sound efficiently.

Because of the positioning of the primary and secondary sources used in the above experiment, the even modes on the plate are always poorly excited. This implies that non-volumetric modes (i.e. not measured by the volume velocity sensor) will not be

largely excited when cancelling the volume velocity. To provide a more challenging test of the robustness of cancellation of the piezofilm's output as an active control strategy, a further experiment was conducted using an inertial actuator as the secondary source. This was positioned off-centre on the plate so that both even and odd modes were excited. The inertial actuator used was a small loudspeaker whose mylar diaphram was attached to the plate using plasticine so that the magnet acted as the inertial mass. The off-centre mass loading provided by the inertial actuator also increases the excitation of the even modes by the primary source. If the volume velocity is actively cancelled using the inertial actuator the level of even mode excitation on the plate will be much larger than in the earlier case. This implies that at higher frequencies, where the radiation efficiency of the non-volumetric modes becomes high, the control system will not be able to achieve good attenuations. At low frequencies, however, the control system is still expected to achieve good attenuations since the non-volumetric modes are very inefficient at radiating sound in this frequency region.

The sum of the squared pressures at four microphones (Nos. 1, 4, 7 and 10) before and after the cancellation of the output of the film sensor are shown in figure 7.8. The dynamics of the plate are changed by the presence of the inertial actuator and therefore the pressure spectrum before control is altered somewhat. The attenuation is still poor below $70Hz$, for the reasons detailed above, but large attenuations are still predicted in the frequency regions 100-250Hz and 450-600Hz. As expected there are now frequency regions where there are significant increases in the sound levels after cancellation of the piezofilm sensor output and this is due to the large excitation of even modes which have little volumetric contribution. The two modes with even order components (n=1, m=2) and (n=2, m=1) which both have natural frequencies at about $300Hz$ account for the increased level after control at this frequency. In general however the predicted sum of the squared pressure levels after control are significantly less after cancellation of the output of the distributed sensor and compare favorably with the optimal control strategy of minimization of the sum of the squared pressures.

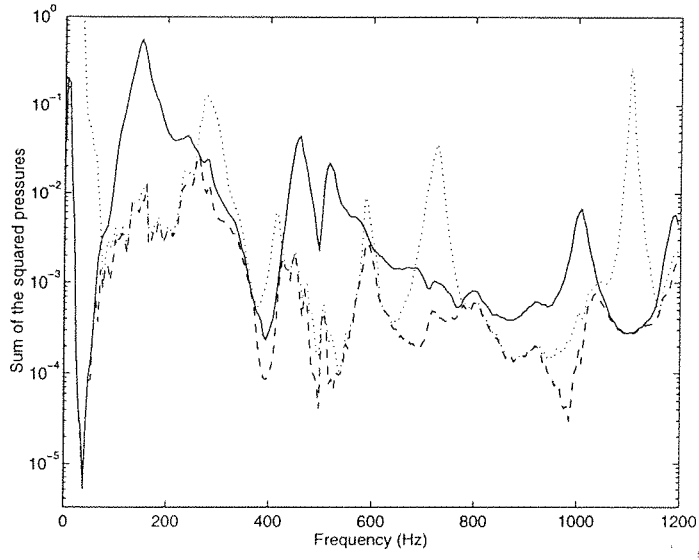

Figure 7.8: The sum of the squared pressures at four microphone positions before control (solid), the predicted pressure squared levels after minimization of the sum of the squared pressures (dashed) and cancellation of sensor output (dotted) using an inertial actuator as a secondary source.

7.2.6 Real time control at single frequencies

The active control results shown in the previous section are all predicted from individually measured frequency responses. To confirm that the predicted attenuations were attainable, a manual control system was used to cancel the output of the volume velocity sensor at a number of discrete frequencies and the observed attenuations were compared with the predicted reductions. To cancel the output of the piezofilm sensor the primary and secondary sources were driven with a two phase oscillator at a single frequency (in a similar arrangement to that shown in figure 6.11). The amplitude and phase of the secondary source was altered until the output of the piezofilm sensor was cancelled (i.e. reduced by at least $40dB$ in practice). The pressure levels at the microphones could then be measured before and after control to determine the attenuation in the sound pressure level. Figure 7.9 shows the predicted attenuations at the microphone in position No.9 (figure 7.6), calculated from the frequency response measurements, as compared with the reductions in pressure level observed when the output of the piezofilm sensor was cancelled manually. The manual control experiment was carried out at eight different frequencies and the results are shown

as crosses in figure 7.9. The results correspond extremely well with the predicted attenuations and in most cases the attenuations achieved by the manual controller are greater than those predicted from the frequency response measurements. This is probably due to noise in the frequency response measurements which on average tend to reduce the predicted attenuations.

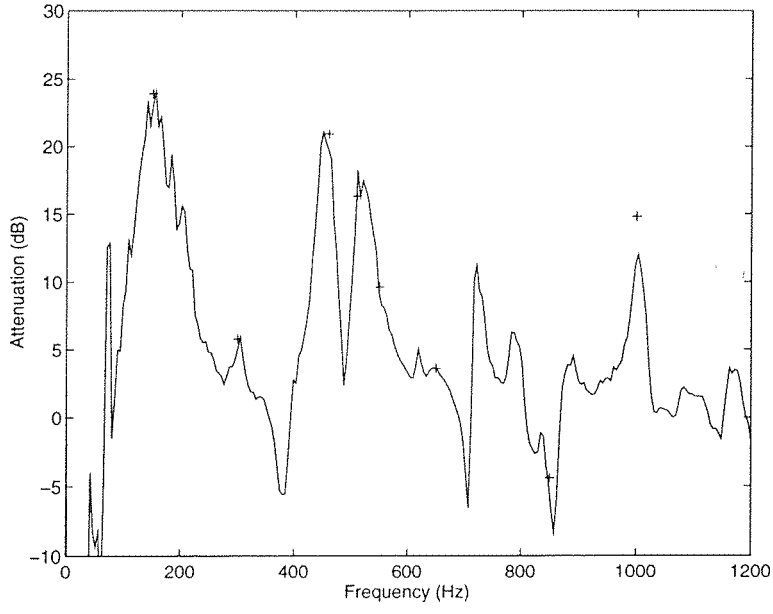

Figure 7.9: The predicted attenuation in pressure squared level at microphone 9 (solid line) and the measured attenuations in pressure squared level at eight different frequencies (crosses).

7.3 Conclusions

The development of distributed sensors allows active structural acoustic control to be achieved over a wide frequency region, using only a single sensor. Cancellation of volume velocity has been shown to be a very useful strategy in achieving active structural acoustic control and compares favorably with the more sophisticated strategy of minimization of the sum of the squared pressures at a number of points in the far field. Previous attempts to use distributed modal sensors have been partially successful in achieving acoustic control but tended to be specific to a particular structure and were only able to achieve attenuations over a very limited frequency range. The design of the sensor developed for use in these experiments was not dependent

on the dynamic properties of the plate used. This was demonstrated by achieving significant reductions in the sound pressure levels after the dynamic properties of the plate were altered by the attachment of an inertial actuator. This shows that the piezofilm sensor is robust to changes in the plate behavior. It has also been shown that over a wide frequency range the attenuations in the far field pressure can be adequately predicted using individually measured frequency responses.

Chapter 8

Feedback control

8.1 Introduction

The active control of sound power radiation from a flexible rectangular panel using feedback control will be investigated in this chapter. Feedback control can be used to cancel broadband disturbances i.e. random or transient, when no reference signal is available. This is in contrast to feedforward control which is most widely used to control harmonic disturbances since it is for these disturbances that reference signals are most commonly available. The results of computer simulations using purely theoretical data and also using measured responses will be presented. This chapter will also present the results of experiments conducted on the plate configuration used in the experiments carried out in chapter 7 of this thesis.

The control systems considered in the previous chapters of this thesis have all been single channel feedforward. This implies that a suitably accurate reference signal is available which can be used to feed the controller (figure 8.1a). There are many circumstances in which no suitable reference signal is available and it becomes necessary to use feedback controllers (figure 8.1b).

To achieve good attenuation, a feedback controller used to control a system with a finite delay must be able to *predict* the disturbance signal in the immediate future. If future disturbance signals can be predicted, then the secondary source can be driven so that it produces an equal and opposite signal to the primary disturbance at the error sensor and therefore the error signal can be greatly attenuated. If the

disturbance signal is periodic then its future behaviour is perfectly predictable and in principle, the error signal can be driven to zero. In the case of a feedforward control system, where the disturbance is non-periodic, prediction is possible if a reference signal is taken sufficiently "upstream" of the error sensor and the reference signal is well correlated with the disturbance signal. Feedback control systems however, act solely on past error signals and rely on the disturbance being correlated in time. Unless the signal is white noise, the future behaviour of a signal will always depend to some extent on the past behaviour of the signal and therefore a degree of prediction can be achieved.

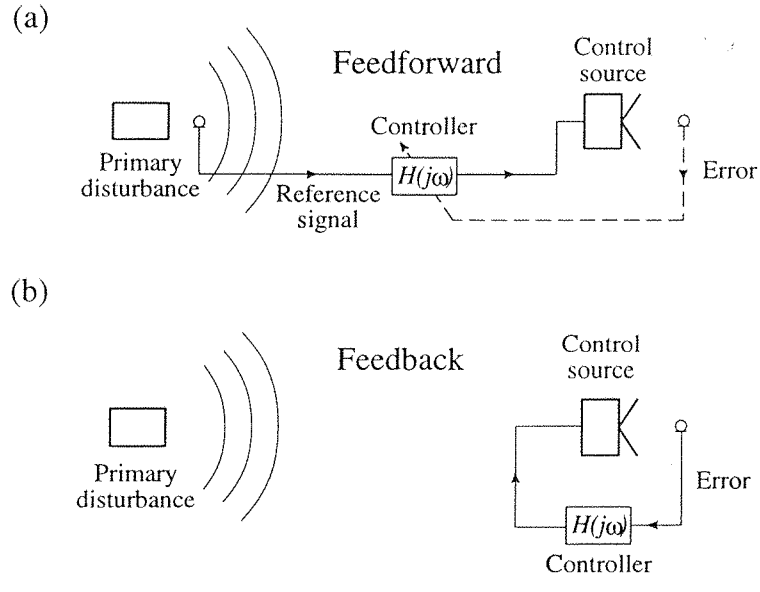

Figure 8.1: Feedforward and feedback control.

8.2 Theory

8.2.1 Analogue feedback

To begin with, a single channel analogue feedback system, whose block diagram is shown in figure 8.2, will be considered. The error signal at the sensor $e(j\omega)$ is comprised of a disturbance due to the primary source, $d(j\omega)$, and the output of the control system $y(j\omega)$. A phase inversion at the error sensor has been assumed (to ensure a negative feedback system) as this will be consistent with the majority of

the control literature. If $y(j\omega)$ is similar to $d(j\omega)$ then large attenuations in $e(j\omega)$ will be achieved. The error signal is first fed through an electronic controller and the output of the controller is used to drive the *plant*. The *plant* represents the transfer function of the path between the output of the controller and the error sensor. The *plant* will in general include electrical components (amplifiers etc.) and acoustic components (for example, the radiation from the secondary loudspeaker and the acoustic propagation). Assuming the feedback system is stable, the error can be described by,

$$e(j\omega) = d(j\omega) - y(j\omega) = d(j\omega) - G(j\omega)H(j\omega)e(j\omega) \tag{8.1}$$

The contribution of the control system to the error signal, $y(j\omega)$, is given by the error signal itself, $e(j\omega)$, filtered by the plant response $G(j\omega)$ and the controller $H(j\omega)$. The above equation can be rearranged to give the transfer function of the entire system.

$$\frac{e(j\omega)}{d(j\omega)} = \frac{1}{1 + G(j\omega)H(j\omega)} \tag{8.2}$$

Unlike fixed feedforward control systems a feedback control system can become unstable if, for example, the denominator in the above equation becomes zero at any frequency. The controller must therefore be carefully specified such that good performance is achieved without causing instability. The stability of the feedback system is more generally assessed using the Nyquist criterion [41]. This implies that there will be a tradeoff between stability and control performance.

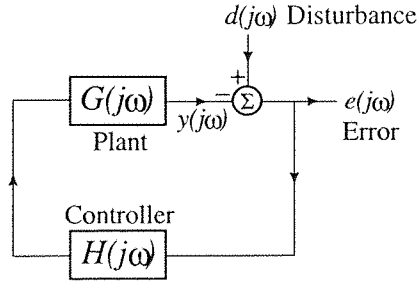

Figure 8.2: Analogue feedback control.

8.2.2 Digital feedback and internal model control

Digital control filters may be used instead of analogue filters because of their flexibility. The use of sampled signals allows the computation of the optimal control filter coefficients and the promise of optimal performance. Digital filter coefficients can also be easily updated to produce real time adaptive systems and the control algorithm can be altered with only a change in software.

A time domain approach to the design of the control filter will be adopted in this section. The q operator notation will be used where q^{-1} is a unit delay (i.e. one sample) such that $q^{-1}x(n) = x(n-1)$. The block diagram for a digital feedback control system is given in figure 8.3. The sampled error is given by $e(n)$, the disturbance by $d(n)$ and the control system's contribution to the error signal by $y(n)$. In operator notation $e(n) = d(n) - G(q)H(q)e(n)$ where the plant's response can be approximated by an arbitrary length FIR filter $G(q)$ such that $G(q) = g_0 + g_1q^{-1} + g_2q^{-2} + ...$ and the controller's response is assumed to be an FIR filter $H(q)$ with I coefficients such that $H(q) = h_0 + h_1q^{-1} + h_2q^{-2} + ... + h_{I-1}q^{1-I}$.

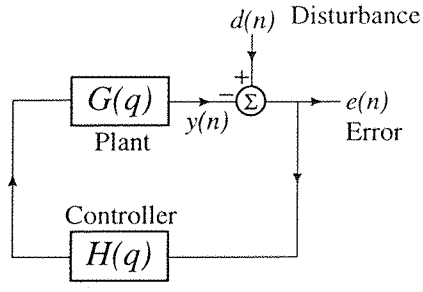

Figure 8.3: Digital feedback control system.

Internal model control

The calculation of the optimal stable control filter $H(q)$ is often a difficult task especially if the controller is required to be adaptive. The internal model control approach [66] is a method of transforming a feedback control system into a system resembling a feedforward control system. The control filter can then be adaptively optimized in real time to produce fully adaptive feedback controllers that are easy to understand and interpret [35, 36, 37, 76, 77].

Figure 8.4a shows the block diagram for an internal model control system. The controller H contains a model of the plant, $\hat{G}(q)$, which compensates for the contribution of real plant $G(q)$ to the error signal, so that the input to the control filter, $W(q)$, is an estimate of the disturbance d rather than of the error e. If the estimate of the plant is good, that is $\hat{G}(q) = G(q)$, then the feedback control system can be considered to act as a purely feedforward system, as shown in figure 8.4b.

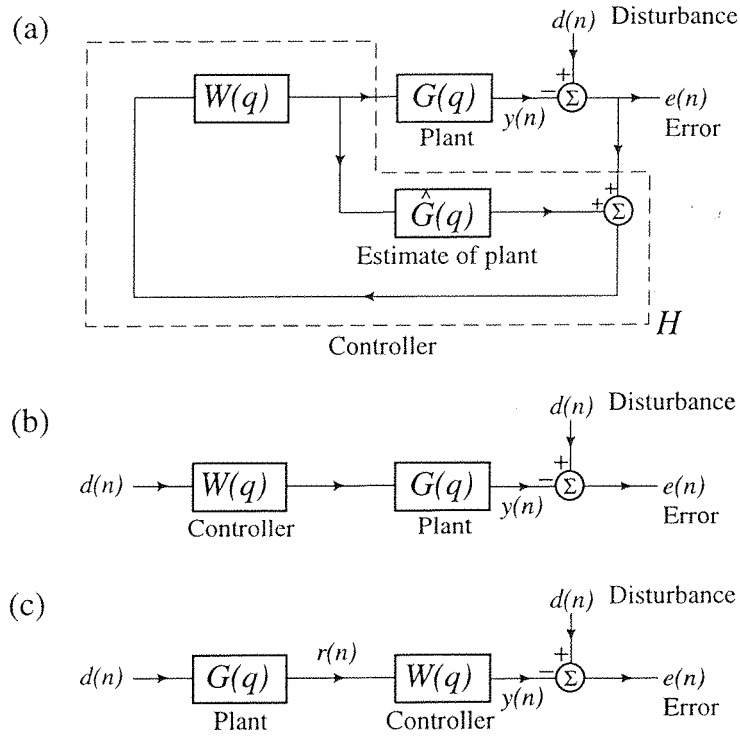

Figure 8.4: Internal model control digital feedback system (a), the equivalent feedforward system (b) and an alternative form of the feedforward system (c).

Under these conditions the error can be expressed as,

$$e(n) = [1 - W(q)G(q)]d(n) \tag{8.3}$$

The feedforward system can be rearranged, as shown in figure 8.4c, to produce an equivalent system where the disturbance is first filtered by the controller $G(q)$ to produce a signal $r(n)$.

The error can now be written as,

$$e(n) = d(n) - W(q)r(n) = d(n) - \sum_{i=0}^{I-1} w_i r(n-i) \tag{8.4}$$

where $r(n) = G(q)d(n)$ is the disturbance signal filtered by the plant response and w_0 to w_{I-1} are the I coefficients of the FIR filter $W(q)$. The expected value of the error squared (i.e. $\mathrm{E}[e^2(n)]$) is taken as the cost function which the control system attempts to minimize. This is equivalent to the minimization of the total power of the signal. Other error criteria may be specified but this is the most common criterion for the active control of acoustic disturbances. If the controller coefficients are optimally adjusted then the error will be totally uncorrelated with the filtered reference signal for the number of samples (I) corresponding to the length of the control filter.

$$\mathrm{E}[e(n)r(n-k)] = 0 \quad \text{for } 0 < k < I-1 \tag{8.5}$$

In other words, if $W(q)$ is optimized, all of the information in the current disturbance signal $d(n)$ which is correlated to the previous $I-1$ samples of the filtered reference signal will be removed, so that the resulting error $e(n)$ is uncorrelated with the last $I-1$ samples of the filtered reference signal. Equation 8.5 and equation 8.4 can be combined to produce an expression which includes the optimal control filter coefficients $w_i(opt)$.

$$\mathrm{E}[d(n)r(n-k)] - \sum_{i=0}^{I-1} w_i(opt)\mathrm{E}[r(n-i)r(n-k)] = 0 \quad \text{for } 0 < k < I-1 \tag{8.6}$$

The first term in the above equation is the expected value of the present disturbance $d(n)$ multiplied by the $(n-k)^{th}$ filtered reference signal $r(n-k)$. To include all values of k, this term is represented by an I length vector $\boldsymbol{p}$ which is the cross-correlation function between $d(n)$ and $r(n)$.

$$\boldsymbol{p} = \left[\begin{array}{cccc} \mathrm{E}[d(n)r(n)] & \mathrm{E}[d(n)r(n-1)] & \ldots & \mathrm{E}[d(n)r(n-I+1)] \end{array} \right]^T \tag{8.7}$$

The expectation value in the second term in equation 8.6 can be represented as an $I \times I$ auto-correlation matrix $\boldsymbol{R}$ for $i = 0$ to $I-1$ and $k = 0$ to $I-1$ which is given by,

$$\boldsymbol{R} = \begin{bmatrix} \mathrm{E}[r(n)r(n)] & \mathrm{E}[r(n)r(n-1)] & \dots & \mathrm{E}[r(n)r(n-I+1)] \\ \mathrm{E}[r(n-1)r(n)] & \mathrm{E}[r(n-1)r(n-1)] & \dots & \mathrm{E}[r(n-1)r(n-I+1)] \\ \vdots & \vdots & \ddots & \vdots \\ \mathrm{E}[r(n-I+1)r(n)] & \mathrm{E}[r(n-I+1)r(n-1)] & \dots & \mathrm{E}[r(n-I+1)r(n-I+1)] \end{bmatrix} \tag{8.8}$$

If the vector of controller coefficients $\boldsymbol{w}$ is given by,

$$\boldsymbol{w} = \begin{bmatrix} w_0 & w_1 & \dots & w_{I-1} \end{bmatrix}^T \tag{8.9}$$

then equation 8.6 can be expressed in matrix form to include all of the values of $k = 0$ to $k = I - 1$.

$$\boldsymbol{p} - \boldsymbol{R}\boldsymbol{w}_{opt} = 0 \tag{8.10}$$

The optimal Wiener control filter coefficients can now be directly calculated from the cross-correlation vector and the auto-correlation matrix.

$$\boldsymbol{w}_{opt} = \boldsymbol{R}^{-1}\boldsymbol{p} \tag{8.11}$$

A direct solution to this equation is possible if the matrix $\boldsymbol{R}$ is positive definite which is assumed if the filtered reference signal persistently excites the control filter $\boldsymbol{w}$ [35]. Given the disturbance signal and the plant response $G(q)$ it is thus possible to calculate the optimal filter coefficients and to calculate the resulting error signal.

If the plant's response G is minimum phase then an arbitrarily long filter W can be specified which perfectly compensates for the plant's response and drives the error to zero. However, if the plant has a delay in it equivalent to K samples, then $r(n)$ is delayed by K samples with respect to $d(n)$, so that the cross-correlation vector $\boldsymbol{p}$ will not include all of the correlated information since $E[d(n)r(n+1)]$ to $E[d(n)r(n+K)]$ will be non-zero. Therefore, the ability of the control system to cancel the output of the error sensor is adversely affected by any delay in the plant. It is therefore desirable in the design of any feedback control system to minimize the delay in the plant.

Adaptive filters: the filtered-x LMS algorithm

The internal model control approach is useful because it allows feedforward adaptive filtering techniques, such as the filtered-x LMS algorithm, to be applied to feedback control systems. The LMS algorithm as developed by Widrow and Hoff [90] is concerned with updating the coefficients in an FIR control filter such that they converge to the optimal filter $\boldsymbol{w}_{opt}$. The error surface associated with an FIR control filter is quadratic with a unique minimum solution. A gradient decent algorithm is therefore guaranteed to converge to the optimal solution. The LMS algorithm uses the instantaneous estimate of the gradient, which is given by the most recent error sample multiplied by the previous I reference signals, to update the coefficients of the I length control filter. The i^{th} filter coefficient at the $n+1$ sample (i.e. $w_i(n+1)$) is thus adjusted according to the equation,

$$w_i(n+1) = w_i(n) + \alpha e(n) x(n-i) \tag{8.12}$$

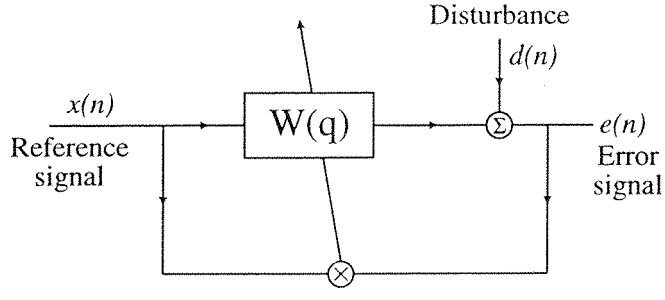

Figure 8.5: An adaptive control system for optimization of the filter $W(q)$.

where $x(n-i)$ is the $(n-i)^{th}$ sample of the reference signal, and α is a convergence coefficient which determines the rate of convergence. This adaptation process is illustrated in figure 8.5. In an active control system for the reduction of sound or vibration, there is generally a plant $G(q)$ through which the output of the filter must travel before it is summed with the disturbance (e.g. as in figure 8.4b) and therefore the reference signal must also be filtered by a model of the plant $\hat{G}(q)$ in order to produce an unbiased estimate of the gradient. This is known as the filtered-x LMS algorithm [91] and is shown in figure 8.6. The update equation then becomes,

$$w_i(n+1) = w_i(n) + \alpha e(n) r(n-i) \tag{8.13}$$

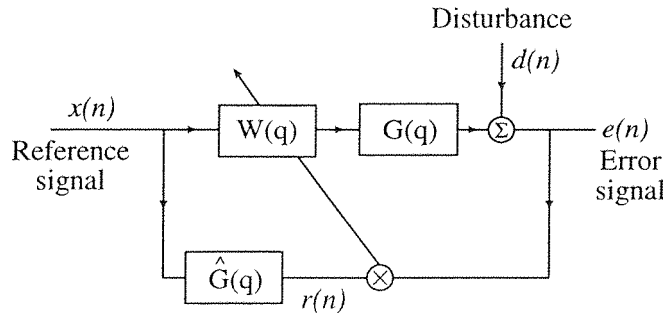

Figure 8.6: An adaptive control system for optimization of the filter $W(q)$ using a reference signal filtered by a model of the plant $\hat{G}(q)$.

where $r(n-i)$ is the filtered reference signal given by filtering the signal $x(n)$ by a J^{th} order FIR estimate of the true plant response $\hat{G}(q)$.

$$r(n) = \hat{G}(q)x(n) = \hat{g}_0 x(n) + \hat{g}_1 x(n-1) + \hat{g}_2 x(n-2) + ...\hat{g}_{J-1} x(n-J+1) \tag{8.14}$$

8.2.3 Feedback control to minimize remote sensors

It is also possible to use a local feedback system to minimize the outputs from a set of remote sensors (figure 8.7a). If the error signal from the local sensor e_1 is correlated with the error signals $\boldsymbol{e}_2$ then it is possible to achieve some level of control at the remote error sensors using a local feedback system. The equivalent feedforward system using internal model control is shown in figure 8.7b.

If the remote error sensors $\boldsymbol{e}_2$ were used to directly feed the controller large time delays would be introduced which would adversely affect the performance of the control system. By using a local error signal e_1 this time delay can be kept to a minimum but the controller can still be adjusted to minimize the remote error signals. This assumes that the local plant response G_1 has a smaller time delay than the remote plant responses $\boldsymbol{G}_2$. The system as a whole will only be effective if the additional time delay in $\boldsymbol{G}_2$ is comparable to the time taken for the disturbance to travel from

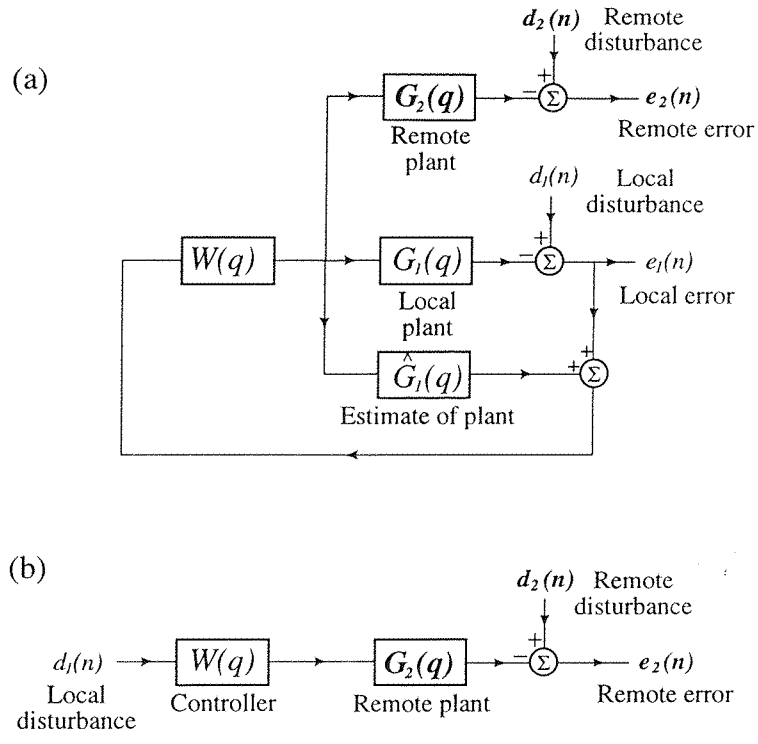

Figure 8.7: An internal model control system used to minimize the errors at a set of remote sensors.

the local error sensor to the remote error sensors. This implies that the local feedback system must be upstream of the remote error sensors. If d_1, $\boldsymbol{d}_2$ and $\boldsymbol{G}_2(q)$ are known then the optimal filter coefficients can be calculated and the resulting error computed. An example of a feedback control system on a structure used to minimize the output of a number of remote microphones is presented by Elliott *et al.* [37]. Although this method could be used to adjust any local feedback loop to minimize sound radiation, the direct minimization of an error signal obtained from a sensor whose mean square output is designed to be proportional to radiated sound power, will be investigated here.

8.2.4 Stability

It is not within the scope of this thesis to give anything but a brief discussion on the stability of feedback control systems. The internal model control architecture, assuming a perfect plant model (i.e. $\hat{G} = G$), will always produce a stable system as long as the control filter W is stable. In any realistic system however some variation

in the plant response will occur and this allows some of the control system's output $y(n)$ to be fed back into the input of the controller thus reinstating a "feedback" path. It is therefore necessary to build a control system whose stability is robust to small changes in the plant response. Methods of achieving a robust internal model control system have been developed and are discussed in a number of publications [36, 35, 76, 77]. In an adaptive controller the robustness can be increased by including a leakage term [91] in the update algorithm for the control filter [36].

8.3 Simulation results

In this section the results of a simulation of feedback control are presented in which the plant response is derived from a computer model of a piezoelectric actuator driving a vibrating plate whose motion is measured by a distributed sensor. The same panel will be used here as was used in the computer simulations presented in chapter 5.

These simulations are designed to determine the upper limit of the performance of a feedback control system designed to control the radiation of broadband noise from a vibrating panel with these actuators and sensors.

8.3.1 Minimization of the output of a volume velocity sensor

Consider a $380mm$ by $300mm$ by $1mm$ aluminium panel with a damping ratio of 0.002 excited by an incoming white noise signal travelling as a plane wave with angles $\theta = 45^o$ and $\varphi = 45^o$ in an arrangement as shown in figure 5.1. The output of a volume velocity sensor is assumed to be minimized using a internal model control feedback system which drives a centrally placed piezoelectric actuator. The reductions in the output of the volume velocity sensor and the resulting changes in the total sound power radiation can then be calculated.

Feedback control systems attenuate the error signal in certain frequency regions at the expense of increasing the signal in other frequency regions [30]. If the intention is to reduce the perceived noise level then an "A-weighting" could be used to filter the error signal before it is minimized by the controller. When using the output of a volume velocity sensor as a broadband error signal, the radiation efficiency of

the structure as a function of frequency must also be taken into account. The error signal in this case should thus be weighted by a radiation efficiency term and an A-weighting term to produce a good estimate of the perceived radiated sound, which can then be minimized by adjusting the controller coefficients. Figure 8.8a shows the weighting filter $B(q)$ used in the simulations which includes an A-weighting term and a radiation efficiency term. An equivalent control system is shown in figure 8.8b which weights the disturbance and the reference signals instead of the error signal. The modulus of the frequency response of $B(q)$ used in these simulations is shown in figure 8.9. To calculate the optimal control filter which minimizes the weighted error $e_0(n)$ equation 8.11 is used with the vector $\boldsymbol{p}$ representing the cross-correlation terms between the weighted disturbance $d_0(n)$ and the weighted disturbance filtered by the plant $r_0(n)$ and the matrix $\boldsymbol{R}$ representing the auto correlation terms of $r_0(n)$.

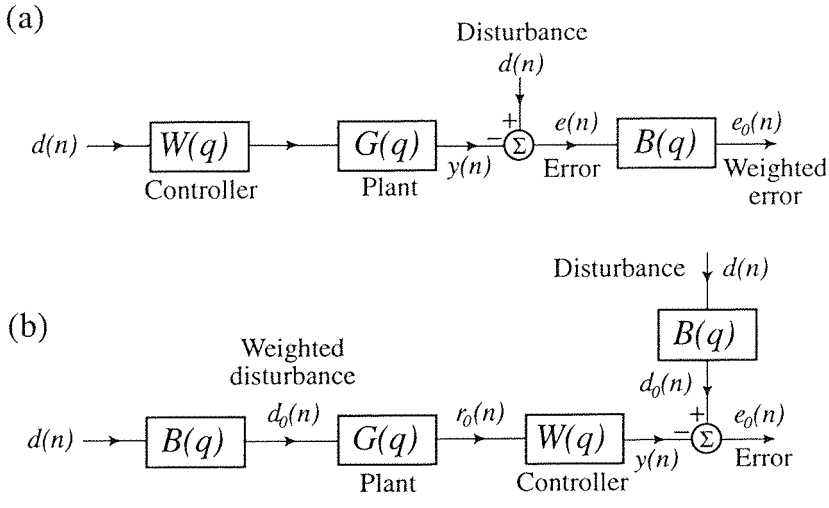

Figure 8.8: (a) An active control system which uses a filter $B(q)$ to the weight the error. (b) An equivalent control system which weights the disturbance and the reference signal instead of the error.

Figure 8.10 shows the power spectral density of the output of the volume velocity sensor, weighted by a radiation efficiency term and an A-weighting term, before and after control. The controller was a 200 coefficient FIR filter with a sample rate of $1400Hz$. Large reductions in the resonant behaviour of the panel are achieved with a total reduction in the error signal of $7.4dB$. These results define the upper performance limit for this control system minimizing this cost function. Time delays due to anti-aliasing filters would inevitably reduce performance. In principle, if very

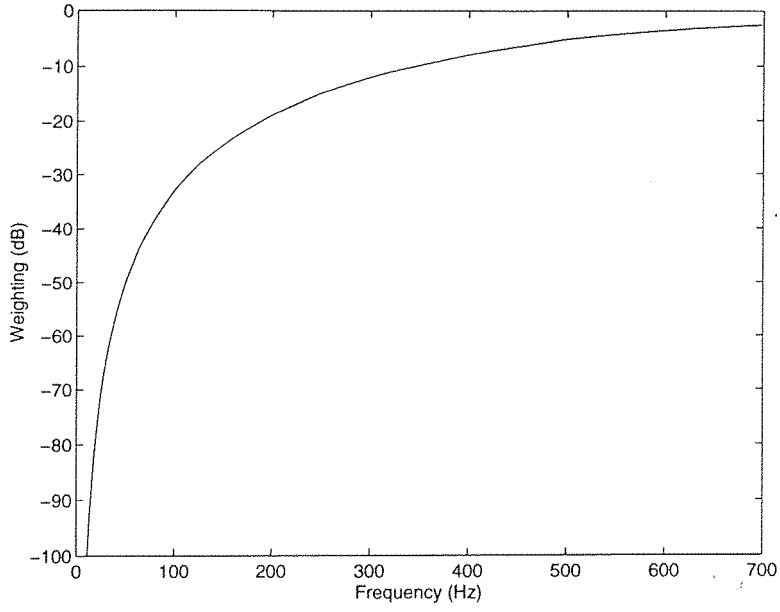

Figure 8.9: The modulus of the frequency response of the filter $B(q)$ used to compensate for the radiation efficiency of the panel and to add an A-weighting term.

fast processing were available, the sample rate of the controller could be made high enough for the delays due to anti-aliasing filters to be negligible.

Although the plane wave incident on the plate was assumed to have a flat spectrum, the vibration of the plate and hence the output of the volume velocity sensor shows resonances due to the plate's modal behaviour. It is this resonant response which is controlled by the feedback system. It should be noted that compared with the multiple single frequency results presented in chapter 5 (e.g. figure 5.3) the A-weighted broadband response shown in figure 8.10 is less dominated by the lowest order plate mode.

Figure 8.11 shows the attenuation of the error signal by the control system as a function of the time delay added to the plant response for two cases, where the damping ratio of the plate was 0.002 and 0.007. If the plate is lightly damped the disturbance exhibits more resonant behaviour (i.e. increased predictability) and hence performance is less likely to be affected by delays. With zero delay the attenuation is finite which implies that the plant's response in this case is non-minimum phase and the causal controller cannot perfectly compensate for the plant's response. Even though the overall level of attenuation is lower for the plate with $\xi = 0.007$, the fall

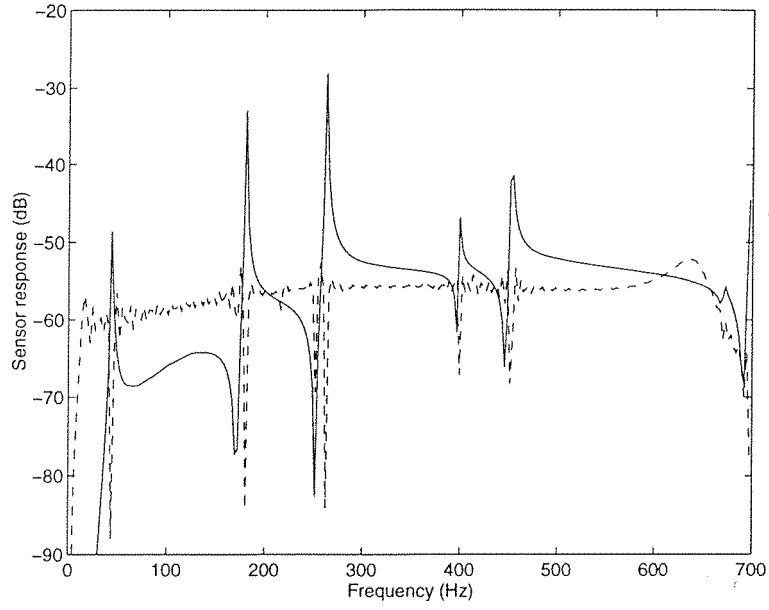

Figure 8.10: The output of a volume velocity sensor on a rectangular simply supported panel which is excited by an acoustic plane wave, before control (solid) and after feedback control using a internal model control approach (dashed).

off in the attenuation with plant delay is similar to that for the plate with $\xi = 0.002$. The relatively small reductions in attenuation shown in figure 8.11, even for $25ms$ of plant delay, are in contrast to the results presented for a purely acoustic feedback control system [36, 37] in which the plant has no resonant response and very little attenuation was possible with plant delays of more than a few milliseconds.

Figure 8.12 shows the A-weighted sound power radiated from the panel before and after control. As expected the A-weighted sound power is very similar to the output of the weighted volume velocity sensor at low frequencies (figure 8.10) although at higher frequencies (e.g. at $640Hz$) even-order structural modes which are not detected by the volume velocity sensor begin to radiate significantly. These results show that significant attenuation of the resonant radiation of the panel can be achieved. The resulting residual spectrum is relatively flat, which implies that the residual error is closer to being white noise. This result is to be expected since the feedback controller removes the predictability from the disturbance signal. The net reduction in the A-weighted sound power radiation is $3.4dB$. In the frequency range $180Hz$ to $500Hz$ the noise reduction is $6.9dB$. The increase of $1dB$ in the noise level in the $500Hz$ to $700Hz$ region, however, accounts for the overall reduction in performance as compared with

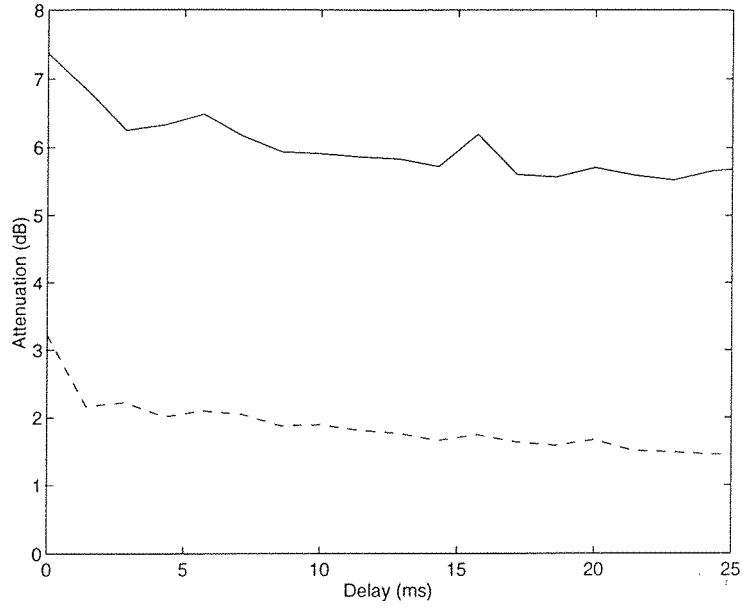

Figure 8.11: The attenuation of the error signal as a function of time delay in the plant for the case of a panel with a damping ratio of 0.002 (solid) and 0.007 (dashed).

the attenuation of the output of the volume velocity sensor, which was $7.4dB$ overall. In circumstances where the higher frequency noise was more highly attenuated by passive absorbers this problem would be reduced.

8.4 Negative-gain feedback on the experimental plate

In this section the possibility of using an analogue, negative-gain, feedback system to control the output of the volume velocity sensor described in chapter 7 is investigated. Figure 8.13 shows a simple analogue negative gain control system whose maximum stable gain is determined by the characteristics of the plant $G(j\omega)$ and the low pass filter $L(j\omega)$.

The frequency response was measured between the input to the piezoelectric ceramic actuator on the rectangular plate and the output of the volume velocity sensor described in chapter 7. This "plant" response could be used to determine the maximum stable feedback gain possible and hence the maximum achievable attenuations. To improve the performance of the control system at low frequencies a low pass filter

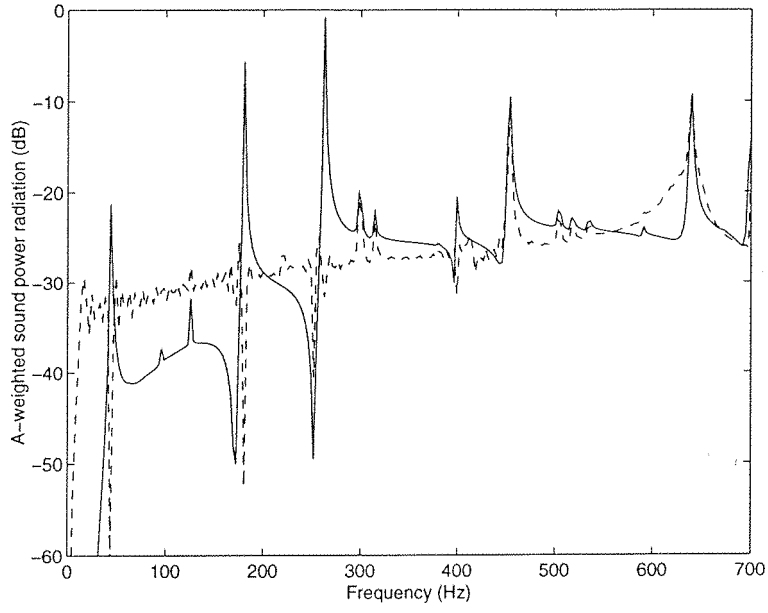

Figure 8.12: The A-weighted sound power radiation from a rectangular simply supported panel which is excited by an acoustic plane wave, before control (solid) and after feedback control using a internal model control approach (dashed).

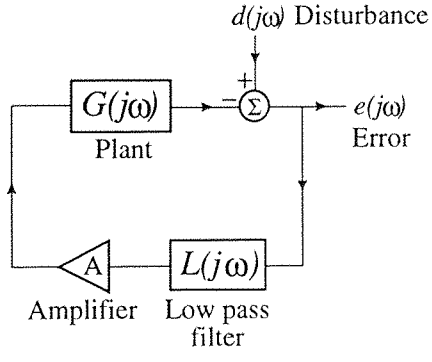

Figure 8.13: A negative gain feedback system with a low pass filter and a loop gain A.

$L(j\omega)$ could be used to roll off the high frequency response of the system and prevent high frequency instabilities. This allows the loop gain to be increased, which results in increased attenuations at low frequencies. A simple second order butterworth filter at $1000Hz$ will be used in the results presented here.

The distributed piezoelectric sensor used in the experiments presented in chapter 7, was designed to measure volume displacement. For the case of controlling single frequency sound the cancellation of volume displacement is equivalent to the cancellation of volume velocity. For the control of broadband disturbances this is not the case and the output of the sensor must be differentiated. This was done using the circuit shown in figure 8.14 [73].

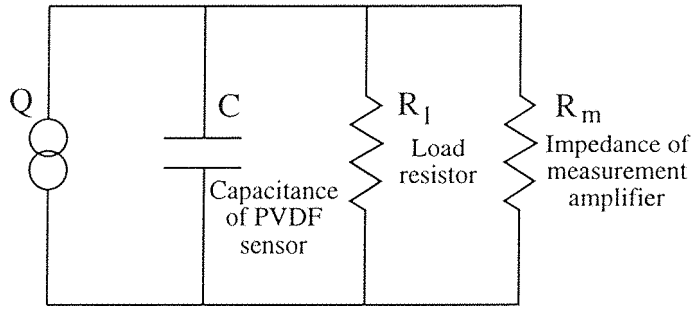

Figure 8.14: The circuit used to measure and differentiate the output of a distributed piezoelectric sensor designed to measure volume displacement.

The capacitance of the sensor was measured as $92nF$. A $2.2k\Omega$ load resistor was used so that the cut-off frequency of the circuit was $790Hz$ ($f_0 = 1/(2\pi RC)$). Below this frequency, the charge from the sensor Q flows almost entirely through the load resistor R_l and hence the output voltage, which is proportional to the current through this resistor, is proportional to $\mathrm{d}Q/\mathrm{d}t$. The measurement amplifier is assumed to have a very high impedance (i.e. $R_m \gg R_l$).

The transfer response of the feedback system shown in figure 8.13 is given by,

$$\frac{e(j\omega)}{d(j\omega)} = \frac{1}{1 + AG(j\omega)L(j\omega)} \tag{8.15}$$

where A is the gain. To ensured that the system is stable the Nyquist plot for the open-loop response $G(j\omega)L(j\omega)$ times the gain A, must not enclose the minus one point. The maximum performance for the system will be achieved if the loop gain A is

increased until the polar plot for the system is very near the Nyquist point although this does not allow any margin for change in the plant response. The frequency response for the system with maximum stable loop gain will determine the maximum attenuation possible.

The magnitude and phase of the frequency response $AG(j\omega)L(j\omega)$ are shown in figure 8.15 when the gain is chosen such that the polar plot of the frequency response (figure 8.16) comes close to but does not enclose the Nyquist point. For this system the gain margin is $4.6dB$ and the phase margin is 36^0.

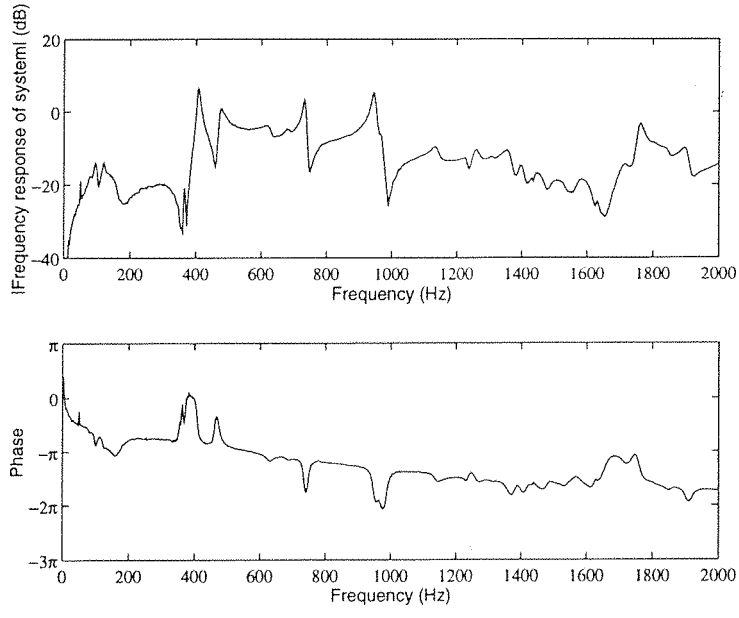

Figure 8.15: The measured magnitude and phase of the open loop response of a control system designed to cancel the output of a volume velocity sensor.

The introduction of a low pass filter reduces the level of the response at high frequencies at the expense of introducing a phase shift at low frequencies. This phase shift, which increases with higher order filters, causes the polar plot to rotate and can potentially cause lower frequency resonances to enclose the Nyquist point and send the system unstable.

The output of the sensor when the plate was acoustically excited by the loudspeaker inside the box (chapter 7) was measured and used as an example of a disturbance signal. This disturbance signal was weighted by the filter $B(q)$ shown in figure 8.8 and figure 8.9 so that it resembled the percieved noise level. The weighted error

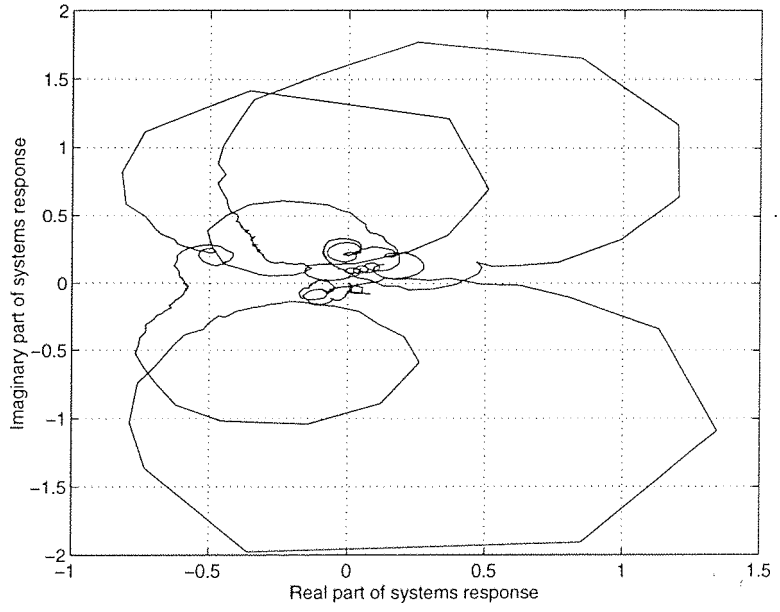

Figure 8.16: The polar plot of the open loop frequency response of the system which includes the plant, the gain and the low pass filter.

before and after control, calculated from equation 8.15, are shown in figure 8.17. The attenuations as a whole are not very large but attenuations of up to $6dB$ are observed at the resonances (e.g. $420Hz$). There can also be large increases, up to $10dB$ in the error at some frequencies. This control method has the advantage of having a simple controller but the attenuations are not very large. Any real control system would probably include a larger gain and phase margin which would reduce the attenuations even further.

8.5 Experimental results

In this section the results of an experiment using an adaptive internal model control system to minimize the output of a structural sensor designed to measure volume velocity are presented. The control system used a TMS320 C30 processor on a PC and the control algorithm was programed by Boaz Rafaely.

The control experiment was conducted on the experimental setup described in chapter 7. The acoustic primary source was driven with white noise that was filtered by a high-pass filter with a cut-on frequency of $300Hz$. It was not possible to include an A-

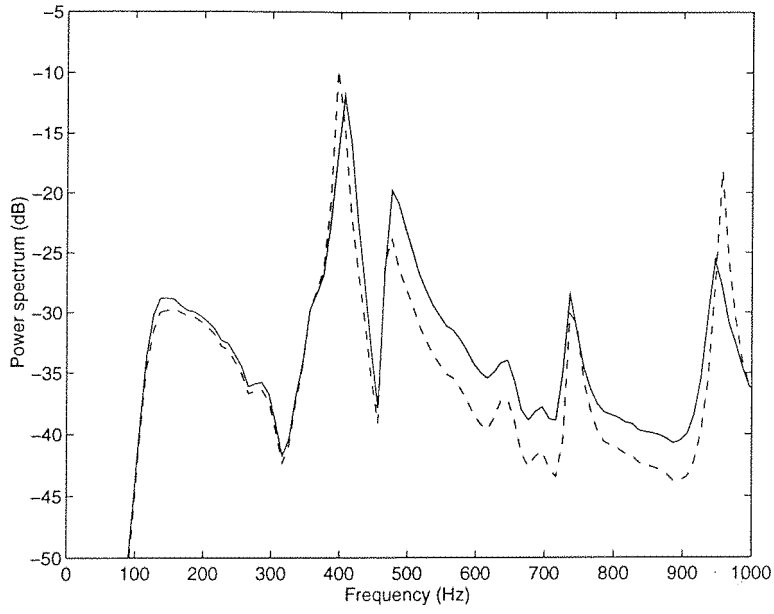

Figure 8.17: The weighted error before (solid) and after control (dotted) when the plate is excited using an acoustic source.

weighting and radiation efficiency weighting term to the error in the filtered-x LMS algorithm and therefore filtering of the disturbance was used to produce a similar effect. Much of the low frequency content of the error signal is unimportant because the radiation efficiency of the panel at these frequencies is very low and the human sensitivity to these frequencies is also low. The sampling frequency used was 6000Hz with an anti-aliasing filter (on the controller output only) set at 3000Hz. An anti-aliasing filter was not required on the input since the disturbance had a natural high frequency roll-off. Anti-aliasing filters produce delay which degrades performance and therefore their unnecessary use was avoided. No leakage term was used in the adaption algorithm for the controller since it was found that the converged system without any leakage factor was stable for up to 100 percent changes in the plant response in this case. Figure 8.18 shows the measured power spectrum of the error at the sensor before and after control. Reductions of up to $12dB$ are measured at certain frequencies with a total reduction in the signal of $6dB$.

Figure 8.19 shows the spectrum of the acoustic pressure at a microphone placed close to the panel before and after control. For these experiments the plate was housed in a laboratory which exhibited a complex acoustic response. Therefore, these results do not allow any generalized conclusions to be drawn about the total reductions in the

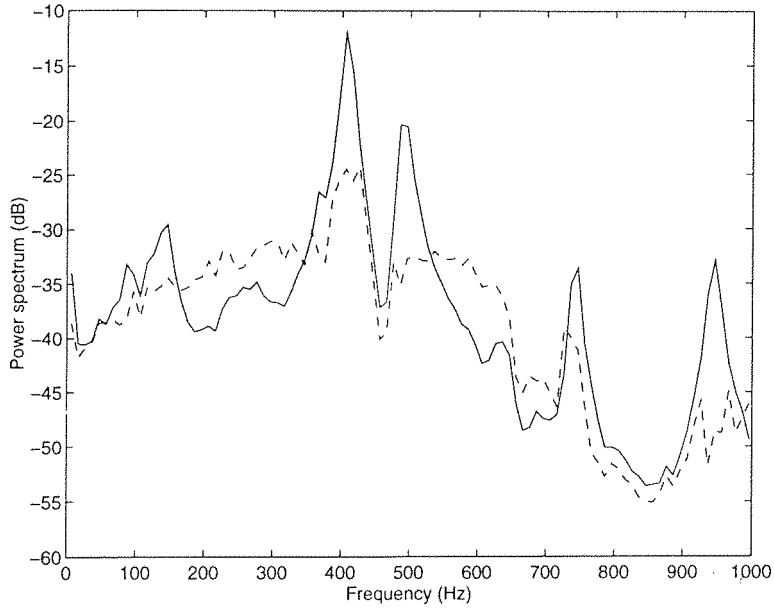

Figure 8.18: The measured spectrum of the error signal before (solid) and after control (dashed) using a real time adaptive internal model control system.

acoustic radiation from the plate but serve as an example of the acoustic reductions which are possible using such a system.

8.6 Conclusions

It this chapter the feedback control of sound radiation from a vibrating panel, excited by a broadband disturbance, using a volume velocity sensor, has been examined. The active control of sound transmission through flexible panels using feedback control systems has also been investigated by other authors [65, 82] but in general these systems have required relatively complex control systems with multiple point sensors. It is suggested here that the use of volume velocity sensors may allow some simplification in the control system without a large loss in performance.

Computer simulations have been used to show that in principle the volume velocity of a plate could be controlled using an adaptive internal model control system. The resonant behaviour of the error from the volume velocity sensor could be controller to produce a "whitened" response. Additional time delay in the plant's response was shown to degrade the performance of the system but not dramatically so. The pos-

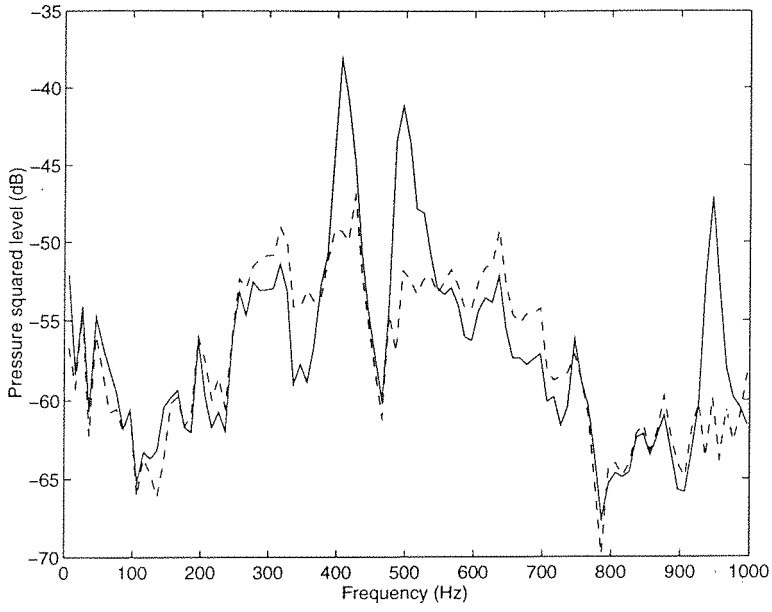

Figure 8.19: The measured spectrum of a microphone error signal before (solid) and after control (dashed) using a real time adaptive internal model control system.

sibility of using a simple negative-gain feedback control system was also investigated using the measured open loop frequency response of the feedback path which included a piezoelectric actuator mounted on a rectangular panel and a volume velocity sensor. It was found that some attenuations were possible at resonant frequencies, although, in this case these attenuations were not very large.

An adaptive internal model control system was also implemented on the panel using the piezoelectric actuator and the volume velocity sensor. Significant attenuations in the sensor output were achieved. The attenuations in the output of the sensor also produced a reduction in the sound pressure levels at a microphone near to the panel.

Significant reductions of broadband noise radiated from a rectangular panel can thus be achieved using a feedback control system. The internal model control feedback system has the ability to reduce the level of the resonant frequencies in the error signal and can be applied to any broadband disturbance that is filtered by a resonant (lightly damped) system such as a light panel. A number of these active panels could potentially be used to control the radiation of broadband sound in small enclosures (e.g. aerodynamic noise into aircraft cabins).

It is believed that a volume velocity sensor acting with a matched constant force

actuator will exhibit minimum phase characteristics and will greatly improve the performance of an analogue or a digital control system.

Chapter 9

Conclusions and recommendations for future work

The work presented in this thesis falls under two main categories: (i) radiation mode theory and (ii) distributed transducers. Recommendations will first be made for further study in these two areas and then a more general discussion on the future of research into the active control of sound transmission into an enclosure will be given.

9.1 Conclusions and recommendations for future work on radiation mode theory

It has been shown that the acoustic radiation from a vibrating surface can be decomposed into an orthogonal set of independently radiating velocity distributions or *radiation modes* (chapter 2). The acoustic power radiated by a vibrating surface into the far-field can be described purely as a function of the normal velocity at the surface and a radiation matrix $\boldsymbol{R}$. The eigenvalues of the matrix $\boldsymbol{R}$ describe the efficiency with which the radiation modes transfer energy from the surface of the structure into the far-field. To some extent the complexity of the energy transfer mechanism from the vibrating surface to the acoustic far-field is determined by the eigenvalues of the matrix $\boldsymbol{R}$. If there are only a few significant eigenvalues then the mechanism is less complex than if there are many significant eigenvalues. For active control purposes the level of complexity will determine the complexity of the control system required

to reduce the energy transfer to the far-field. In the work carried out in this thesis the values of these eigenvectors as a function of frequency have been calculated under a number of different circumstances (chapter 3). It was shown that at low frequencies the eigenvalues associated with the radiation of sound from baffled surfaces tended to change at a constant rate with respect to frequency. This rate of change is similar to the rate of change of efficiency associated with the radiation of sound from spherical harmonics. Spherical harmonics are themselves a special set of radiation modes for spherical radiators and it may be possible to link the rate of change of radiation efficiency for the radiation modes of arbitrarily shaped sources to the rate of change of radiation efficiency for spherical harmonics.

Although the radiation modes derived in this thesis concern the acoustic radiation from vibrating surfaces, this theory could be used to describe the transfer of energy from any section of a system to any another section of a system. The radiation of sound from a baffled source is a convenient example because the boundary between the two sections is well defined and the matrix of transfer impedances can be easily calculated. The generalization of this theory to include the transfer of energy in more complex structural and/or acoustic systems could potentially facilitate reductions in the complexity of the control systems required for control by allowing distributed sensors, equivalent to radiation mode sensors, to be used in the control system.

9.2 Conclusions and recommendations for future work on distributed transducers

In this thesis the design of a distributed transducer for measuring volume velocity is tested both theoretically and experimentally (chapters 4 and 7). It has also been shown that the cancellation of volume velocity is a useful strategy for the control of sound power radiation from a vibrating structure at low frequencies (chapters 5 and 7). If a volume velocity sensor and its reciprocal transducer, i.e. a constant force actuator, are used as an actuator/sensor pair then there will potentially be a number of useful effects:

- the levels of attenuation will increase and the system will continue to be effective at higher frequencies
- it will reduce control spillover and hence reduce undesirable side effects such as increased vibration levels and increased near field pressure levels
- the resulting plant response will be minimum phase and hence a simple analogue feedback control system could be used to achieve similar reductions in the control of broadband disturbances as those achieved using a single channel feedforward control system in the control of tonal disturbances.

In principle, the design of a constant force actuator is similar to that of a volume velocity sensor. Unfortunately when being used as an actuator the thin PVDF film used here cannot generate sufficient force to produce a practical system. The production of piezoelectric materials which can be etched or cut into shapes but are stiffer and more sensitive than a thin sheet of PVDF will potentially solve this problem. Recently, composite materials which are made from piezoelectric ceramic powder fixed in a polymer matrix have come into production and these materials should be investigated to determine if they are suitable for this application.

The etching techniques which have been used to produce a single distributed sensor with a spatially weighted sensitivity could also be used to produce large numbers of point sensors on a single sheet of piezoelectric material. The large number of electrical connections required to connect all of these sensors could also be etched into the surface of the film electrode to produce a simple junction at which the external cables could be connected. A large number of such sensors could be used as error sensors in a feedforward control system or an equivalent internal model control feedback system (chapter 8). The control system could use these sensors to monitor performance and could in principle scan through these error sensors sequentially to achieve slow adaptive control if a separate sensor was used to detect the primary disturbance. These error sensors could also be connected to an analogue weighting network to produce, for example, a volume velocity sensor or a higher order radiation mode sensor. The output of the analogue weighting filter could then be used directly as a reference signal or an error signal depending on the application. This allows some flexibility, since the weighting filter (or filters) could be changed without changing the

physical film sensor.

9.3 Conclusions and recommendations for future work on the active control of sound transmission

There are a number of systems in commercial production for the feedforward active control of low frequency tonal noise. Active control of the transmission of low frequency broadband disturbances into enclosures is a major subject for future active control research. The sources of broadband noise, such as aerodynamic flow, are often distributed. Therefore, for most broadband disturbances, unless they are contained in an environment such as a duct, it is difficult to obtain a suitable reference signal to use in a feedforward active control system. It is likely that feedback control systems will be required in many cases to control the transmission of broadband noise into enclosures.

The case of the transmission of broadband noise into a cylinder is a good example on which some ideas about the active control of broadband disturbances can be explored. The use of acoustic sources and error microphones is unlikely to be effective in a feedback system since they would introduce large delays and hence heavily degrade the performance of any feedback control system. It is therefore likely that structural sensors and actuators would be required to reduce the delays in the system.

In a multichannel control system it is generally necessary, as it is in an internal model control system, to filter a number of reference signals with models of the multiple paths in the plant in real time. For a system with an equal number of sensors and actuators the number of plant models required increases with the square of the number of control signals. This implies that multichannel internal model control systems will require large processing power and there will be a need to restrict the number of channels required to a minimum. If processing power were not a constraint then a large multichannel internal model control system could be used to minimize the sum of the squared pressures at a number of remote microphones inside the cylinder (chapter 8). This could potentially remove most of the resonant behaviour of the system. In

any realistic system where the processing power is likely to be very limited it may be necessary to use distributed sensors and actuators in an attempt to reduce the complexity of the control system. A system using structural modal sensor/actuator pairs each with an independent analogue feedback control system could be used to dampen the response of certain structural modes (chapter 6). For this system to be successful the output of the modal actuators must be poorly coupled to all of the other modal sensors and if the structural modes are orthogonal then this is likely to be the case. It would be also possible to use structural modal sensor/actuator pairs in an internal model control system designed to minimize the sum of the squared pressures at a number of microphones inside the cylinder.

The restrictions imposed by different applications will determine the choice and success of a given control system. For the aerospace application described in chapter 6, large weight restrictions will be placed on the system but less financial restrictions will probably be made. The aerospace structure however is likely to be more simple than an aircraft structure and there is a possibility of a successful system being produced using current technology. As processing power becomes faster and cheaper those applications in which performance increases rapidly with an increase in processing power will become more viable and more likely to be topics of active control research. Radiation mode theory provides a convenient method of quantifying the complexity of the energy transfer mechanism between a source and a receiver and therefore the complexity of the control system required to significantly reduce this energy transfer. A slow rate of change in the complexity of the energy transfer mechanism with frequency will identify the applications which will benefit most from an increase in processing power.

Bibliography

[1] E. H. Anderson and N. W. Hagood, "Simultaneous piezoelectric sensing/actuation: analysis and application to controlled structures," Journal of Sound and Vibration **174**(4), 617-639 (1994).

[2] *Atochem Sensors Technical Notes* Pg 14 (1987)

[3] T. Bailey and J. E. Hubbard, "Distributed piezoelectric-polymer active vibration control of a cantilever beam," J. Guidance and Control **8**, Pg 605-611 (1985)

[4] M. J. Balas "Direct velocity feedback control of large space structures" J. Guidance and Control **2**, 232-253 (1979).

[5] O. Bardou, S. J. Elliott and R. J. Pinnington "Active control of structured vibrations using power transmission methods," ISVR Technical Memorandum No. 749 (1995)

[6] O. Bardou, S. J. Elliott and R. J. Pinnington "Power minimisation and power absorption for force and moment excitation sources on finite and infinite plates," ISVR Technical Memorandum No. 750 (1995)

[7] W. T. Baumann, W. R. Saunders and H. R. Robertshaw, "Active suppression of acoustic radiation from impulsively excited structures," J. Acoust. Soc. Am. **90**(6) Pg 3202-3208 (1991)

[8] A. Berry, J. Guyader and J. Nicolas, "A general formulation for the sound radiation from rectangular, baffled plates with arbitrary boundary conditions," J. Acoust. Soc. Am. **88**(6) Pg 2792-2802 (1990)

[9] G. V. Borgiotti, "The power radiated by a vibrating body in an acoustic fluid and its determination from boundary measurements," J. Acoust. Soc. Am. **88**(4), Pg 1884-1893 (1990).

[10] G. V. Borgiotti and K. E. Jones, "The determination of the acoustic far field of a radiating body in an acoustic fluid from boundary measurements," J. Acoust. Soc. Am. **93** (5), Pg 2788-2797 (1993).

[11] R. A. Burdisso and C. R. Fuller, "Design of active structural acoustic control systems by eigenproperty assignment," J. Acoust. Soc. Am. **96**(3), Pg 1582-1591 (1994).

[12] S. E. Burke, J. E. Hubbard and J. E. Meyer, "Distributed transducers and colocation," J. Mech. Sys. and Sig. Proc. **7**(4), Pg 349-361 (1993)

[13] S. E. Burke and J. M. Sullivan, "Distributed transducer shading via spatial gradient electrodes," Proc. SPIE. 1995 North Am. Conf. on Smart Struct. and Mat. Vol. 2443, Pg 716-726 (1995)

[14] S. E. Burke and R. L. Clark, "Transducer tolerance theory for structural control," Proc. SPIE. 1995 North Am. Conf. on Smart Struct. and Mat. Vol. 2443, Pg 410-421 (1995)

[15] D. M. Carey and F. B. Stulen, "Experiments with a two-dimensional multi-modal sensor," Recent Adv. in Act. Con. of Sound and Vib. Pg S41-S52, supplement (1993)

[16] F. Charette, C. Guigou and A. Berry, "Development of volume velocity sensors for plates using PVDF film," Proc. ACTIVE 95, Pg 241-252 (1995)

[17] R. L. Clark and C. R. Fuller, "Experiments on the active control of structurally radiated sound using multiple piezoceramic actuators," J. Acoust. Soc. Am. **91**(6), Pg 3313-3320 (1992)

[18] R. L. Clark and C. R. Fuller, "Modal sensing of efficient acoustic radiators with polyvinylidene floride distributed sensors in active structural acoustic control approaches," J. Acoust. Soc. Am. **91**(6), Pg 3321-3329 (1992)

[19] R. L. Clark and C. R. Fuller, "A model reference approach for implementing active structural acoustic control," J. Acoust. Soc. Am. **92**(3), Pg 1534-1544 (1992)

[20] R. L. Clark, G. P. Gibbs and C. R. Fuller, "An experimental study implementing model reference acoustic control," J. Acoust. Soc. Am. **93**(6), Pg 3258-3264 (1993)

[21] R. L. Clark, R. A. Burdisso and C. R. Fuller, "Design approaches for shaping PVDF sensors in active structural acoustic control," J. of Intelligent Mat. Sys. and Struct. Vol. 4. Pg 354-365 (1993)

[22] R. L. Clark, "A Hybrid, autonomous control approach," Proc. Recent Advances in Structural Dynamics **5**(2) 934-944 (1994).

[23] K. A. Cunefare, "The minimum multimodal radiation efficiency of baffled finite beams," J. Acoust. Soc. Am. **90**, Pg 2521-2529 (1991).

[24] K. A. Cunefare and G. H. Koopman, "Global optimum active noise control: surface and far-field effects," J. Acoust. Soc. Am. **90**(1), Pg 365-373 (1991)

[25] K. A. Cunefare and M. N. Currey, "On the exterior acoustic radiation modes of structures," J. Acoust. Soc. Am. **96**(4), Pg 2302-2312 (1994)

[26] P. Curie and J. Curie, Comptes Rendus **91**, Pg. 294 (1880)

[27] M. N. Currey and K. A. Cunefare, "The radiation modes of baffled finite plates," J. Acoust. Soc. Am. **98**(3), Pg 1570-1580 (1994)

[28] John P. Dakin, "Multiplexed and Distributed Optical Fibre Sensors," Proc. Internat. Symp. on Advanced materials for lightweight structures, ESTEC, (1992)

[29] J. J. Dosch, D. J. Inmann and E. Garcia, "A self-sensing piezoelectric actuator for collocated control," Journal of Intelligent Material Systems and Structures, **3**, 166-185 (1992).

[30] J. C. Doyle, B. A. Francis and A. R. Tannenbaum, *Feedback control theory*, Maxwell Macmillan (1992)

[31] S. J. Elliott and P. A. Nelson, "The active control of sound," Elect. and Comm. Eng. J, Pg 127-136 (August 1990)

[32] S. J. Elliott and J. Rex, "Adaptive algorithms for underdetermined active control problems," ICASSP, II Pg 237-240 (1992)

[33] S. J. Elliott and M. E. Johnson, "Radiation modes and the active control of sound power," J. Acoust. Soc. Am. **94**(4), Pg 2194-2204 (1993).

[34] S. J. Elliott and M. E. Johnson, "Active control of structurally radiated sound," lecture given as part of the short course on *Active control of sound and vibration* by S. J. Elliott and P. A. Nelson at Penn State University (1993).

[35] S. J. Elliott, "Active control using feedback," ISVR Technical Memorandum No. 732 (1994)

[36] S. J. Elliott and T. J. Sutton, "Feedforward and feedback methods for active control," Proc. of Institute of Acoustics **16**(2), Pg. 255-273 (1994)

[37] S. J. Elliott, T. J. Sutton, B. Rafaely and M. Johnson, "Design of feedback controllers using a feedforward approach," Proc. ACTIVE 95. (1995)

[38] F. Fahy, *Sound and Structural Vibration* Academic Press, London (1985)

[39] F. Fahy, *Sound intensity* Elsevier Science Publishers (1989)

[40] J. E. Ffowcs-Williams, "Anti-sound," Proc. R. Soc. London, A395, Pg 63-88 (1984)

[41] G. F. Franklin, J. D. Powell and A. Emani-Naeini, *Feedback control of dynamic systems* 2^{nd} ed. Addison-Wesley (1991)

[42] C. R. Fuller and J. D. Jones, "Experiments on reduction of propeller induced interior noise by active control of cylinder vibration," Journal of Sound and Vibration **112**, Pg 389-395 (1987)

[43] C. R. Fuller, "Active control of sound transmission/radiation from elastic plates by vibration inputs: I. Analysis," Journal of Sound and Vibration **136**(1), Pg 1-15 (1991)

[44] Y. Gu, R. L. Clark, C. R. Fuller and A. C. Zander, "Experiments on active control of plate vibration using piezoelectric actuators and polyvinylidene floride (PVDF) modal sensors."ASME Journal of Vibration and Acoustics. **116**, Pg. 303-308 (1994)

[45] C. Guigou and A. Berry, "Design strategy for PVDF sensors in active control of simply supported plates," Internal report, GAUS, Dept. of Mech. Eng. Sherbrooke University (1993).

[46] J. R. Hassall and K. Zaveri, *Acoustic noise measurements*, Bruel and Kjaer, Pg 135-136. (1979)

[47] M. D. Jenkins, P. A. Nelson, R. J. Pinnington and S. J. Elliott, "Active isolation of periodic machinery vibrations," Journal of Sound and Vibration **166**(1), Pg 117-140 (1993)

[48] M. E. Johnson, "Active absorption and a power output approach to active control," Part III Project report, I.S.V.R. Univ. of Southampton (1991)

[49] M. E. Johnson and S. J. Elliott, "Volume velocity sensors for active control," Proc. Inst. Acoust. **15**(3), Pg 411-420 (1993)

[50] M. E. Johnson, S. J. Elliott and J. Rex, "Volume velocity sensors for the active control of acoustic radiation," ISVR Technical Memorandum No. 723 (1993)

[51] M. E. Johnson and S. J. Elliott, "Experiments on the active control of sound transmission into a stiff cylinder using a piezoelectric actuator," Proc. Inst. Acoust. **16**(1), Pg 201-210 (1994)

[52] M. E. Johnson and S. J. Elliott, "Minimisation of volume velocity as an active control strategy," Proc. 5th Conf. Rec. Adv. Struct. Dyn. Pg 962-972 (1994)

[53] M. E. Johnson and S. J. Elliott, "Active control of sound radiation using volume velocity cancellation," J. Acoust. Soc. Am. **98**(4), Pg 2174-2186 (1995)

[54] M. E. Johnson and S. J. Elliott, "Experiments on the active control of sound radiation using a volume velocity sensor," Proc. SPIE. 1995 North Am. Conf. on Smart Struct. and Mat. (1995).

[55] M. E. Johnson and S. J. Elliott, "Properties of radiation modes," ISVR Technical Memorandum No. 764 (1995)

[56] H. Kawai, "The piezoelectricity of polyvinylidene floride," Jpn. J. Appl. Phys. **8**, Pg 975-976 (1969)

[57] A. J. Kempton, "The ambiguity of acoustic sources - a possibility for active control?" Journal of Sound and Vibration, **48**, Pg 475-483 (1976)

[58] L. E. Kinsler, A. R. Frey, A. B. Coppens and J. V. Sanders, *Fundamentals of acoustics* (1950).

[59] S. M. Kuo and J. J. Min, "Development and analysis of an adaptive noise equalizer," IEEE Trans. on Speech and Audio Processing, Vol. 3, No.3, Pg 217-222 (1995)

[60] A. S. Knyazev and B. D. Tartakovskii, "Abatement or radiation from flexurally vibrating plates by means of active local vibration dampers," Soviet Physics - Acoustics, Vol. 13, No.1, 115-116 (1967).

[61] J. F. Lamb, C. G. Ingram, I. A. Johnston and R. M. Pitman, *Essentials of Physiology* Blackwell Scientific Publications Pg. 14-16 (1991)

[62] C. K. Lee, "Theory of laminated piezoelectric plates for the design of distributed sensors/actuators. Part I: Governing equations and reciprocal relationships," J. Acoust. Soc. Am. **87**, Pg 1144-1158 (1990)

[63] C. K. Lee and F. C. Moon, "Modal Sensors / Actuators," ASME Transactions Journal of Applied Mechanics, Vol.57 Pg 434-441 (1990)

[64] H. C. Lester and S. Lefebvre, "Piezoelectric Actuator Models for Active Sound and Vibration Control of Cylinders" Journal of Intelligent Material Systems and Structures. Vol. 4 Pg. 295-306 (1993)

[65] J. P. Millard and C. R. Fuller, "Advanced time domain wave-number sensing for structural acoustic systems. Part III. Experiments on the active broadband radiation control of a simply supported plate," J. Acoust. Soc. Am. **98** (5), Pg 2613-2621 (1995)

[66] M. Morari and E. Zafiriou, *Robust Process Control*, Prentice Hall (1989)

[67] P. M. Morse and K. U. Ingard, *Theoretical Acoustics* McGraw-Hill (1968)

[68] K. Naghshineh, G. H. Koopman and A. D. Belegundu, "Material tailoring of structures to achieve a minimum radiation condition," J. Acoust. Soc. Am. **92**(2), Pg 841-855 (1992).

[69] K. Naghshineh and G. H. Koopman, "A design method for achieving weak radiator structures using active vibration control," J. Acoust. Soc. Am. **92**(2), Pg 856-870 (1992).

[70] K. Naghshineh and G. H. Koopman, "Active control of sound power using acoustic basis functions as surface velocity filters," J. Acoust. Soc. Am. **93**(5), Pg 2740-2752 (1993).

[71] P. A. Nelson and S. J. Elliott, *Active Control of Sound* Academic Press, London (1992).

[72] P. A. Nelson, A. R. D. Curtis, S. J. Elliott and A. J. Bullmore, "The minimum power output of free field point sources and the active control of sound," Journal of Sound and Vibration **116**(3), Pg 397-414 (1987).

[73] M. J. Newman, *Active vibration control using a distributed controller* PhD Thesis, University of Southampton (1994)

[74] D. M. Photiadis, "The relationship of singular value decomposition to wave-vector filtering in sound radiation problems," J. Acoust. Soc. Am. **88**(2), Pg 1152-1159 (1990).

[75] J. N. Pinder, M. E. House and F. J. Fahy, "A Preliminary Study of the Ariane 5 Payload Bay Given by the Fairing and SPELTRA," Final report, ESA Contract No 6675/86/F/FL (1987)

[76] B. Rafaely and S. J. Elliott, "The use of internal model control in the design of feedback controllers for active headsets," ISVR Technical Memorandum No. 776 (1996)

[77] B. Rafaely and S. J. Elliott, "An adaptive and robust feedback controller for active control of sound and vibration," To be presented at the International Conference on Control (1996)

[78] J. Rex, *The use of Integrated Transducers for the Active Control of Structural Vibration*, M.Sc Thesis University of Southampton (1991)

[79] J. Rex and S. J. Elliott, "QWSIS A new sensor for structural radiation control," Proceedings of the 1st International Conf. on Motion and Vibration Control, Pg 339-343 (1992)

[80] S. D. Snyder and N. Tanaka, "On feedforward active control of sound and vibration using vibration error signals," J. Acoust. Soc. Am. **94**(4), Pg 2181-2194 (1993)

[81] S. D. Snyder, N. Tanaka and Y. Kikushima, "The use of optimally shaped piezoelectric sensors in the active control of free field radiation, Part 1: Feedforward control." J. Vib. Aco. Trans of ASME. Vol 3, Pg 311-322 (1995)

[82] D. R. Thomas and P. A. Nelson, "Feedback control of sound radiation from a plate excited by a turbulent boundary layer," J. Acoust. Soc. Am. **98**(5), Pg 2651-2662 (1995)

[83] M. Tohyama and R. H. Lyon, "Zeros of a transfer function in a multi-degree-of-freedom vibrating system," J. Acoust. Soc. Am. **86**, 1854-1862 (1989).

[84] I. Tolstoy, *Ocean acoustics* Am. Inst. of Phy. (1966)

[85] P. Vitiello, P. A. Nelson and M. Petyt, "Numerical studies of the active control of sound transmission through double partitions," ISVR Technical Report No. 183 (1989)

[86] C. E. Wallace, "Radiation resistance of a baffled beam," J. Acoust. Soc. Am. **51**(3) Pt.1, Pg 936-945 (1972)

[87] C. E. Wallace, "Radiation resistance of a rectangular panel," J. Acoust. Soc. Am. **51**(3) Pt.2, Pg 946-952 (1972)

[88] B. T. Wang, C. R. Fuller and E. K. Dimitriadis, "Active control of noise transmission through rectangular plates using multiple piezoelectric or point force actuators," J. Acoust. Soc. Am. **90**, Pg 2820-2830 (1991)

[89] G. B. Warburton, "The vibration of rectangular plates," Proc. Inst. Mech. Eng. Vol.168, 371-383 (1954).

[90] B. Widrow and M. Hoff, "Adaptive switching circuits," Proceedings IRE WESCON convention record, Part 4, Session 16, Pg 96-104 (1960)

[91] B. Widrow and S. D. Sterns, *Adaptive signal processing.* Prentice Hall, Englewood Cliffs, New Jersey. (1985)

[92] A. van der Ziel, *Solid state physical electronics* (1968)